



Amite River Basin Numerical Model

March 25, 2019

Project Report



PREPARED BY:

Dewberry Engineers Inc.
1615 Poydras Street, Suite 650
New Orleans, LA 70112

**Louisiana Department of Transportation &
Development (LA DOTD)**
1201 Capital Access Road Baton Rouge, LA 70802

Page intentionally left blank.

TABLE OF CONTENTS

Introduction.....	14
Numerical Model Purpose and Selection	17
HEC Software Used to Develop the ARBNM.....	18
Tiered Modeling Approach.....	20
<i>The 6-tiers:.....</i>	20
<i>Application of Modeling Approaches</i>	21
Data Gap Analysis and Collection.....	23
LiDAR, Bathymetry, and Ground Survey Collection	26
2018 LA DOTD ARB LiDAR.....	26
2017/18 LA DOTD ARB Survey and Bathymetry Collection	28
<i>Survey Methodologies.....</i>	28
<i>Cross Section Survey.....</i>	28
<i>Detailed Bridge Surveys.....</i>	30
<i>Limited Detail Survey.....</i>	30
High Water Mark (HWM) and Observed Data Collection	31
August 2016 Flood HWM Data.....	32
<i>Review of ARBC HWM Data</i>	32
<i>Other Sources of HWMs for the August 2016 Flood</i>	35
March 2016 Flood HWM Data.....	36
October 2017 Flood HWM Data	36
August 2017 Flood HWM Data.....	36
Hydrologic Model	37
Model Geometry, Input, and Parameters	38
<i>Subbasins.....</i>	38
<i>Routing.....</i>	40
<i>Meteorological Models.....</i>	41
Hydraulic Model.....	42
Dynamic HEC-RAS Hydraulic Model	42
<i>Computation Methods</i>	43
<i>Model Geometry</i>	43
<i>Model Parameters</i>	51
HEC-RAS Model Stability	58
<i>1D Flow Stability.....</i>	58
<i>2D Flow Stability.....</i>	61
Steady State ARB HEC-RAS Hydraulic Models.....	68
<i>Computation Methods</i>	70
<i>Model Geometry</i>	70
<i>Hydrologic Flows</i>	70
Calibration.....	71
Historic Precipitation Reconstruction for Floods.....	75
<i>August 2017 Precipitation Event.....</i>	77
<i>October 2017 Precipitation Event.....</i>	80

<i>March 2016 Precipitation Event</i>	82
<i>August 2016 Precipitation Event</i>	84
HEC-HMS Calibration	86
<i>Validation of Excess Precipitation Observations</i>	92
HEC-RAS Calibration	96
<i>Use of HEC-RAS Flow Roughness Factors in the ARB HEC-RAS Model 1D Reaches</i>	96
<i>Low Flow Calibration for January 2018 and June 2018 Flow Events</i>	97
<i>Calibration of the August 2017, October 2017, March 2016 and August 2016 Flood Events</i>	97
Design Flood Simulations	100
Flood Frequency Analysis	100
<i>Methodology and Software</i>	102
<i>Estimated Frequency of the August 2016 Flood</i>	105
<i>Summary of Flood Frequency Estimates</i>	106
Development of Design Storm Spatial and Temporal Distributions and Magnitude	108
<i>Design Storm Spatial Distribution</i>	109
<i>Design Storm Temporal Distribution</i>	111
<i>Design Storm Centers and Magnitudes</i>	112
Boundary Conditions	122
<i>Average or "Typical" Conditions</i>	123
<i>Wind and Storm Surge Influenced Conditions</i>	124
<i>"Typical" Flood Conditions</i>	125
<i>Period of Record Peak Flood Conditions</i>	126
Stationarity Analysis of Historic Precipitation and Flow	135
<i>Summary of Stationarity Assessment</i>	135
Consequence Model.....	136
Base Input Data.....	136
<i>Building Footprint Development</i>	138
<i>Agricultural Grid</i>	139
<i>Inundation Grids</i>	139
Model Parameters	140
<i>Economic Losses</i>	140
<i>Agricultural Data</i>	142
<i>Life-Loss</i>	143
<i>Impact Area Parameters and Warning Issuance Scenario</i>	146
<i>Alternatives</i>	149
Results and Validation.....	151
<i>Economic Damages</i>	151
<i>Number of Structures</i>	152
<i>Life-Loss</i>	153
HEC-WAT Implementation and Demonstration Projects	154
Summary and Recommendations	157
References	160
Appendix 1: HEC-HMS Model Parameter Summary	A1-1
Appendix 2: HTab Curves for Bridges in the Dynamic ARB HEC-RAS Model.....	A2-1
Appendix 3: HEC-SSP Statistical Analysis Reports	A3-1

Appendix 4: Boundary Conditions Supporting Research	A4-1
Appendix 5: Hydrologic and Hydrometeorologic Stationarity Assessment.....	A5-1

LIST OF FIGURES

Figure 1: Amite River Basin.....	15
Figure 2: Generalized Geologic Regions of Louisiana	16
Figure 3: Modeling approaches applied throughout the ARB	22
Figure 4: 2018 LA DOTD LiDAR	26
Figure 5: 2004 LSU LiDAR	26
Figure 6: Example bridge scan point cloud.....	30
Figure 7: Example bridge scan point cloud illustrating the bridge skew and pier locations	30
Figure 8: Example mudline on exterior of building.	31
Figure 9: Example mudline within a residential building.	31
Figure 10: Example debris line on fence.....	32
Figure 11: Example mudline on vegetation.....	32
Figure 12: Triple validation of HWMs.....	33
Figure 13: HWM location examples	34
Figure 14: Example visualization of observed and modeled data using the HEC-RAS Plot Stage and Flow Hydrographs function.	35
Figure 15: ARB HEC-HMS Hydrologic Model Overview	37
Figure 16: HEC-HMS basin Grid Cell File.....	39
Figure 17: ARBNM HEC-RAS Hydraulic Model Geometry Overview.....	42
Figure 18: Example of 2D Mesh with varying cell resolution and breaklines used to enforce streamlines and ridgelines within the upper reaches of the Bayou Manchac 2D Flow Area.....	46
Figure 19: Example of a bridge approximated as multiple culverts within SA/2D connections.....	47
Figure 20: Example of a bridge approximated using LiDAR data to simulate the opening for the Weir/Embankment within SA/2D Connections.	48
Figure 21: Example of bridge coding from ground survey at Highway 22 at the Amite River Diversion Canal.....	48
Figure 22: Example of multiple opening bridge at highway 37/63 on the Amite River	49
Figure 23: Amite Diversion Weir geometry, Amite River Lateral Structure146750.0 (right bank of Amite River).....	52
Figure 24: Variations of Weir Coefficients in the ARB HEC-RAS Hydraulic Model at the Amite River Diversion Weir Compared to Observed Flow Split on June 15, 2018 (flow split data collected by USGS).	53
Figure 25: Amite River, Cross Section 399176.7 (approximately 20 miles upstream of the Comite River Confluence), looking upstream. The basic channel Manning’s N value is estimated to be 0.037.	55

Figure 26: Amite River, Cross section 399176.7 (approximately 20 miles upstream of the Comite River Confluence), looking at right over bank. The basic right overbank Mannings's N value is estimated to be 0.12. <i>Photo: Forte & Tablada, 2018</i>	55
Figure 27: Chinquapin Canal, Cross Section 16041.2 looking upstream. The channel Manning's N value is estimated to be 0.03.....	56
Figure 28: Chinquapin Canal, Cross Section 16041.2 looking at left overbank. The left overbank Manning's N value is estimated to be 0.11.	56
Figure 29: Creating identical inverts and sections at sections 2, BRD, BRU and 3 of the HEC-RAS bridge routine generally resulted in greater stability for both single and multiple bridge openings.....	60
Figure 30: Gradual transition of cell sizes resulted in improved stability.	62
Figure 31: Example of 2D cell with two independent flooding elevations on the east and west edges of the cell which result in instabilities. The use of the red break lines along ridgelines divides these independent flood elevations coming from the east and west and consequently would improve model stability and run times..	63
Figure 32: Refinement of 2D mesh around ponds and borrow pits similar in size to the 2D mesh resolution resulted in improved stability. (Grey lines represent original mesh, black lines represent refined mesh)	64
Figure 33: Example of non-optimal cell alignment between 2D Flow Areas where faces are not collinear	65
Figure 34: Example of more optimally aligned cell faces between adjacent 2D Flow Areas	66
Figure 35: Optimization of Cell Sizes Adjacent to Culverts.....	67
Figure 36: Steady State Amite River Tributaries HEC-RAS Hydraulic Model Geometry Overview	68
Figure 37: Steady State Comite River Tributaries HEC-RAS Hydraulic Model Geometry Overview	69
Figure 38: Reconstructed rainfall with observations overlaid for the August 2017 event. Areas circled in red (blue) are underestimated (overestimated) by reconstructed Stage IV data.	78
Figure 39: Scatter plot of the reconstructed Stage IV rainfall and observed data with a 10% and 20% error bound.	79
Figure 40: Reconstructed rainfall with observations overlaid for the October 2017 event. Areas circled in red (blue) are underestimated (overestimated) by reconstructed Stage IV data.	80
Figure 41: Scatter plot of the reconstructed Stage IV rainfall and observed data with a 10% and 20% error bound.	81
Figure 42: Reconstructed rainfall with observations overlaid for the March 2016 event. Areas circled in red (blue) are underestimated (overestimated) by reconstructed Stage IV data.	82
Figure 43: Scatter plot of the reconstructed Stage IV rainfall and observed data with a 10% and 20% error bound.	83
Figure 44: Reconstructed rainfall with observations overlaid for the August 2016 event. Areas circled in red (blue) are underestimated (overestimated) by reconstructed Stage IV data.	84
Figure 45: Scatter plot of the reconstructed Stage IV rainfall and observed data with a 10% and 20% error bound.	85
Figure 46: Estimation of initial water content for the August 2016 flood event for the basin upstream of USGS Gage 07377500, Comite River near Olive Branch. At approximately 12:00 AM on August 12th, 2016, the river began to respond after receiving 2.3 in. of cumulative precipitation.	87
Figure 47: Validation of Gages for October 2017 Event.....	93

Figure 48: Adjusted reconstructed rainfall with observations and mask overlaid for the August 2016 event. Three sets of masks were created for the event as observations of rainfall and streamflow (Comite at Olive Branch and Darlington) indicated underestimations in the reconstructed rainfall.	95
Figure 49: HEC-RAS Flow Roughness Factors Option	96
Figure 50: HWMs were added to RAS Mapper and labeled to enable a rapid assessment of the accuracy of the HEC-RAS model by simply activating the Water Surface Elevation Grid (WSE) and hovering the cursor over the observed HWM.	98
Figure 51: The HEC-RAS Plot Stage and Flow Hydrographs function can be misleading when comparing observed and modeled hydrographs in areas of coupled 1D and 2D modeling since it does not account for 2D overbank flows as demonstrated here for the Amite River Near Denham Springs where flows are under estimated by only reporting flows contained within the 1D portion of the floodplain.....	99
Figure 52: By utilizing the Plot Flow Time Series function for Profile Lines drawn across both the 1D and 2D regions of a model will provide a comprehensive insight into the observed hydrograph where both 1D and 2D modeling methods are used as demonstrated here for the Amite River Near Denham Springs, more accurately representing the floodplain than the method demonstrated in Figure 51.....	99
Figure 53: USGS streamflow gages used in the Flood Frequency Analysis	101
Figure 54: Bulletin 17C AEP flow estimates including the August 2016 flood for the Amite River with the 90% confidence limits illustrated.	107
Figure 55: Bulletin 17C AEP flow estimates including the August 2016 flood for the Comite River with the 90% confidence limits illustrated.	108
Figure 56: The design storm at each storm center is represented by elliptical isohyets with a ratio of the major axis to the minor axis of 2.5 to 1 using the HMR 52 Standard Isohyetal Pattern.	109
Figure 57: The axis ratios for the August 2016 and March 2016 events were approximated to validate the HMR 52 assumption of 2.5:1. Both the March and August 2016 events demonstrated approximately a 2:1 ratio as illustrated here for the August 2016 event.....	110
Figure 58: HMR 52 Temporal Distribution.....	111
Figure 59: The HMR 52 temporal distribution accumulation was compared to the August 2016 storm accumulations to validate the assumption.	112
Figure 60: Design storm centered over the Comite River near Olive Branch Gage (OB).	113
Figure 61: Design storm centered over the Amite River near Darlington Gage (DAR).....	114
Figure 62: Design storm centered over the Amite River near Denham Springs Gage (DS).	115
Figure 63: Design Storm Flows for the Comite River near Olive Branch with Multiple Storm Centers.....	119
Figure 64: Design Storm Flows for the Comite River near Comite with Multiple Storm Centers	119
Figure 65: Design Storm Flows on the Amite River at Darlington with Multiple Storm Centers.....	120
Figure 66: Design Storm Flows on the Amite River at Magnolia with Multiple Storm Centers	120
Figure 67: Design Storm Flows on the Amite River at Denham Springs with Multiple Storm Centers	121
Figure 68: Design Storm Flows on the Amite River at Port Vincent with Multiple Storm Centers	121

Figure 69: ARB HEC-FIA Consequence Model Overview	136
Figure 70: Example of the NSI (yellow triangles) in East Baton Rouge Parish.	137
Figure 71: Comparison of LiDAR derived structures (red squares) and the NSI (yellow triangles) in East Baton Rouge parish.	138
Figure 72: HEC-FIA grids only event set-up.	139
Figure 73: Depth-damage curve associated with structure occupancy type REL 1, Church.	141
Figure 74: Depth-damage curve associated with structure occupancy type RES1-1SNB, Residential one story with no basement.	142
Figure 75: Crop loss editor table in HEC-FIA.	143
Figure 76: Safe zone parameters for structure occupancy type RES1-1SNB, Residential one story with no basement	144
Figure 77: Safe zone parameters for structure occupancy type RES1-2SNB, Residential two story with no basement.	145
Figure 78: Impact area editor showing the default values chosen for the ARB.	146
Figure 79: “Additional Parameters” editor for computing life-loss with uncertainty.	147
Figure 80: Warning issuance scenario for the August 2016 flooding event.	148
Figure 81: Timeline of watches and warnings issued by the NWS for Louisiana.	149
Figure 82: Alternative editing GUI	150
Figure 83: ARB HEC-WAT Model	154
Figure 84: HEC-WAT Model Linking Editor	155
Figure 85: Software Linking in HEC-WAT	155
Figure 86: Create a new HEC-WAT Alternative Simulation.	156

LIST OF TABLES

Table 1: River Characteristics	17
Table 2: Datasets Used to Develop the ARBNM	23
Table 3: ASPRS V1.4 Lidar Point Classes Required For The 2018 LA DOTD Lidar	27
Table 4: Summary of HWM Quality Assessment and Count	33
Table 5: Summary of Terrain Data Used for 2D Flow Areas	45
Table 6: Summary of Geometric Data Used for High Detail Cross Sections	50
Table 7: Summary of Manning’s N Values for 1D Cross Sections	54
Table 8: Summary of Manning’s N Values for 2D Flow Areas	57
Table 9: NWS Flood Stage Categorization	72
Table 10: USGS Recorded Stage (Cell colors correspond to Table 9 Flood Stage Categorization)	73
Table 11: USGS Recorded Flows (Cell colors correspond to Table 9 Flood Stage Categorization)	73
Table 12: Selected Historical Flood Events	74
Table 13: Amite Watershed Calibration Events	76
Table 14: August 2017 Precipitation Event Observations	88
Table 15: October 2017 Precipitation Event Observations	89
Table 16: March 2016 Precipitation Event Observations	90
Table 17: August 2016 Precipitation Event Observations	91
Table 18: Summary of Excess Precipitation	92
Table 19: Summary of Stream Gages used within the Analysis	102
Table 20: Comparison of Software and Statistical Methodologies for the 1% AEP Estimates (through 2017)	103
Table 21: Low Outliers Detected by Software and Method Including and Excluding the August 2016 Flood	104
Table 22: Sensitivity of the inclusion and exclusion of the August 2016 flood on the 1% AEP flow estimates	104
Table 23: Estimated Frequency Range of the August 2016 Flood	105
Table 24: Peak Flow Estimates for Gages with 2016 event included in analysis except as noted	106
Table 25: Peak Design Flood Streamflow Estimates for Olive Branch (OB) Storm Center with Estimated AEP or AEP Range	116
Table 26: Peak Design Flood Streamflow Estimates for Darlington (DAR) Storm Center with Estimated AEP or AEP Range	117
Table 27: Peak Design Flood Streamflow Estimates for Denham Springs (DS) Storm Center with Estimated AEP or AEP Range	118
Table 28: Average or “typical” conditions downstream boundary condition water surface elevation hydrograph	123

Table 29: Average Daily Wind Speed vs. Measured Lake Maurepas water surface elevation.	125
Table 30: Amite River Peak Discharges vs. Measured Lake Maurepas water surface elevation.	126
Table 31: Period of record flood conditions downstream boundary condition water surface elevation hydrograph.	127
Table 32: HEC-FIA Structure Inventory inputs for HEC-FIA.....	137
Table 33: Occupancy Type and Count Estimated for the ARB.....	140
Table 34: Summary of HEC-FIA Computed Economic Damages Estimated for the August 2016 Flood	151
Table 35: Summary of HEC-FIA Computed Damaged Structures Counts Estimated for the August 2016 Flood	152
Table 36: Summary of observed and HEC-FIA simulated life loss for the August 2016 Flood for the ARB	153

LIST OF ACRONYMS

Annual Exceedance Probability	AEP
Amite River Basin	ARB
Amite River Basin Drainage & Water Conservation District	ARBC
Amite River Basin Numerical Model	ARBNM
Annual Maximum Series	AMS
Base Level Engineering	BLE
Bridge Downstream Internal Cross Section	BRD
Bridge Selection Method	BR Sel Method
Bridge Upstream Internal Cross Section	BRU
Centimeter	cm.
Cubic Feet Per Second	cfs
Coastal Protection and Restoration Authority	CPRA
Coastwide Reference Monitoring System	CRMS
Community Collaborative Rain, Hail, & Snow Network	CoCoRaHS
Cooperating Technical Partner	CTP
Digital Elevation Model	DEM
Engineering and Construction Bulletin	ECB
Federal Emergency Management Agency	FEMA
Flood Insurance Rate Map	FIRM
Flood Insurance Study	FIS
Flood Risk Analysis	FRA
foot/feet	ft.
Freedom of Information Act	FOIA
Hydrologic Engineering Center	HEC
HEC-Data Storage System Visual Utility Engine	HEC-DSSVue
HEC-Ecosystem Function Model	HEC-EFM
HEC-Flood Impact Analysis	HEC-FIA
HEC-Hydrologic Modeling System	HEC-HMS
HEC-Meteorological Visual Utility Engine	HEC-MetVue
HEC-River Analysis System	HEC-RAS
HEC-Statistical Software Package	HEC-SSP
HEC-Watershed Analysis Tool	HEC-WAT
High Water Mark	HWM

Hour	hr
Hydrometeorological Report	HMR
Inch	in.
Inertial Navigation System	INS
Integrated Climate and Land-Use Scenarios	ICLUS
Louisiana Department of Transportation & Development	LA DOTD
Louisiana Economic Development	LED
Louisiana State University	LSU
Louisiana Watershed Initiative	LWI
Mile	mi.
Multi-Resolution Land Cover Characteristics Consortium	MRLC
National Hydrology Dataset Plus	NHD+
National Land Cover Database	NLCD
National Oceanic and Atmospheric Administration	NOAA
National Structure Inventory	NSI
National Weather Service	NWS
Non-vegetated Vertical Accuracy	NVA
North American Datum of 1983	NAD 83
North American Vertical Datum of 1988	NAVD 88
Natural Resources Conservation Service	NRCS
One Dimensional	1D
Quality Level 1	QL1
Quality Level 2	QL2
Real-time Network	RTN
Root Mean Square Error in the Z direction	RMSEz
Seconds	sec
Soil Survey Database	SSURGO
square miles	sq. mi.
Standard Hydrologic Grid	SHG
The Annual Exceedance Probability	AEP
Two Dimensional	2D
U.S. Army Corps of Engineers	USACE
United States Geological Survey	USGS
Water Surface Elevation	WSEL / WSE
World Meteorology Organization	WMO

INTRODUCTION

Dewberry Engineers Inc. (Dewberry) was contracted by the Louisiana Department of Transportation and Development (LA DOTD) for this project to develop the suite of modeling tools referred to as the Amite River Basin Numerical Model (ARBNM), to simulate hydrology and hydraulics within the Amite River Basin (ARB), and to quantify the potential consequences of floods simulated with the tools. Forte & Tablada, Inc. and FTN Associates, Ltd supported Dewberry on this project. Forte & Tablada, Inc. provided survey services, and FTN Associates, Ltd provided independent quality control, stakeholder engagement and hydraulic modeling support.

This report documents the process used to develop Version 1.0, of the ARBNM, the sources of data utilized for the model and the technical methodologies applied as a resource to future users. In addition to this report, the *Amite River Basin Numerical Model Quick Guide* provides hands-on guidance using the ARBNM tools with references back to this document and other technical references pertinent to the successful utilization of the ARBNM.

The Amite River is a tributary to Lake Maurepas in southeastern Louisiana. The river's headwaters begin in Mississippi as the East Fork Amite River and the West Fork Amite River, and flow south, confluenting approximately 1 mi. downstream of the Louisiana-Mississippi state line. The Amite River continues and confluenting with the Comite River just upstream of the City of Denham Springs and continues on for approximately 55 mi. before reaching Lake Maurepas. **Figure 1** below illustrates the Amite River Basin (ARB) and its major tributaries.

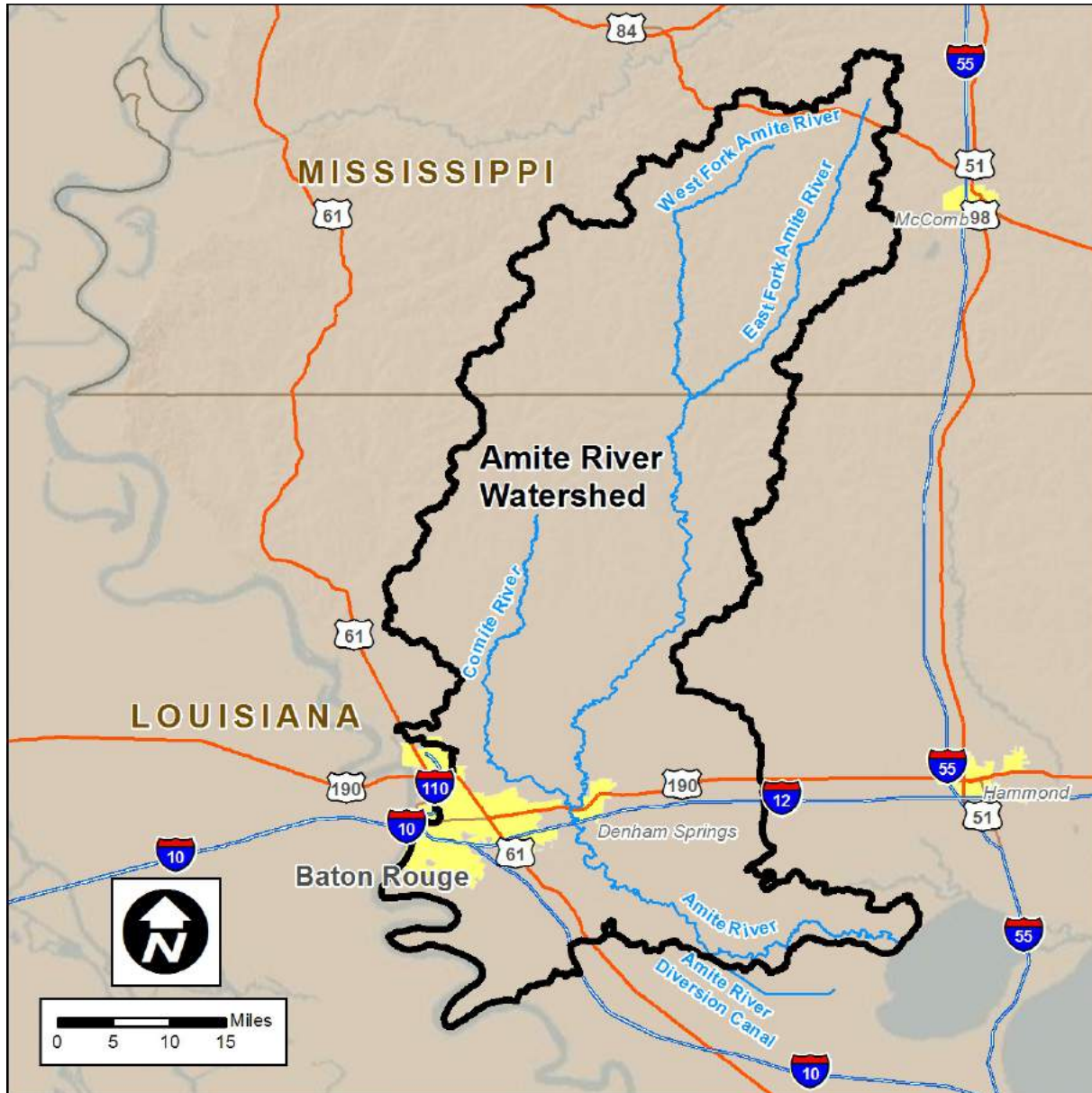


Figure 1: Amite River Basin.

The Amite River and its tributaries pass over three generalized geologic regions. These regions, illustrated in **Figure 2**, include the Citronelle and Willis Formations (Pliocene) region, the Terraces (Pleistocene) region, and the Alluvium (Holocene) region. Characteristics of the Amite River and major tributaries found within these regions are described in **Table 1**.

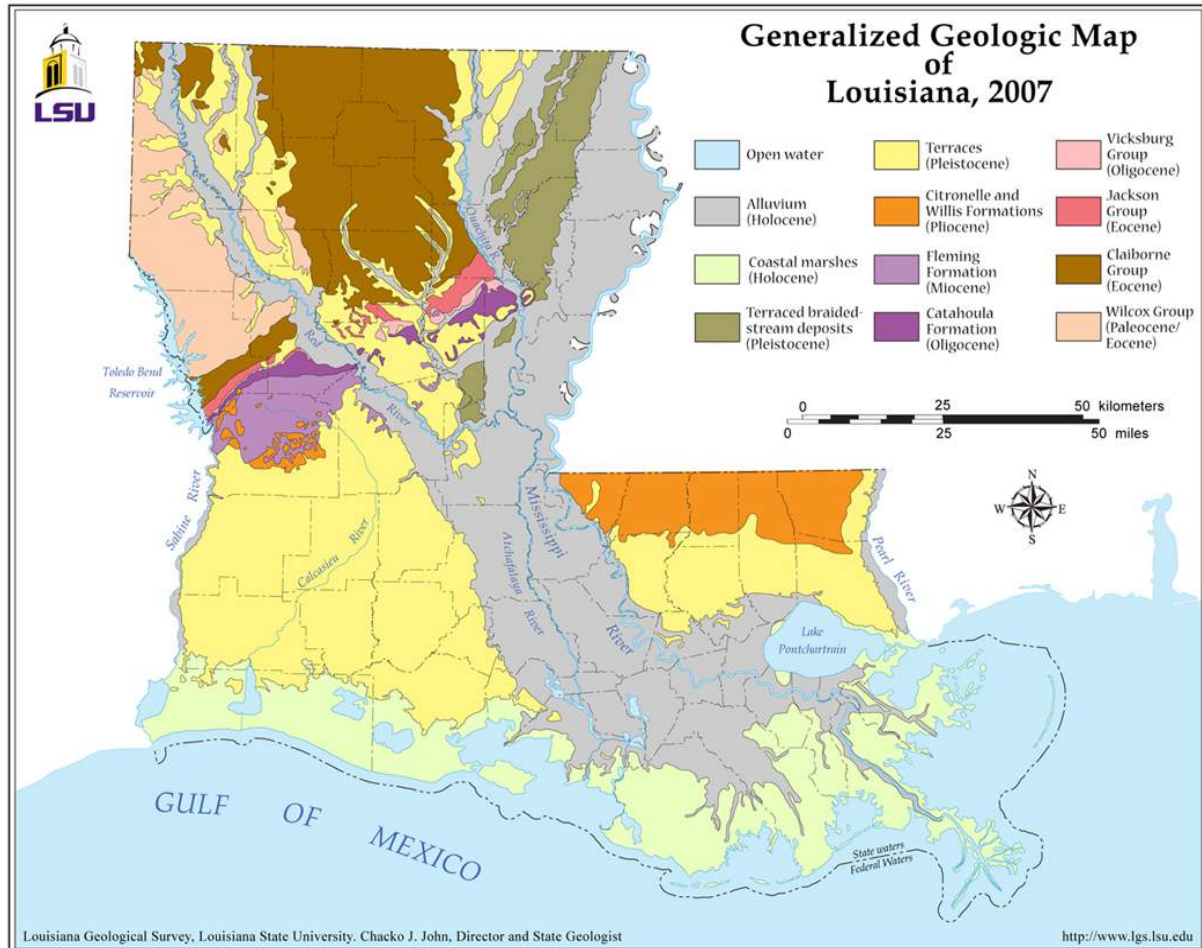


Figure 2: Generalized Geologic Regions of Louisiana.

Source: Louisiana Geological Survey and Louisiana State University

Table 1: River Characteristics	
Generalized Geologic Region	River Characteristics
Citronelle and Willis Formations (Pliocene)	<ul style="list-style-type: none"> • Extensive coarse sand/gravel bars with partially filled channels during base flows. • Confined floodplains, • Approximately 3.5 ft./mi. water surface slope
Terraces (Pleistocene)	<ul style="list-style-type: none"> • Extensive sand/gravel bars with partially filled channels during base flows. Highly meandering channels, extensive evidence of channel migration and changing morphology. • Less confined floodplains. • Approximately 2.2 ft./mi. water surface slope
Alluvium (Holocene)	<ul style="list-style-type: none"> • Deep, slow moving tidally influenced flows. Base flows permanently at or near bank full. Poorly drained soils. • Wide, unconfined floodplains • Approximately 0.5 ft./mi. water surface slope

Numerical Model Purpose and Selection

The modeling tools provide engineers and planners with a system-wide model representing the ARB's existing hydrologic and hydraulic conditions. The model can be used as a baseline to support the assessment of manmade and natural watershed changes that may alter flood risk. Using these tools users can quantify changes to flood volumes, flood elevations, and frequencies as a result of physical changes, while simultaneously assessing and quantifying life-safety and economic consequences.

Proprietary and freely available software was reviewed to determine their suitability for development of the ARBNM. The U.S. Army Corps of Engineers (USACE) Hydrologic Engineering Center (HEC) produces the HEC suite of software which has become widely used for hydrologic and hydraulic modeling throughout the U.S. The software is freely available to non-USACE users, and is the most commonly used suite of software for the Federal Emergency Management Agency (FEMA) Flood Insurance Studies.

The HEC suite is a consistent framework for hydrologic and hydraulic modeling through its HEC-Hydrologic Modeling System (HEC-HMS) and HEC-River Analysis System (HEC-RAS) applications. HEC-RAS's recent enhancements include industry leading two dimensional (2D) modeling capabilities, ideally suited to complex unconfined floodplains found throughout Louisiana. HEC-RAS's 2D capabilities are becoming more widely embraced both in Louisiana and within the national community of practice.

While some future projects will require the modification of HEC-HMS hydrologic models, the majority will likely only require the modification of HEC-RAS hydraulic models to assess potential project impacts, including new roads, levees, channel modifications, and diversions. While there are many local engineering firms in Louisiana who are experienced users of the one dimensional (1D) hydraulic modeling capabilities of HEC-RAS, as a result of the relatively new 2D technology, there are far fewer that are familiar with 2D hydraulic modeling. Therefore, model features, such as channels and hydraulic structures that will most frequently

be subject to further study and investigation, have been modeled using 1D features, thus making the models generally more accessible to a wider range of end users and maximizing the use of embedded design and analysis functions within HEC-RAS which are generally more extensive for 1D features.

In addition to the hydrologic and hydraulic capabilities of the HEC suite, additional HEC applications ideally suited to Louisiana include HEC-Flood Impact Analysis (HEC-FIA) which quantifies the life safety and economic impacts of floods and projects, HEC-Ecosystem Function Model (HEC-EFM) which assesses the ecosystem impacts of projects, and the HEC-Watershed Analysis Tool (HEC-WAT) which integrates multiple models into a single environment and provides users with an advanced suite of tools to assess projects through both traditional and advanced risk assessment methodologies, all of which are available to non-USACE users at no cost.

HEC Software Used to Develop the ARBNM

Software used for the ARBNM was classified into two broad categories: Primary Software and Secondary Software. Definitions of each category for purposes of this report are as follows:

- 1. Primary Software:** Includes software that will be frequently used by the local community of practice to assess risk and the potential impact of projects within the ARB.

HEC-Hydrologic Modeling System (HEC-HMS)

- HEC-HMS allows users to simulate the complete hydrologic processes of dendritic watershed systems, and includes many traditional hydrologic analysis procedures such as event infiltration, unit hydrographs, and hydrologic routing. HEC-HMS was used to develop a hydrologic model of the ARB that allows easy integration of computed flows to a HEC-RAS hydraulic model. While this software will not require updating for every use of the ARBNM by the local community of practice, it is anticipated that many users will choose to refine the model and create additional hydrologic simulations.

HEC-River Analysis System (HEC-RAS)

- HEC-RAS allows users to perform 1D steady flow, 1D and 2D unsteady flow calculations, sediment transport/mobile bed computations, and water temperature/water quality modeling. HEC-RAS was used to develop a hydraulic model of the ARB using the unsteady coupled 1D and 2D engines. It is anticipated that this software will be the most commonly used software by the local community of practice.

HEC-Flood Impact Assessment (HEC-FIA)

- HEC-FIA allows users to perform consequence assessments from a single event including economics and life safety. HEC-FIA was used to develop a consequences model for the ARB to quantify economic and life safety impacts of simulations. While this software will likely not be used for most local scale applications of the ARBNM, it is anticipated that the local community of practice will most commonly utilize it to assess the consequences of larger, regional scale flood mitigation and planning projects.

- 2. Secondary Software:** Includes software used to help develop the ARBNM, software that will only require occasional use, and software needed only for advanced applications.

HEC-Statistical Software Package (HEC-SSP)

- HEC-SSP allows users to perform statistical analyses of hydrologic data. HEC-SSP can perform flood flow frequency analysis based on Bulletin 17B (Interagency Advisory Committee on Water Data, 1982) and Bulletin 17C (England, et al., 2015) methodologies, generalized frequency analysis on flow and other hydrologic data, volume frequency analysis on high and low flows, duration analysis, coincident frequency analysis, and balanced hydrograph analysis. HEC-SSP was not an integral part of the ARBNM, but was used extensively to analyze historical data to support calibration of simulations for specific annual exceedance probabilities within the ARB. It is anticipated that HEC-SSP will not be widely implemented by the local community of practice since its primary purpose was to advise the development of probabilistic design floods during the initial development of the ARBNM. However, as additional years of historic data are collected, it may again be utilized to perform updated analysis of streamflow statistics to advise the updated calibration for the ARBNM.

HEC-Meteorological Visual Utility Engine (HEC-MetVue)

- HEC-MetVue is a tool that provides users with a suite of functions for precipitation viewing and processing. HEC-MetVue was utilized for the development of design storms within the ARBNM and enabled several storm centers to be efficiently simulated. HEC-MetVue is anticipated to be used by advanced users for the analysis of various storms including those to meet specific community design criteria. One potential application is the ability to move the center of observed and design storms within the ARB to adjacent watersheds if needed to simulate ‘what if’ scenarios. Examples could include ‘what if the August 2016 flood was centered over the headwaters of the ARB, or 30 mi. further east.

HEC-Watershed Analysis Tool (HEC-WAT)

- HEC-WAT provides an overarching interface for many of the HEC suite of software and is designed for interactive use in a multi-tasking environment to provide information for decision makers to support alternative analysis. HEC-WAT was used to integrate HEC-HMS, HEC-RAS and HEC-FIA models adding a wealth of functionality to the modeling system for future advanced analysis and research. It is anticipated that HEC-WAT will not be commonly implemented by the local community of practice at this time, partially due to the development of HEC-WAT still being in the early stages of implementation, however it does provide advanced tools for integration of models and flood risk analysis that provides strong potential for future and more advanced analysis.

HEC-Data Storage System Visual Utility Engine (HEC-DSSVue)

- HEC-DSSVue is a Java-based visual utilities program that allows users to plot, tabulate, edit, and manipulate data in a HEC-DSS database file format. These advanced functions infused efficiencies when developing the ARBNM for data stored within the DSS database. It is anticipated that advanced users of the ARBNM will likely utilize HEC-DSSVue to manipulate and analyze data, however many of

the advantages realized were associated with the initial development of the ARB HEC-HMS and HEC-RAS models.

Tiered Modeling Approach

The ARB within Louisiana contains approximately 1,165 mi. of floodplain as identified on FEMA's Flood Insurance Rate Maps (FIRMs). A 6-tier modeling approach was scoped using both 1D and 2D hydraulic approaches to meet the challenges of the unique hydrologic conditions and provide added detail in areas of greater flood risk and complexity.

The 6-tiers:

#1. Low Detail 1D (300 Stream Miles)

- Steady state 1D hydraulic modeling using instantaneous peaks from the HEC-HMS model
- Applied to minimally developed areas with confined floodplains
- Consistent with FEMA model backed Zone A methodologies
- Key modeling techniques include:
 - Cross sections cut directly from LiDAR
 - Major structures modeled using data approximated from aerials and topography

#2. Medium Detail 1D (70 Stream Miles)

- Unsteady 1D hydraulic model using inflows from the HEC-HMS model
- Applied to areas of minor development and major rivers with confined floodplains
- Consistent with FEMA Detailed Zone AE methodologies
- Key modeling techniques include:
 - Cross sections cut directly from LiDAR with some bathymetric assumptions
 - Detailed survey performed for major hydraulic structures. Minor structures modeled using data approximated from aerials and topography

#3. High Detail 1D (15 Stream Miles)

- Unsteady 1D hydraulic model using inflows from the HEC-HMS model
- Applied to areas of high development along the Amite, Comite and select tributaries with confined floodplains
- Consistent with FEMA Detailed Zone AE methodologies
- Key approaches include:
 - Cross sections cut from LiDAR and supplemented with bathymetry and/or bathymetric assumptions
 - Detailed structure coding from survey and/or available plans for all structures

#4. Low Detail 2D (450 Stream Miles)

- Unsteady 2D modeling
- Applied to smaller flooding sources with unconfined floodplains
- Consistent with FEMA Limited Detail Model Backed Zone AE methodologies

- Channels modeled in 2D with break line refinement
- Major structures modeled in 1D using dimensions approximated from aerials and topography

#5. Medium Detail 2D (250 Stream Miles)

- Unsteady 2D modeling
- Applied to moderately developed areas with unconfined floodplains typically shown as FEMA Zone A or AE floodplain
- Consistent with FEMA Limited Detail Model Backed Zone AE methodologies
 - Channels modeled in 2D with break line refinement and minor hydro enforcement
 - Basic level survey performed for major hydraulic structures. Minor structure coding assumed from aerials and topography. Structures coded as 1D features

#6. High Detail 2D (120 Stream Miles)

- Unsteady coupled 1D/2D modeling
- Applied to developed areas with unconfined floodplains typically shown as FEMA Zone AE floodplain
- Consistent with FEMA Detail Zone AE methodologies
 - Channels modeled bank to bank in 1D with the unconfined overbanks modeled in 2D
 - Structures coded as 1D features using survey and/or available plans for all structures

Application of Modeling Approaches

Figure 3 illustrates the modeling approaches for the 1,165 mi. of study streams within the ARB. It should be noted that both Low and Medium detail studies will be scalable and can be enhanced during future studies where greater detail is needed.

A single HEC-HMS hydrologic model was developed for the entire ARB to provide inflows for all study reaches regardless of model detail. This included routed flows to support instantaneous peaks applied to the low detail 1D steady state HEC-RAS study reaches in addition to point inflows from individual subbasins to apply to the dynamic 1D and 2D HEC-RAS model. This model is referred as the *ARB HEC-HMS Model* throughout this document.

A single HEC-RAS hydraulic model was developed for all medium and high detail 1D study reaches in addition to all 2D study reaches regardless of detail. Routed inflows from the ARB HEC-HMS model were applied to the Amite River at the Mississippi State Line in addition to the routed lateral inflows from low detail 1D reaches within the ARB HEC-HMS model. All other flows from the ARB HEC-HMS model were applied from subbasin flows as point inflows to either the 1D or 2D reaches and were routed dynamically within HEC-RAS which uses the Saint Venant equations as further detailed in the Hydrology and Hydraulic sections of this report. This model is referred to as the *Dynamic ARB HEC-RAS Model*. This will be the main model used for analysis within the ARB and includes all areas of higher flood risk and development potential. It should be noted that streams within Mississippi were not included in

the ARB hydraulic models, however the ARB within Mississippi was include in the ARB hydrologic model.

Two HEC-RAS hydraulic models were developed for the low detail 1D reaches representing the Comite River tributaries and the Amite River tributaries above the confluence of these two rivers. These models are referred to as the *Steady State ARB HEC-RAS Models* throughout this document. It is expected that these models will be used far less frequently than Dynamic ARB HEC-RAS.

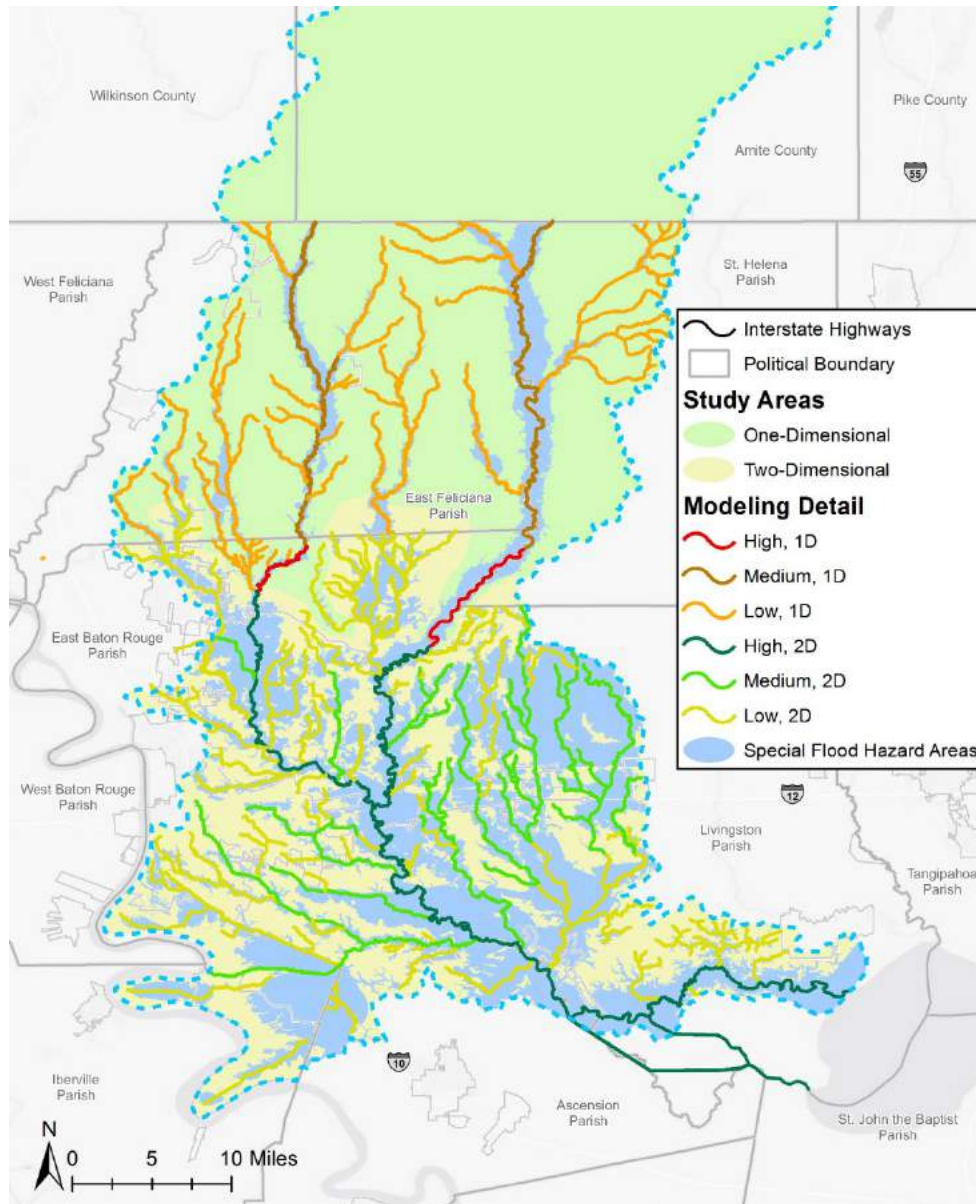


Figure 3: Modeling approaches applied throughout the ARB

DATA GAP ANALYSIS AND COLLECTION

The purpose of this task was to identify, collect and review existing technical data including models and survey that could be leveraged for development of the ARBNM.

To perform this task, extensive research and stakeholder engagement was performed to identify potential sources of data. This included Freedom of Information Act (FOIA) requests to Federal agencies including FEMA and USACE as well as direct requests to local agencies, stakeholders and experts.

Stakeholder engagement included presenting an overview and status update for the ARBNM development at the *Improving the Amite River Basin Flood Forecasting and Hazard Analysis, 2nd Annual Technical Workshop*, cohosted by the ARB Drainage and Water Conservation District and the Louisiana State University (LSU) Center for River Studies on October 19, 2017 at the Patrick F. Taylor Hall. More than 90 professionals attended the workshop including representatives from federal agencies, state agencies, local agencies, non-profits, academia and the private sector. After the one hour presentation, attendees received a request to share available technical data and information to support the development of the ARBNM. As a result of direct solicitations and data request, a number of datasets were received including high water marks, GIS data, modeling data, survey and technical reports. These were individually evaluated to identify data availability and inform the need for additional data collection including ground based structure and bathymetric survey. **Table 2** summarizes those datasets received that were directly utilized to develop the ARBNM.

Dataset	Source	Data Type	Description	Assessment	Application for Watershed
2018 LA DOTD ARB LiDAR	LA DOTD	LiDAR LAS and DEM files.	QL1 LiDAR developed between January and April 2018 by Dewberry for LA DOTD.	High quality recent LiDAR exceeding FEMA's minimum standards for detailed floodplain studies.	Data used for 2D mesh development and 1D cross section extraction where bathymetric survey is not available.
2016 FEMA Base Level Engineering Study of Amite River HUC 8 watershed	FEMA RVI	HEC-HMS/HEC-RAS hydraulic models	FEMA First Order Approximation (FOA) of flood risk using HEC-HMS/HEC-RAS 2D Rain-on-Grid Methodologies.	Approximate model providing an overview of flood conditions, flow paths and flood risk utilizing the LSU statewide LiDAR dated 2006.	Results used as guidance for model layout including 1D cross section alignment and 2D flow areas.
ARBC, August 2016 Flood HWM	Various Sources	Survey points	Survey points of HWM for the August 2016 flood.	449 HWM. 374 of 449 were assessed to be high confidence.	Used for calibration of the August 2016 flood simulation.

Table 2: Datasets Used to Develop the ARBNM

Various ARB datasets	Gulf Engineers & Consultants	Hydrologic and hydraulic models.	Variety of hydrologic and hydraulic models including the Amite River, Comite River, Amite River Diversion, and Bayou Manchac	HEC-HMS and HEC-RAS models of varying age and detail.	Geometry from bridges and culverts leveraged for limited detail study areas where feasible.
Spatial file	HNTB	ESRI Shapefile	GIS polygon of 2D model domain from model being developed by HNTB for various parishes.	Boundary polygon of 2D modeling domain.	Boundary utilized to ensure accurate edge-match between model and the ARBNM to streamline future model integration/merging.
Amite and Comite River 2017 Bathymetric Survey	USACE New Orleans District	Survey files	Post August 2016 bathymetric survey of the Amite River, Comite River and Amite River Diversion Canal.	High quality survey data representative of existing river conditions. Extents include bathymetric cross sections approximately 250 ft. apart for the Amite River from Lake Maurepas, to Denham Springs and the Comite River from the Amite River confluence upstream to Dyer Road.	Survey utilized for wet portions of all 1D model cross sections within the extent of the survey.
1992 Darlington Reservoir Feasibility Study	USACE New Orleans District	PDF	Plans and specifications for Darlington Reservoir concepts	Various project alternatives for concept project.	Plans used to demonstrate use of HEC-WAT for assessment of project alternatives.
Stream gaging for Amite River Diversion Weir	USGS	.KMZ	Results of stream gaging for a single event at the Amite Diversion Weir	Measured flows upstream and downstream of the diversion weir for a low flow event.	Utilized to validate flow split modeled within HEC-RAS.
August 2016 Oblique Imagery	Civil Air Patrol	.JPG	Oblique imagery captured at various times during the August 2016 flood	Aerial imagery captured at various times giving insight into the flood extent.	Utilized to validate 2016 flood simulation where appropriate.

Table 2: Datasets Used to Develop the ARBNM

2017 CPRA LiDAR	CPRA	LiDAR LAS and DEM files.	QL2 LiDAR collected in 2017.	High quality recent LiDAR exceeding FEMA's minimum standards for detailed floodplain studies.	Data used for 2D mesh development beyond the extent of the 2018 LA DOTD LiDAR.
--------------------	------	--------------------------------	---------------------------------	--	--

LIDAR, BATHYMETRY, AND GROUND SURVEY COLLECTION

The purpose of this task was to collect additional survey and LiDAR data to supplement the data collected during the Data Gap Analysis and Collection task. Additional information regarding the application of this information for model geometry on both regional and node specific levels is provided in the Hydrologic and Hydraulic Model sections of this report.

2018 LA DOTD ARB LiDAR

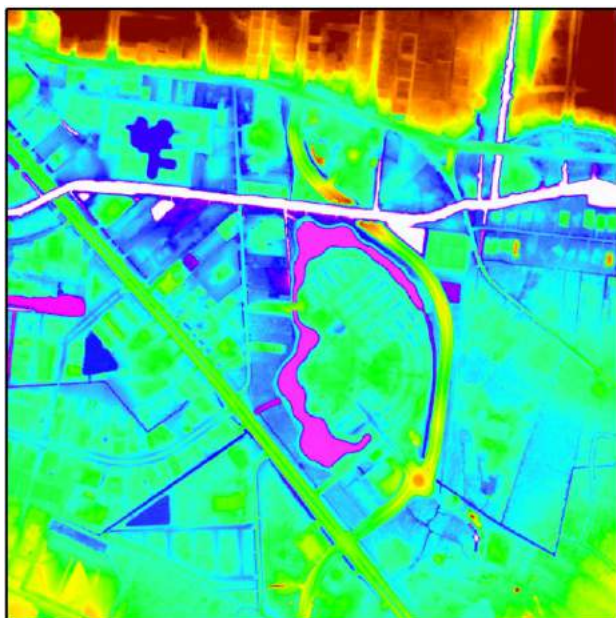


Figure 4: 2018 LA DOTD LiDAR

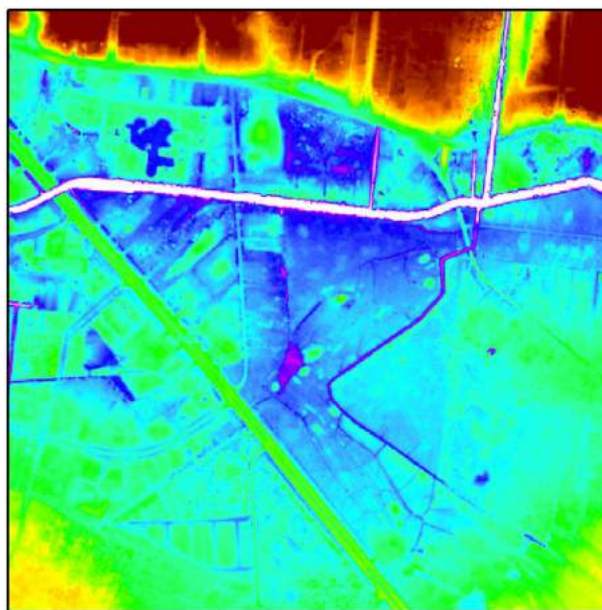


Figure 5: 2004 LSU LiDAR

Review of the existing 2004 LSU LiDAR indicated significant changes throughout the ARB since the LiDAR was captured. Additionally, technological advances in LiDAR sensors and processing techniques supported the development of higher accuracy data for the purpose of developing hydrologic and hydraulic models within the ARB. To provide more accurate and up to date terrain data for the development of the ARBNM, LiDAR was captured during the timeframe of March 01, 2018 to April 12, 2018 for the entire ARB using USGS National Geospatial Program LiDAR Base Specifications for Quality Level 1 (QL1). **Figure 4** and **Figure 5** highlight the differences between the 2004 and 2018 LiDAR datasets within an area of Baton Rouge.

Aerial data acquisition was performed by Precision Aerial Reconnaissance and all ground survey including checkpoints was performed by Forte & Tablada. Dewberry was responsible for LiDAR classification, breakline production, Digital Elevation Model (DEM) production, any derivative product development, and quality assurance. The tested Root Mean Square Error in the Z direction (RMSEz) of the classified LiDAR data for checkpoints in non-vegetated terrain equaled 3.6 cm. compared with the 10 cm. specification. Meanwhile, the Non-vegetated Vertical Accuracy (NVA) of the classified LiDAR data computed using $\text{RMSEz} \times 1.9600$, was equal to 7 cm. compared with the 19.6 cm. specification.

Detailed breaklines and bare-earth Digital Elevation Models (DEMs) were produced for the project area. Data was formatted according to tiles with each tile covering an area of 1,500 meters by 1,500 meters. A total of 2,410 tiles were produced for the project encompassing an area of approximately 1,900 sq. mi. LAS files use an industry standard binary format for storing airborne LiDAR point cloud data in a classified manner. LAS allows LiDAR data to be examined in its native format and through use of classification codes that allow users to determine what points represent as shown in **Table 3**.

Table 3: ASPRS V1.4 Lidar Point Classes Required For The 2018 LA DOTD Lidar	
Classification Value	Meaning
1	Unclassified
2	Ground (Bare Earth)
7	Low Noise
8	Model Key Points
9	Water
17	Bridge Deck
18	High Noise

The bare earth DEMs supplemented with ground survey and bathymetry of channels were primarily used to develop the Dynamic ARB HEC-RAS model geometry, however LAS point cloud information was utilized to supplement survey data for structures critical to hydraulic modeling including portions of bridges and roadways.

2017 QL2 LiDAR was obtained from the Louisiana Coastal Protection and Restoration Authority (CPRA) which covered much of the lower Amite River watershed including adjacent areas beyond the Amite River HUC8 boundary not captured by the 2018 LA DOTD LiDAR. For isolated areas beyond the extent of the HUC 8 2018 LA DOTD LiDAR and 2017 CPRA LiDAR datasets, 2004 LSU LiDAR was used.

2017/18 LA DOTD ARB Survey and Bathymetry Collection

To supplement the USACE 2017 bathymetric survey, additional survey data was collected to support the development of the Dynamic ARB HEC-RAS hydraulic model geometry. This data was collected by Forte & Tablada as a subcontractor to Dewberry and included detailed channel cross section survey, major bridge structure survey, weir survey and limited detail culvert survey.

All survey data was collected using the North American Datum of 1983 (NAD 83) horizontal datum, Epoch 2010. The projected coordinate system used for survey data is the State Plane Coordinate System, Louisiana South Zone (1702). The vertical datum is the North American Vertical Datum of 1988 (NAVD 88) utilizing Geoid 12B.

Survey collection included:

- 30 high detail surveys of major bridge structures located on the Amite River, Comite River, Amite River Diversion Canal, Bayou Chenne Blanc and the Chinquapin Canal
- High detailed survey of the Amite River Diversion Weir
- High detail survey of 51 bathymetric channel surveys
- Limited detail survey of 198 hydraulic structures including bridges and culverts located on tributaries to the Amite and Comite Rivers

Survey Methodologies

A range of survey methods were implemented using a variety of surveying equipment. Control and cross section data, where applicable, was collected using Trimble R10 GNSS/GPS receivers tied to LSU C4G NET or Leica Smart Net Real-time Network (RTN). Cross section data was collected using Trimble S-series robotic total station & Trimble TSC-3 Data Collector, and Leica Sprinter 150 Digital Level. Additionally the Sonarmite Single Beam Fathometer, R2Sonic 2024 Multibeam Echosounder, I2NS Type II (Applanix WaveMaster Inertial Navigation System (INS)), and AML BASE X2 Sound Velocity Profiler systems were utilized to collect bathymetric survey where these methods provided improved efficiency.

Cross Section Survey

Detailed channel cross sections were surveyed at strategic locations beyond the extent of the 2017 USACE bathymetric survey. These cross sections included locations along the Amite River, Comite River, Old River and Bayou Chinquapin. The channel surveys captured all significant grade changes within the channel including the top of banks, bottom of banks, low and high points of the channel and numerous intermediate points. The survey extended approximately 100 ft. beyond the top of the channel bank to enable a direct comparison with LiDAR to be performed supporting the validation of both datasets.

Data was gathered using both GPS and Conventional surveying. Control was set on each cross section by using GPS and taking 3-180 epochs (180 epochs = 1 session) on each control point and averaging the three sessions together. For quality assurance, each epoch was analyzed for outliers before averaging. Sessions that were not within a 0.165-ft. tolerance were discarded and additional sessions were collected. Once control was established, cross section data was obtained by conventional ground survey methods. If excessive water depths were encountered, bathymetric surveying methods were used instead.

When excessive water depths were encountered at cross-sections, a boat mounted Sonarmite fathometer integrated with GPS was used to gather data of the river bathymetry. The Sonarmite combined with the Trimble R-10 and TSC-3 made an “easy-to-use” system that produced a horizontal and vertical position with the GPS and a water depth with the Sonarmite. For quality control, the Sonarmite’s depth reading were field verified against a hard depth readings taken with a level rod. If the two readings matched within 10 cm., the data was considered acceptable and the process was repeated on each cross-section.

The second bathymetric surveying method was the R2Sonic Echosounder system. This system integrated the GPS method for position, R2Sonic Echosounder for acoustic ranging, with INS for navigational corrections, and AML BASE X2 for sound velocity profile adjustment to produce a point cloud of the water bottom in locations that included the Amite River Diversion Canal and weir.

Other unconventional methods were used when tree coverage engulfed the top of bank and/or dry ground and GPS method became unsuitable to set control or when excessive water depths were encountered. When tree coverage engulfed the top of bank, first a surface water elevation shot was taken at the cross-section for vertical control before two stakes were placed on the cross section in the water bottom and coordinates were established on each stake. With the digital level setup on the cross-section, a distance was taken from one of the stakes to establish a location of the level. Once a horizontal position of the instrument was gathered, a vertical position was established using the water surface as a temporary benchmark. Elevations and distances were then recorded at a +/- 25 ft. interval along the cross-section to establish horizontal and vertical positions.

Detailed Bridge Surveys

All detailed bridge structures were captured using Faro Focus 120 and Focus X330 for terrestrial laser scans. The data was registered together and tied to survey control with Faro Scene Software. It was then exported using a 1-in. spatial filter to reduce the file size. This provided full point cloud coverage of the structures including piers, abutments and decks from which hydraulic engineers were able to extract critical information for development of the Dynamic ARB HEC-RAS hydraulic model bridge geometry. **Figures 6** and **Figure 7** illustrate example point clouds from bridge scans.

Terrestrial bridge scanning provided notable efficiencies when compared to traditional survey of large bridges with the added benefit of a more comprehensive capture of bridge features. This virtually eliminated the issue of survey omissions of critical hydraulic features that traditionally require surveyors to remobilize at the request of hydraulic engineers who require further data to accurately code bridge geometry. This empowered the hydraulic engineers to extract the data they needed such as low chord elevations, pier shapes and skew angles rather than rely on the limited points traditionally collected by surveyors. This was particularly valuable for unusual structures.

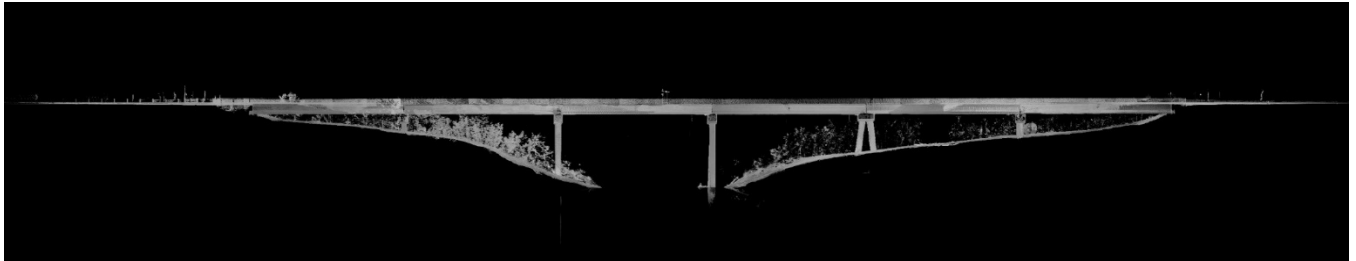


Figure 6: Example bridge scan point cloud

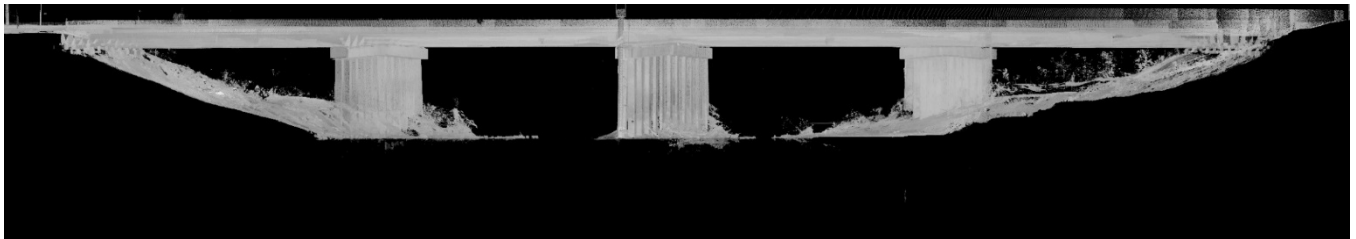


Figure 7: Example bridge scan point cloud illustrating the bridge skew and pier locations

Limited Detail Survey

For study reaches scoped as medium detail, limited detail survey of bridges and culverts was collected. For bridges, sketches were developed and annotated with field measurements to include number and size of bents and piles, skew angle, bridge length and width, low chord, length between bents, height of bridge deck and guardrail, and bridge material. For culverts, sketches were developed and annotated with field measurements to include opening shape, width and height, skew angle, amount of sediment, materials and height between road surface and invert of opening. All bridge and culvert sketches were supplemented with photographs of the structures and adjacent channels.

HIGH WATER MARK (HWM) AND OBSERVED DATA COLLECTION

This task consolidated various sources of High Water Mark (HWM) data into GIS formats, assessed quality, and determined potential application for calibration and verification of the ARBNM. HWMs provide crucial information for historical documentation of floods and can be used for a number of applications including:

- Estimation of flood frequency
- Assessment of the accuracy of FIRMs
- Preparation of inundation maps
- Input to building performance assessments
- Calibration of models that simulate the flood
- Prioritization of mitigation projects and preparation of benefit-cost analyses
- Determination of depth of flooding of structures

In addition to HWM data available from USGS and other streamflow gages, HWMs can be identified after floods through various indicators. Examples of these indicators include mudlines and stains on buildings and other objects (**Figures 8-9**), debris lines on fences (**Figure 10**), and mudlines on the ground and vegetation (**Figure 11**). The quality of surveyed HWMs can vary greatly due to a number of factors including the perishable nature of HWMs as a result of the time lapse and weather conditions before HWMs can be flagged, the quality of the HWM and human judgement. Typically, larger rivers with longer duration floods leave higher quality, more easily identifiable HWMs. This is due to the longer duration of the high water and the higher turbidity of the water, both which result in more easily recognizable marks. Additionally, multiple peaks may result in multiple HWMs, as can be seen in **Figure 9**. Often the secondary peaks can leave a more visible water mark than the true HWM which due to a reduced duration may leave less evidence and mislead the HWM flagger or surveyor.



Figure 8: Example mudline on exterior of building.

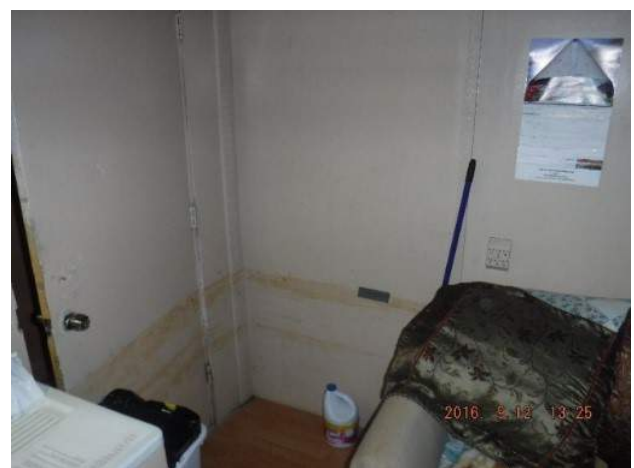


Figure 9: Example mudline within a residential building.

August 2016 Flood HWM Data

As previously noted, various sources of HWM survey data were received through the efforts of the Amite River Basin Drainage & Water Conservation District (ARBC) and their partners following the August 2016 flood. 449 HWMs were provided to LA DOTD from the ARBC for this study.

In addition to HWM survey for the August 2016 flood, multiple USGS and Coastwide Reference Monitoring System (CRMS) gages were available that provided observed stage information for the August 2016 flood and various additional events. This data included stage-time series as well as flow-time series.

Review of ARBC HWM Data

The HWM data was carefully reviewed to assess the quality. This included comparing HWMs with surrounding HWMs to identify outliers through the process of triple validation. Triple validation is a widely utilized method of quality control whereby three or more HWMs located within the same general vicinity are compared to ensure that they yield similar elevations. When two or more HWMs yield similar elevations, users can have a higher level of confidence that the data is accurate by eliminating the outlier HWM.



Figure 10: Example debris line on fence.

Source: SJB Group, LLC



Figure 11: Example mudline on vegetation.

Source: T. Baker Smith

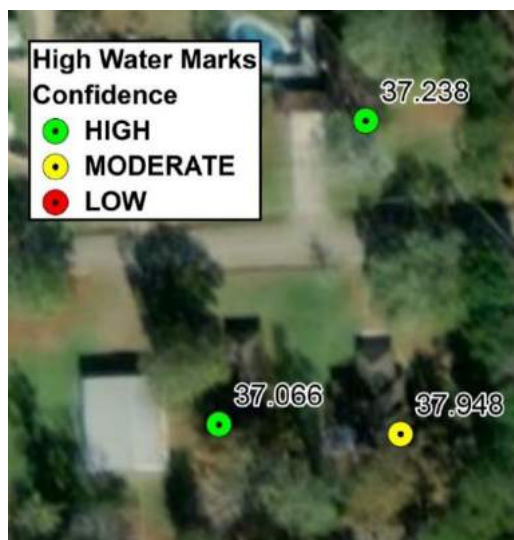


Figure 12: Triple validation of HWMs

Figure 12 illustrates the triple validation process whereby two HWMs (37.238 and 37.066) agree relatively closely and are classified as high confidence, while a third elevation (37.948) appears slightly higher than expected and is therefore classified as only moderate confidence. Additionally, HWMs were reviewed for expected trends in water surface elevation. This was generally based on the assumption that water surface elevations will decrease in the downstream direction of flow and that in wide, flat floodplain areas such as the lower Amite River below Denham Springs, water surface elevations will exhibit only minimal changes.

Table 4 provides a summary of the methodology used to assess and classify the quality of HWM and the count of HWMs per classification.

Table 4: Summary of HWM Quality Assessment and Count		
Confidence Assessment	Description of Confidence Assessment*	Number of HWMs
High	HWM elevations that generally agree within approximately 0.5 ft. of one or more HWMs in the general vicinity expected to demonstrate minimal changes in water surface elevation.	373
Moderate	HWM elevations that generally agree within approximate 0.5 - 1 ft. with one or more HWMs in the general vicinity expected to demonstrate minimal changes in water surface elevation. Or HWM elevations that do not follow an expected trend such as water surface elevations decreasing in the downstream direction, or irregular outlier changes in water surface elevations in flat, wide floodplain areas.	50
Low	HWM elevations that are an outlier by approximately 1 ft. or greater when compared against 2 or more adjacent HWMs in the general vicinity expected to demonstrate minimal changes in water surface elevation. Or HWM elevations that differ greatly from an expected trend such as water surface elevations decreasing in the downstream direction, or large, irregular outlier changes in water surface elevations in flat, wide floodplain areas.	26
Total:		449

*Engineering judgement is used when applying tolerances for HWM quality classification with these ranges generally being increased when HWMs are spaced further apart.

Figure 13 provides an example of the HWM locations within a portion of the ARB. Of the ARBC's 449 HWM's reviewed and classified:

- 373 were classified as having a high confidence (83%);
- 50 were classified as having a moderate confidence (11%);
- And 26 were classified as having low confidence (6%).

The HWMs were included as observed data within the 1D portions of the ARB HEC-RAS model in addition to being spatially referenced and labeled within RAS Mapper.

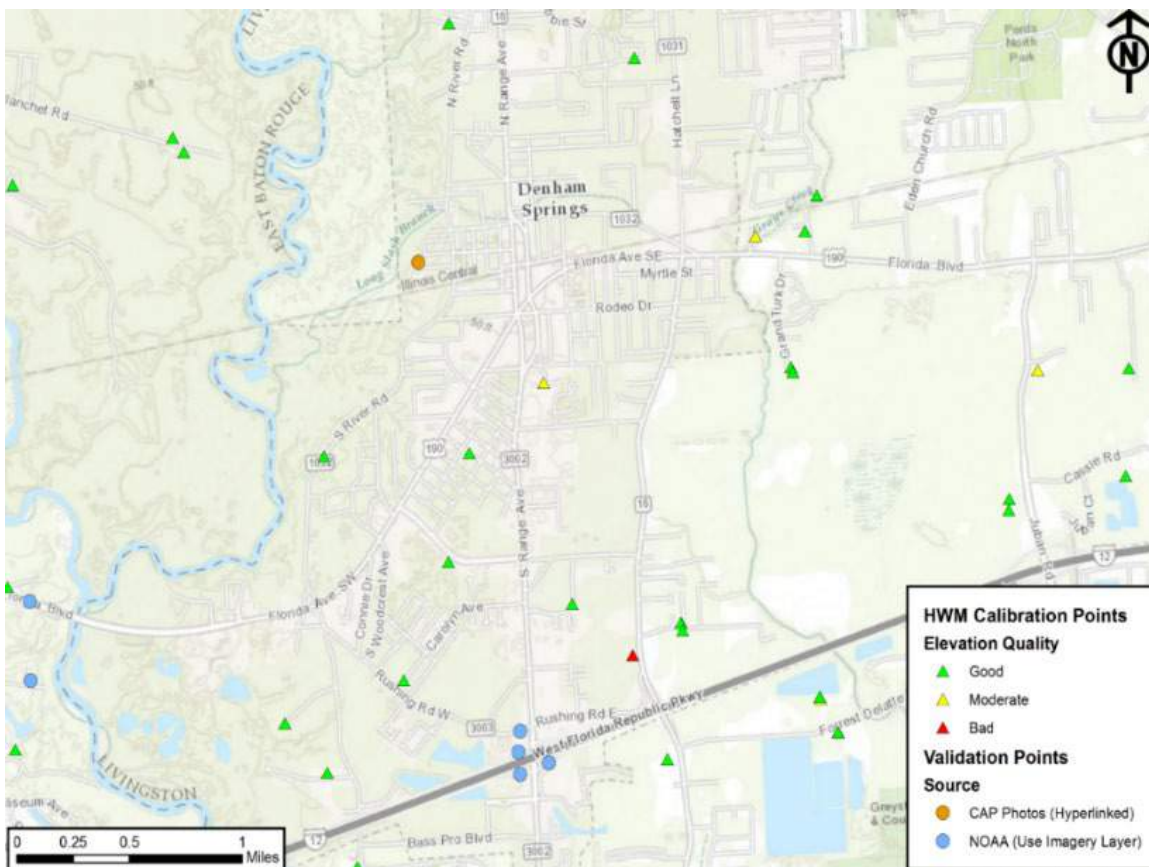


Figure 13: HWM location examples

Other Sources of HWMs for the August 2016 Flood

Time series data including stage and flow from USGS and CRMS gages were obtained from online sources and converted from stage to the NAVD 88 vertical datum. This data was saved within the ARBNM HEC-DSS database enabling the time series data for both stage and flow to be directly read into HEC-HMS and HEC-RAS as observed data that can be dynamically viewed using some of the visualization tools within HEC-HMS and HEC-RAS. **Figure 14** demonstrates the display of modeled and observed data for USGS gage 073770500 Amite River near Darlington, LA, for an initial calibration run using the HEC-RAS Plot Stage and Flow Hydrographs function enabling a quick comparison of results to inform the calibration actions of the HEC-RAS model. It should be noted that the simulated flows reported by HEC-RAS Plot Stage and Flow Hydrographs only represent the flows within the 1D cross section. Therefore in areas where coupled 1D/2D approaches are used, this function will underestimate the peak flow and volume of the hydrograph since it does not account for coupled 2D flows.

The observed peak stage for the August 2016 Flood were also extracted from all available USGS and CRMS gages and consolidated with the ARBC HWMs.

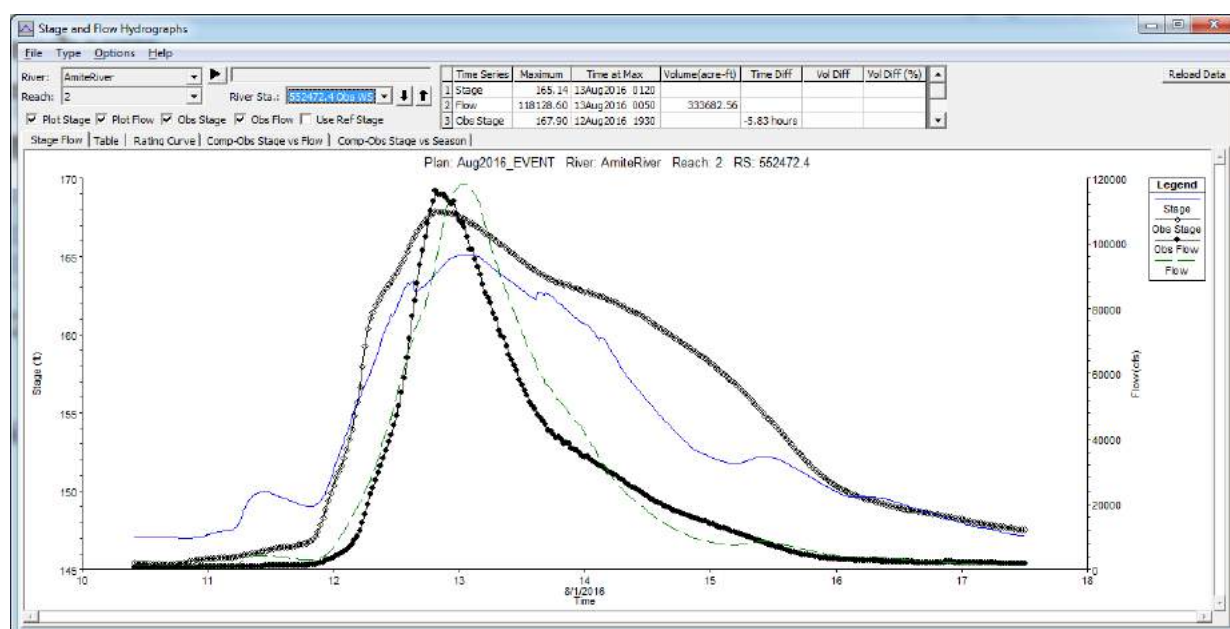


Figure 14: Example visualization of observed and modeled data using the HEC-RAS Plot Stage and Flow Hydrographs function.

March 2016 Flood HWM Data

Similarly to the August 2016 flood, multiple USGS and Coastwide Reference Monitoring System (CRMS) gages were available that provided observed stage information for the March 2016 flood that were saved to the HEC-DSS database. Additionally the USGS Flood Event Viewer (<https://stn.wim.usgs.gov/FEV/#LouisianaMarch2016>) provided an additional seven HWMs which were combined with the observed peak elevations from the USGS and CRMS gages. The HWMs were included as observed data within the 1D portions of the ARB HEC-RAS model in addition to being spatially referenced and labeled within RAS Mapper.

October 2017 Flood HWM Data

No sources of HWM data were available for the October 2017 minor flood event with exception to those available from USGS and CRMS gages. Time series from these sources were saved to the HEC-DSS database in addition to peak elevations.

August 2017 Flood HWM Data

No sources of HWM data were available for the August 2017 minor flood event with exception to those available from USGS and CRMS gages. Time series from these sources were saved to the HEC-DSS database in addition to peak elevations.

HYDROLOGIC MODEL

Version 1.0, February 2019 of the ARB hydrologic model was developed in HEC-HMS Version 4.2.1 and represented all study reaches within the study including those modeled in low, medium and high detail.

As further illustrated in **Figure 15**, the geometry of the ARB HEC-HMS model is comprised of more than 2,000 hydrologic elements including:

- More than 700 subbasins representing 1,960 square mi. of watershed;
- More than 550 hydrologic routing reaches; and
- More than 700 hydrologic junctions

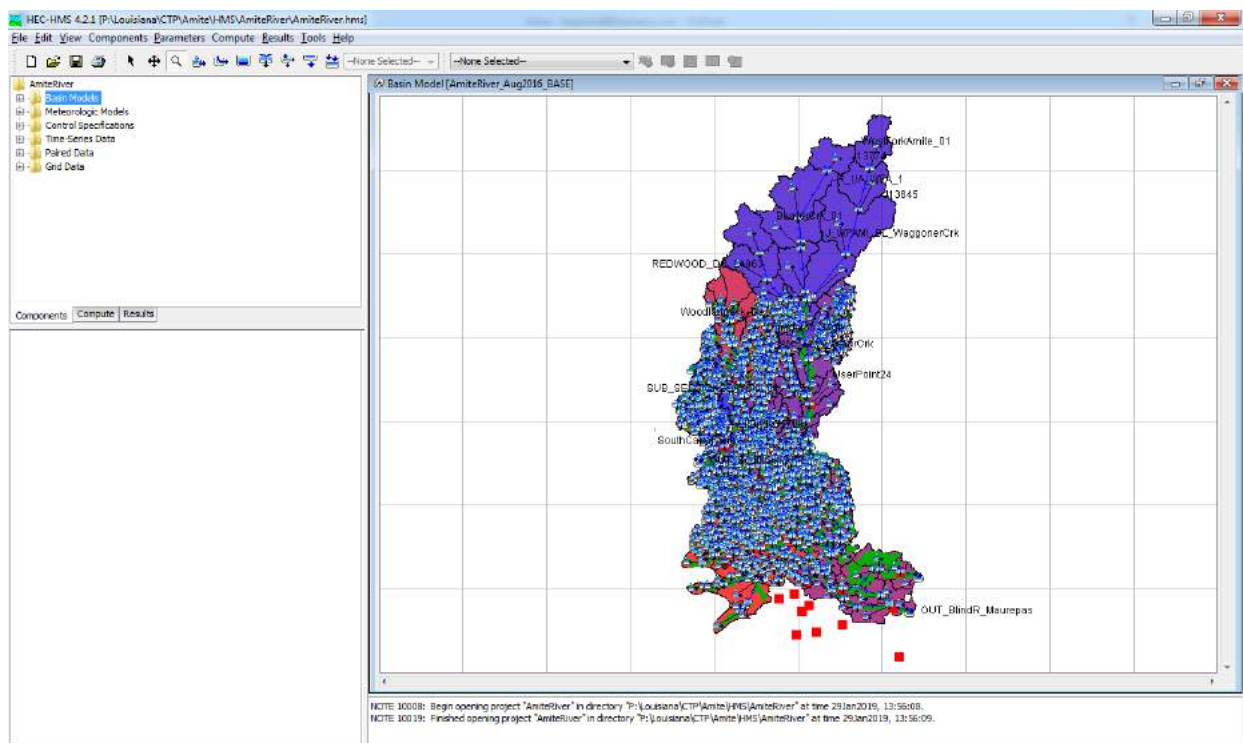


Figure 15: ARB HEC-HMS Hydrologic Model Overview

Model Geometry, Input, and Parameters

The ARB HEC-HMS model uses a variety of data sources for development of model geometry and input data. This includes terrain data, land use data, soils data, precipitation and hydraulic data.

Subbasins

Hydrologic subbasins within HEC-HMS were delineated using the 2004 LSU LiDAR dataset. It should be noted that at the initial time of hydrologic model development, this was the best available dataset since the 2018 LA DOTD LiDAR was not available. However, since the data is only used to delineate watershed boundaries, differences between this dataset and 2018 datasets will be negligible in hydrologic terms. This data was converted to a 20 ft. cell DEM.

The DEM was processed within GIS to determine flow accumulation patterns throughout the basin. This was done through careful hydro enforcement to ensure that embankments do not create artificial barriers within the hydrologic model and that natural sinks are able to drain appropriately. Where available, local storm water inventory was utilized to identify flow paths and storm water infrastructure that was critical to determining drainage paths. Subbasins were delineated at critical hydrologic locations to adequately capture the volume and magnitude of runoff. Subbasin parameters including Transform and Losses are summarized in **Appendix 1**.

Subbasin Transform

Subbasin transform utilized the ModClark methodology which accounts explicitly for variations in travel time to the watershed outlet from all regions of the watershed. As such, the ModClark method can be categorized as a quasi-distributed method rather than a lumped method like the more traditional Clark Unit Hydrograph method. This methodology was required due to the gridded NEXRAD radar rainfall which was used. The ModClark Method eliminates the time-area curve and time of concentration to develop a translation hydrograph and instead uses a separate travel time index for each grid cell which is then scaled by the overall time of concentration. Note that a time-area curve defines the cumulative area of the watershed contributing runoff to the subcatchment outlet as a function of time (expressed as a proportion of T_c).

To use the ModClark model, a gridded representation of the basin is defined. For the ARB HEC-HMS model, the standard hydrologic grid (SHG) was used. The SHG is a variable-resolution-cell map grid defined for the conterminous United States and the coordinate system is based on the Albers equal-area conic map projection. A 1,000 meter grid resolution was selected for the study area as that was determined suitable for the general purpose hydrologic modeling with the Stage IV radar precipitation that was calibrated during hydrometeorology. In **Figure 16**, an image of the grid cell file is shown for the project which contains the subbasin name, the lower X and Y coordinates, hydrologic travel length of the grid cell, and area of the subbasin within the grid cell.

```

1 Parameter Order: Xcoord Ycoord TravelLength Area
2 End:
3
4 Subbasin: ByuBraud_US_LOC
5 GridCell: 466 801 10.977755905511811 0.19884194224694704
6 GridCell: 467 801 10.603777463804926 0.012887570630035271
7 GridCell: 465 802 11.088266367157734 0.10552841362294477
8 GridCell: 466 802 10.360635874396749 0.98497227077932914
9 GridCell: 467 802 10.011452247904495 0.71121454095832415
10 GridCell: 468 802 11.045309721869444 0.069071467990177132
11 GridCell: 465 803 9.4744411988823973 0.064775033820444167
12 GridCell: 466 803 8.6377956724663427 0.97119006379483552
13 GridCell: 467 803 8.2298956613538223 1.0000030738474075

```

Figure 16: HEC-HMS basin Grid Cell File

Parameters required for the ModClark method include the time of concentration (T_c) and a storage coefficient (R). The time of concentration defines maximum travel time in the subbasin from the point farthest away from the outlet and the storage coefficient represents the linear reservoir of each grid cell which represents an index of temporary storage of precipitation excess in the watershed as it drains to the outlet point. These parameters were calculated using the Fort Bend, Texas Stormwater Design Manual. This methodology was selected because the hydrological characteristics of the equations are very similar in the ARB.

The Fort Bend, Texas Stormwater Design Manual defines parameters through drainage area physiographic characteristics which include the length, slope and roughness of the basins longest flow path (T_c), average basin slope, and the effective impervious area. The effective impervious area is further defined by the percent of the subbasin that is developed and the average percent of impervious cover of the developed area. The parameters related to effective impervious area were developed from the 2011 National Land Cover Dataset (NLCD) Landcover and Impervious datasets while the other parameters were developed from the LiDAR topography. Due to the inherent nature of hydrologic routing, the presence of significant ponding in a subbasin can have a pronounced effect on the nature of the runoff hydrograph. Storage in ponding area tends to flatten and delay the hydrograph.

The storage coefficient is then further refined by ponded storage within a subbasin. The value for ponded storage was taken from the National Hydrology Dataset Plus (NHD+). Subbasin transforms were validated through the review of the HEC-RAS results and were demonstrated to provide only minor sensitivity to the flows within the ARBNM, however this sensitivity is likely to become more pronounced if the study ARBNM is used for assessment of very small drainage features.

Loss Methods

The Green and Ampt loss method is used for all subbasins. The Green and Ampt method uses five parameters to determine precipitation infiltration losses:

- **Initial Water Content:** Represents the initial saturation of the soil at the start of the simulation and is given in terms of volume ratio.
- **Saturated Water Content:** Represents the maximum water holding capacity in terms of volume ratio and is often assumed to be the total porosity of the soil.
- **Wetted Suction Front:** This is generally assumed to be a function of the soil texture.
- **Hydraulic Conductivity:** Represents the constant percolation rate of saturated soil.
- **Percentage Impervious:** This specifies the percentage of area for which no losses will be calculated.

Initial water content was estimated through the review of initial losses for historical streamflow and precipitation data whereby cumulative precipitation totals were compared to streamflow at available gages. The initial abstraction was assumed to have been met when the streamflow was observed to begin positively responding to rainfall. This parameter is further discussed in the section Calibration.

The saturated water content, wetted suction front and hydraulic conductivity for each subbasin was estimated using GIS by correlating the Natural Resources Conservation Service (NRCS) Soil Survey Database (SSURGO) which provides classified soil polygons, to the recommend values in Table 12 of the March 2000, *HEC-HMS Technical Reference Manual*. By attributing each individual soil class within SSURGO to this table, subbasin averages were determined.

The percentage impervious for each subbasin for existing landuse conditions was estimated using the 2011 NLCD published by the Multi-Resolution Land Cover Characteristics (MRLC) Consortium. The NLCD is updated every five years. As of February 2019, the 2016 NLCD dataset has not yet been finalized and therefore was not available for use at time of model development. This data was used to determine subbasin total impervious percentage.

Routing

Hydrologic routing sections were developed to connect subbasins within the ARB HEC-HMS model using the Modified Puls routing methods with parameters being derived from a variety HEC-RAS hydraulics model simulations. All hydrologic routing within the high and medium detail reaches of the ARBNM are performed using the dynamic HEC-RAS model within both 1D and 2D domains. Within the Dynamic ARB HEC-RAS model, inflows are generally received directly from the HEC-HMS subbasins outflows via the HEC-DSS database. This allows for more advanced dynamic routing to be performed using the full Saint Venant equation as used for both the 1D and 2D HEC-RAS unsteady-flow computation engines.

For the East and West Fork's of the Amite River in Mississippi, a simplified HEC-RAS model was developed utilizing a range of arbitrary flows to determine the stage-storage relationships needed for Modified Puls Routing to enable flows to be routed to the confluence of the two forks. For small tributaries modeled in low detail that flow into the Amite and Comite

Rivers, the low detail HEC-RAS models were used to extract routing parameters for use within the HEC-HMS model.

Meteorological Models

Meteorological models within the ARB HEC-HMS model utilize both gridded and point precipitation datasets stored within the HEC-DSS database for a selection of historical precipitation events and generalized designs storms intended to facilitate the simulation of a range of Annual Exceedance Probability floods.

Meteorological models include:

- Four Historic Precipitation Events (gridded precipitation)
 - August 2017 flood event
 - October 2017 flood event
 - March 2016 flood event
 - August 2016 flood event
- 30 Design Precipitation Events (One design storm with 10 precipitation depths and three centers)
 - 8 in.
 - 10 in.
 - 12 in.
 - 14 in.
 - 16 in.
 - 18 in.
 - 20 in.
 - 22 in.
 - 24 in.
 - 26 in.

The selection and development of the historical precipitation events is further discussed in the Calibration section and the development and application of design precipitation events is further discussed in Design Flood Simulations section.

HYDRAULIC MODEL

As previously discussed, three HEC-RAS hydraulic models were developed. This includes the Dynamic ARB HEC-RAS Hydraulic Model which will be the primary model for the ARB as well as two Steady State ARB HEC-RAS hydraulic models which covers smaller tributaries to the Amite River and Comite River that were studied using 1D methods.

Dynamic HEC-RAS Hydraulic Model

Version 1.0, February 2019 of the Dynamic ARB HEC-RAS hydraulic model was developed in HEC-RAS Version 5.0.6. As further illustrated in **Figure 17**, the geometry of the ARBNM comprises of:

- More than 800 1D cross sections within seven reach segments;
- 30 major 1D bridges (many with multiple openings);
- More than 400 1D lateral structures primarily connecting 1D reaches to 2D flow areas and 2D flow areas to other 2D flow areas;
- 21 2D flow areas;
 - More than 265,000 2D cells with over 3,200 enforced breaklines;
- Nearly 500 Storage Area/1D connections representing bridges and culverts in 2D flow areas; and
- More than 400 boundary condition

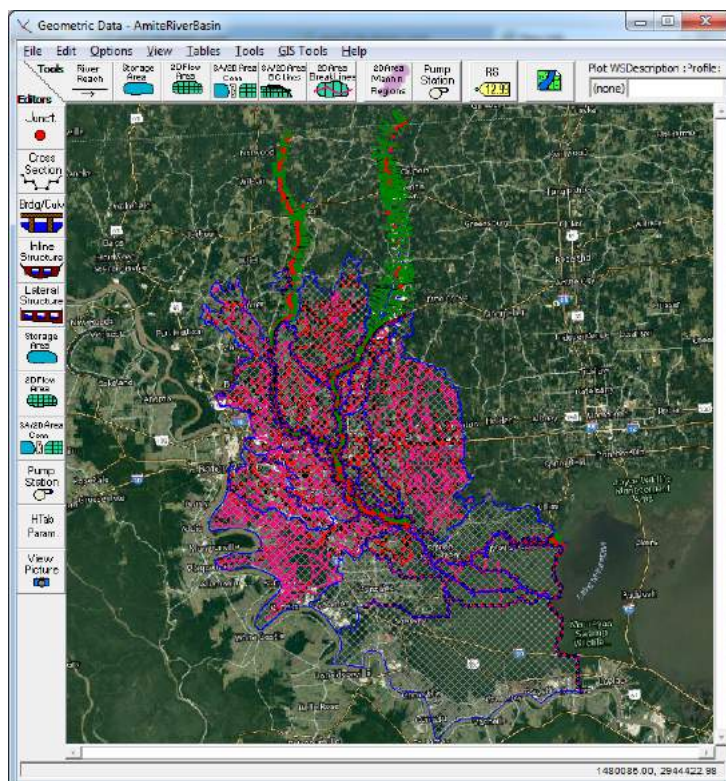


Figure 17: ARBNM HEC-RAS Hydraulic Model Geometry Overview

Computation Methods

For 1D model reaches, the ARBNM uses the Finite Difference 1D Numerical Solution (Classic HEC-RAS methodology) with the default Skyline/Gaussian matrix solver. Due to the relatively flat terrain and low velocities found throughout the ARB, 1D simulations were run without the 1D Mixed Flow Option selected since super critical flow was not expected to occur anywhere within the study area.

For 2D flow areas, the ARBNM uses the Finite Volume, Full Momentum (Saint Venant) solution. HEC-RAS also provides a simplified solution based on the Diffusion Wave equations which may be suitable for some applications although this simplified approach has not been utilized in the ARBNM. The ARBNM was optimized to run using a fixed 30-sec time step with resulting water surface calculation tolerances generally being targeted to be less than 0.1 ft. for detailed 1D reaches and less than 0.2 ft. for 2D areas. Due to the medium detail approach applied in many 2D flows areas, these tolerances may be exceeded in isolated areas.

Future releases of HEC-RAS are anticipated to include a Finite Volume 1D numerical solution which is expected to provide improved stability and efficiency between the 1D and 2D solutions since 1D and 2D simulations will be solved simultaneously within a single engine rather than separately. This approach is anticipated to reduce compute times and significantly improve 1D numerical stability. It is strongly recommended to perform thorough testing and validation prior to utilizing this option if included in future releases.

Model Geometry

The ARBNM uses a variety of data sources for development of model geometry within HEC-RAS including ground survey, bathymetric survey, field measurements, estimations from aerial imagery and LiDAR data. Geometric features within HEC-RAS using these data sources include 1D cross sections, bridges, weirs, culverts and lateral structures in addition to the 2D mesh.

2D Flow Area Mesh

The ARBNM consists of 21 2D Flow Areas which define the extent of an individual computational mesh. Each 2D Flow Area contains a generally regular mesh with varying resolutions of cells. Two primary terrain data sources were utilized for the underlying terrain used to generate the 2D mesh properties as highlighted in **Table 5**. Mesh cells were generally created using regular squares of varying resolutions ranging from as coarse as 1,000 ft. squares in very flat areas of minimal development, to 100 ft. squares in areas of higher flood risk and more complex terrain. Since HEC-RAS uses a finite volume approach, whereby each cell face is represented as an irregular cross section extracted from the underlying terrain, cell resolution can be considered comparable to the concept cross section spacing. Therefore larger cell sizes can be used than typically used with traditional finite difference and finite element approaches to 2D hydraulic modeling which normally use cell averaged elevations for cell faces.

To further refine 2D meshes in areas critical for the accurate simulation of overland flows, breaklines have been used to enforce key features of the terrain and ensure that the model reasonably simulates the movement of overland flow. This includes breaklines along notable channels which concentrate flows and ridge lines that allow flows to spill from one area to another across features such as road embankments, levees and natural ridgelines. Breakline enforcement along ridges also helps to minimize computational ‘*cell leakages*’, whereby 2D cells straddling a ridge line rather than following it can artificially allow water to flow upstream to

downstream as if the embankment was not there. **Figure 18** illustrates an area of the Bayou Manchac 2D Flow Area which contains multiple cell resolutions and breaklines. More than 3,200 breaklines were enforced into the 2D Flow Areas of the ARBNM. While the model was primarily developed for the Amite River HUC 8 watershed, spills between adjacent HUC8s necessitated 2D Flow Areas beyond the study area.

This included the following 2D Flow Areas:

- **HNTB Placeholder:** This area was included as an approximate study area to refine the external boundary conditions of the BayouManchac and AmiteR_Div_SW 2D Flow Areas which include the Marvin Braud and Laurel Ridge levee systems. This 2D Flow Area extent utilized the polygon feature from models developed by HNTB on behalf of Ascension Parish with the goal of streamlining the future integration of models. Since it is modeled only in approximate detail without any internal hydrologic inflows, the results of this area are not intended to be utilized at this time.
- **BlindRiver:** This 2D Flow Area was included as an approximate area to refine the boundary conditions of the AmiteR_Div_SW 2D flow area. Since it is modeled only in approximate detail without any internal hydrologic inflows, the results of this area are not intended to be utilized at this time.

Table 5: Summary of Terrain Data Used for 2D Flow Areas

2D Flow Area	Terrain Source
AmiteComite	2018 LA DOTD LiDAR
AmiteEast	2018 LA DOTD LiDAR
AmiteR_Div_NE	2018 LA DOTD LiDAR supplemented with 2017 CPRA LiDAR
AmiteR_Div_SW	2018 LA DOTD LiDAR supplemented with 2017 CPRA LiDAR
AmiteR_Grays	2018 LA DOTD LiDAR
AmiteWest	2018 LA DOTD LiDAR
Amite_AmiteEast	2018 LA DOTD LiDAR
BayouManchac	2018 LA DOTD LiDAR
BlindRiver	2017 CPRA LiDAR supplemented with 2004 LSU LiDAR
ClaycutJones	2018 LA DOTD LiDAR
ColyellCreek	2018 LA DOTD LiDAR supplemented with 2004 LSU LiDAR
ComiteEast	2018 LA DOTD LiDAR
ComiteR_NP	2018 LA DOTD LiDAR
ComiteR_US	2018 LA DOTD LiDAR
ComiteWest	2018 LA DOTD LiDAR supplemented with 2004 LSU LiDAR
FrenchSettlement	2018 LA DOTD LiDAR
GraysCrk	2018 LA DOTD LiDAR
HNTB_Placeholder	2018 LA DOTD LiDAR supplemented with 2017 CPRA LiDAR
Maurepas	2018 LA DOTD LiDAR supplemented with 2017 CPRA LiDAR
RedwoodCreek	2018 LA DOTD LiDAR
Unt_ComiteR	2018 LA DOTD LiDAR
WardsCreek	2018 LA DOTD LiDAR

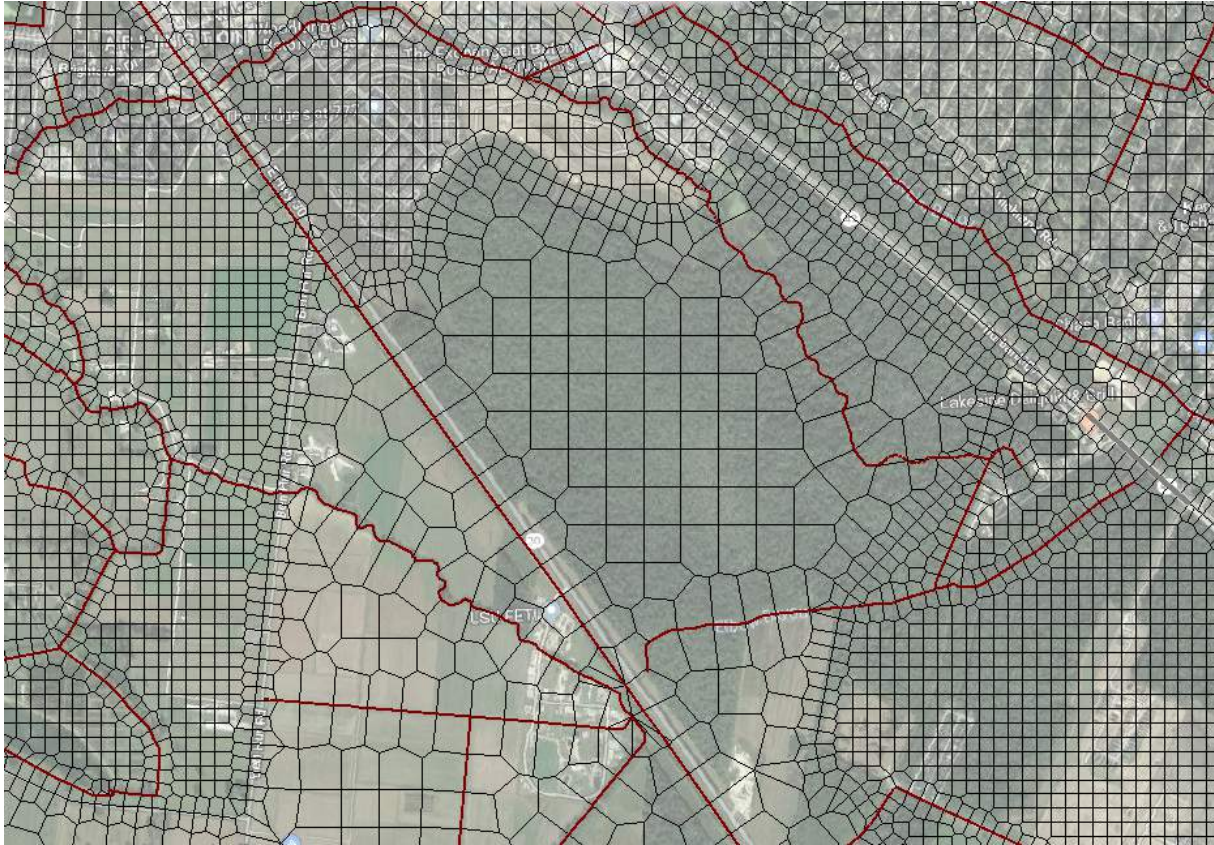


Figure 18: Example of 2D Mesh with varying cell resolution and breaklines used to enforce streamlines and ridgelines within the upper reaches of the Bayou Manchac 2D Flow Area.

2D Flow Area Hydraulic Structures

All hydraulic structures within 2D areas have been modeled in medium detail. HEC-RAS utilizes Storage Area/2D Connections (SA/2D Connections) to model hydraulic structures both between and within 2D Flow Areas. HEC-RAS Version 5.0.6 supports the use of weirs, gates and culverts, but bridges are currently not supported.

Geometric data for all hydraulic structures within 2D flow areas were coded using a variety of data sources. For all embankments, elevation data within the SA/2D Connections were extracted from the 2018 LA DOTD LiDAR. For all structures modeled within 2D areas, inverts were assumed from the 2D mesh head water and tail water elevations. Since the 2D mesh does not include channel survey, many structure inverts were artificially raised to ensure that they are higher than the adjoining 2D cell headwater and tailwater since HEC-RAS does not allow structure inverts or road deck inverts to be below the adjoining 2D minimum cell elevations.

Dimensions for hydraulics structures were obtained for a variety of sources including:

- Bridge openings approximated from LiDAR data and modeled as a slot in the SA/2D Connection
- 2017/2018 limited detail ground survey by LA DOTD which included basic information pertaining to structure shapes, materials and opening dimensions.

- 2018 ground survey provided by CSRS on behalf of the City of Central – Note that while this survey included inverts, as noted previously, these were often artificially raised within the model to ensure that they were higher than the adjacent 2D cell minimum elevations per HEC-RAS limitations.
- Dimensions taken from historical hydraulic models gathered during data collection
- Dimension approximations using various sources of aerial imagery and terrain data

Since HEC-RAS 5.0.6 does not support bridges within 2D Flow Areas, bridges were simulated using one of two methods. Firstly, bridges were modeled by assuming multiple culverts, approximately representing bridge spans between piers as demonstrated in **Figure 19**. Secondly, bridges without survey data and those that created excessive numerical instability within the 2D Flow Area were modeled as slotted embankment openings. Where LiDAR data approximated the embankment with the bridge deck removed, this was used directly to simulate the bridge opening within the Weir/Embankment as demonstrated in **Figure 20**. Where LiDAR data did not represent the bridge opening, the bridge opening in the Weir/Embankment was estimated from aerial imagery and terrain.

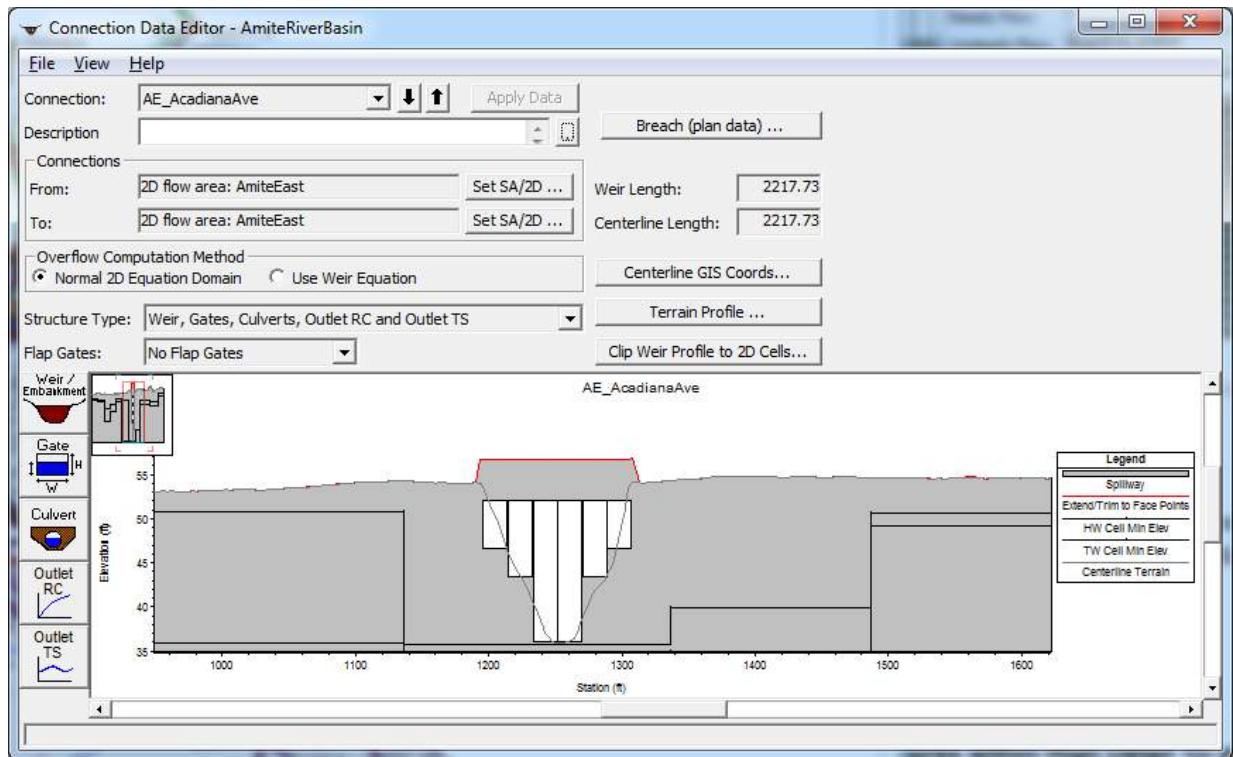


Figure 19: Example of a bridge approximated as multiple culverts within SA/2D connections

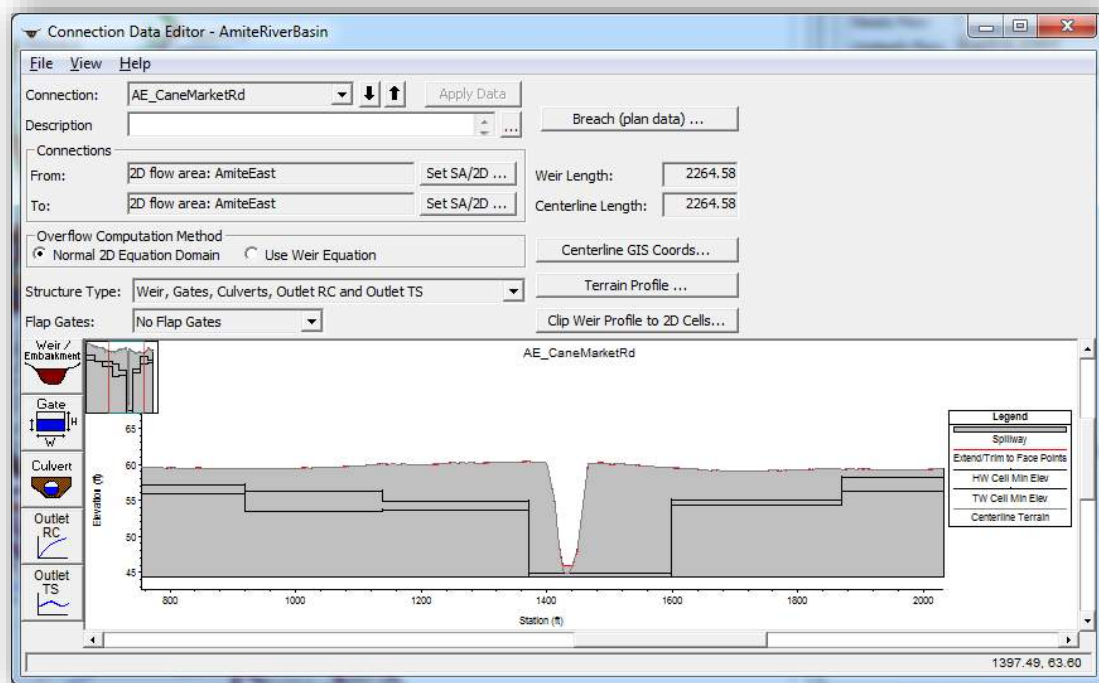


Figure 20: Example of a bridge approximated using LiDAR data to simulate the opening for the Weir/Embankment within SA/2D Connections.

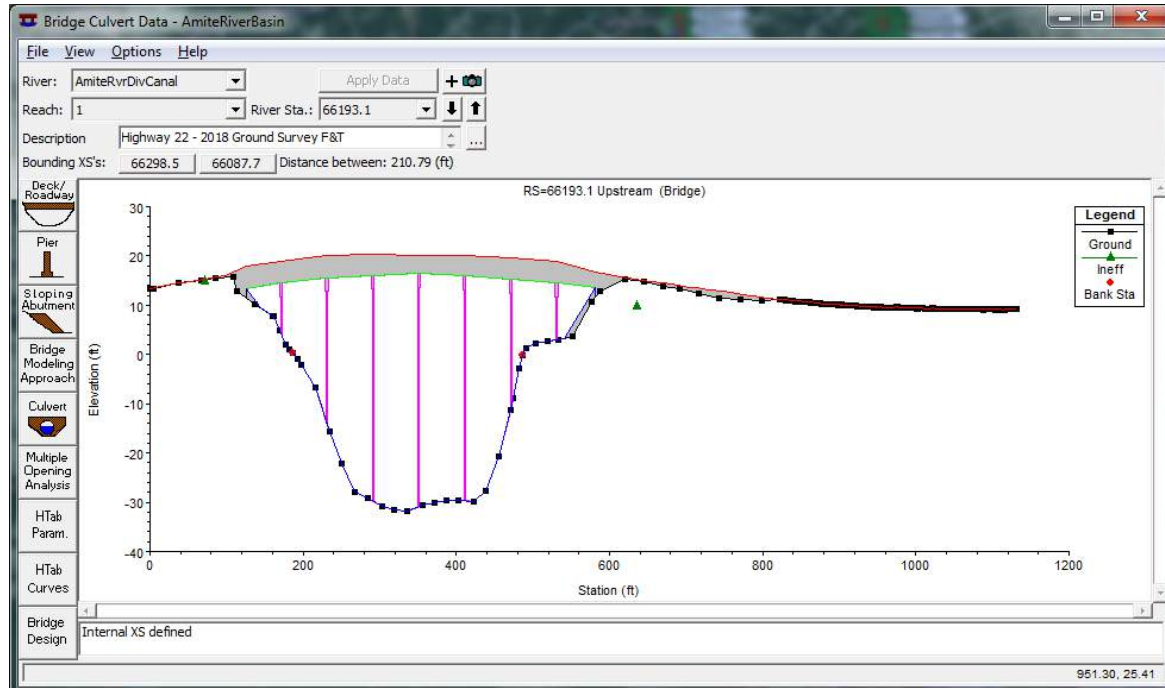


Figure 21: Example of bridge coding from ground survey at Highway 22 at the Amite River Diversion Canal.

High Detail Study Area 1D Hydraulic Structures, including 1D structures within High Detail 1D and 2D Areas

Hydraulic structures located within the high detail study reaches of the Amite River, Comite River, Amite River Diversion Canal, Bayou Chenne Blanc, and the Chinquapin Canal were coded into the Dynamic ARB HEC-RAS geometry using combinations of traditional ground run survey methods and newer terrestrial laser scanning techniques collected through the 2017/2018 LA DOTD survey collection performed by Forte & Tablada. Hydraulic structures included the Amite River Diversion Weir in addition to 30 major bridges and their relief openings in road and railroad embankments. As seen above, **Figure 21** illustrates the Highway 22 Bridge coding on the Amite River Diversion Canal using the 2017/2018 LA DOTD survey.

Multiple Bridge Analysis

Where a road or rail embankment contains multiple bridges or culvert openings, the HEC-RAS Multiple Opening Analysis option has been used to define openings and conveyance areas as illustrated in **Figure 22**. This function allows the user to define multiple bridge openings and areas of conveyance while automatically determining stagnation points between openings to more accurately estimate flow and elevations through the multiple openings. Further information regarding this technique can be found in the HEC-RAS User Manual and Hydraulic Reference Manual.

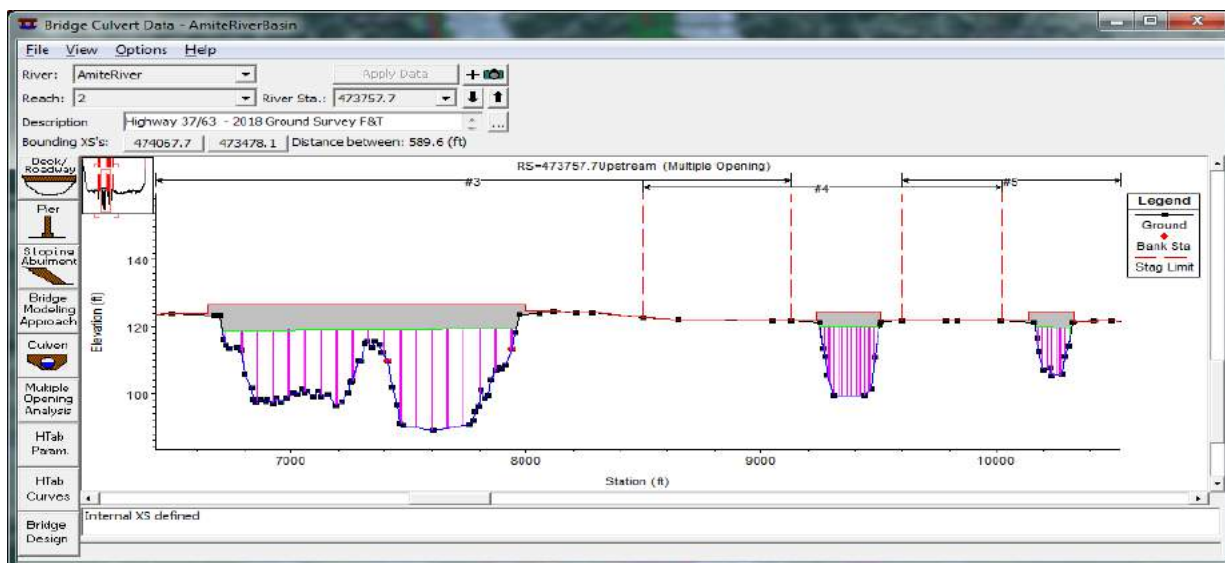


Figure 22: Example of multiple opening bridge at highway 37/63 on the Amite River

High Detail Cross Sections

Cross sections for all 1D study reaches including 1D channels within high detail 2D study areas were coded using combinations of ground based survey, LiDAR and bathymetric survey. High detail cross sections were located along the main channels of the Amite River, Comite River, Amite River Diversion Canal, Blind River (downstream of the Amite River Diversion Canal), Bayou Chenne Blanc, Old River and the Chinquapin Canal. **Table 6** provides a summary of the geometric data source used for the HEC-RAS cross sections.

Table 6: Summary of Geometric Data Used for High Detail Cross Sections

HEC-RAS Study Reach (River Code, Reach Code)	Return Interval	
	Cross Section Range	Geometric Data Source
Amite River upstream of the Comite confluence (AmiteRiver, Abv_ComiteR)	455732.8 – 624771.4	Channel: 2018 LA DOTD LiDAR Overbanks: 2018 LA DOTD LiDAR
	329636.3 – 452434.7	Channel: 2017/2018 LA DOTD Survey (with bathymetric interpolations made between surveyed cross sections) Overbanks: 2018 LA DOTD LiDAR
	296046.6 -327917.9	Channel below waterline: 2017 USACE Bathymetric Survey Channel above waterline: 2018 LA DOTD LiDAR Overbanks: 2018 LA DOTD LiDAR
Amite River downstream of the Comite confluence (AmiteRiver, Blw_ComiteR)	All Cross Sections	Channel below waterline: 2017 USACE Bathymetric Survey Channel above waterline: 2018 LA DOTD LiDAR Overbanks: 2018 LA DOTD LiDAR
Comite River upstream of the Pretty Creek confluence (ComiteRiver, Abv_PrettyC)	All Cross Sections	Channel: 2018 LA DOTD LiDAR Overbanks: 2018 LA DOTD LiDAR
Comite River downstream of the Pretty Creek confluence (ComiteRiver, Blw_PrettyC)	153840.6 - 230474.3	Channel: 2018 LA DOTD LiDAR Overbanks: 2018 LA DOTD LiDAR
	87620.9 - 152667.2	Channel: 2017/2018 LA DOTD Survey (with bathymetric interpolations between surveyed cross sections) Overbanks: 2018 LA DOTD LiDAR
	1188.23 - 87367.09	Channel below waterline: 2017 USACE Bathymetric Survey Channel above waterline: 2018 LA DOTD LiDAR Overbanks: 2018 LA DOTD LiDAR
Amite River Upstream of the Blind River (AmiteRvrDivCanal, Abv_BlindR and BlindRiver)	All Cross Sections	Channel below waterline: 2017 USACE Bathymetric Survey Channel above waterline: 2018 LA DOTD LiDAR Overbanks: 2018 LA DOTD LiDAR
Old River, Chinquapin Canal, and Chenne Blanc Bayou (OAR_CC_CBB, Above_BlindR)	All Cross Sections	Channel: 2017/2018 LA DOTD Ground Survey Overbanks: 2018 LA DOTD LiDAR

Model Parameters

The ARB HEC-RAS model uses a wide array of model parameters including weir coefficients, cross sections roughness coefficients and expansion/contraction coefficients to name a few of the most common. These parameters were generally applied using the guidance provided by HEC-RAS documentation in addition to other technical references. Those parameters that are a little more subjective are further discussed here.

Weir Coefficients for Bridge Decks/Roadway

1D Bridge Deck/Roadways were generally allowed to use the default broad crested weir coefficient of 2.6. However in many situations where road embankments were generally at grade or very low, the HEC-RAS Bridge Modeling Approaches were forced to Energy Only, bypassing the use of the weir equation.

Weir Coefficients for Lateral Structures and Storage Area/2D Area Connections

Weir coefficients for lateral structures were assigned using the guidance provided in the Table 3-1 of the HEC-RAS 2D Modeling User's Manual, Version 5.0, dated February 2016. Values ranged from 0.2 for lateral connections that exhibited no or very small embankment heights between the upstream and downstream connection to 3 for those that exhibited a sharp crest such as a concrete interstate barrier connecting two 2D flow areas.

Weir Coefficient for the Amite River Diversion Weir

The Amite River Diversion Weir within the Dynamic ARB HEC-RAS hydraulic model is illustrated in **Figure 23**. While the Amite River Diversion Weir is not a common weir type since only very minor head losses are observed at the headwater versus the tailwater, flows do have to pass over the weir to reach the Diversion Canal. Table 3-1 *Lateral Weir Coefficients* in the *HEC-RAS 2D User Manual* states that weir coefficients are in the range of 0.5 to 1.0 for a weir that “Does not really act like a weir but water must flow over high ground to get into the 2D flow area” which is similar to what is observed at the Amite River Diversion Weir. To better estimate the weir coefficient, LA DOTD coordinated with the USGS who performed flow gaging upstream and downstream of the weir on June 15, 2018. Flows during the gaging period ranged from 1,860 cfs to 2,150 cfs immediately upstream of the diversion weir on the Amite River which is comparable to the mean flow at USGS streamflow gage 07380120, Amite River at Port Vincent based on a review of daily mean flows. The observed flow data indicated a flow split of approximately 26% downstream of the weir on the Amite River and 74% downstream of the weir on the Amite River Diversion Canal during this time window.

To estimate the weir coefficient using the observed data, the hydrograph from USGS streamflow gage 07380120 was applied to the model at this location and scaled up slightly to match observed flows just upstream of the weir. The model was then run six times with the weir coefficients of 0.2, 0.5, 0.75, 1.0, 1.5, and 2.0. As illustrated in **Figure 24**, a weir coefficient of 0.713 was interpolated to match the observed flow split measured by the USGS.

While the observed data only represented a very limited range which very closely matches the mean annual flow on this section of the Amite River, its magnitude is only a fraction of that estimated to result in flooding of the lower Amite River. However, the weir coefficient observed to best match the observed conditions is based on the best available observed data at the time of this study and is well within the range recommended by the HEC-RAS 2D User Manual. Due to the lack of additional data, the weir is assumed to follow the general hydraulic assumption that weir coefficients are constant.

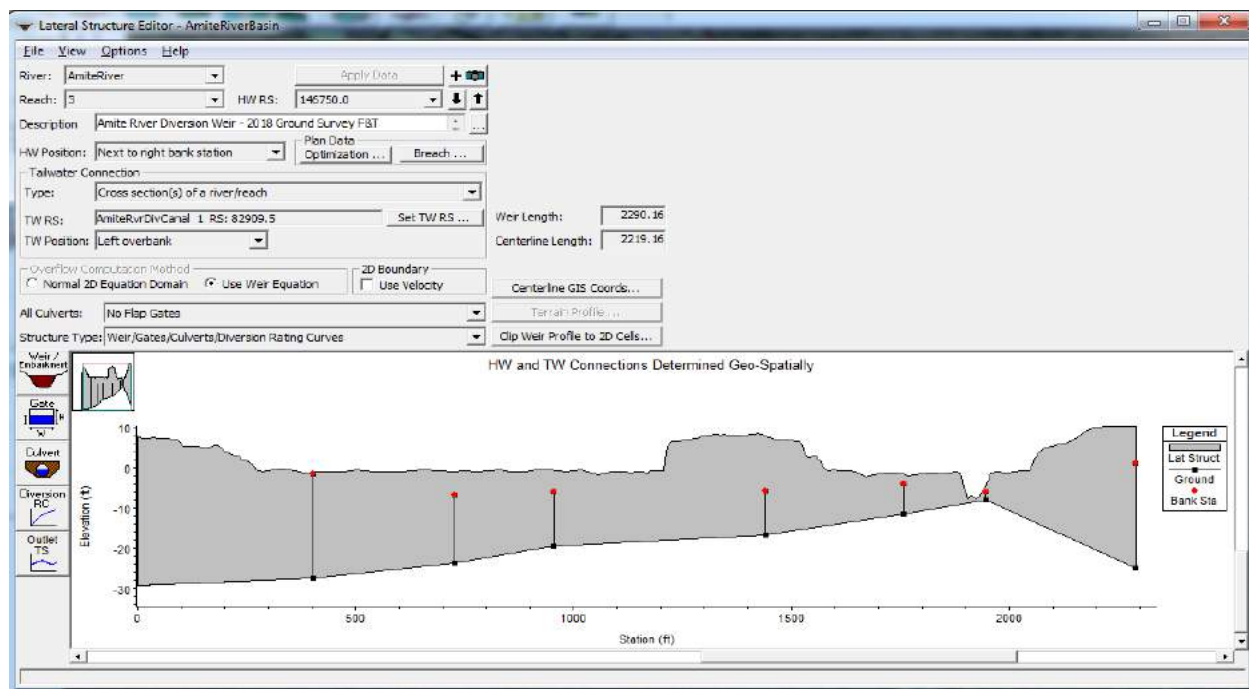


Figure 23: Amite Diversion Weir geometry, Amite River Lateral Structure 146750.0 (right bank of Amite River).

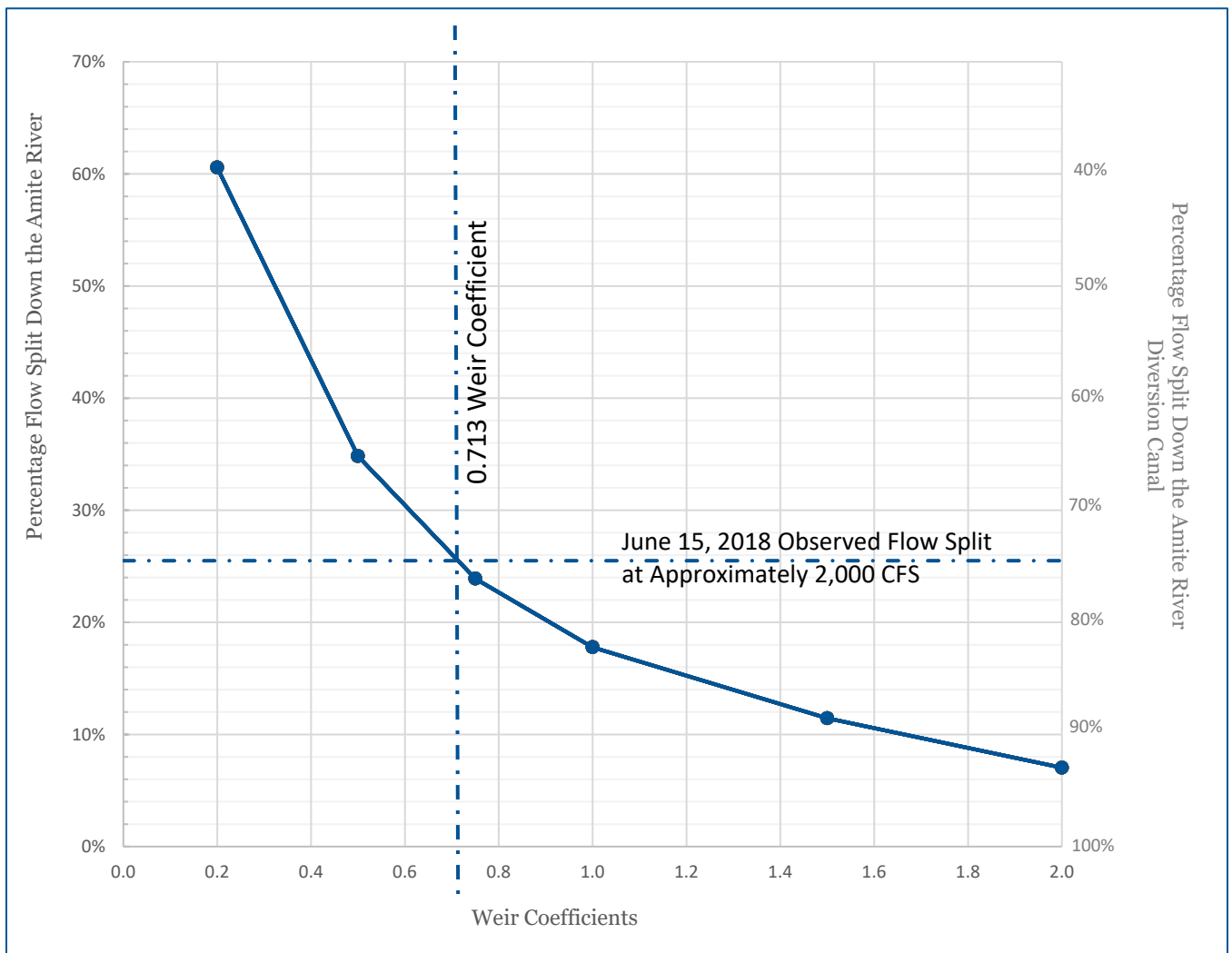


Figure 24: Variations of Weir Coefficients in the ARB HEC-RAS Hydraulic Model at the Amite River Diversion Weir Compared to Observed Flow Split on June 15, 2018 (flow split data collected by USGS).

Manning's Roughness Values for 1D Reaches

Aerial imagery, field reconnaissance and survey photography were all utilized where available to visually evaluate cross sections and assign Manning's N values using guidance provided in Open Channel Hydraulics by V.T. Chow, 1959. Additional refinements were made using engineering judgement to apply a degree of meandering factor as recommended by Cowan (Cowan, 1956). Cowan recommends applying a multiplier of 1, 1.15 or 1.3 for minor, appreciable, and severe meanders respectively. **Figures 25 to 28** illustrate the selection of N values for several cross sections within the Dynamic ARB HEC-RAS model.

Review of historical flow records indicated that travel times through the study reaches varied considerably for different magnitudes of flow, suggesting that Manning's N values were not constant at all flow magnitudes. To account for this, Flow Roughness Factors were used within HEC-RAS. The Flow Roughness Factors option can be found within the Tools menu in the Geometric Data window.

The Flow Roughness Factors option allows the user to adjust roughness coefficients with changes in flow. This feature is very useful for calibrating unsteady flow models with a large range of flows and is further discussed in the Calibration section. Roughness generally decreases with increases in flow and depth and is especially true on large river systems. **Table 7** provides a summary of the basic channel and overbank N values assigned to the 1D cross sections prior to the application of Flow Roughness Factors. These factors were selected generally assuming bank full discharges.

Location	Left Overbank	Channel	Right Overbank
Amite River Upstream of the Comite River Confluence	0.09 – 0.12	0.035 – 0.045	0.09 – 0.12
Amite River Reach Downstream of the Comite River Confluence	0.08 – 0.12	0.028 – 0.045*	0.07 – 0.12
Comite River Upstream of the Pretty Creek Confluence	0.1 – 0.12	0.045 – 0.06	0.08 – 0.12
Comite River Reach Downstream of the Pretty Creek Confluence	0.08 – 0.12	0.035 – 0.055	0.08 – 0.12
Amite River Diversion Canal	0.08 – 0.12	0.022 – 0.025*	0.08 – 0.12
Amite River Diversion Canal (Blind River)	0.12	0.022 – 0.024	0.12
Chenne Blanc Bayou/Chinquapin Canal	0.09 – 0.12	0.028 – 0.045	0.09 – 0.12
Pretty Creek (Medium Detail Study)	0.12	0.05	0.12

*Values were increased to 0.06 adjacent to the Amite River Diversion weir to account for irregular, non-parallel flow patterns that are observed as flow exchanges between the River and Canal.



Figure 25: Amite River, Cross Section 399176.7 (approximately 20 miles upstream of the Comite River Confluence), looking upstream. The basic channel Manning's N value is estimated to be 0.037.



Figure 26: Amite River, Cross section 399176.7 (approximately 20 miles upstream of the Comite River Confluence), looking at right over bank. The basic right overbank Manning's N value is estimated to be 0.12. Photo: Forte & Tablada, 2018

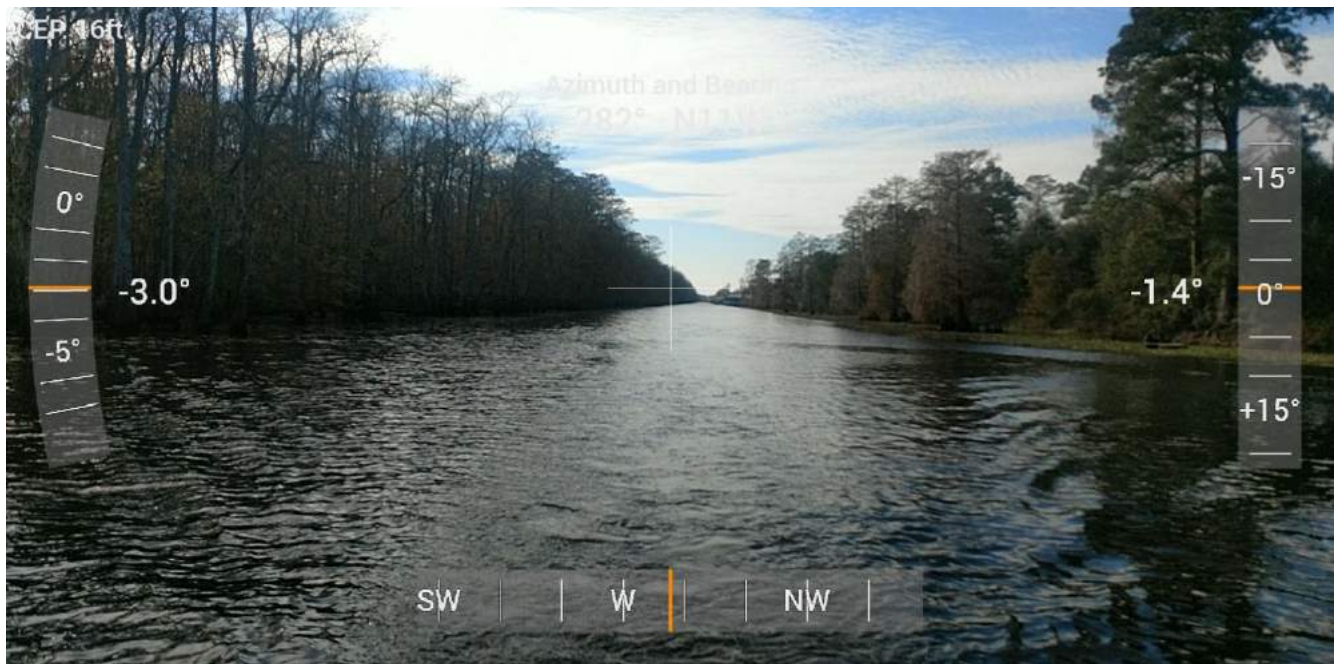


Figure 27: Chinquapin Canal, Cross Section 16041.2 looking upstream. The channel Manning's N value is estimated to be 0.03.

Photo: Forte & Tablada, 2018



Figure 28: Chinquapin Canal, Cross Section 16041.2 looking at left overbank. The left overbank Manning's N value is estimated to be 0.11.

Photo: Forte & Tablada, 2018

Manning's Roughness Values for 2D Flow Areas

2D flow areas were assigned Manning's N values using the Land Cover to Manning's N function within HEC-RAS 2D Flow Areas. This function allows spatially varied N values to be applied within 2D areas using GIS polygon regions. The 2011 NLCD, the most current at the time of model development was utilized to assign Land Cover to 2D flow areas. As of January 2019, the Multi-Resolution Land Characteristics Consortium indicates that the 2016 NLCD dataset will not be available until sometime in 2019 and therefore was not available for use with the ARBNM Version 1.0. **Table 8** provides a summary of the Manning's N values assigned to NLCD land use codes. Since flooding sources studied by 2D methods were only performed in medium detail, the NLCD was not refined to apply separate Manning's N values to channel areas. This would be highly recommended as a model upgrade in the event that the Dynamic ARB HEC-RAS model is to be used for detailed analysis of flood risk and project measures within the medium detail 2D study reaches.

Table 8: Summary of Manning's N Values for 2D Flow Areas		
2011 NLCD Code	Description	Manning's N
11	Open Water	0.035
21	Developed, Open Space	0.09
22	Developed, Low Intensity	0.10
23	Developed, Medium Intensity	0.10
24	Developed High Intensity	0.15
31	Barren Land (Rock/Sand/Clay)	0.10
41	Deciduous Forest	0.12
42	Evergreen Forest	0.12
43	Mixed Forest	0.12
51	Shrub/Scrub	0.12
71	Grassland/Herbaceous	0.07
81	Pasture/Hay	0.09
82	Cultivated Crops	0.10
91	Woody Wetlands	0.12
95	Emergent Herbaceous Wetlands	0.12

HEC-RAS Model Stability

Model stability is an inherent challenge of dynamic 1D and 2D hydraulic modeling. There is no analytical solution for the Saint Venant equations (two hyperbolic differential equations) which are used to calculate how flow changes in space over time. Consequently, they must be solved by numerical approximation. Model stability refers to whether or not the solution of the numerical approximations of the governing differential equations at each computational time-step is able to converge on a reasonable solution or not. A stable model converges on a solution and completes an entire simulation and an unstable model diverges away from a solution, causing the model to abort or “crash”, ending the simulation prematurely. An otherwise stable model can become unstable if the flow regime is changed; a culvert, bridge, or other hydraulic structure (i.e., an internal boundary condition) is added to the system; or the initial conditions are changed to something that is unrealistic to name just a few causes. The larger the model, the greater the challenge to create a stable model.

During the development of the ARB HEC-RAS model, numerous instabilities were encountered. Run time messages were carefully reviewed to identify fatal instabilities (those that result in HEC-RAS aborting), critical instabilities (those that results in erroneous results but allow HEC-RAS to run to completion) and minor instabilities (those that give reasonable results but result in multiple iterations and larger convergence errors which increase program execution or “run” times). All fatal and critical instabilities were eliminated from the runs through a variety of methods while all minor instabilities were carefully reviewed and actions were taken where feasible to reduce instabilities and minimize convergence errors. Fatal and critical instabilities were most often associated with the 1D reaches. 2D areas were most commonly associated with minor instabilities which had the most significant impact on run times. Some of the more common causes of instability for 1D and 2D study areas included:

1D Flow Stability

Free and Submerged Flow Rating Curves at Hydraulic Structures

Due to the large size of many of the bridges along the Amite and Comite rivers, the default Parameters for Hydraulic Properties Table (HTab Param icon within the Bridge Culvert Data editor) often resulted in irregular Free and Submerged Flow Rating Curves that exhibited rapid changes in water surface elevation with minor changes in flow. A Free Flow rating curve describes the flow-elevation relationship when tailwater submergence does not occur such as free flow over a weir. A family of Submerged Flow rating curves is calculated by RAS for a given flow for a range of tailwater conditions. These abnormal rating curves created significant instabilities which often prevented RAS from converging on a solution. Notable differences were observed when comparing Free and Submerged Flow Rating Curves developed within HEC-RAS version 4.1 and 5.0.6 as well as unexplained changes to the rating curves following minor geometry edits.

To improve stability, all structure Free and Submerged Flow Rating Curves were carefully reviewed to ensure that the selected curve accurately matches the expected hydraulics through the bridge opening. Where sudden changes in the curves were irregular and unexplainable, the default parameters for the number of points on the free flow curve (50), the number of submerged curves (50) and number of points on each submerged curves (20) were increased up to the maximum allowable. Additionally, where needed, headwater maximum elevations, tailwater maximum elevation and maximum flow values were entered to limit the

extent of the curves. The maximum flow and elevation observed during the August 2016 flood was used as a guidance with an appropriate buffer applied. While this resulted in significantly longer Geometry Preprocessor times, it also resulted in smoother curves and reduced Unsteady Flow Simulation run times as a result of improved stability.

All final HTab curves for bridges along the Amite and Comite River main channels have been included in the **Appendix 2** as reference to future users as a direct comparison in the event of instabilities during future simulations.

Bridge Modeling Approaches

Adding to the stability issues associated with Free and Submerged Flow Rating Curves, Bridge Modeling Approaches were a further source of instability. In particular the use of Momentum for low flow methods resulted in questionable results for some bridges. Where visible model instabilities were present, the HEC-RAS Standard Table for Bridge Comparison was reviewed at time steps before, during and after the instability to determine the Bridge Selection Method (BR Sel Method). Often the instabilities occurred when the low flow method switched from Energy to Momentum methods. When reviewing the hydraulic profile through bridge openings, erroneous large drawdowns in both energy grade and hydraulic grade were often observed at internal bridge sections BRU and BRD. When this was observed, the bridge modeling approach was forced to the Energy method for low flows which typically resulted in reasonable results and improved stability.

Multiple Bridge Openings

The Multiple Bridge Opening option was used for many bridges where true multiple openings were present. This did present challenges with stability and resulted in significantly longer Preprocessing of HEC-RAS geometry data but was critical for the accurate and stable modeling of bridges. The best stability and results were obtained by using identical cross sections for sections 2 and 3 of the bridge modeling routine ensuring that the stationing of sections 2, 3 and all internal bridge sections BRU and BRD are identical. This provided a flat bed profile though the bridge as illustrated in **Figure 29**.

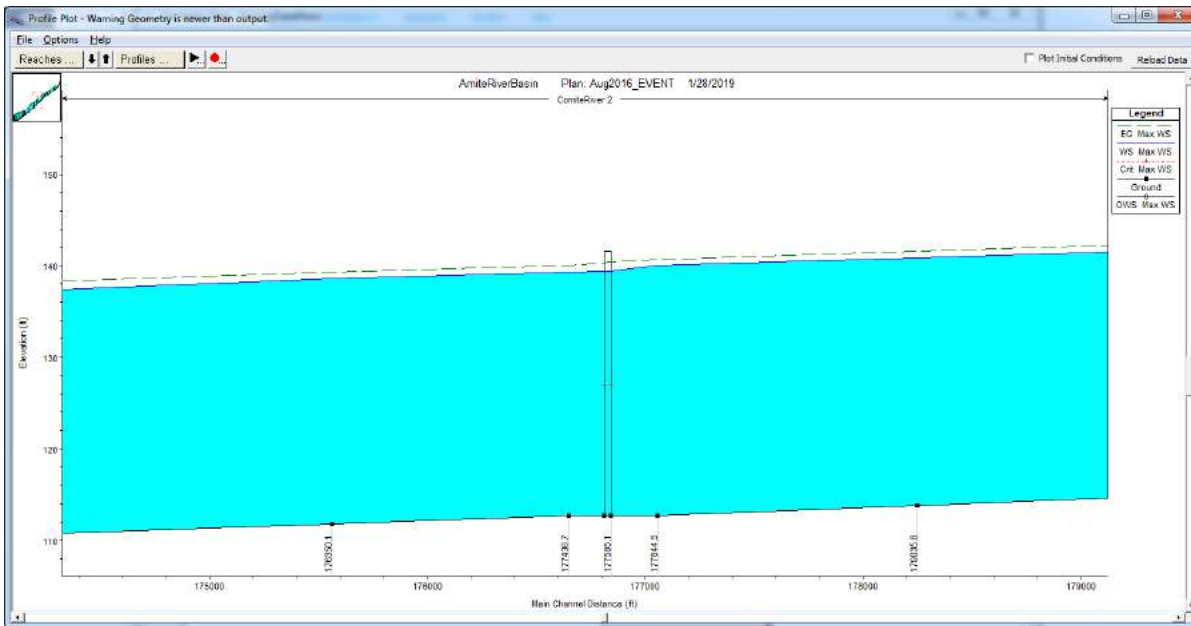


Figure 29: Creating identical inverts and sections at sections 2, BRD, BRU and 3 of the HEC-RAS bridge routine generally resulted in greater stability for both single and multiple bridge openings.

Weir Flow at Bridges

Unexplained issues were accounted at several single opening bridges whereby HEC-RAS did not appear to be allowing weir flow to occur despite both the energy and hydraulic grade lines exceeding the minimum weir flow elevation. The Multiple Bridge Opening routine was used as a workaround by defining the road embankments as conveyance areas which allowed weir flow to occur and provided more realistic results.

Low Flows

Low flows are notoriously challenging to obtain numerical stability within HEC-RAS 1D. Applying Initial Flow values to the Unsteady Flow Data Initial Conditions improved stability at the start of simulations, however, this was often only temporary since the Initial Flow is only used by HEC-RAS to perform a steady state simulation to establish initial elevations at all cross sections. It does not function as a minimum flow. Therefore unless significant flow is applied to the model before the initial conditions drain out of the system, the model will often exhibit poor numerical stability. This is particularly critical during observed simulations which may often result in extended time steps of low or minimal flow to portions of the model. To improve the stability, a minimum flow of 1 cfs per square mi. of drainage area was assigned to every hydrograph boundary applied to the ARB HEC-RAS model Unsteady Flow Data. While the impact of this was negligible during flood flows, it resulted in improved stability at all flow conditions resulting in a more robust model that will present end users with fewer challenges.

Multiple Boundary Conditions at a Single Cross Section adjacent to the Amite River Diversion Weir

While potentially just an irregularity with the unique characteristics of the Amite River Diversion Weir, fatal instabilities were observed at the upstream-most cross section of the Amite River Diversion Canal. At this cross sections there was a boundary condition inflow from Flat Lake within the AmiteR_Div_SW 2D Flow Area in addition to a lateral inflow from the Amite River Diversion Weir. By disconnecting the boundary condition from the 2D Flow Area and allowing this minor flow to pond up and enter the Amite River and Diversion Canal upstream and downstream of the weir resulted in improved stability. Since the inflow from Flat Lake was very small (approximately 50 cfs when gaged during an approximately 2,000 cfs flow along the Amite River) and quickly becomes overwhelmed by unconfined upstream flow break outs from the Amite River, the removal of this connection was considered insignificant. If the model is to be used for low flow studies in this area, it is recommended that the connection be reestablished and additional effort be performed to improve stability.

2D Flow Stability

When compared to the HEC-RAS 1D computation engine, the 2D computation engine resulted in far fewer fatal and critical instabilities when developing and testing the model. Often fatal and critical instabilities reported to be within the 2D engine were not as a direct result of the 2D engine but rather instabilities inherited from coupling with an unstable 1D reach. Minor instabilities, while typically not resulting in erroneous results, did result in slow computation run times as a result of multiple iterations. Wherever feasible, the causes of these instabilities were identified and remedied.

To identify areas of instability the computation run time messages were transferred to Excel and sorted to rank the cells by those with the largest error in addition to summarizing and ranking the individual cells with the most convergence errors reported within the Run Time Messages that are over the default RAS tolerance. Some of the most common causes of large and multiple errors included:

Cell Size Transitions

HEC-RAS allows the utilization of refinement regions that enable users to create regular 2D meshes of differing resolution. While this function saves considerable time creating meshes and allows increased detail in more critical areas, sudden changes in cell size can create computational instability and significantly increase run times. As a general rule of thumb, it was determined that to achieve reasonable stability and run times, adjacent cells should be no more than 0.5 to 2 times the size of adjacent cells. To create more gradual transitions, refinement areas were either strategically delineated to result in gradual transitions or additional break lines were utilized to create a more regular transition as illustrated in **Figure 30**.

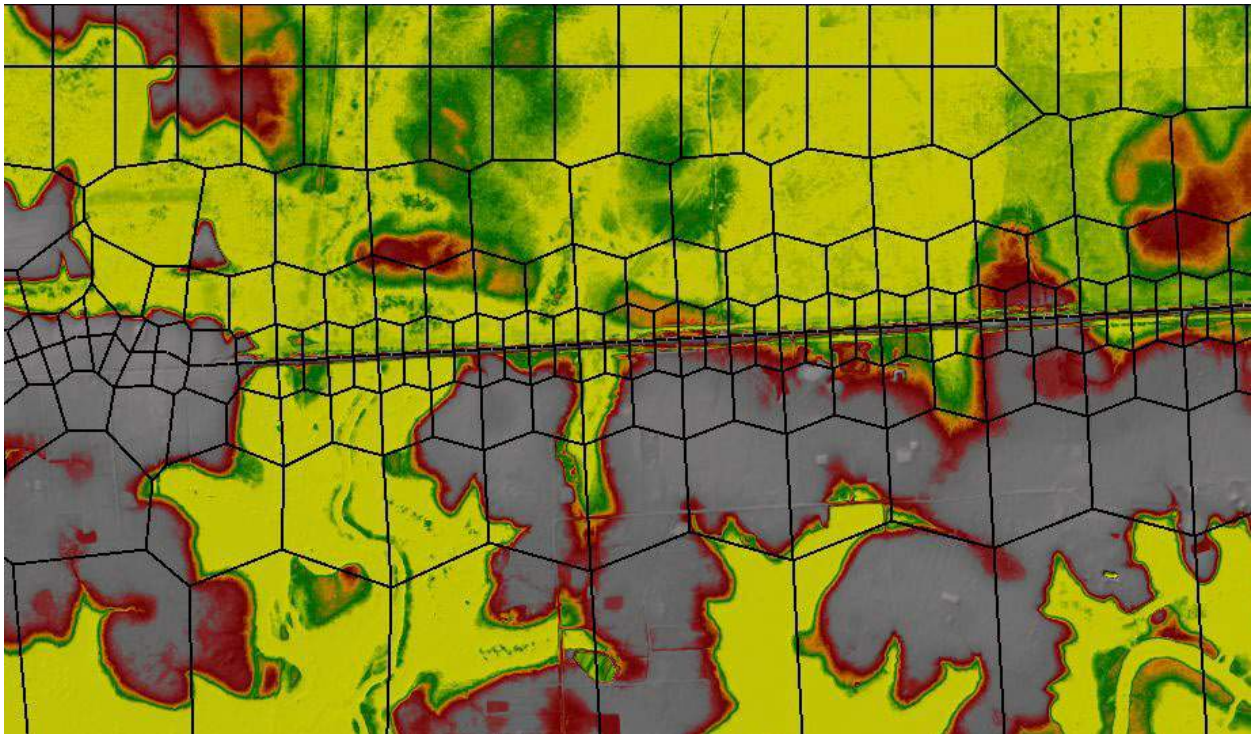


Figure 30: Gradual transition of cell sizes resulted in improved stability.

Multiple Water Surfaces within a Single Cell

Cells that straddle high ground between two independent flood elevations as illustrated in **Figure 31** were a common cause of instability and increased run times. While this is typically only a temporary situation until water elevations rise and the adjacent floods merge, cells that become wetted only during the peak of the flood or during an extended time of stable water elevation did have significant impacts on run times. This was most notable for 2D cells at the edge of the middle and lower Amite River where inundation times were significantly longer than those in more confined areas upstream.

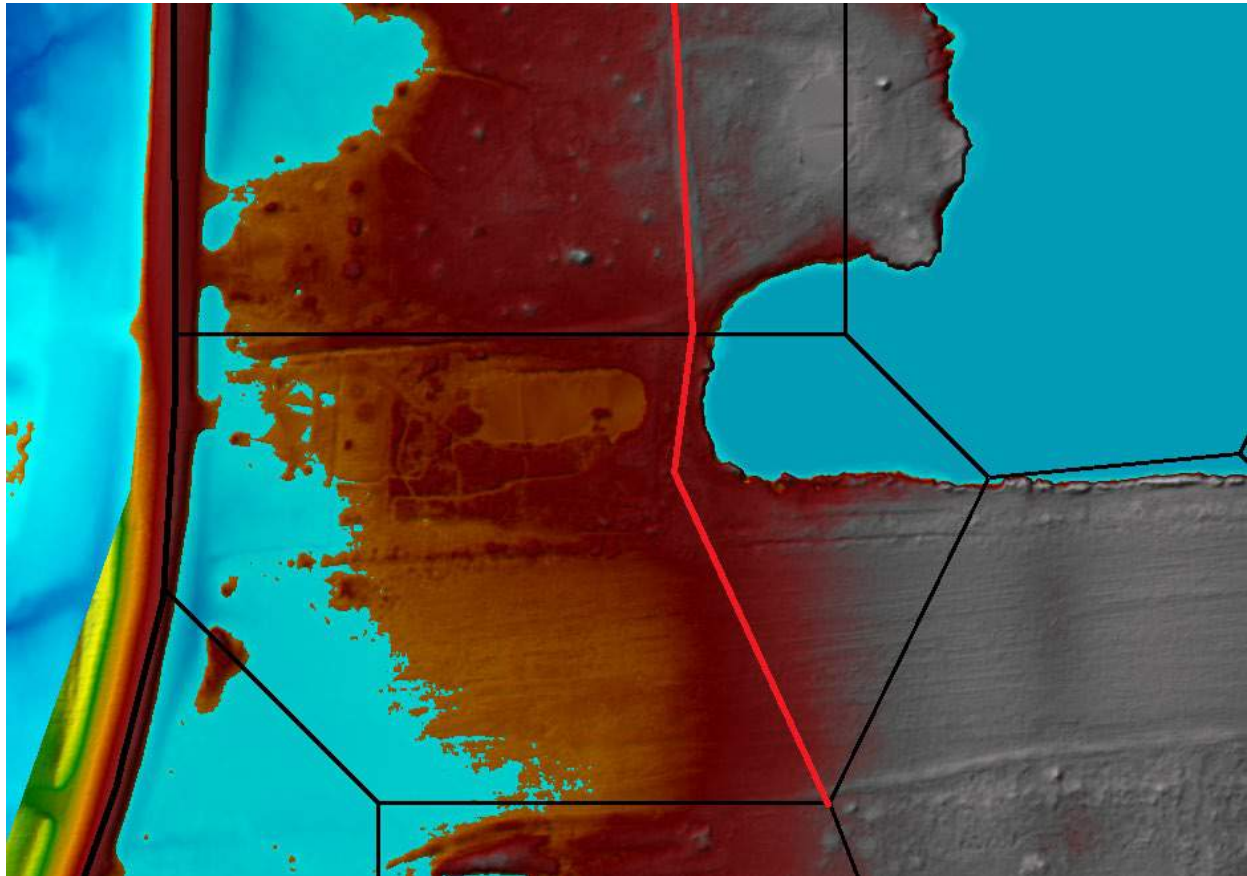


Figure 31: Example of 2D cell with two independent flooding elevations on the east and west edges of the cell which result in instabilities. The use of the red break lines along ridgelines divides these independent flood elevations coming from the east and west and consequently would improve model stability and run times.

This issue was particularly prevalent in areas of multiple small ponds or borrow pits which were generally one to two times the size of 2D cells. Due to the close vicinity of many of these ponds and pits, 2D cells would frequently straddle two depressed areas and therefore cause instabilities. For areas which caused significant instability, the 2D cells were manipulated to ensure that cell faces either encircled these areas or breaklines were used to enforce the high ground around them as illustrated in **Figure 32**.

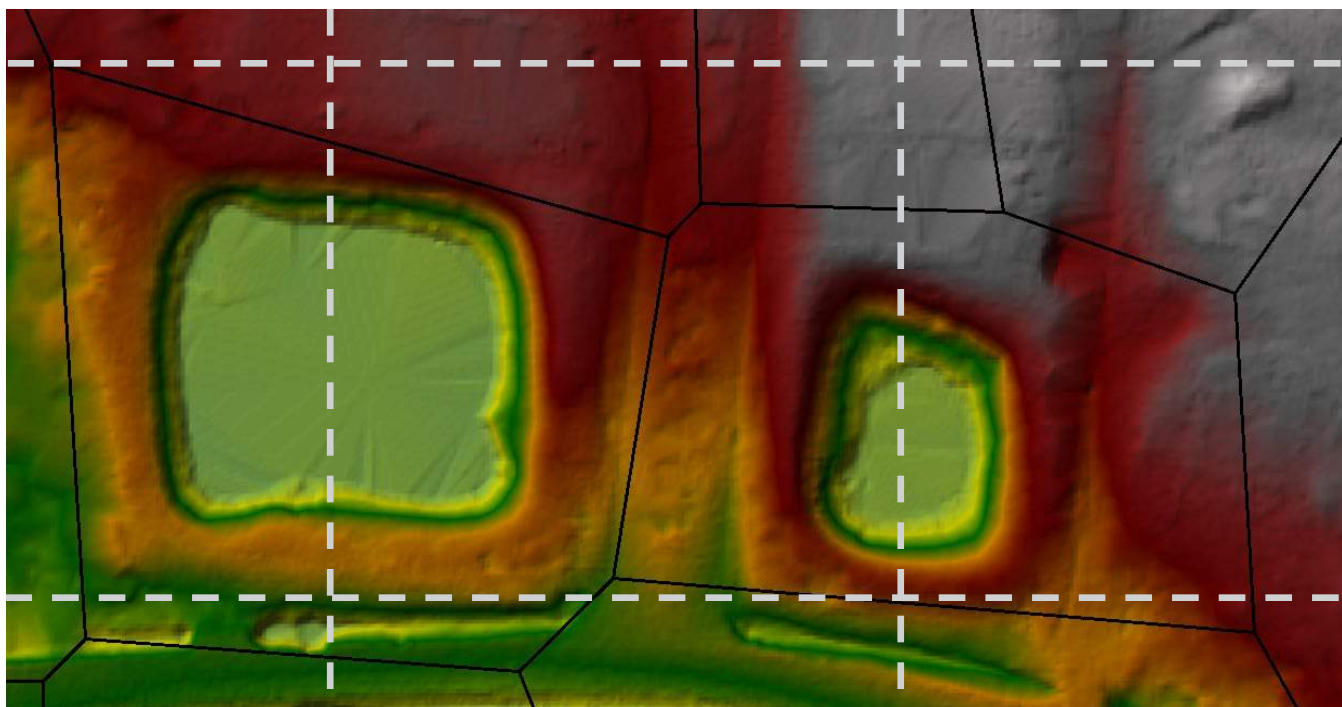


Figure 32: Refinement of 2D mesh around ponds and borrow pits similar in size to the 2D mesh resolution resulted in improved stability. (Grey lines represent original mesh, black lines represent refined mesh)

SA/2D Area Connections

Storage Area/2D connections were often a source of instability within 2D Flow Areas when used to model bridges and culverts. As discussed previously, current limitations of HEC-RAS prevent the coding of bridges within SA/2D Connections. Therefore, bridges were modeled either as slots through the weir or as a series of culverts. While weirs provided reasonable stability within 2D Flow Areas, culverts frequently caused instabilities. Many of these issues were likely as a result in the limited detail modeling of channels in medium detail 2D areas which did not include bathymetry. This required culvert inverts to be artificially raised since HEC-RAS does not allow SA/2D Area Connections to have inverts lower than the adjoining 2D cells.

To reduce the instabilities associated with modeling culverts within 2D Flow Areas and improve run times, many bridges were converted from multiple culverts to weir openings as previously highlighted in **Figure 20**. Additionally true culverts coded into 2D Flow Areas which exhibited significant instabilities were also converted to weir openings which approximately replicated the culvert opening. When the ARB HEC-RAS model is needed for more detailed analysis in the 2D Flow Areas, it is recommended that bathymetry be enforced to improve accuracy and model stability at structures enabling them to be modeled more accurately.

Time Slicing

Time slicing within the HEC-RAS Unsteady Computation Options and Tolerances allows the user to set a computational time step for a specific 2D flow area that is a fraction of the overall unsteady flow computation interval. Review of the initial runs in several 2D Flow Areas indicated clearly erroneous velocities, sometimes in excess of 1,000 ft/s. suggesting localized numerical instability. This issue was eliminated through the use of time slices in several 2D Flow Areas allowing the Courant conditions for stability to be met and resulted in reasonable

results. A maximum of six slices was required to achieve this stability, effectively reducing time steps on the fly from 30 seconds to 5 seconds where needed.

Lateral Structures

Lateral structures were a source of instabilities. Selection of weir coefficients as low as 0.2 did result in improved stability, however this often underestimated the exchange of flow between 1D and 2D areas. Often instabilities at lateral structures were inherited from instabilities in the 1D reaches which once resolved resulted in improved stability at the lateral structures.

Cell Size Enforcement around Structures

When a 2D area is created, the automated mesh generation tool in HEC-RAS generally works well. However, cell formation does not account for proper alignment along topographic or hydraulically significant features. If breaklines are not enforced within a 2D area it will not cause instabilities, but if breaklines are not enforced along the boundary of a 2D area where there is flow transfer it will cause computational issues. In **Figure 33** below the boundary of the ComiteWest, ClaycutJones, and WardsCreek 2D Flow Area's can be seen. Notice how the cells along the 2D Areas are not collinear meaning that the cells faces do not align properly. In this instance it is not a problem because the 2D areas connect along a ridge where flow does not transfer from one area to another.

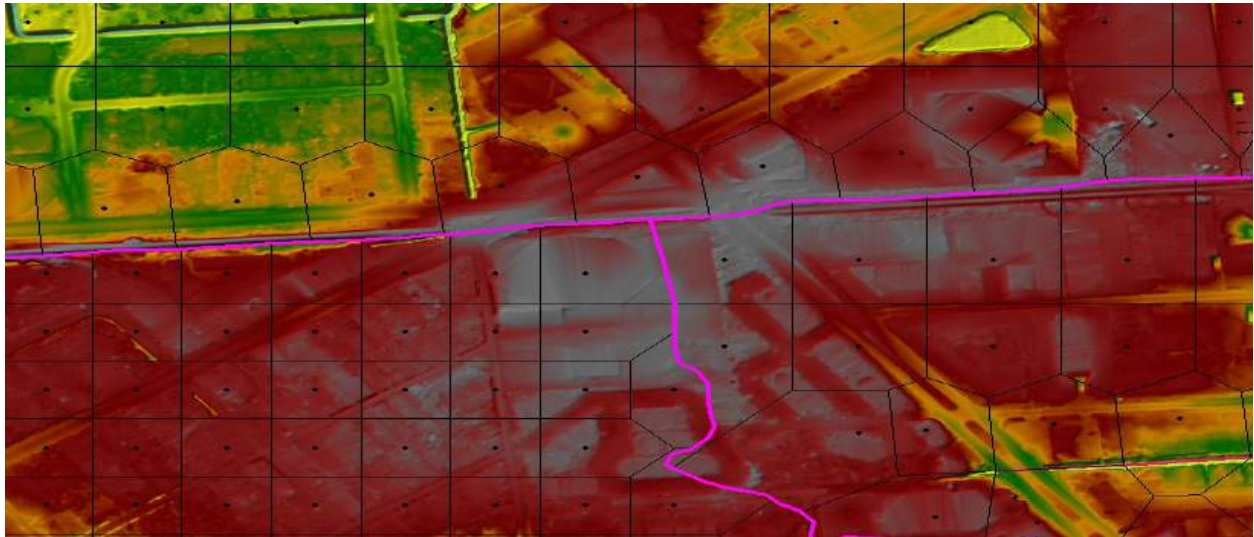


Figure 33: Example of non-optimal cell alignment between 2D Flow Areas where faces are not collinear

In **Figure 34**, the cell faces are aligned more optimally to properly model flow transfers between 2D Flow Areas. Enforcing and aligning the cells along a lateral structure connection of a 1D reach and 2D area can also increase overall model stability.

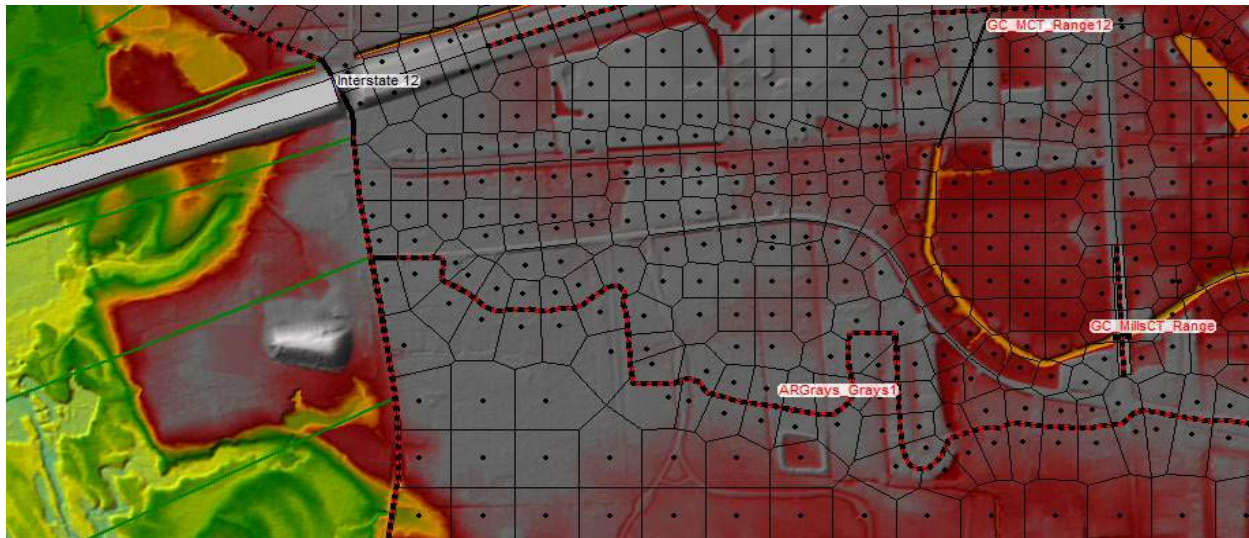


Figure 34: Example of more optimally aligned cell faces between adjacent 2D Flow Areas

Cell Size Selection Immediately Adjacent to SA/2D Connections

Optimal performance and stability was realized when strategically selecting cells sizes at the faces of bridge openings and culverts within SA/2D Connections. Larger 2D cells at the faces of culverts generally resulted in improved stability whereas smaller cells at the opening of weir slots used to simulate bridges openings generally resulted in improved stability when smaller cells sizes were used. This is believed to be as a result of flow going from 1D (culvert) to an individual 2D cell causing instabilities related to volume conservation. One small 2D cell may not have the same volume of a large submerged culvert. So to increase stability around modeled culverts, a larger cell was used to convey the culvert flow upstream to downstream. An example of this can be seen in **Figure 35**.

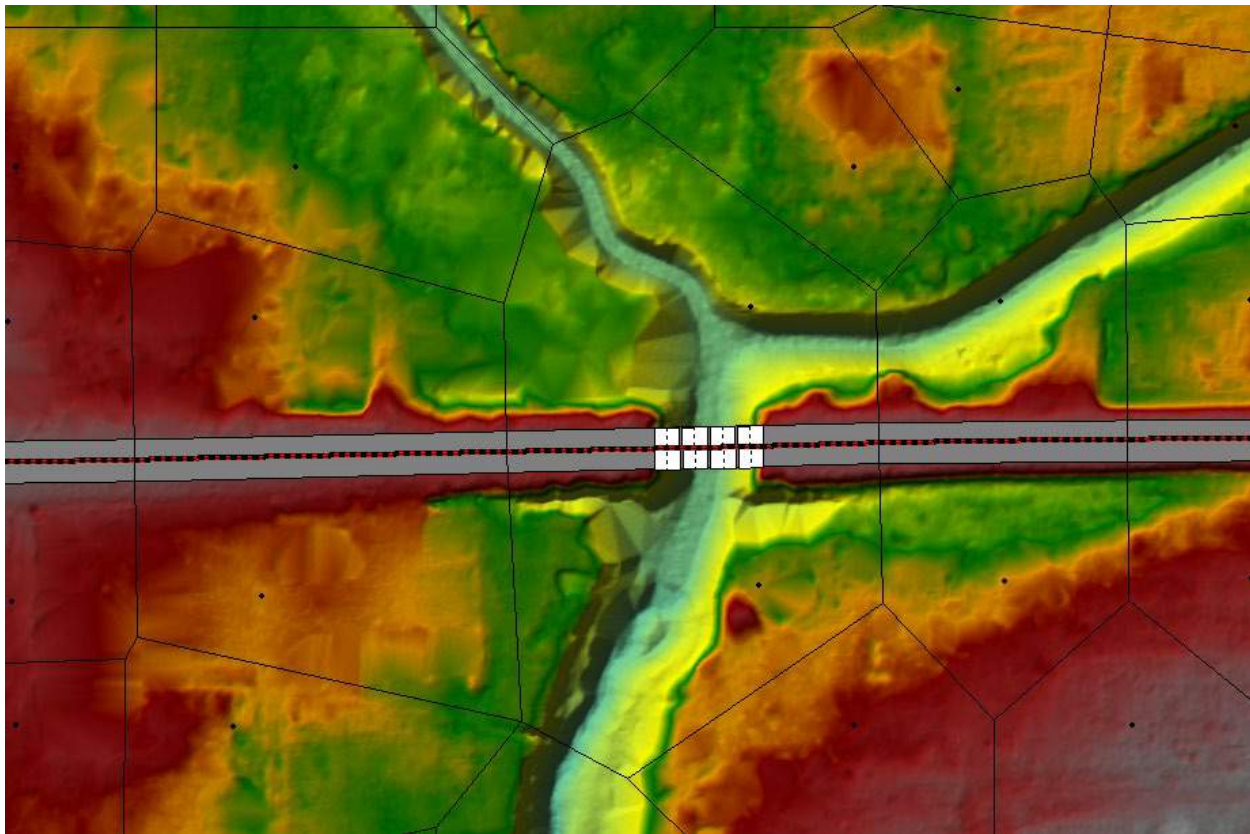


Figure 35: Optimization of Cell Sizes Adjacent to Culverts

Steady State ARB HEC-RAS Hydraulic Models

Version 1.0, February 2019 of the Steady State ARB hydraulic models were developed in HEC-RAS Version 5.0.6. As previously noted the models represent the Amite River and Comite River Tributaries studied in low detail 1D methodologies.

As further illustrated in **Figure 36**, the geometry of the Steady State Amite Tributaries model comprises of:

- More than 1200 1D cross sections within 45 reach segments;
- 68 limited detail hydraulic structures;
- Approximately 140 flow change locations

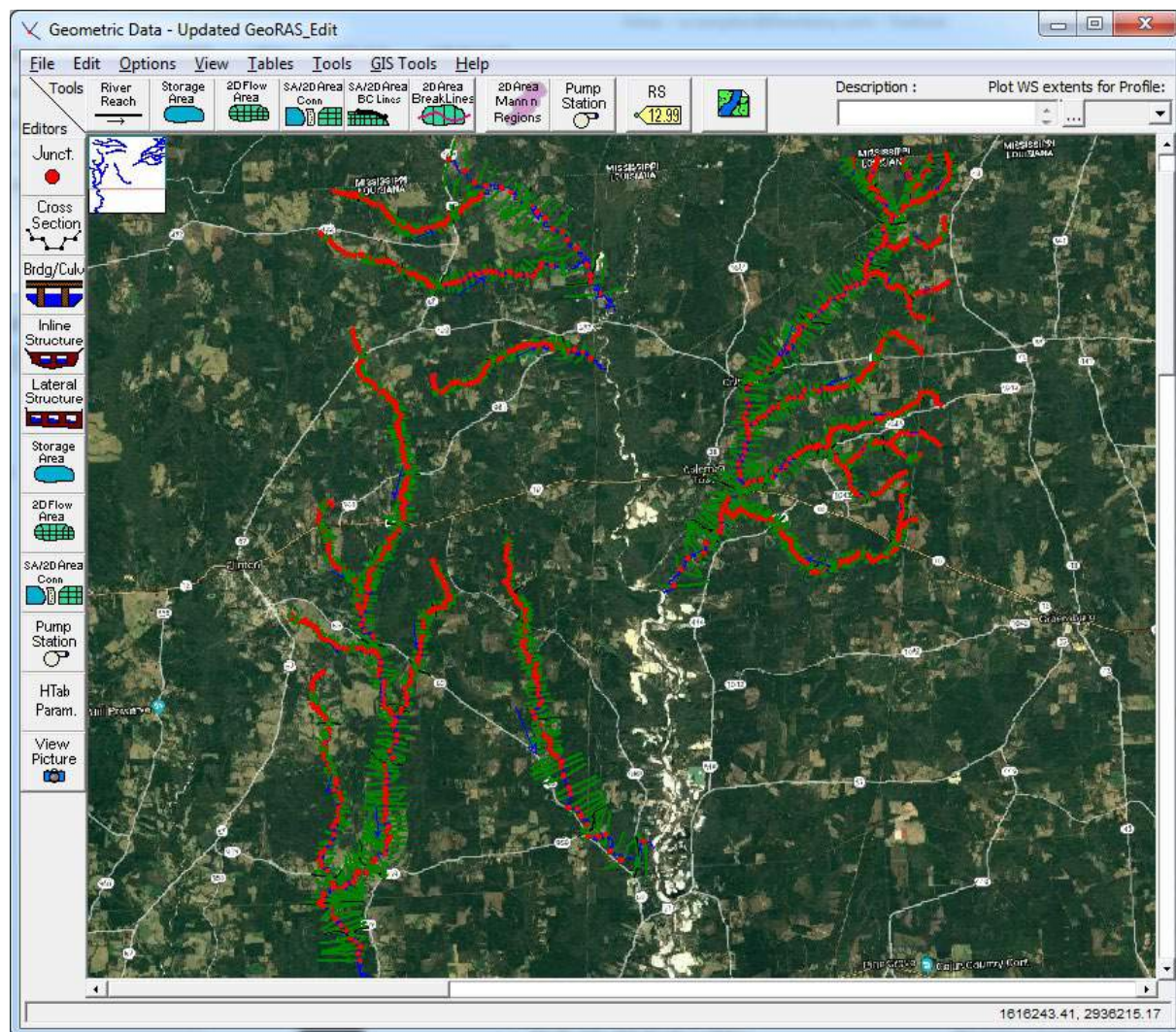


Figure 36: Steady State Amite River Tributaries HEC-RAS Hydraulic Model Geometry Overview

As further illustrated in **Figure 37**, the geometry of the Steady State Comite Tributaries model comprises of:

- More than 900 1D cross sections within 33 reach segments;
- 77 limited detail hydraulic structures and;
- Approximately 95 flow change locations.

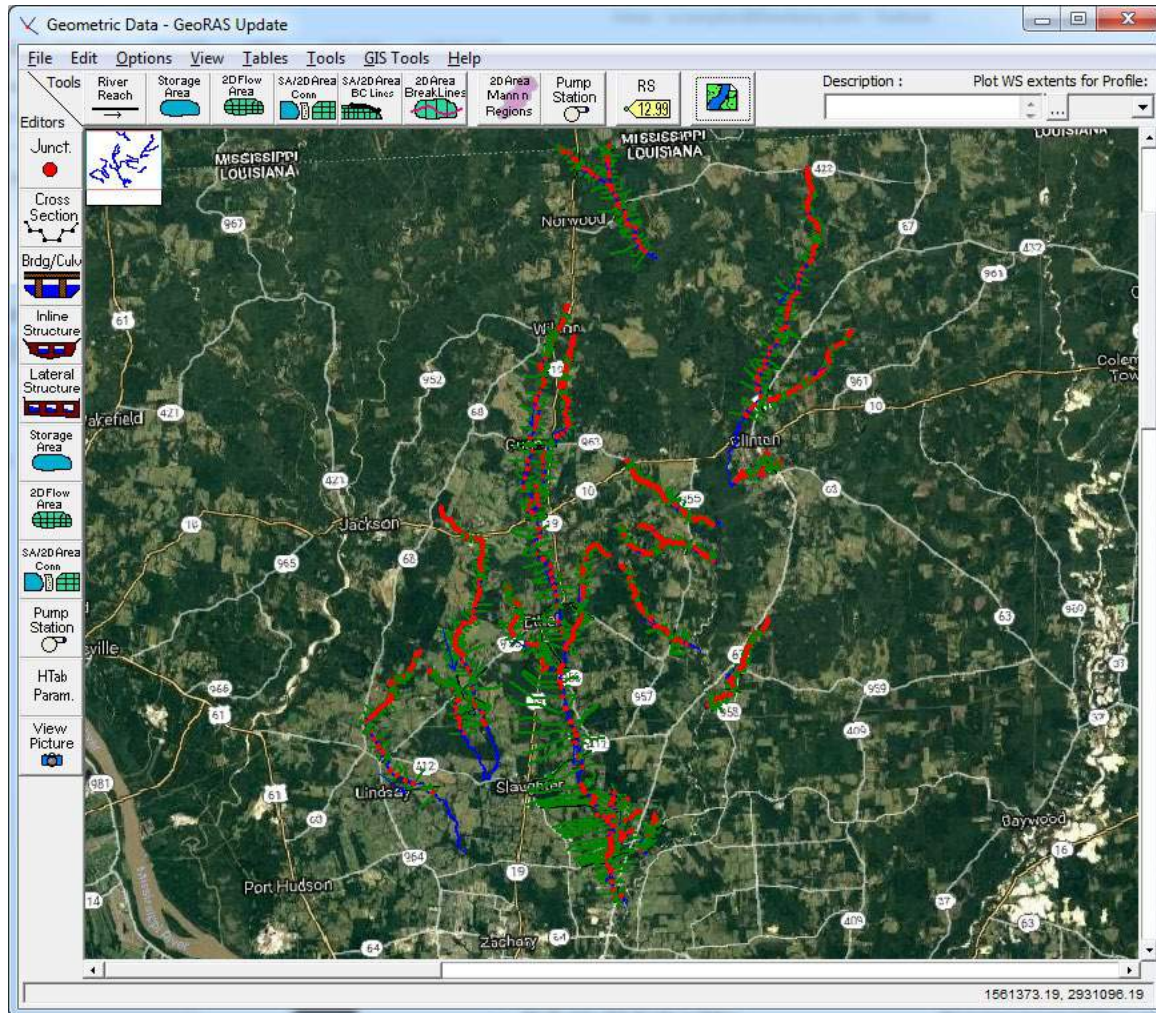


Figure 37: Steady State Comite River Tributaries HEC-RAS Hydraulic Model Geometry Overview

Computation Methods

The steady state ARB HEC-RAS models use the standard step back water method within the Steady State Flow Analysis engine to solve the energy equations. Sub critical flow was assumed for all reaches.

Model Geometry

The ARB steady state HEC-RAS models use the 2018 LA DOTD LiDAR for all cross sections. Due to the scoped low level of detail, no bathymetric assumptions were made for portions of the channel not captured by the LiDAR. Hydraulic structures modeled within these reaches were assumed from LiDAR and or aerial images.

Manning's N values were approximated using the same methodology as medium and high detail study areas, however the Flow Roughness Factors option was not utilized in low detail areas.

Hydrologic Flows

Instantaneous peak flows from the ARB HEC-HMS model were applied to the model through the Steady Flow Data option in HEC-RAS. These flow were validated using the 2001 USGS Publication Methods for estimating Flood Magnitude and Frequency in Rural Areas in Louisiana. Individual flow change locations and magnitudes can be found in the State Flow Analysis option.

CALIBRATION

Six historical floods were selected for calibration of the ARB HEC-HMS and Dynamic ARB HEC-RAS models. These flood events were selected to meet the following criteria to best characterize a range of flows within the entire basin and allow the models to be accurately calibrated:

- Low flow, in-channel discharges to enable calibration of channel celerity through Manning's N values.
- Bank-full and near bank full discharges to enable calibration of bank-full Manning's N values with primary focus on channel celerity and a secondary focus on elevations.
- Minor flood discharges to enable shallow overbank roughness N values to be refined with a focus on both channel celerity, and overbank Manning's N values.
- Major flood discharges to enable calibration of deep overbank flooding Manning's N values.
- Flood of record to simulate the recent 2016 flood with a primary focus on calibration of peak elevations.

Where multiple comparable historical events were observed that met this criteria, preference was given to those events that occurred after the August 2016 storm since notable changes in channel geometry had occurred as a result of scour, erosion, channel migration and sediment deposition. Additionally, high-resolution radar precipitation data and USGS stream gage information is generally more abundant for more recent events.

The National Weather Service (NWS) flood stage categorization at flood forecast locations corresponding to USGS gages included in **Table 9** were used as a guide to assess historical flood magnitudes at the five key stream gages located along the Amite River and Comite River. In general, the term flood stage is defined as the gage height of the lowest bank of the reach in which the gage is situated. The term "lowest bank" is, however, not to be taken to mean an unusually low place or break in the natural bank through which the water inundates an unimportant and small area. The common definition is the stage at which overflow of the natural banks of a stream begins to cause damage in the local area from inundation (flooding).

Table 9: NWS Flood Stage Categorization				
Location	Major Flood Stage	Moderate Flood Stage	Flood Stage	Action Stage
USGS 07380120 Amite River at Port Vincent, LA	12	10	8	7
USGS 07377000 Amite River near Darlington, LA	23	21	18	16
USGS 07378500 Amite River near Denham Springs, LA	39	35	29	26
USGS 07378000 Comite River near Comite, LA	28	25	20	16
USGS 07377500 Comite River near Olive Branch, LA	24	22	19	16

After a careful review of historic floods, six events were selected to meet the criteria. These floods are listed in **Tables 10** and **11** and are annotated with the colors previously defined in **Table 9** to characterize the flood stage.

Table 10: USGS Recorded Stage (Cell colors correspond to Table 9 Flood Stage Categorization)

Event	Description	USGS 07380120 Amite River at Port Vincent, LA (ft.)	USGS 07377000 Amite River near Darlington, LA (ft.)	USGS 07378500 Amite River near Denham Springs, LA (ft.)	USGS 07378000 Comite River near Comite, LA (ft.)	USGS 07377500 Comite River near Olive Branch, LA (ft.)
June 2018	Low, in-channel discharges	1.84	1.35	15.81	7.92	0.15
January 2018	Partial bank full discharges	2.92	4.61	20.37	8.03	3.12
August 2017	Minor flood discharges	4.88	5.58	23.35	10.26	3.88
October 2017	Minor flood discharges	3.64	13.04	29.03	24.59	19.40
March 2016	Major Flood	11.20	16.82	36.09	26.18	14.00
August 2016	Flood of Record	17.90	22.54	46.20	34.22	26.96

Table 11: USGS Recorded Flows (Cell colors correspond to Table 9 Flood Stage Categorization)

Event	Description	USGS 07380120 Amite River at Port Vincent, LA (CFS)	USGS 07377000 Amite River near Darlington, LA (CFS)	USGS 07378500 Amite River near Denham Springs, LA (CFS)	USGS 07378000 Comite River near Comite, LA (CFS)	USGS 07377500 Comite River near Olive Branch, LA (CFS)
June 2018	Low, in-channel discharges	4,560	978	2,830	2,230	185
January 2018	Partial bank full discharges	7,030	3,330	5,460	2,560	1,190
August 2017	Minor flood discharges	9,430	4,200	7,980	3,220	1,510
October 2017	Minor flood discharges	13,900	15,000	25,100	11,000	30,000
March 2016	Major Flood	41,700	29,800	65,200	12,100	11,100
August 2016	Flood of Record	199,000	116,000	266,000	71,000	78,000

The basic description and calibration method intended for each of the six flood events is summarized in **Table 12**:

Table 12: Selected Historical Flood Events			
Event	Date	Description	Description and Calibration Methodology
1	June 2018	Low, in-channel discharges	Small peak, generally $\frac{1}{4}$ to $\frac{1}{2}$ bank full. Observed hydrographs from USGS gages were input into HEC-RAS model and flow roughness factors were applied to applicable flow range to calibrate timing of floodwave by matching observed timing at downstream gage.
2	January 2018	Partial bank full discharges	Small peak, generally about $\frac{1}{2}$ bank full. Observed hydrographs from USGS gages were input into HEC-RAS model and flow roughness factors were applied to applicable flow range (above that of previous event) to calibrate timing of floodwave by matching observed timing at downstream gage.
3	August 2017	Minor flood discharges	Very minor flood with bank full or near bank full discharges and isolated minor overbank flooding. Full recreation of gridded radar precipitation data was applied to HEC-HMS to generate flows for HEC-RAS. Flow roughness factors were applied to applicable flow range (above that of previous events) to primarily calibrate the timing of the floodwave by matching observed timing at downstream gage. Calibration to observed high water marks was also performed, however this was second priority to timing.
4	October 2017	Minor Flood discharges	Very minor flood with bank full or near bank full discharges and isolated minor overbank flooding. Full recreation of gridded radar precipitation data was applied to HEC-HMS to generate flows for HEC-RAS. Flow roughness factors were applied to applicable flow range (above that of previous events) to primarily calibrate the timing of the floodwave by matching observed timing at downstream gage. Calibration to observed high water marks was also performed, however this was second priority to timing.
5	March 2016	Major Flood	Large flood with significant overbank flow generally throughout watershed. Full recreation of gridded radar precipitation data applied to HEC-HMS to generate flows for HEC-RAS. Timing of floodwave and runoff volumes in addition to flood elevations were the focus of calibration.
6	August 2016	Flood of Record	Very large flood event with major overbank flows generally throughout the watershed. Full recreation of gridded radar precipitation data applied to HEC-HMS to generate flows for HEC-RAS. Calibration of elevations was primary focus.

Historic Precipitation Reconstruction for Floods

To recreate the four floods within the ARB where HEC-HMS models were developed for calibration, the National Oceanic and Atmospheric Administration (NOAA) Stage IV gridded precipitation data was collected. The data was obtained from the University Corporation for Atmospheric Research data server (<https://data.eol.ucar.edu/dataset/113.003>).

Stage IV is an hourly quality controlled rainfall product available on a 4 km (2.6 mi.) grid across the United States. The hourly rainfall data was bi-linearly spatially interpolated to a 1 km grid and rounded to the nearest hundredth. In addition, the hourly data was temporally linearly disaggregated to a 15-min. timestep (i.e. hourly precipitation was equally divided into 15-minute bins). All calculations were done using R statistical software (version 3.2.2). The output from R was individual gridded 15-min. ascii files, which were then concatenated in a HEC-DSS file using the HEC Asc2dssGRid.exe tool which is a function within HEC-GeoHMS tools. The HEC-DSS file format allowed the precipitation grids to be directly read into HEC-HMS.

The gridded rainfall reconstruction was quality controlled using rain gages from a variety of data sources. The primary sources are listed below, although not all sites had data for each event:

- USGS - <https://waterdata.usgs.gov/ga/nwis/rt>
- NCEI - <https://www.ncei.noaa.gov/>
- Community Collaborative Rain, Hail & Snow Network (CoCoRaHS) - www.cocorahs.org
- Weather Underground Personal Weather Stations – <http://www.wunderground.com>
- MesoWest - <http://mesowest.utah.edu/index.html>
- RAWS - <http://www.raws.dri.edu/index.html>
- NADP - <http://nadp.sws.uiuc.edu/>
- HADS - https://mesonet.agron.iastate.edu/request/dcp/fe.phtml?network=LA_DCP
- Louisiana Agrilclimatic Information System (LAIS) - <http://weather.lsuagcenter.com/>

The temporal extent for the rainfall reconstruction was determined using the time series of rainfall and streamflow data within and in close proximity (for rain gages) to the basin. All events exhibited both bank-full discharges and minor flood discharges, which aided calibration and timing/routing of the hydrologic model. Streamflow hydrographs were collected for each event and centered on the peak flow. Paired with rain gage data, this process allowed antecedent rainfall and subsequent rainfall unrelated to the main event to be excluded from the core precipitation period. The pairing of these two datasets also helped capture ongoing flooding relating to runoff from subsequent rainfall over saturated soils. Thus, the core precipitation period of a storm could be extended as necessary. **Table 13** shows the temporal extent of each rainfall event used in the study.

Table 13: Amite Watershed Calibration Events	
Event	Dates
March 2016	March 10 (1000 CST) – March 12 (2100 CST)
August 2016	August 10 (1000 CDT) – August 21 (1900 CDT)
August 2017	August 26 (1600 CDT) – August 31 (2200 CDT)
October 2017	October 21 (1400 CDT) – October 22 (1300 CDT)

Quality control of the reconstructed Stage IV precipitation was completed for each event to ensure the gridded data was properly capturing the spatiotemporal patterns of the rainfall. Due to the highly inhomogeneous nature of heavy rainfall, a perfect rainfall reconstruction is impossible. However, with the use of nearby rainfall gages, accuracy can be estimated as to how the gridded precipitation compares to ground observations.

Stage IV accumulations are generally within 25% of independent rainfall gages, but often times are more accurate (within 10%). Daily observational data used in the analyses may be capturing a different time period than the hourly total from the reconstructed Stage IV. These errors are expected to be minimal and would only represent the fractions of rain that fell before or after the core precipitation period. For each analysis, areas of possible underestimations or overestimations by the reconstructed rainfall were circled in red and blue, respectively.

August 2017 Precipitation Event

Rainfall from the August 2017 event was associated with remnants of Hurricane Harvey that notoriously dropped over 40 in. of rain within the Houston Metroplex. As the system moved through the Amite Watershed, the southern portion of the watershed received up to 12 in. of rain. Embedded convection within the storm likely caused some underestimations by the reconstructed Stage IV rainfall as seen in **Figure 38**. However, almost all these underestimations were within the 20% bound (**Figure 39**). Interestingly, all USGS observations were ~10% less than the gridded rainfall. Typically, their gages are mounted to the side of a bridge, so perhaps this caused interference with the tipping bucket. Analysis of wind speeds and USGS gage climatology were outside the focus of this study, but could also help explain the low estimates of the USGS gage totals. A bias correction was applied to the USGS gages (not shown) and storm totals at these gages were moved to within 10% of reconstructed Stage IV precipitation data.

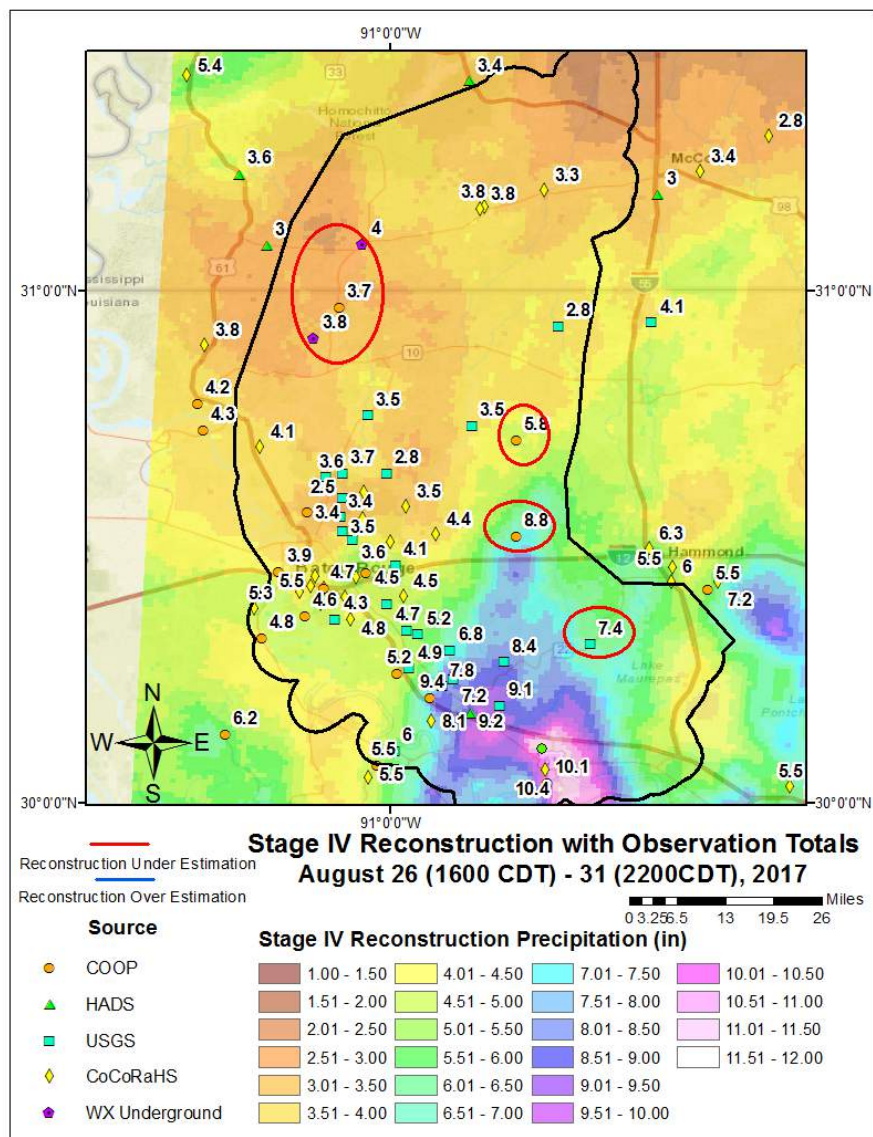


Figure 38:
 Reconstructed rainfall with observations overlaid for the August 2017 event. Areas circled in red (blue) are underestimated (overestimated) by reconstructed Stage IV data.

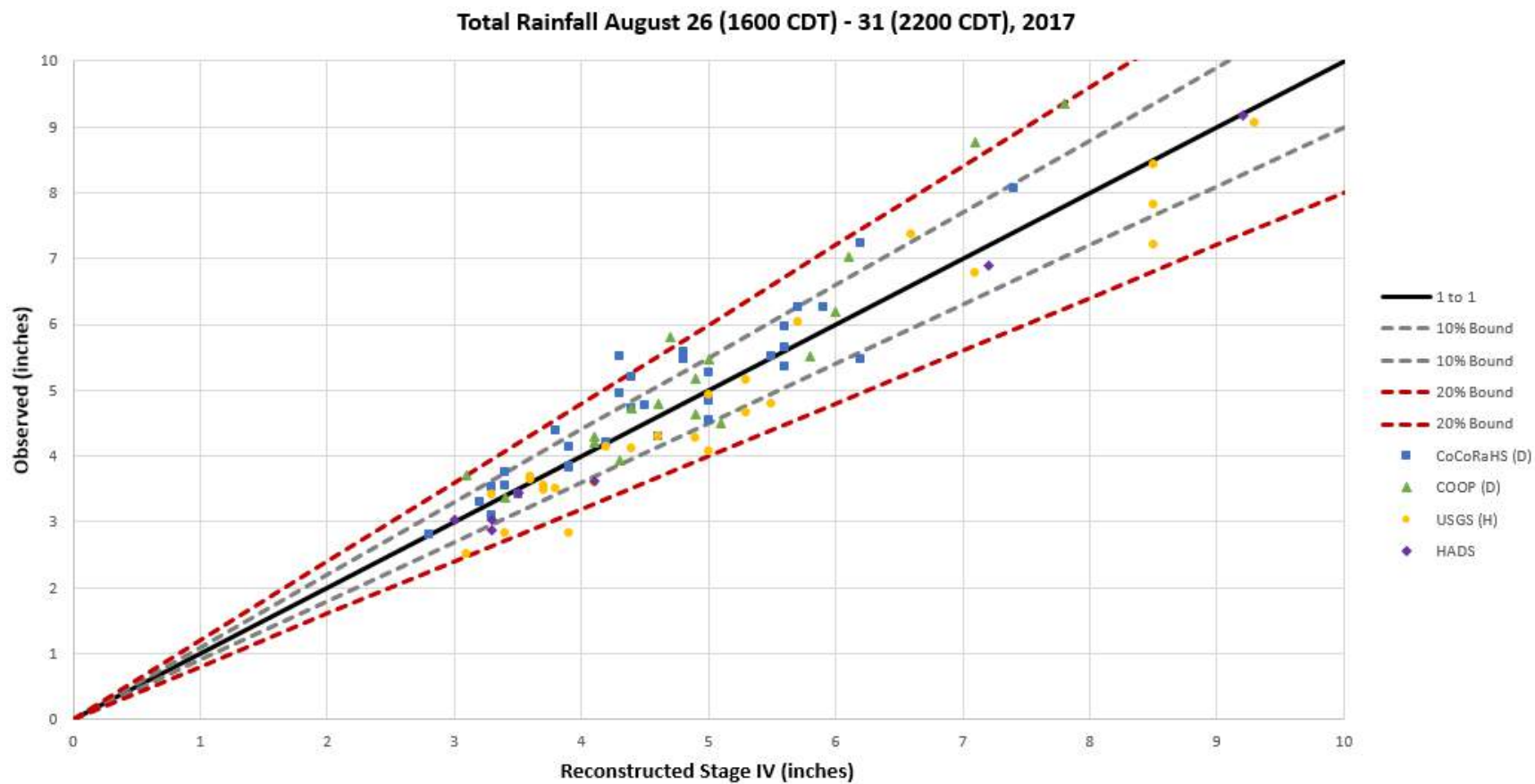


Figure 39: Scatter plot of the reconstructed Stage IV rainfall and observed data with a 10% and 20% error bound.

October 2017 Precipitation Event

Heavy rainfall from the October 2017 event was generally limited to the Mississippi and Louisiana border with totals up to 9.5 in. (**Figure 40**). Unfortunately, this remote area has limited gage data, so the quality control check was limited. Over gaged areas, the reconstruction and observation data were mostly within 10% agreement. **Figure 41** once again shows USGS gages being underestimated when compared to the reconstructed precipitation. After another bias correction, the two are within 10% of one another (not shown). Within the domain, the largest difference between the observations and reconstructed rainfall were up to 0.5 in. Thus, the gridded rainfall was deemed reasonable to serve as input into H&H modeling.

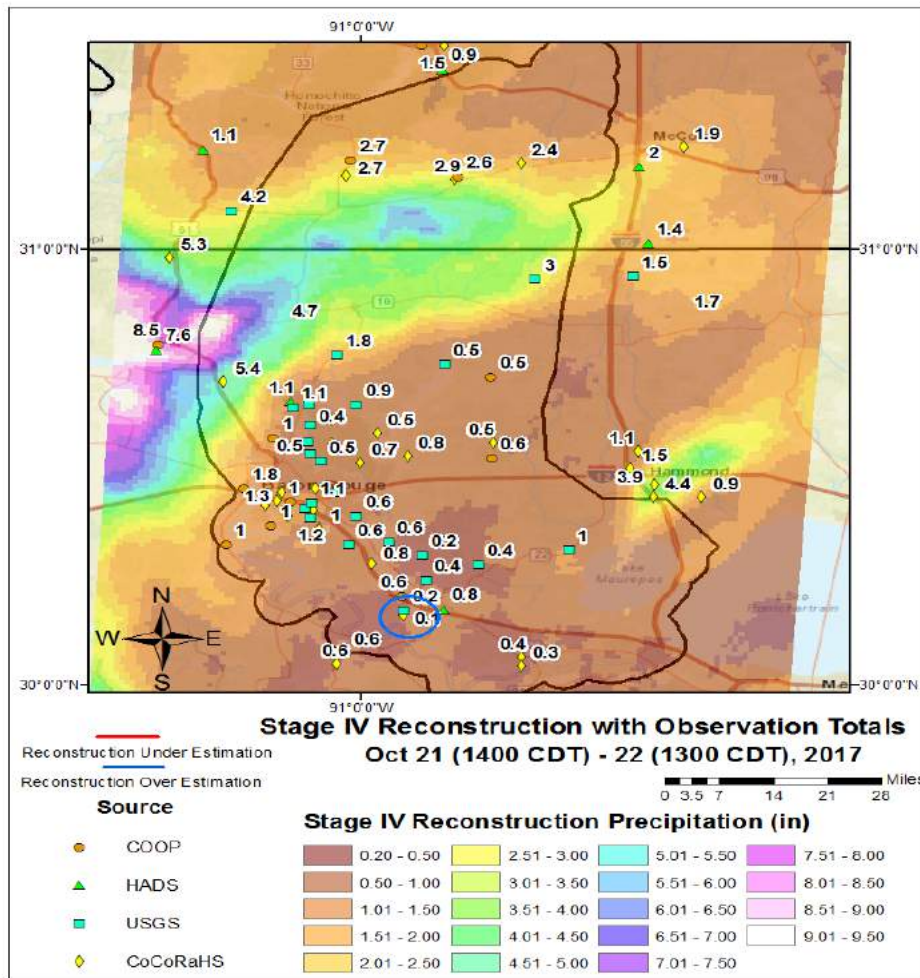


Figure 40: Reconstructed rainfall with observations overlaid for the October 2017 event. Areas circled in red (blue) are underestimated (overestimated) by reconstructed Stage IV data.

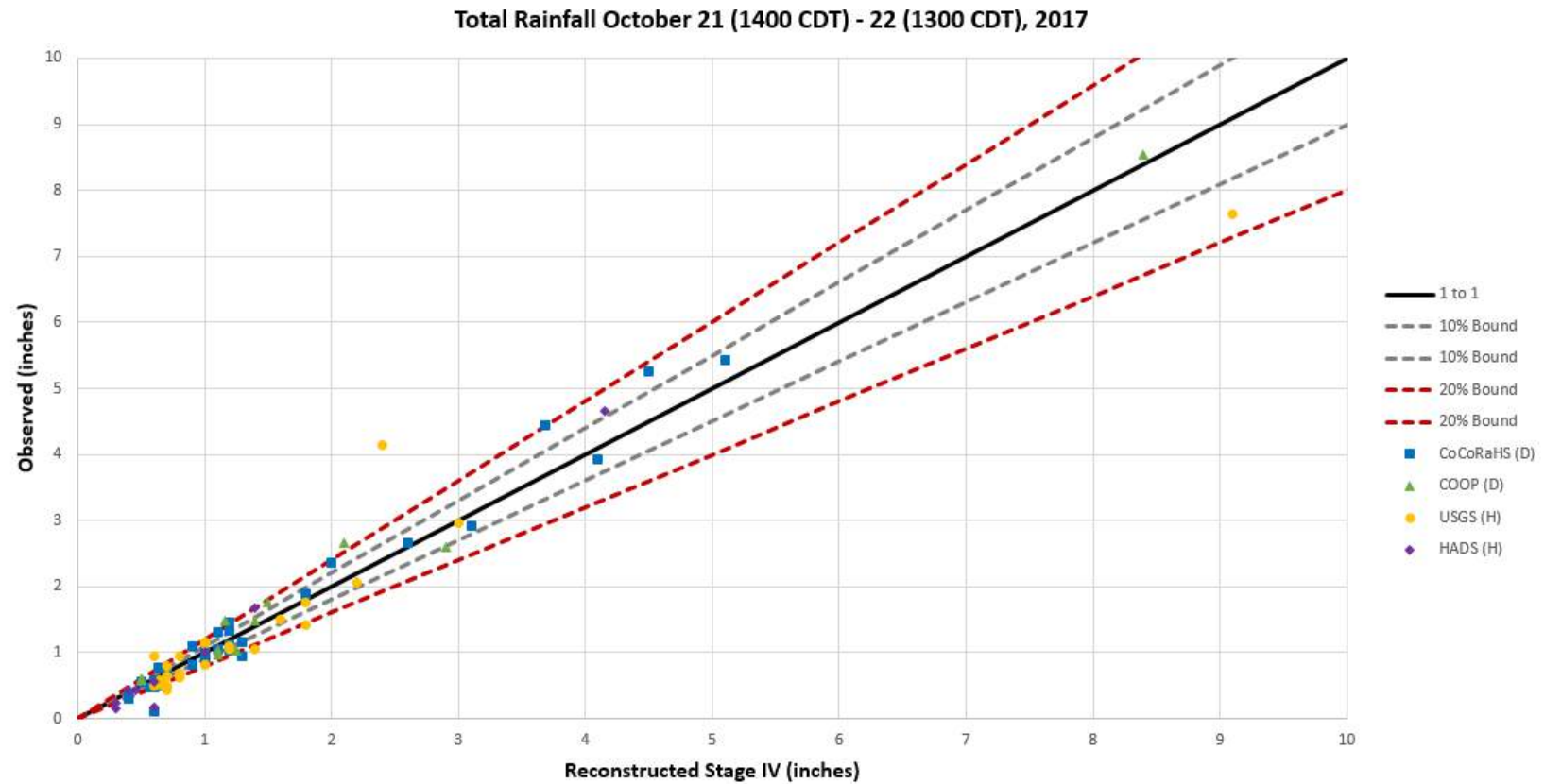


Figure 41: Scatter plot of the reconstructed Stage IV rainfall and observed data with a 10% and 20% error bound.

March 2016 Precipitation Event

Figure 42 and **Figure 43** show the reconstructed Stage IV with observations overlaid and the scatter plot comparing the reconstructed Stage IV totals at the observation gages for the March 2016 event. The 60-hr event is characterized by moderate rainfall over the south, central portion of the domain with storm totals up to 13 in. Underestimations by the reconstructed Stage IV rainfall north of Donaldsville (circled in red) were up to 2 in. However, the area of underestimation was limited in areal extent and therefore did not decrease flows in the area within the hydrology model.

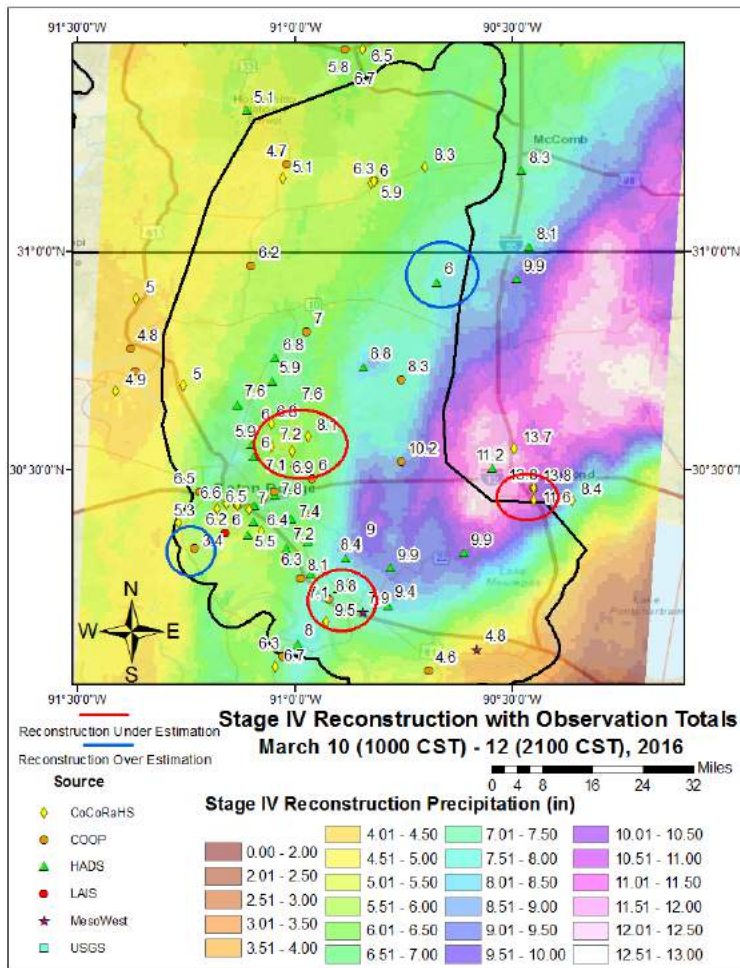


Figure 42: Reconstructed rainfall with observations overlaid for the March 2016 event. Areas circled in red (blue) are underestimated (overestimated) by reconstructed Stage IV data.

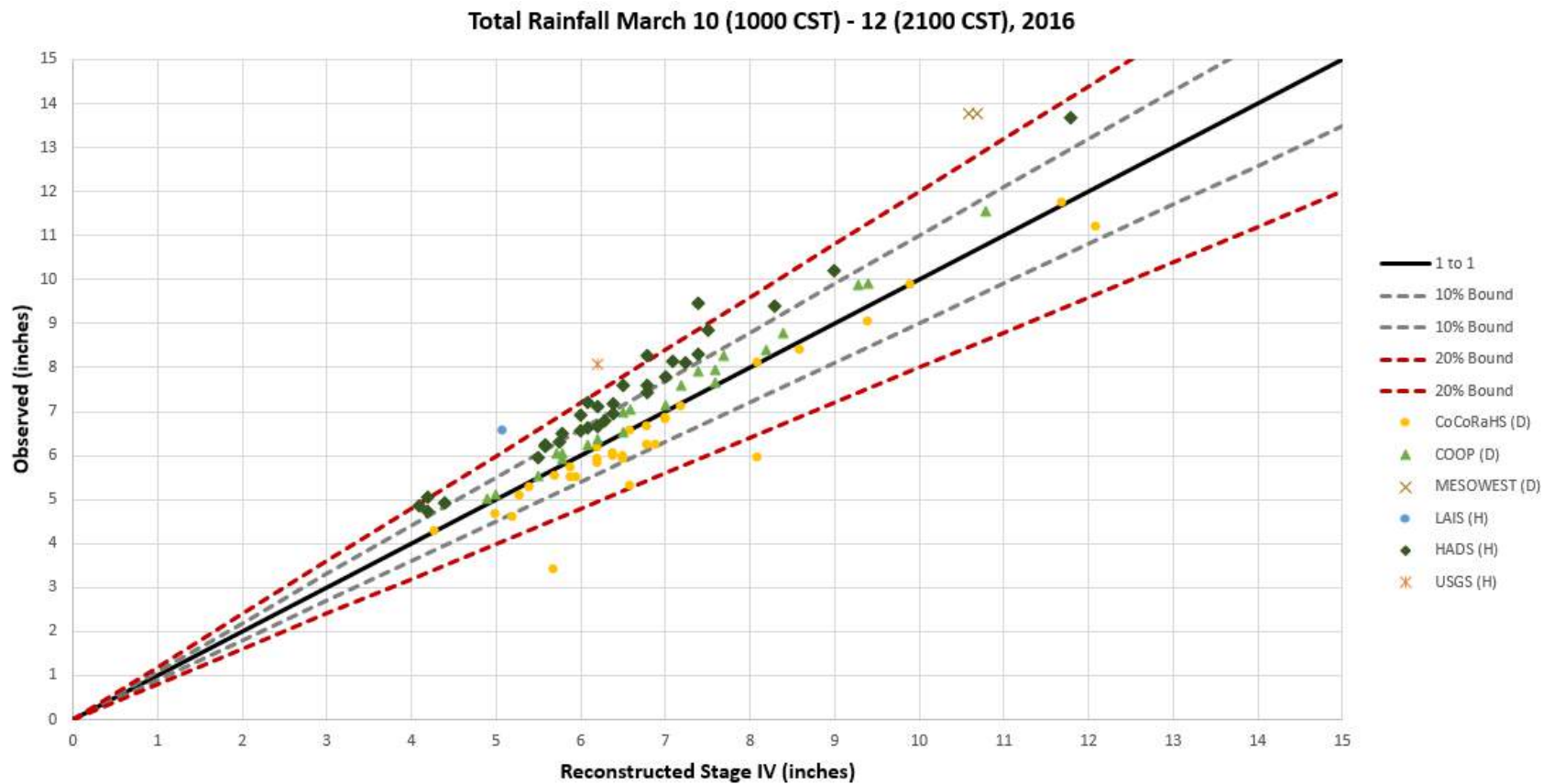


Figure 43: Scatter plot of the reconstructed Stage IV rainfall and observed data with a 10% and 20% error bound.

August 2016 Precipitation Event

Figure 44 shows a comparison of the reconstructed and observed data for the August 2016 event, on the interpolated Stage IV 1-km grid. A slow moving Low pressure system paired with high amounts of atmospheric moisture lead to historical flooding in southeast Louisiana. The highest recorded value for the storm was 31.39 in. just outside of Watson, Louisiana. **Figure 45** is a scatter plot comparing Stage IV estimates with observations, along with 10% error bound for reference. All errors were under 20%, and the majority of estimates were within 10% of the gage reading. Furthermore, the final amounts did not conflict with other literature published by the National Weather Service or other reliable media sources. Areas circled in red show possible underestimation by the reconstructed Stage IV data, and areas overestimated by Stage IV are circled in blue. Most of these errors occur in areas of tight precipitation gradients. After comparing to all precipitation gages, total rainfall values were initially deemed reasonable to serve as input into H&H modeling.

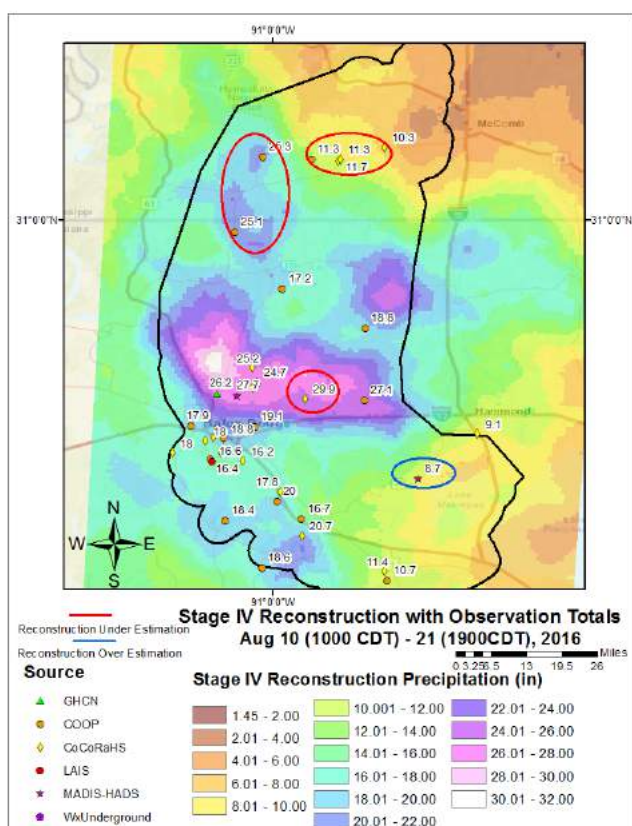


Figure 44: Reconstructed rainfall with observations overlaid for the August 2016 event. Areas circled in red (blue) are underestimated (overestimated) by reconstructed Stage IV data.

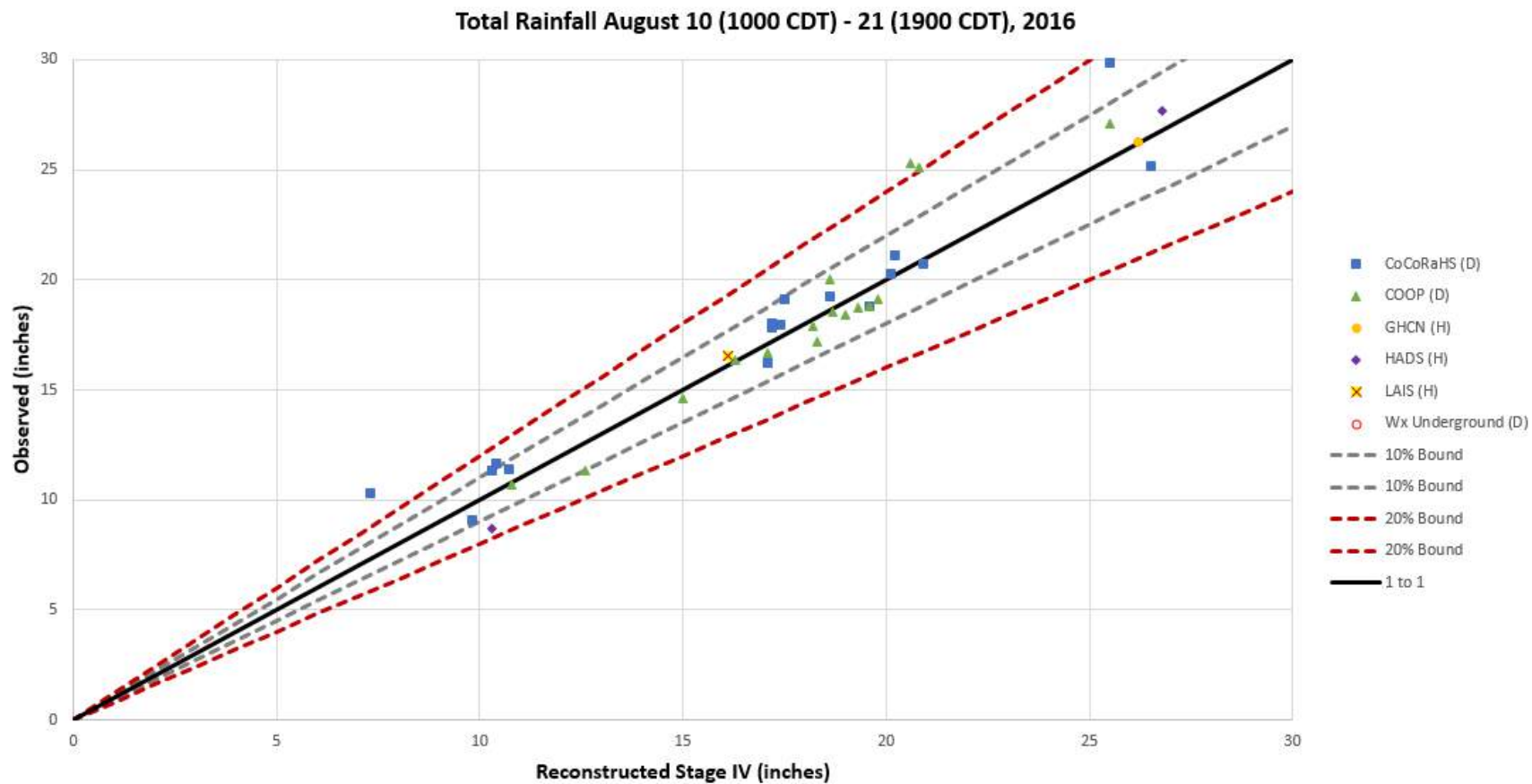


Figure 45: Scatter plot of the reconstructed Stage IV rainfall and observed data with a 10% and 20% error bound.

HEC-HMS Calibration

The ARB HEC-HMS model was calibrated using the four precipitation events reconstructed using Stage IV data. The gridded rainfall data was applied to the HEC-HMS model to simulate the observed flood hydrographs which deliver flow inputs to the HEC-RAS hydraulic model. It should be noted that while the ARB HEC-HMS model does contain hydrologic routing reaches, only routed reaches within the state of Mississippi and those in a limited number of reaches leading to the 1D Amite River and Comite River reaches are used by the Dynamic ARB HEC-RAS model.

All hydrologic routing within the Louisiana portions of the Amite River and Comite River are performed using the dynamic HEC-RAS model within both 1D and 2D domains receiving inflows directly from the HEC-HMS subbasin outflows through the connected HEC-DSS database. This allows for more advanced dynamic routing to be performed using the full Saint Venant equation as used for both the 1D and 2D HEC-RAS computation engines. Therefore with the exception of the limited number hydrologic routing reaches within Mississippi, only subbasin losses were calibrated within HEC-HMS. Subbasin transforms were validated through the review of the HEC-RAS results and were demonstrated to provide only minor sensitivity to the flows within the ARBNM.

The sensitivity of the Green & Ampt parameters used in the HEC-HMS model was tested by varying each parameter individually. Initial water content and hydraulic conductivity appeared to be the two most sensitive loss parameters for sub basins and were the primary focus for calibration.

To calibrate the subbasin losses, observed losses were determined for the four precipitation events by estimating the excess precipitation. Excess precipitation was estimated at all locations where USGS streamflow data was available for the precipitation events. This was determined as:

$$\text{Excess Precipitation (\%)} = \frac{\text{Hydrograph Volume} - \text{Baseflow Volume}}{\text{Basin Averaged Precipitation Volume}}$$

Whereby:

- Hydrograph Volume represented the total volume of water for the flood event observed at the USGS gage (area under hydrograph).
- Baseflow Volume represented the volume of water estimated to be from baseflow (area under linear interpolation of initial and end of storm baseflow hydrograph).
- Basin Averaged Precipitation Volume represented the average precipitation depth upstream of the USGS gage determined from Stage IV data multiplied by the drainage area.

Initial water content was estimated by comparing the cumulative basin averaged precipitation with the hydrograph response at USGS Streamflow gages. When a significant hydrograph response was observed, the cumulative precipitation for that instance in time was noted and assumed to be representative of the initial water content as illustrated in **Figure 46**. Basin average initial water contents were applied to the HEC-HMS model for individual storms.

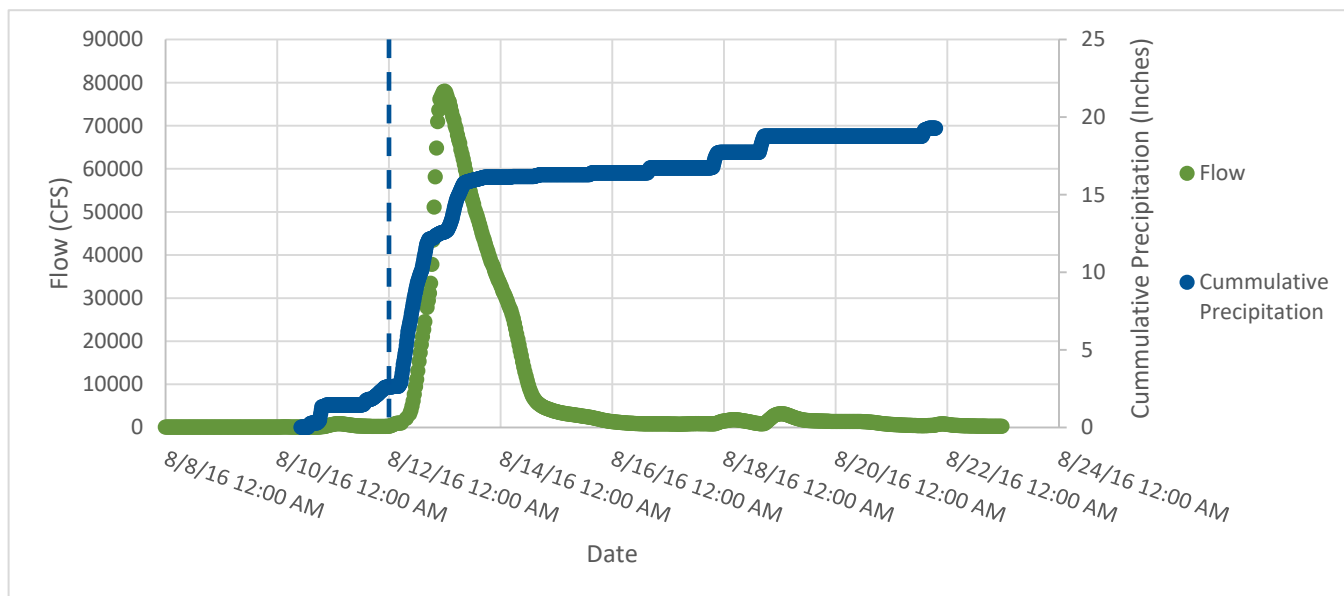


Figure 46: Estimation of initial water content for the August 2016 flood event for the basin upstream of USGS Gage 07377500, Comite River near Olive Branch. At approximately 12:00 AM on August 12th, 2016, the river began to respond after receiving 2.3 in. of cumulative precipitation.

Excess precipitation and initial water content for each of the five USGS streamflow gages locations are summarized in **Tables 14-17** for the four observed precipitation events. It should be noted that during the August 2016 flood, several streamflow gages were unable to report peak discharges due to a number of reasons including damage to gages and backwater influences which invalidated rating curves.

Table 14: August 2017 Precipitation Event Observations

USGS Gage Location	Observed Hydrograph Volume at Gage (acre.ft.)	Drainage Area at Gage (square mi.)	Average Precipitation Depth Upstream of Gage from Radar Rainfall (in.)	Initial Abstraction Estimated from Hydrograph/Hyetographs (in.)	Observed Excess Rainfall (observed hydrograph volume/precipitation volume)
07377500 Comite River Nr Olive Branch	9,400	145	3.3	1.3	37%
07378000 Comite River Nr Comite	22,000	284	3.3	0.6	44%
07377000 Amite River Nr Darlington	27,500	580	3.3	1.3	27%
07378500 Amite River Nr Denham Springs	78,000	1,280	3.4	1.5	34%
07380120 Amite River at Port Vincent	98,000	1,596	3.6	1.2	32%

Table 15: October 2017 Precipitation Event Observations

USGS Gage Location	Observed Hydrograph Volume at Gage (acre.ft.)	Drainage Area at Gage (square mi.)	Average Precipitation Depth Upstream of Gage from Radar Rainfall (in.)	Initial Abstraction Estimated from Hydrograph/Hydrographs (in.)	Observed Excess Rainfall (observed hydrograph volume/precipitation volume)
07377500 Comite River Nr Olive Branch	46,000	145	4.2	1.6	144%
07378000 Comite River Nr Comite	34,000	284	3.3	0.7	69%
07377000 Amite River Nr Darlington	33,000	580	2.7	3.3	39%
07378500 Amite River Nr Denham Springs	98,000	1280	2.5	0.6	57%
07380120 Amite River at Port Vincent*	79,500	1596	2.2	0.3	42%

Table 16: March 2016 Precipitation Event Observations

USGS Gage Location	Observed Hydrograph Volume at Gage (acre.ft.)	Drainage Area at Gage (square mi.)	Average Precipitation Depth Upstream of Gage from Radar Rainfall (in.)	Initial Abstraction Estimated from Hydrograph/Hyeto graphs (in.)	Observed Excess Rainfall (observed hydrograph volume/precipitation volume)
07377500 Comite River Nr Olive Branch	38,000	145	5.9	2.3	84%
07378000 Comite River Nr Comite	73,000	284	6.1	1.0	79%
07377000 Amite River Nr Darlington	137,500	580	6.1	2.0	73%
07378500 Amite River Nr Denham Springs	426,000	1280	6.3	2.4	99%
07380120 Amite River at Port Vincent*	344,000	1596	6.4	1.0	64%

Table 17: August 2016 Precipitation Event Observations

USGS Gage Location	Observed Hydrograph Volume at Gage (acre.ft.)	Drainage Area at Gage (square mi.)	Average Precipitation Depth Upstream of Gage from Radar Rainfall (in.)	Initial Abstraction Estimated from Hydrograph/Hyeto graphs (in.)	Observed Excess Rainfall (observed hydrograph volume/pre cipitation volume)
07377500 Comite River Near Olive Branch	191,500	145	19.8	2.3	125%
07378000 Comite River Near Comite	NA	284	22.4	1.5	NA
07377000 Amite River Near Darlington	305,500	580	11.5	1.2	86%
07378500 Amite River Near Denham Springs	107,000	1280	17.0	2.4	92%
07380120 Amite River at Port Vincent*	NA	1596	17.1	1.1	NA

Validation of Excess Precipitation Observations

To validate the excess precipitation observations, the data was reviewed and cross-checked to identify and verify potential outliers or potential issues requiring further consideration. **Table 18** summarizes the range of precipitation excess and potential outliers for each of the four precipitation events. As can be seen, three potential outliers have been flagged. These are generally those with hydrograph volumes that approach or exceed the observed precipitation that fell upstream of the gage. In at least two instances, the observed hydrograph volume exceeds the actual precipitation volume that is estimated to have fallen on the basin.

Table 18: Summary of Excess Precipitation				
Precipitation Event	Range of Excess Precipitation	Potential Outliers	Range Excluding Outliers	Average Excess Precipitation Excluding Any Outliers
August 2017	27% - 44%	None	N/A	35%
October 2017	39% - 144%	144% (07377500)	39% - 69%	52%
March 2016	64% - 99%	99% (07378500)	64% - 84%	75%
August 2016	86% - 125%	125% (07377500)	86% - 92%	89%

The largest outlier is the 144% excess precipitation estimated at Gage 07377500, Amite River near Olive Branch for the October 2017 flood event. To verify this, the volume at this gage was compared to gage 07378000 Comite River near Comite which indicated a decrease in hydrograph volume from 46,000 acre.ft. at Olive Branch to 34,000 acre.ft. at Comite demonstrating a decrease in the downstream direction. Since there were no major diversions upstream of these gages, this indicated a potential error in either precipitation or stream flow records.

To isolate the potential outlier, the Comite River Near Comite gage was compared to the Amite Near Darlington gage (upstream of the Comite River confluence) and Amite Near Denham Springs gage (downstream of the Comite River confluence) to determine a drainage area weighted comparison between observed hydrograph volumes both upstream and downstream of the Amite River and Comite River confluence as illustrated in **Figure 47**.

This would strongly suggest that the streamflow estimated at 07377500 Comite River near Olive Branch for the October 2017 flood is erroneous and was therefore discounted as an outlier in the calibration. The hydrograph shape however was utilized for calibration of hydrograph timing. Since other potential outliers were not so extreme, the source of potential error could not so easily be isolated.

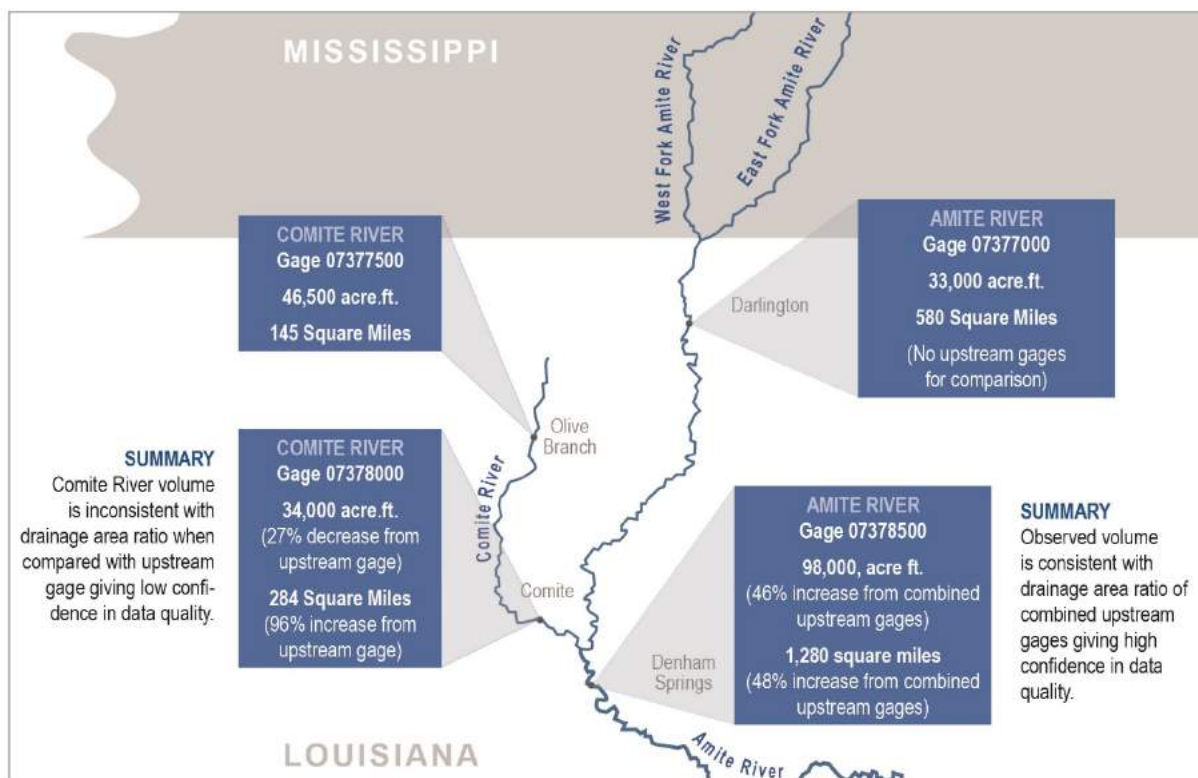


Figure 47: Validation of Gages for October 2017 Event

Initial HEC-HMS runs generally indicated that all four precipitation events underestimated the rainfall totals required to generate observed flood volumes at USGS gages.

Upon closer look, over the Comite at Olive Branch, rainfall was underestimated by 17 to 19% when compared to the NWS Cooperative Observer Program (COOP) stations at Norwood and Gloster. Precipitation was increased over this area using a mask approach. First, storm centers were identified and isohyets were drawn appropriately. Then, storm total rainfall was increased by using multiple factors for each of the isohyet areas. The factor was applied uniformly across time as to not alter the temporal distribution of the storm, but only the magnitude. Adjusted storm totals at the COOP stations after applying the mask were then within 1% of the observations.

Looking upstream, there were also extreme underestimations in streamflow over the Darlington sub-basin implying rainfall was also underestimated by the Stage IV data over this sub-basin. Over the southern portion of the basin, there were two CoCoRaHS stations and one COOP station that indicated a strong rainfall gradient. The COOP station (orange circle in the middle mask **Figure 48**) indicated the reconstructed Stage IV data was overestimating rainfall by 12%, whereas the CoCoRaHS stations (yellow diamonds in the middle mask **Figure 48**) indicated the reconstructed Stage IV data was underestimating rainfall by 9-11%. The distance from the COOP station to the CoCoRaHS stations was only about 4 mi., which is why it is believed a strong rainfall gradient was present. The northern most CoCoRaHS station (yellow diamond in the northern mask, **Figure 48**), also suggests rainfall was underestimated upstream

of Darlington. The difference between the reconstructed Stage IV data and CoCoRaHS observation further north was 29%.

Rather than apply one mask over the entire northern area, two masks were created in hopes to smooth the strong rainfall gradient and account for the different magnitudes of underestimation. Starting with the central mask, it was important to make sure a realistic gradient between the other two areas was achieved as well as staying within the 10% rainfall error bound. After applying the mask, the adjusted storm totals at the two CoCoRaHS stations stayed within the 10% error bounds; however, the adjusted storm total at the COOP station did not. The adjusted storm total at the COOP station was 15.5 in., which is 4.2 in. higher than the observation or a 37% overestimation. Several interactions of the mask were completed to try to reduce the error, but none properly captured the necessary rainfall gradient and produced the observed streamflows. Subjectively, the mask used was the best compromise although there was the possibility of some overestimation of rainfall near the COOP station. The area of error should be small enough to not affect the basin-wide rainfall. Over the larger, northern mask, the adjusted storm totals at the CoCoRaHS station were within 0.7 in. of the observation, which reduced the error from 29% to 7%. Unfortunately, no other observations were available, so this mask and subsequent increase in rainfall are assumptions for the ARB upstream of Darlington.

One source of potential error was identified to be from the NRCS SSURGO data whereby soils were observed to change suddenly from Clay Loam in Louisiana to more pervious Silt Loam in Mississippi at the state line. Since it was unreasonable for soils to change at state lines and all indications were that runoff volumes were being underestimated by either the Green Ampt methodology or as a result of rainfall underestimation, it was assumed that the Mississippi Silt Loam was the same soil type as the less pervious Clay Loam in Louisiana, consequently reducing the soil conductivity. Additionally, to more closely replicated observe flood volumes, soil conductivity values were reduced globally to more reasonably match observed runoff volumes for all four calibration events. Care was taken to avoid over forcing parameters given the uncertainty of observed data and methodologies.

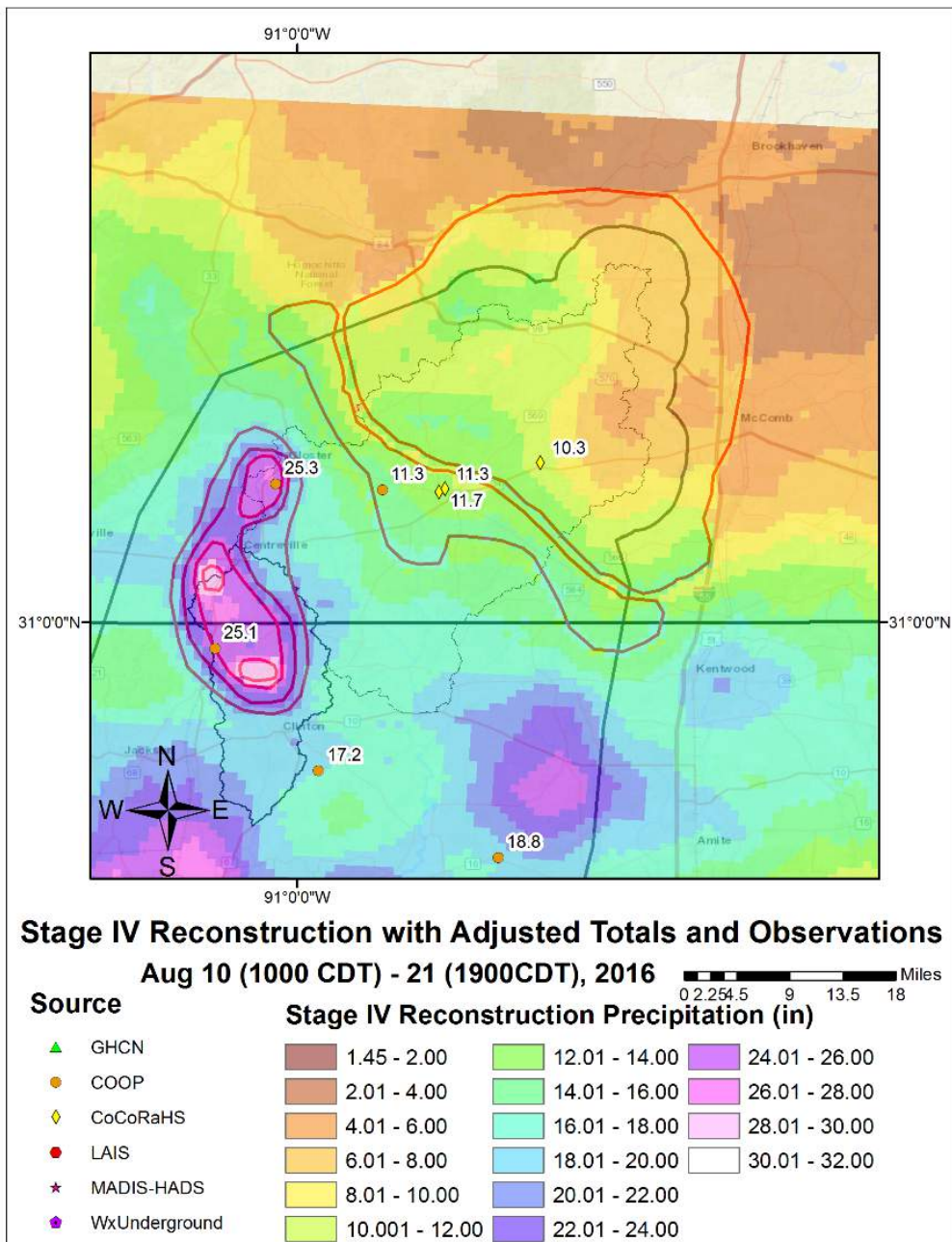


Figure 48: Adjusted reconstructed rainfall with observations and mask overlaid for the August 2016 event. Three sets of masks were created for the event as observations of rainfall and streamflow (Comite at Olive Branch and Darlington) indicated underestimations in the reconstructed rainfall.

HEC-RAS CALIBRATION

The ARB HEC-RAS model was calibrated using the four precipitation events reconstructed using Stage IV rainfall data in addition to the January 2018 and June 2018 observed hydrographs for small in channel flows. As previously noted, the dynamic HEC-RAS model within both 1D and 2D domains receives inflows directly from the HEC-HMS subbasin outflows through the connected HEC-DSS database allowing the flows to be routed using the full Saint Venant equation rather than the simplified HEC-HMS hydrologic routing methods.

The process of hydraulic calibration was performed incrementally beginning with the smaller floods and building up to the larger floods. Initially hydrograph timing was the primary focus for smaller events including those in channel events, however as the magnitude of events increased, an incrementally greater focus was given to the peak discharges and flood elevations.

When calibrating flood elevations, the modeled profile within HEC-RAS was carefully reviewed to make a visual determination as to whether normal flow was occurring. Where normal flow was observed, Manning's N values were adjusted to reasonably recreate observed elevations. Where backwater impacts were observed from hydraulic structures including bridges, culverts and weirs, the associated parameters including bridge modeling approaches and weir coefficients were adjusted to better calibrate to observed elevations.

Use of HEC-RAS Flow Roughness Factors in the ARB HEC-RAS Model 1D Reaches

The timing of hydrographs at USGS gages throughout the basin were reviewed for a range of historic flow events to determine the flood wave travel time between gages. This indicated that the flood wave travel time varied considerably for different events suggesting that a single Manning's N value would be inappropriate to recreate a range of flood magnitudes. To further validate this theory, steady state simulations were performed using the ARB HEC-RAS model for observed instantaneous peak flows. Manning's N values were adjusted to match observed stages for several historic flow events. When performing these simulations, it was observed that Manning's N values varied considerably and generally

Geometry - Roughness Change Factors

Roughness Factor Data

Set: *riv: ComiteRiver rch: Abv_PrettyC rs: 342648.6 to 309785.9*

Add Copy Delete

River: ComiteRiver

Reach: Abv_PrettyC

Upstream Riv Sta: 342648.6

Downstream Riv Sta: 309785.9

Auto-Generate Flow Column

Uniform Spacing ... Exponentially Increasing ...

	Flow	Roughness Factor
1	0	4
2	45	2.5
3	100	2
4	200	1.6
5	450	1.15
6	1000	1.1
7	10000	1.25
8		
9		
10		
11		
12		
13		

Import Calibration Factors ... OK Cancel

Figure 49: HEC-RAS Flow Roughness Factors Option

decreased with increasing flows. To account for these observations, the HEC-RAS Flow Roughness Factors option was utilized for all reaches along the Amite River and Comite River within the dynamic model. The HEC-RAS Flow Roughness Factors option allows users to apply a multiplication factor to the assigned N values corresponding to flow thresholds as illustrated in **Figure 49**.

Low Flow Calibration for January 2018 and June 2018 Flow Events

Low flow calibration using the January 2018 and June 2018 flow events was performed on the Amite River and Comite River simply by applying observed hydrographs individually at cross sections that corresponded to USGS gage locations. The flood wave was then tracked downstream to the next USGS gage where the arrival and peak timing of the flood wave was compared to observed data. For low flows, the flood wave was generally observed to arrive early on initial runs. Therefore flow roughness factors greater than 1 were applied to the range of flows being simulated and the simulation was rerun until a reasonable agreement of flood wave timing was observed. Calibration of the January 2018 event, which was generally less than a half bank full event typically required flow roughness factors in the range of 2 to 4 to achieve a reasonable match. Flow roughness factors rapidly decreased as the flows approached bank full where a factor close to 1 was typically appropriate.

Calibration of the August 2017, October 2017, March 2016 and August 2016 Flood Events

The calibrated HEC-HMS flows for the August 2017, October 2017, March 2016 and August 2016 floods were used to incrementally calibrate the HEC-RAS models. The August 2017 and October 2017 floods generally represented near bank full flows with some shallow flooding in the overbanks. These were used to calibrate the in channel N values while also adjusting Flow Roughness Factors to obtain better timing of the flood hydrographs and better match peak discharges. The March 2016 and August 2016 floods represented large and major floods respectively. While some adjustments were made to Flow Roughness Factors, a primary focus was on calibrating to the observed HWMs previously documented. RAS Mapper was utilized extensively to compare results to the HWMs as illustrated in **Figure 50** for the August 2016 flood event. It should be noted that generally only minor changes to N values were required during these high events which can be attributed to the detailed calibration of N values during smaller events. Often discrepancies in elevations were attributed to model geometry requiring refinements to 2D Flow Areas generally to allow flow through embankments which would pond up flows.

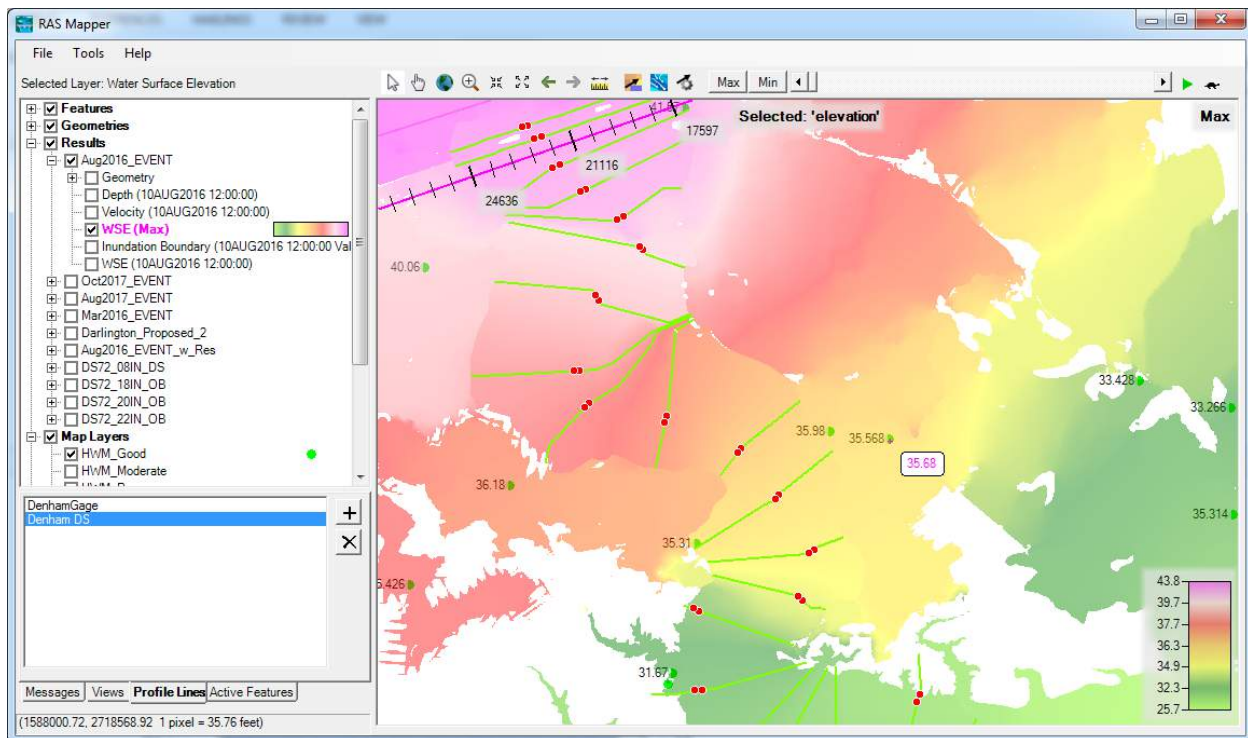


Figure 50: HWMs were added to RAS Mapper and labeled to enable a rapid assessment of the accuracy of the HEC-RAS model by simply activating the Water Surface Elevation Grid (WSE) and hovering the cursor over the observed HWM.

It should be noted that when the HEC-RAS Plot Stage and Hydrograph function is used to compare observed and modeled flows, the observed flow represents the full flow reported at the USGS gage, however the modeled flow reported only represents the portion of the location modeled in 1D. **Figure 51** would initially appear that the model underestimates the observed flow by approximately 45% at the USGS gage near Denham Springs for the August 2016 flood since overbank flow modeled in 2D is not reported. In these situations where modeled flows are represented by both 1D and 2D methods, RAS Mapper should be used to draw Profile Lines which can be used to plot Flow Time Series across both 1D and 2D reaches as illustrated in **Figure 52**. This indicated that the modeled flow is actually within 9% of the observed peak and well within the expected uncertainty of the flow reported by the USGS gage given the unconfined nature of the overbank flooding.

Figure 51: The HEC-RAS Plot Stage and Flow Hydrographs function can be misleading when comparing observed and modeled hydrographs in areas of coupled 1D and 2D modeling since it does not account for 2D overbank flows as demonstrated here for the Amite River Near Denham Springs where flows are under estimated by only reporting flows contained within the 1D portion of the floodplain.

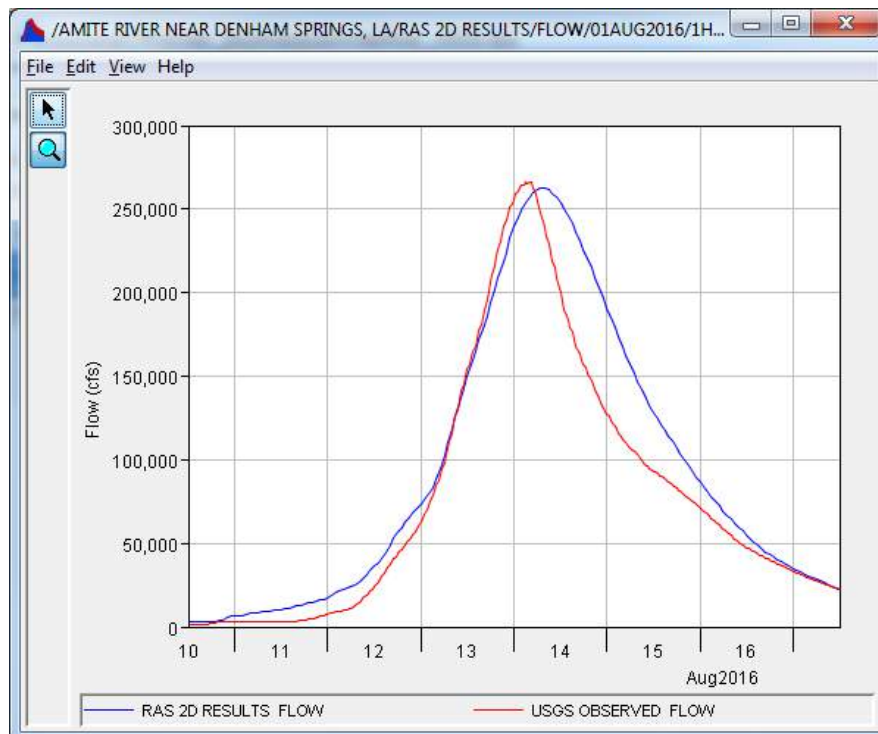
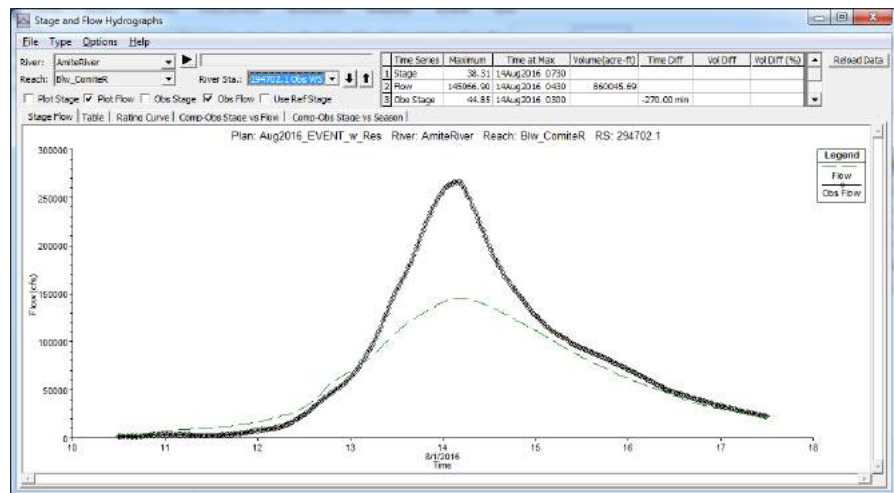


Figure 52: By utilizing the Plot Flow Time Series function for Profile Lines drawn across both the 1D and 2D regions of a model will provide a comprehensive insight into the observed hydrograph where both 1D and 2D modeling methods are used as demonstrated here for the Amite River Near Denham Springs, more accurately representing the floodplain than the method demonstrated in Figure 51.

DESIGN FLOOD SIMULATIONS

The design flood plans within the ARBNM are intended to provide users with an array of options to simulate the 20%, 10%, 4%, 2%, 1%, 0.2% and 1%+ Annual Exceedance Probability (AEP) floods (also referred to as the 5-, 10-, 25-, 50-, 100-, 500- and 100+-year flood respectively). Due to the large size of the ARB and the highly irregular nature of precipitation events, it would be impossible to simulate a flood event with a single meteorological storm that would generate a consistent AEP flood throughout the basin. As is demonstrated during the observed August 2016 flood, the AEP of the peak flood discharge varied significantly along the Amite River. At Darlington the peak was estimated to be approximately a 1% AEP flood, and at Denham Springs, the peak discharge exceeded the 0.2% AEP flood (as will be further demonstrated in **Table 23**). However upstream on the East Fork of the Amite River near Peoria, MS, the August 2016 flood did not even register as the largest peak of that water year.

A design storm approach was developed that can be used for multiple storm centers selected by the user within the ARB. It should be noted that there are many factors associated with a precipitation event and resultant flood that impact the AEP of the flood including the basin antecedent moisture conditions, storm duration, storm intensity, storm center, storm track and current streamflow conditions. Therefore, the AEP of a precipitation event rarely equals the same AEP of the resultant flood event, and storms have the ability to generate floods of both more and less frequent AEPs.

The development of the design storm plans within the ARBNM involved four key steps:

- Flood frequency analysis at all suitable USGS stream gages to estimate AEP magnitude
- Development and selection of design storm spatial distribution, temporal distribution, and magnitude
- Simulation of design storms with multiple centers and precipitation depths to make recommendations on which storms to use to generate a specific AEP flood
- Development of a suite of design boundary Conditions

Flood Frequency Analysis

To estimate the peak magnitude of an AEP flood at key locations within the watershed, a flood frequency analysis was performed on all of the USGS gages reporting annual peak streamflow measurements with at least 15 years of record. To advise users of the potential uncertainty in estimates, the 90% confidence interval was calculated for both the upper and lower bounds of the estimate. The potential range of uncertainty of an AEP estimate at the 90% confidence level generally decreases when a larger period of record is available while similarly the range of uncertainty will be smaller for more frequent AEP floods.

There are over 33 active USGS stream gage sites in the ARB although many of these report only stage and not flow. Of these 33 gages, 22 are located upstream of the Amite River Diversion Canal and only 7 had at least 15 years of streamflow. Of those, five of the seven had flow estimates for the 2016 flood. Five gages from the adjacent Tangipahoa and Tickfaw watersheds were added to the analysis to ensure the results were consistent throughout the

region and help validate areas within the upper ARB that do not have adequate gaging. **Figure 53** demonstrates the location of the gages analyzed within the ARB and **Table 19** provides a summary of the data available at these gages.

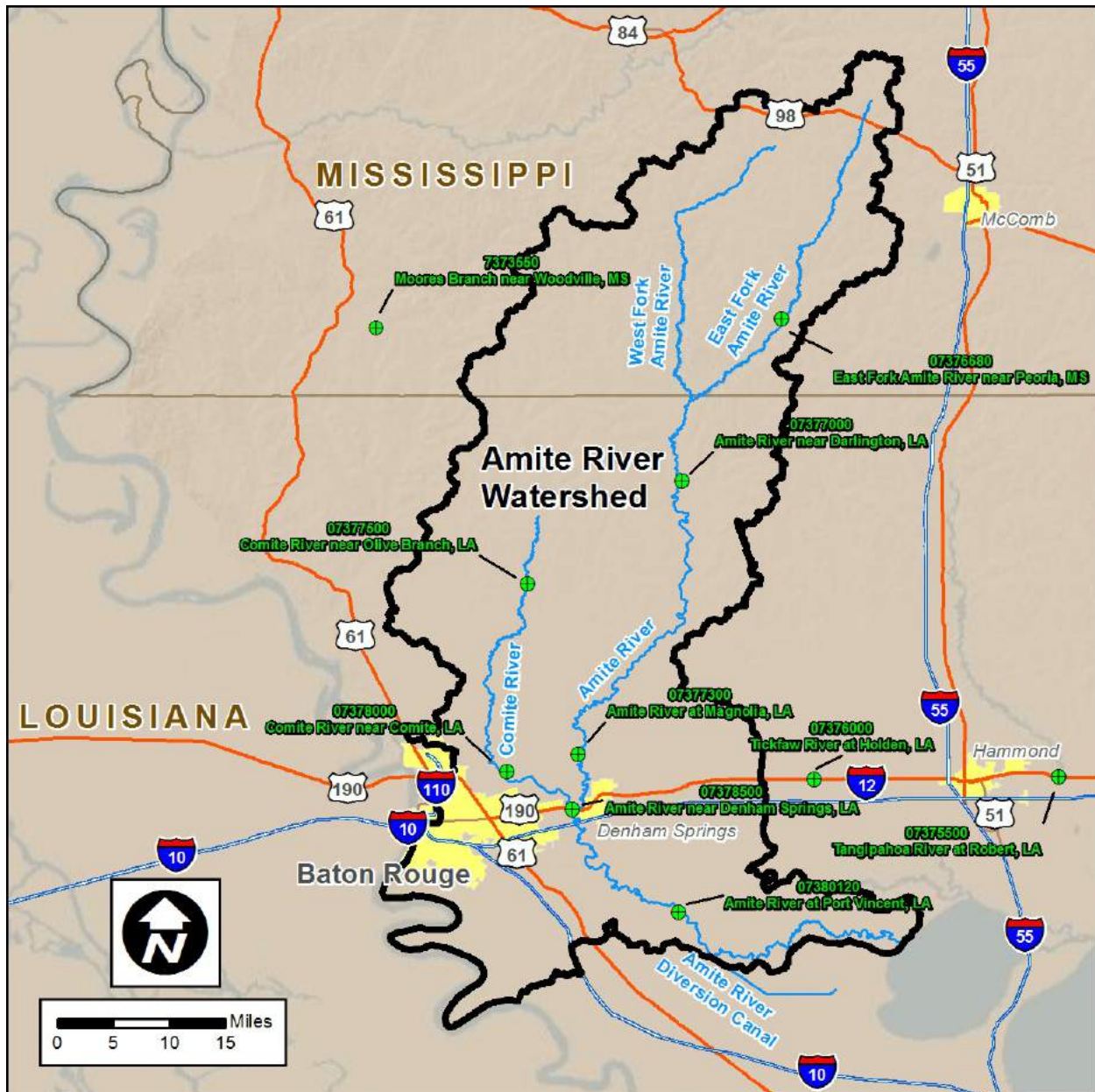


Figure 53: USGS streamflow gages used in the Flood Frequency Analysis

Table 19: Summary of Stream Gages used within the Analysis

USGS Station	Gage Name	Drainage Area (sq mi)	# of Records	Period of Record	2016 Flow Estimate	Watershed
07373550	Moore's Branch nr Woodville, MS	0.21	62	1955-2017	Yes	Tangipahoa
07375500	Tangipahoa River at Roberts	646	79	1939-2017	Yes	Tangipahoa
07376000	Tickfaw R at Holden, LA	247	77	1941-2017	Yes	Tickfaw
07376679	East Amite R nr Peoria, MS	179	21	1990-2016	Yes	Amite
07377000	Amite R nr Darlington, LA	580	69	1949-2017	Yes	Amite
07377300	Amite R at Magnolia, LA	884	58	1949-2017	Yes	Amite
07377500	Comite R nr Olive Br, LA	145	75	1943-2017	Yes	Amite
07378000	Comite R nr Comite, LA	284	73	1944-2016	Yes	Amite
07378500	Amite R nr Denham Springs, LA	1,280	80	1921-2017	Yes	Amite
07380120	Amite R at Port Vincent, LA	1,596	33	1985-2017	Yes	Amite

Methodology and Software

The flood frequency analysis is based on the methodologies documented in Bulletin 17C, Guidelines for Determining Flood Flow Frequency, 2018. Bulletin 17C revises the procedures of Bulletin 17B, 1982. The most significant differences between the two methodologies are how historical events are treated and the addition of the Multiple Grubbs–Beck method of identifying outliers. A historical event is an event that precedes a gap in the annual peak data series that is larger than any flood event that occurred during the gap. Historical events are identified in the USGS data sets with the code ‘7’ following the historical flow. If there is no code ‘7’ after the last flow prior to the gap, it means that it is unknown whether larger events occurred during the gap. Data with gaps and historical events are now analyzed differently under the 17C guidance. The hydrologist must provide a Perception Threshold and a range of possible values for the missing years. It is typically assumed that the Perception Threshold is the value of the historical event. This assumes that had a larger event occurred, witnesses would have recorded the incident and noted that it was greater than the historical event. If the gap is not preceded by a historical event, the Perception Threshold is set relatively low and the upper bound of the range is infinity.

Prior to the adoption of Bulletin 17C, the USGS PeakFQ or HEC-SSP software only provided the Single Grubbs-Beck test where multiple low outliers could potentially adversely affect the accuracy of the frequency curve for larger events.

To validate HEC-SSP and the new Bulletin 17C methodology, tests were performed to compare the Peak FQ, and HEC-SSP results using the Bulletin 17B methods while also comparing the HEC-SSP Bulletin 17B results with the HEC-SSP Bulletin 17C results for the 1% annual chance flood at seven USGS stream gages. As can be seen in **Table 20**, all three approaches provided very similar results and consequently did not highlight any reasonable concerns with using HEC-SSP or the Bulletin 17C methodologies.

Location	PeakFQ 17B	HEC-SSP 17B	HEC-SSP 17C
07377500 Comite R nr Olive Br, LA	46,710	42,887	47,651
07376679 East Amite R nr Peoria, MS	35,270	34,566	38,404
07377000 Amite R nr Darlington, LA	111,900	111,661	117,083
07378500 Amite R nr Denham Springs, LA	148,300	148,268	150,376
07380120 Amite R at Port Vincent, LA (1985-2017)	135,800	141,042	135,814
07377300 Amite River at Magnolia, LA	117,200	125,606	126,449
07378000 Comite River Near Comite, LA (1944-2016)	45,360	45,277	44,224

Number of Outliers

The results of the flood frequency analysis were observed to be sensitive to the number of observations that are considered as outliers when using the Bulletin 17C methodology. Adding or subtracting one event can potentially have significant impacts on the estimates. For example, USGS gage 07377500 Comite River near Olive Branch, has 74 years of record. In 1980, the peak flow of 2,560 cfs was flagged with a code 'D', "Base Discharge changed during this year". If the 'D' is not removed, the program designates 28 peaks as outliers and estimates the 1% AEP flow as 42,990 cfs. If the 'D' is removed, the program designates none of the peaks as Low Outliers and estimates the 1% AEP flow as 47,230 cfs, an approximately 10% increase. Another example is for the record from USGS gage 07377000 Amite River near Darlington. When excluding the August 2016 record, HEC-SSP designates 18 of the 67 peaks as low outliers. When including the August 2016 record, it does not identify a single low outlier. **Table 21** summarizes the number of outliers identified using Bulletin 17B and Bulletin 17C methodologies when including and excluding the August 2016 flood.

Table 21: Low Outliers Detected by Software and Method Including and Excluding the August 2016 Flood

Location	PeakFQ 17B		HEC-SSP 17B		HEC-SSP 17C	
	Inc. 2016	Exc. 2016	Inc. 2016	Exc. 2016	Inc. 2016	Exc. 2016
07377500 Comite R nr Olive Br, LA	30	31	32	31	0	28
07376679 East Amite R nr Peoria, MS	2	5	4	0	4	2
07377000 Amite R nr Darlington, LA	0	18	20	18	0	0
07378500 Amite R nr Denham Springs, LA	0	0	17	0	0	17
07380120 Amite R at Port Vincent, LA	0	0	0	0	0	0

Table 22 demonstrates the sensitivity of including and excluding the August 2016 flood on the 1% AEP flow estimates for various USGS gages. As can be seen, the resultant increase of including the August 2016 flood ranges from insignificant, to large. To better determine the appropriateness of including or excluding the August 2016 flood, an analysis was performed to determine the estimated AEP magnitude of the event and make a determination of whether it was representative of the AEP of floods that would be used for future analysis or whether it represented an event too extreme that its results would be of little interest to end users.

Table 22: Sensitivity of the inclusion and exclusion of the August 2016 flood on the 1% AEP flow estimates

Stream Gage	Drainage Area (sq mi)	Bulletin 17C 1% AEP Flood Estimate (cfs)		Percent Increase in 1% AEP flow when Including August 2016.
		Inc. 2016	Exc. 2016	
07377500 Comite R nr Olive Br, LA	145	47,650	33,090	56
07376679 East Amite R nr Peoria, MS	179	38,404	35,928	4
07378000 Comite R nr Comite, LA	284	44,224	36,665	21
07377000 Amite R nr Darlington, LA	580	117,083	103,426	13
07377300 Amite R nr Magnolia, LA	884	126,285	90,311	40
07378500 Amite R nr Denham Springs, LA	1,280	150,376	122,492	23
07380120 Amite R at Port Vincent, LA	1,596	135,814	138,087	-2

Estimated Frequency of the August 2016 Flood

Using the results of the Bulletin 17C analysis, the peak streamflow recorded at each USGS streamflow gage included in the analysis were reviewed to interpolate the estimated flood frequency of the August 2016 flood event on both the Amite and Comite Rivers.

As summarized in **Table 23**, the AEP of the August 2016 flood was estimated to range from a < 0.2% (ie more extreme than a 0.2% AEP (500-year) flood event) to approximately a 1% AEP when either including or excluding the event in the statistical analysis. The most significant impact of including or excluding the August 2016 event was the increase in the 0.2% AEP for several gages which can be attributed to the increased uncertainty when performing estimates for extreme events. While the August event resulted in extensive damages and is considered a major flooding event, the magnitude is not excessively extreme. Therefore it was concluded that the August 2016 flood was appropriate to include in the analysis.

Location	Bulletin 17C AEP Peak Streamflow Estimates (cfs)		
	Observed Peak Streamflow (cfs)	Estimated AEP Range	
		Inc. 2016	Exc. 2016
07377500 Comite R nr Olive Br, LA	78,000	<0.2%	<0.2%
07376679 East Amite R nr Peoria, MS	Unavailable, August storm was not the largest event	Unavailable	Unavailable
*07378000 Comite R nr Comite, LA	71,000	<0.2%	<0.2%
07377000 Amite R nr Darlington, LA	116,000	1%	1% – 0.5%
*07377300 Amite R nr Magnolia, LA	202,000	<0.2%	<0.2%
07378500 Amite R nr Denham Springs, LA	266,000	<0.2%	<0.2%
07380120 Amite R at Port Vincent, LA	199,000	1% - 0.2%	< 0.2%

* Flow was not included for the August 2016 flood since no estimate was available.

Summary of Flood Frequency Estimates

Table 24 summarizes the peak flow estimates at the USGS gages analyzed for all AEP events when including the August 2016 record in the Bulletin 17C analysis. Full results of the HEC-SSP Bulletin 17C analysis including input data and confidence limit outputs are included in **Appendix 3**.

Table 24: Peak Flow Estimates for Gages with 2016 event included in analysis except as noted.							
Location	Bulletin 17C AEP Peak Streamflow Estimates Including the August 2016 Record (cfs)						
	20%	10%	4%	2%	1%	0.2%	1%+ (90% Confidence)
07377500 Comite R nr Olive Br, LA	14,900	21,100	30,400	38,600	47,700	73,000	67,400
07376679 East Amite R nr Peoria, MS	16,800	21,600	28,100	33,100	38,400	51,500	57,900
07378000 Comite R nr Comite, LA	20,400	26,000	33,300	38,800	44,200	57,000	55,600
07377000 Amite R Darlington, LA	39,300	54,800	77,400	96,400	117,100	172,100	164,200
07377300 Amite R nr Magnolia, LA	46,000	61,200	84,200	104,000	126,400	190,100	184,000
07378500 Amite R nr Denham Springs, LA	57,000	76,800	104,400	126,800	150,400	210,500	193,000
07380120 Amite R at Port Vincent, LA	44,900	60,900	86,100	109,000	135,800	217,400	239,100

Figures 54 and 55 illustrate the 1% AEP estimates including the upper and lower bounds of the 90% confidence interval (including the August 2016 flood) with respect to drainage area on the Amite and Comite Rivers. As can be seen, the range of the 90% confidence interval and resultant uncertainty in the estimate is significantly larger for gages with limited years of records such as the Amite River at Port Vincent with 33 years of record used when compared to the adjacent gage Amite River at Denham Springs with 80 years of record.

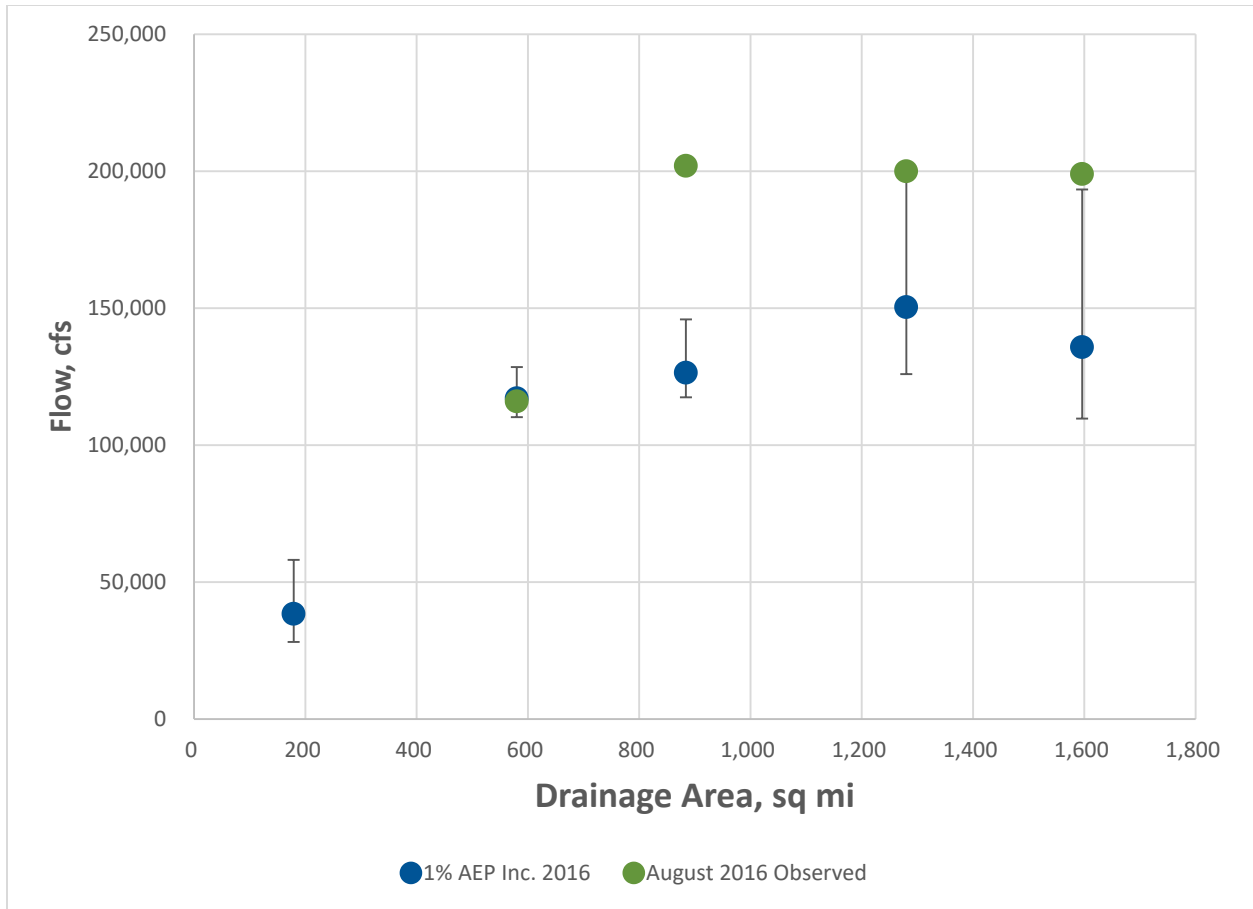


Figure 54: Bulletin 17C AEP flow estimates including the August 2016 flood for the Amite River with the 90% confidence limits illustrated.

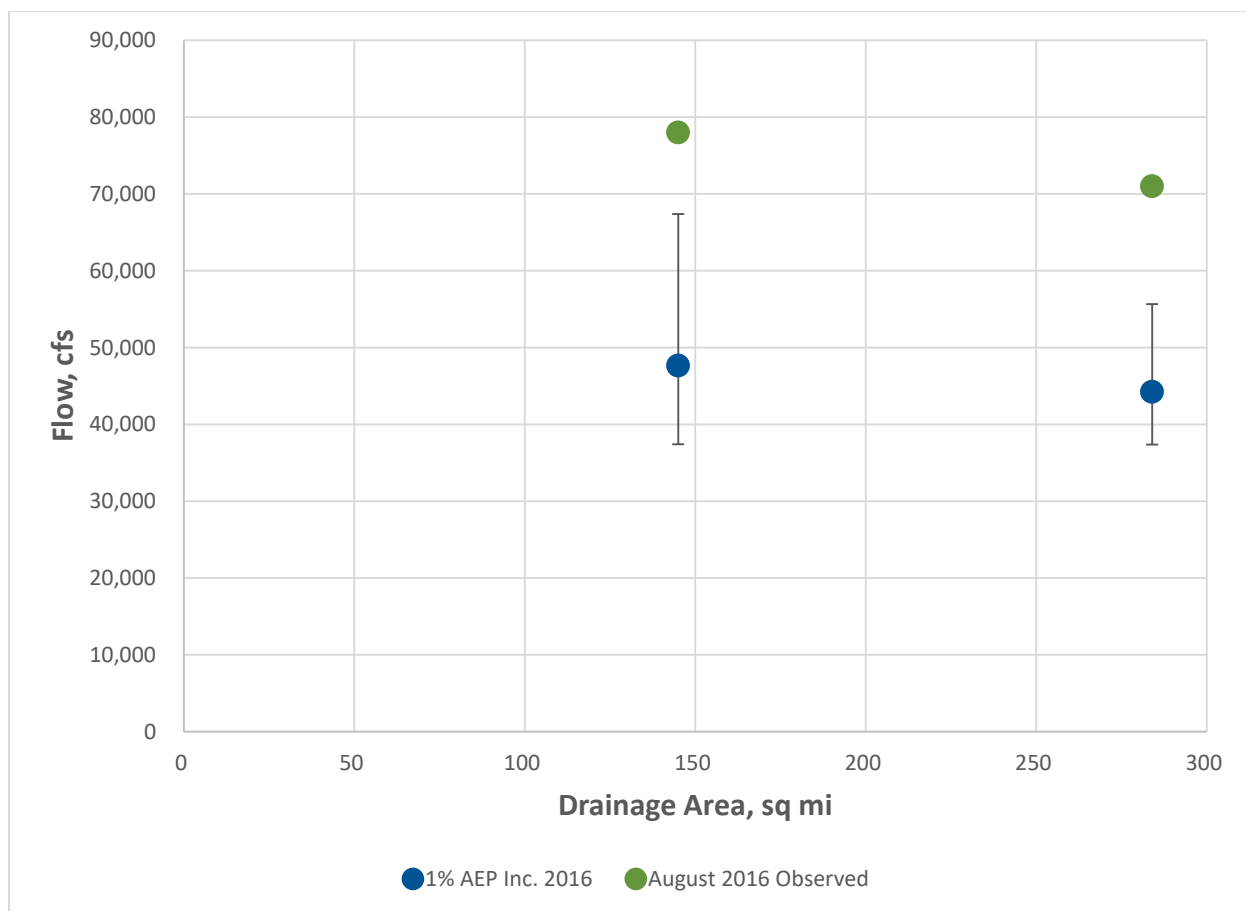


Figure 55: Bulletin 17C AEP flow estimates including the August 2016 flood for the Comite River with the 90% confidence limits illustrated.

Development of Design Storm Spatial and Temporal Distributions and Magnitude

The procedures of NOAA Hydrometeorological Report Number 52 (HMR 52) were used to guide the development of a design storm for the ARBNM that could be scaled and centered anywhere within the ARB and beyond. Review of major floods within the ARB including the March 2016 and August 2016 flood events indicated that storm durations causing major flooding were generally in the range of 48 hrs to 72 hrs. For purposes of developing a design storm, a 72 hr duration storm was assumed.

To provide an efficient platform for future analysis and refinement of the ARBNM, HEC-MetVue was utilized to apply the HMR52 procedures. HEC-MetVue is an interactive precipitation visual and analysis tool created by the HEC. This program allows the user to refine, translate, rotate, scale and animate storms over their basin of interest. The model also adheres to accepted NWS and World Meteorology Organization (WMO) standards which simplifies the process for the end user and will provide a long term solution for analysis of the ARB.

Design Storm Spatial Distribution

For the spatial distribution of the design storm, storm-area size, orientation and spatial variability were optimized using HEC-MetVue to produce maximum precipitation over the basin using HMR 52 guidelines. The isohyetal shape for the basin centroid was represented by elliptical isohyets drawn at the standard HMR area sizes as illustrated in **Figure 56**. The orientation for the storm was optimized by HEC-MetVue, and no storm was oriented by more than 40 degrees from the preferred orientation presented in HMR 52. The standard ratio of the major axis to minor axis recommended by HMR52 is 2.5 to 1. To validate this assumption, the axis ratio was compared to the observed March 2016 and August 2016 storms which each demonstrated a comparable ratio of approximately 2 to 1 as illustrated in **Figure 57**.

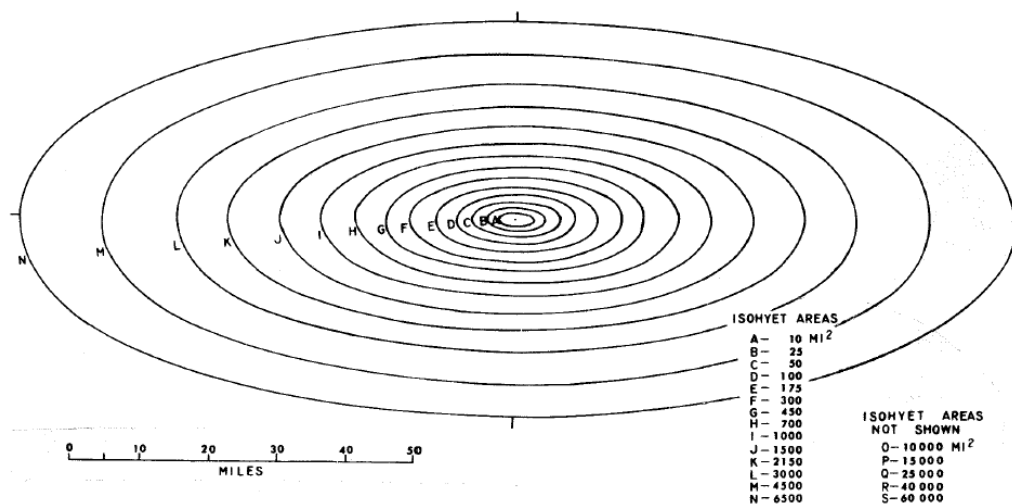


Figure 56: The design storm at each storm center is represented by elliptical isohyets with a ratio of the major axis to the minor axis of 2.5 to 1 using the HMR 52 Standard Isohyetal Pattern.

Source: HMR52 Probable Maximum Storm (Eastern United States) User's Manual. March 1984, Updated April 1987

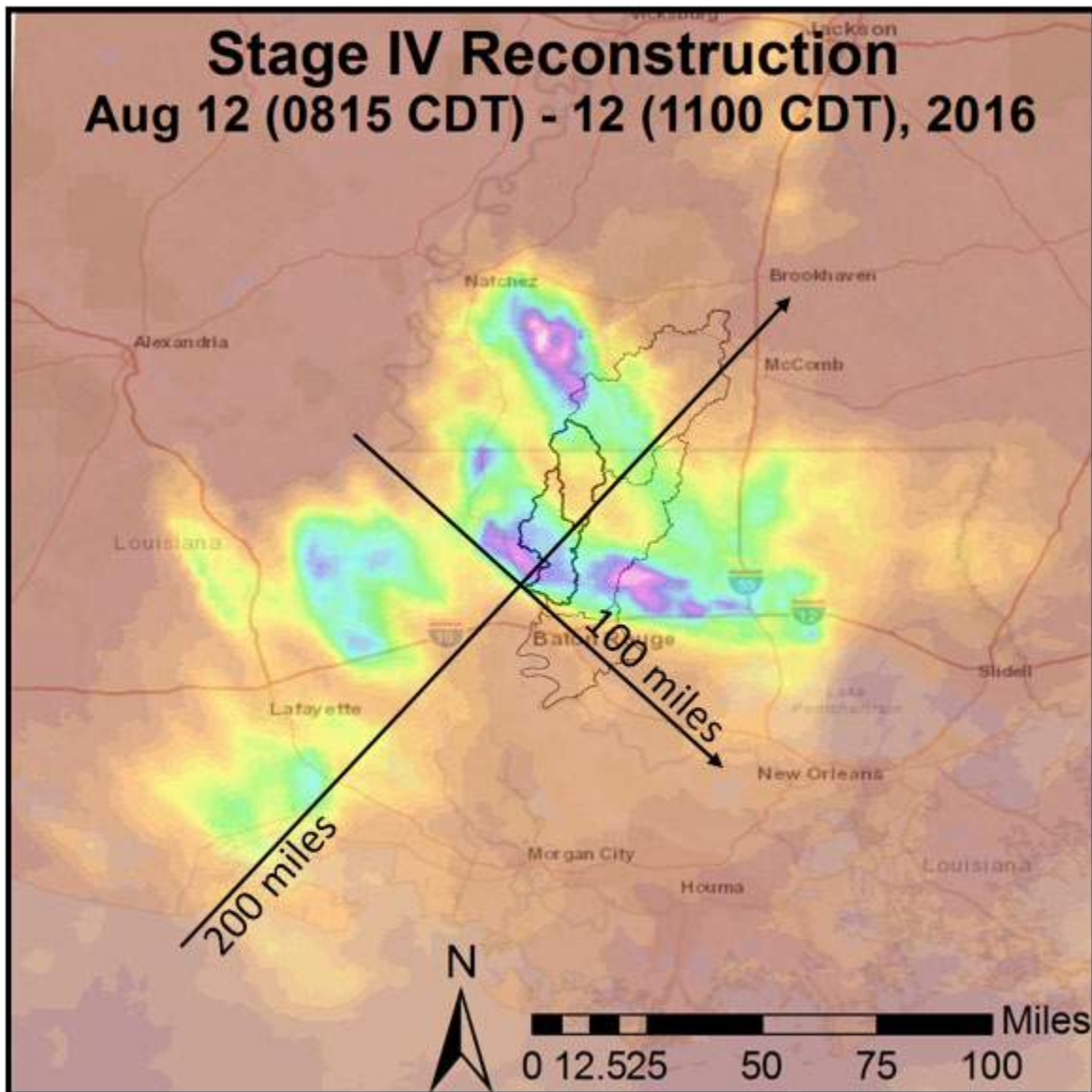


Figure 57: The axis ratios for the August 2016 and March 2016 events were approximated to validate the HMR 52 assumption of 2.5:1. Both the March and August 2016 events demonstrated approximately a 2:1 ratio as illustrated here for the August 2016 event.

Design Storm Temporal Distribution

Analysis of rainfall accumulation during the August 2016 flood event and subsequent streamflow aided in the guidance of choosing an appropriate temporal pattern. The standard HMR 52 6-hr distribution for each hyetograph was used for the temporal distribution. The factors governing the temporal distribution of the design storm included using a 72-hr duration, making sure four of the 6-hr periods with the greatest precipitation occurred after the first 24-hr and 6-hr increments were arranged such that the increments decreased progressively on either side of the greatest 6-hour increment as illustrated in **Figure 58**. The 6-hr increments were reduced to 1-hr intervals using the standard 4 periods, and the ratio of the 1-hr to 6-hr precipitation at the storm-center was used to properly adjust ratios for each isohyet within the storm-area size. **Figure 59** shows the fraction of rainfall accumulation over time for the standard HMR distribution used in the analyses. Overlaid is the August 2016 event 72-hr maximum accumulation, which shows the assumptions of the HMR 52 temporal distribution to be of comparable rainfall intensity.

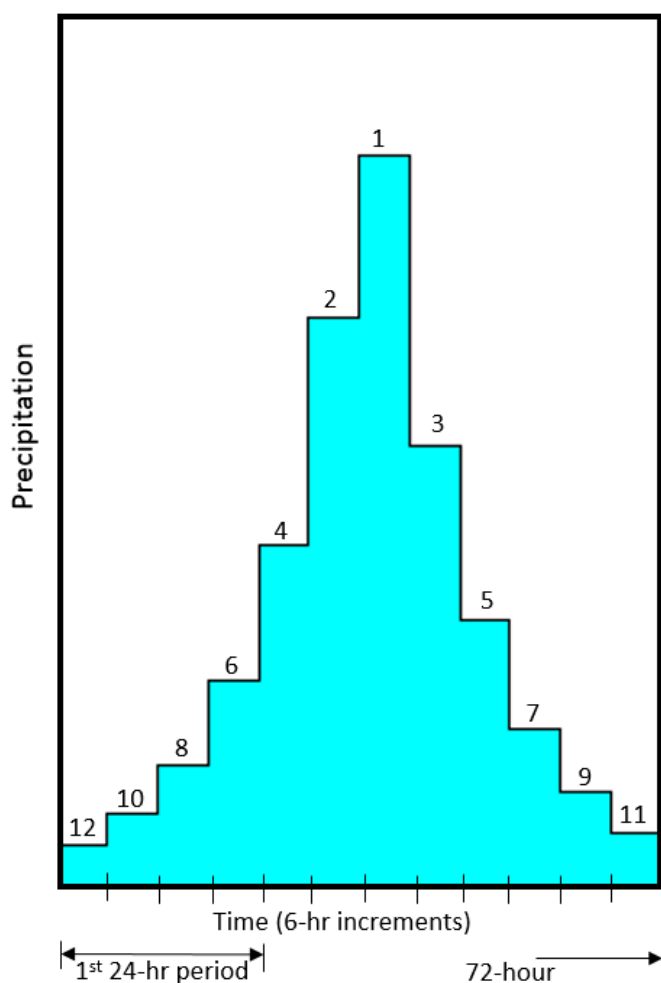


Figure 58: HMR 52 Temporal Distribution

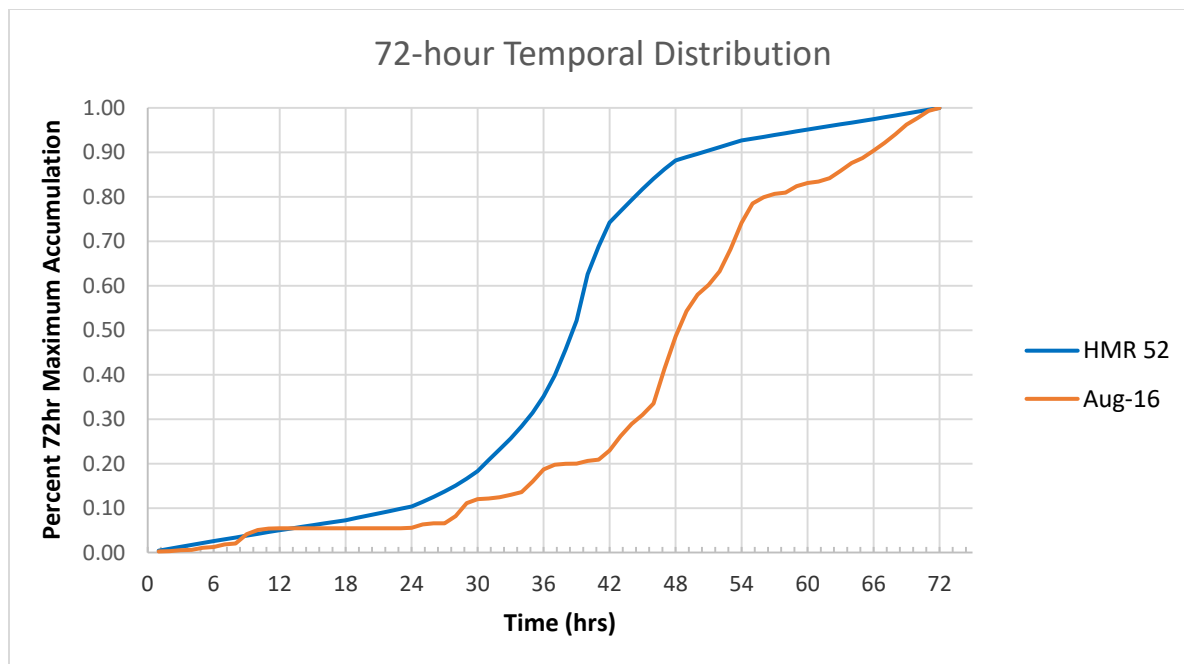


Figure 59: The HMR 52 temporal distribution accumulation was compared to the August 2016 storm accumulations to validate the assumption.

This design storm was then transposed to different locations over the ARB, which allowed the design storm storm-area size and spatial variability to remain constant.

Design Storm Centers and Magnitudes

Three storm centers were created for the ARBNM which were optimized to enable a range of AEP floods to be simulated throughout the basin. The storm center locations selected were the USGS Olive Branch gage on the Comite River which represented a central location within the Comite basin, the USGS Darlington gage on the Amite River which represented a central location for the ARB upstream of the Comite River confluence, and the USGS Denham Springs gage on the Amite River which represented a central location for the area of greatest flood risk, just downstream of the confluence with the Comite River.

As previously discussed, due to the size of the ARB, it cannot be assumed that a single storm will produce a consistent AEP flood, therefore it was determined that modeling different rainfall depths would be a better process to provide users with the tools to successfully simulate a range of AEP at different locations throughout the basin. Guidance would then be provided to users to help select an appropriate storm center and depth based on location within the basin. Rainfall depths of 8-, 10-, 12-, 14-, 16-, 18-, 20-, 22-, 24- and 26-in. were selected for analysis. Since the default PMP rainfall depth generated by HEC-MetVue using the HMR 52 procedures was much larger than the selected precipitation depths, the individual hyetographs were reduced by the ratio of the selected rainfall depths (at the centroid) to the PMP value (at the centroid) for each simulated storm. This was done by taking the mean areal average of precipitation for the HMS subbasin that the PMP was centered on. **Figures 60-62** illustrate the three centers and spatial distribution of the design storm provided within the ARBNM.

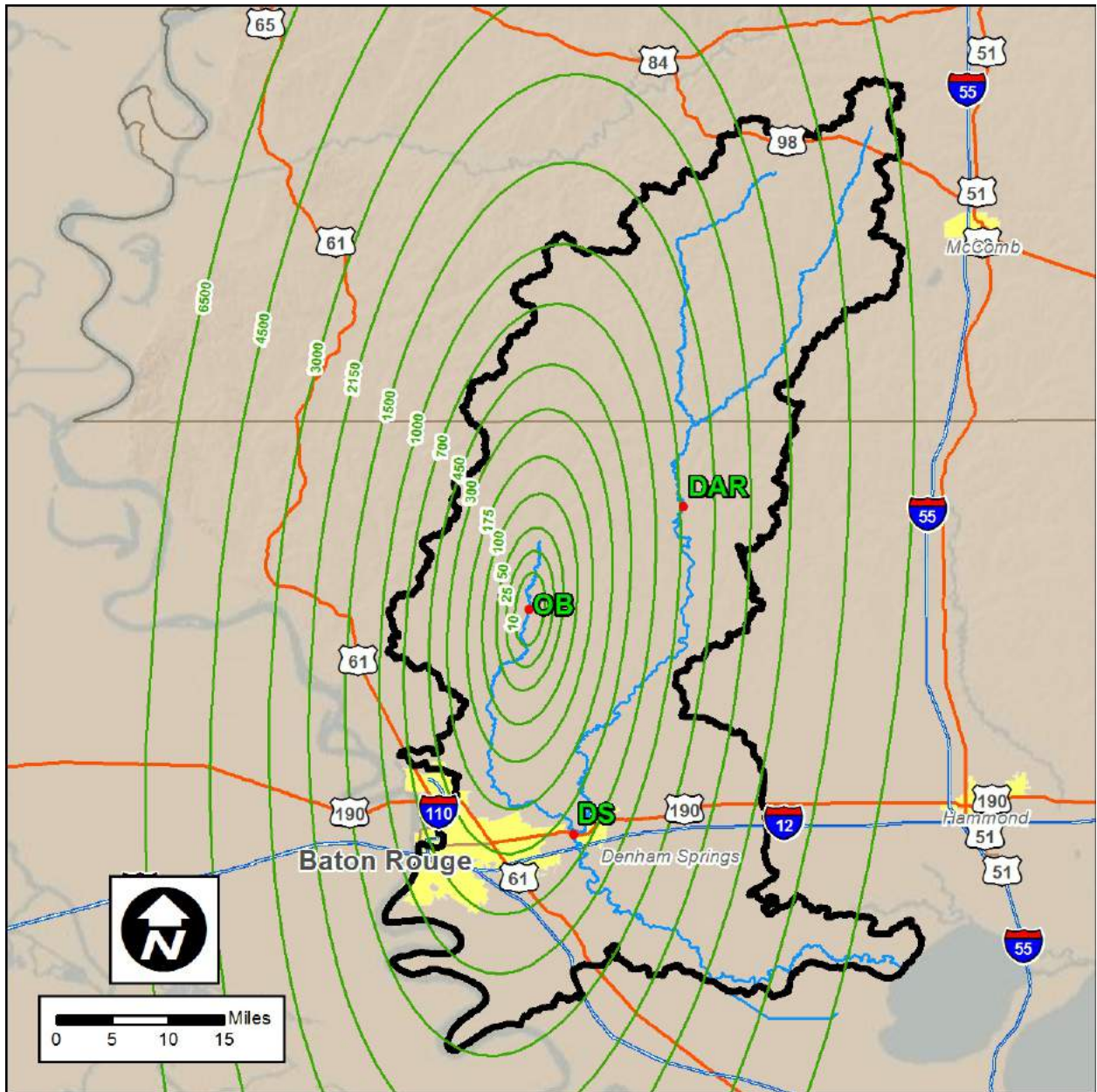


Figure 60: Design storm centered over the Comite River near Olive Branch Gage (OB).

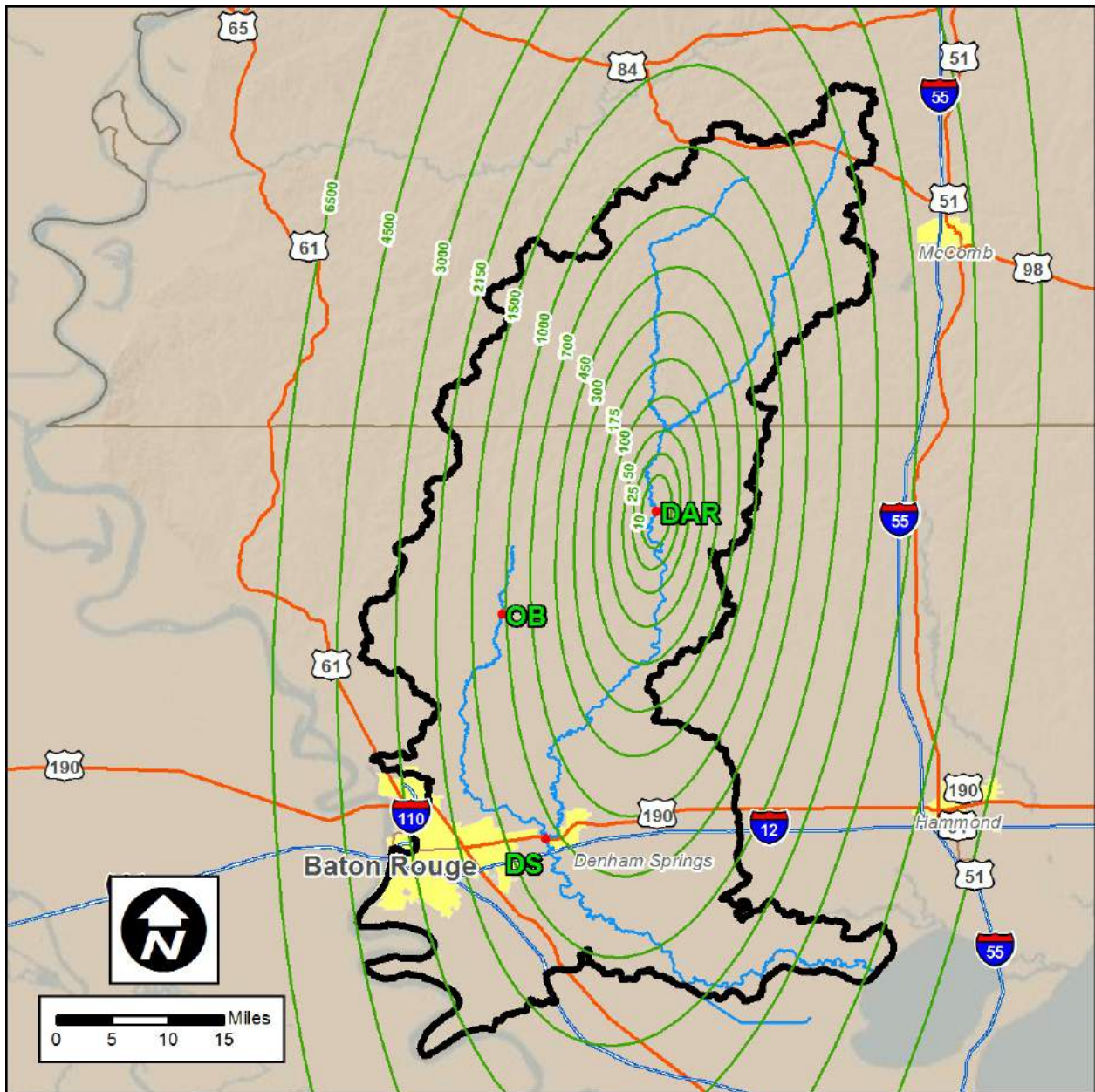


Figure 61: Design storm centered over the Amite River near Darlington Gage (DAR).

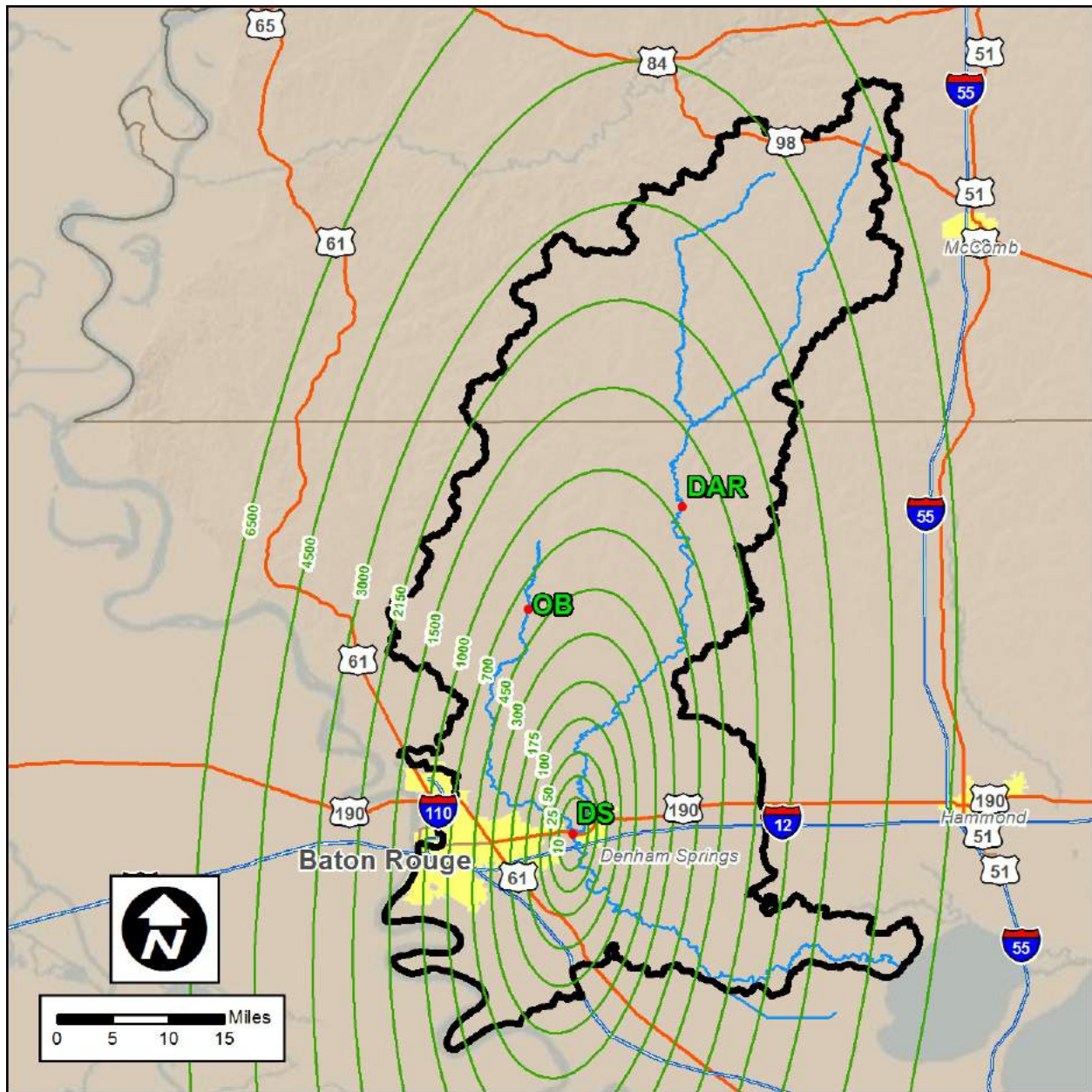


Figure 62: Design storm centered over the Amite River near Denham Springs Gage (DS).

Results of Design Storm Simulations

A total of 30 HEC-HMS and HEC-RAS model runs representing the ten rainfall depths and three centers were performed. The HEC-RAS routed flows extracted from RAS Mapper using profile lines at a selection of locations within the ARB can be seen in **Tables 25-27** for each storm center with corresponding AEP or range **Figures 63-68**. Note that the 1% AEP can be achieved with different rainfall depths depending on the storm center. For example, at Denham Springs an approximately 1% AEP flow will result if the storm is centered directly over it with a rainfall depth of 22 in. However, if the storm is centered over Darlington, then it only takes an 18 in. rainfall depth to achieve nearly the same flow. It should be noted that due to the unconfined nature of floodplains in many regions of the ARB, the alignment of profile lines is very subjective. The profile lines were carefully chosen to best match the observed flows reported by the USGS during the August 2016 flood.

Table 25: Peak Design Flood Streamflow Estimates for Olive Branch (OB) Storm Center with Estimated AEP or AEP Range												
Cumulative Rainfall Depth (in.)	Peak Discharge (cfs) Estimate AEP or range											
	07377500 Comite Nr Olive Branch		07378000 Comite Nr Comite		07377000 Amite Nr Darlington		07377300 Amite Nr Magnolia		07378500 Amite Nr Denham Springs		07380120 Amite at Port Vincent	
8	11,010	>20%	20,080	20%	25,970	>20%	38,010	>20%	52,630	20%	41,560	20%
10	13,890	20%	25,430	10%	36,860	20%	49,170	20%	68,480	20%-10%	55,580	10%
12	17,470	20%-10%	30,720	10%-4%	47,910	20%-10%	61,520	10%	84,360	10%-4%	69,500	10%-4%
14	22,180	10%	35,540	4%-2%	58,560	10%	74,240	10%-4%	100,170	4%	82,580	4%
16	26,880	10%-4%	40,810	2%-1%	69,620	10%-4%	87,120	4%	117,210	4%-2%	97,100	4%-2%
18	32,110	4%-2%	45,810	1%	80,460	4%-2%	99,400	2%	134,500	2%-1%	111,500	2%
20	37,950	2%	50,000	1%-0.2%	91,150	2%	111,930	2%-1%	153,540	1%	124,420	2%-1%
22	43,400	2%-1%	54,520	0.2%	101,910	2%-1%	124,040	1%	174,690	1%-0.2%	140,650	1%
24	48,020	1%	58,460	0.2%	112,920	1%	135,620	1%-0.2%	194,000	0.2%	157,360	1%-0.2%
26	52,230	1%-0.2%	62,200	<0.2%	123,540	1%-0.2%	148,390	1%-0.2%	212,740	0.2%	170,240	1%-0.2%

Table 26: Peak Design Flood Streamflow Estimates for Darlington (DAR) Storm Center with Estimated AEP or AEP Range

Cumulative Rainfall Depth (in.)	Peak Discharge (cfs)											
	07377500 Comite Nr Olive Branch		07378000 Comite Nr Comite		07377000 Amite Nr Darlington		07377300 Amite Nr Magnolia		07378500 Amite Nr Denham Springs		07380120 Amite at Port Vincent	
8	8,310	>20%	15,150	>20%	40,550	20%	49,750	20%	57,440	20%	46,450	20%
10	11,120	>20%	19,380	20%	55,670	10%	66,310	10%	77,030	10%	62,800	10%
12	14,250	20%	24,140	20%- 10%	70,750	4%	83,470	4%	97,740	10%- 4%	77,720	10%- 4%
14	18,130	20%- 10%	27,940	10%	85,370	4%-2%	99,550	2%	116,640	4%- 2%	94,020	4%- 2%
16	22,250	10%	31,810	4%	99,730	2%	114,730	2%- 1%	135,770	2%- 1%	110,370	2%
18	26,320	10%- 4%	35,830	4%-2%	114,170	1%	129,550	1%	155,420	1%	124,680	2%- 1%
20	30,910	4%	40,500	2%-1%	127,050	1%- 0.2%	144,990	1%- 0.2%	175,420	1%- 0.2%	142,340	1%
22	35,790	4%-2%	44,630	1%	142,410	1%- 0.2%	159,600	1%- 0.2%	195,130	1%- 0.2%	159,430	1%- 0.2%
24	39,600	2%	47,110	1%- 0.2%	154,430	1%- 0.2%	171,040	0.2%	209,750	0.2%	169,760	1%- 0.2%
26	44,210	1%	50,820	1%- 0.2%	170,450	0.2%	187,200	0.2%	232,310	<0.2 %	180,550	1%- 0.2%

Table 27: Peak Design Flood Streamflow Estimates for Denham Springs (DS) Storm Center with Estimated AEP or AEP Range

Cumulative Rainfall Depth (in.)	Peak Discharge (cfs)											
	07377500 Comite Nr Olive Branch		07378000 Comite Nr Comite		07377000 Amite Nr Darlington		07377300 Amite Nr Magnolia		07378500 Amite Nr Denham Springs		07380120 Amite at Port Vincent	
8	7,230	>20%	15,120	>20%	16,440	>20%	31,640	>20%	43,470	>20%	35,480	>20%
10	9,340	>20%	19,190	20%	23,590	>20%	42,440	20%	57,390	20%	47,240	20%
12	11,810	>20%	23,570	20%- 10%	32,040	>20%	52,440	20%- 10%	70,910	10%	59,880	10%
14	14,460	20%	27,500	10%	39,340	20%	62,150	10%	83,930	10%- 4%	71,760	10%- 4%
16	17,620	20%- 10%	31,280	4%	48,370	20%- 10%	73,040	10%- 4%	97,710	4%	83,080	4%
18	20,910	10%	35,170	4%-2%	56,300	10%	84,520	4%	111,030	4%- 2%	96,200	4%-2%
20	24,120	10%- 4%	39,830	2%	64,970	10%- 4%	95,390	4%- 2%	126,040	2%	109,070	2%
22	27,870	10%- 4%	42,530	1%	73,410	4%	105,850	2%	140,280	2%- 1%	120,100	2%-1%
24	31,800	4%	46,420	1%	81,590	4%-2%	117,470	2%- 1%	157,090	1%	133,060	1%
26	36,000	2%	50,110	1%	89,840	2%	128,160	1%	174,100	1%- 0.2%	146,230	1%- 0.2%

The Darlington location appears to be the most sensitive location as far as temporal rainfall distribution goes and this is likely because it is the most upstream location modeled. The Olive Branch location displays similar sensitivity although it is muted a bit since it is closer in proximity to the Darlington gage and the watershed will still receive a significant amount of rainfall from the Darlington centered location. The Denham Springs location appears to be almost equally affected by a storm centered over the upstream reaches of the Amite River or Comite River watersheds which shows the significance of how timing can affect a flooding event.

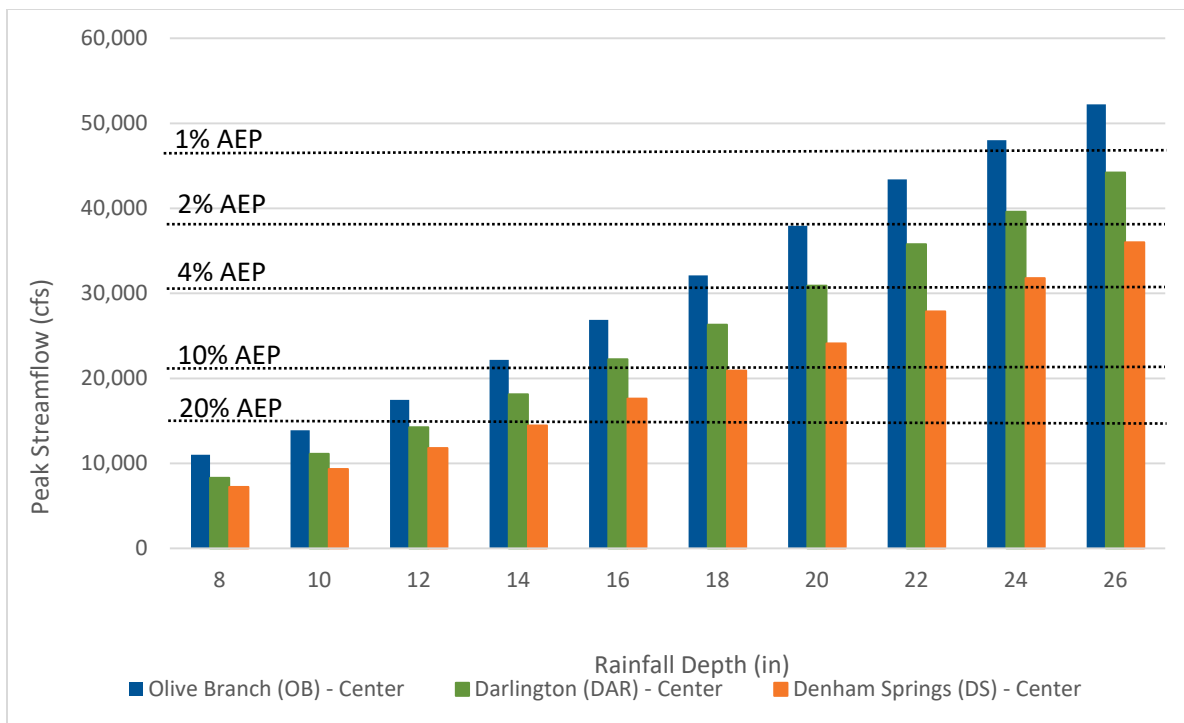


Figure 63: Design Storm Flows for the Comite River near Olive Branch with Multiple Storm Centers

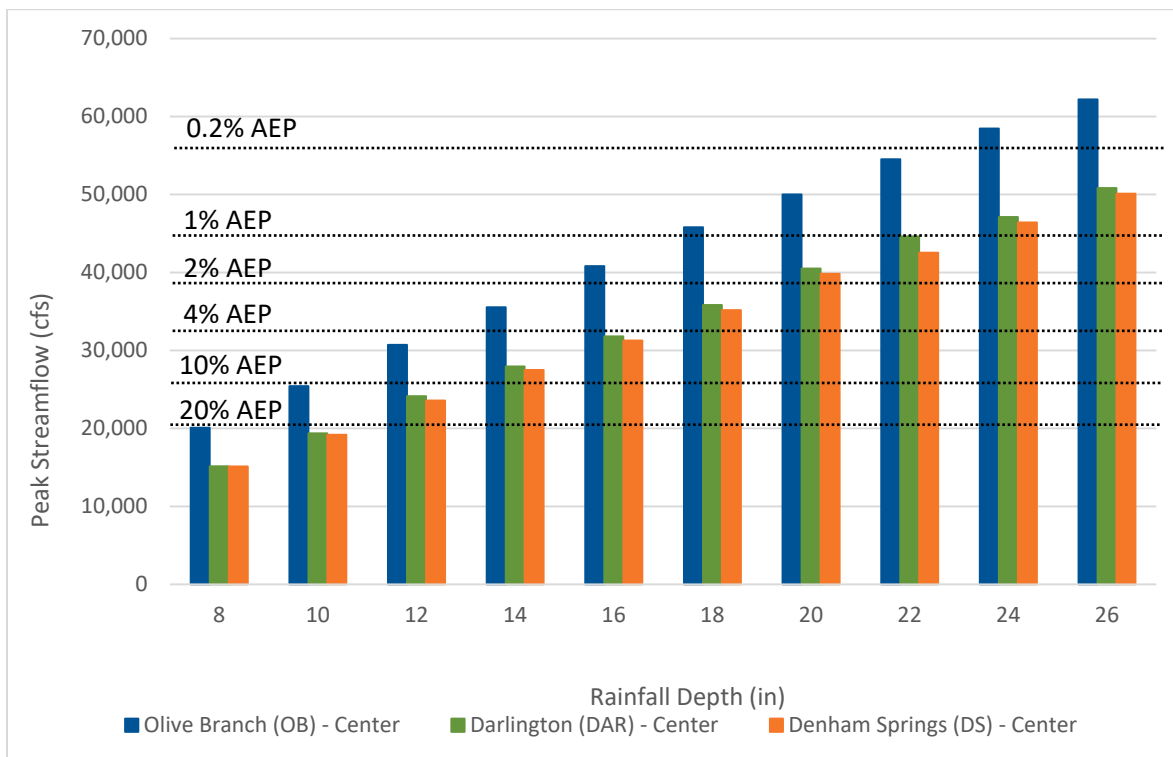


Figure 64: Design Storm Flows for the Comite River near Comite with Multiple Storm Centers

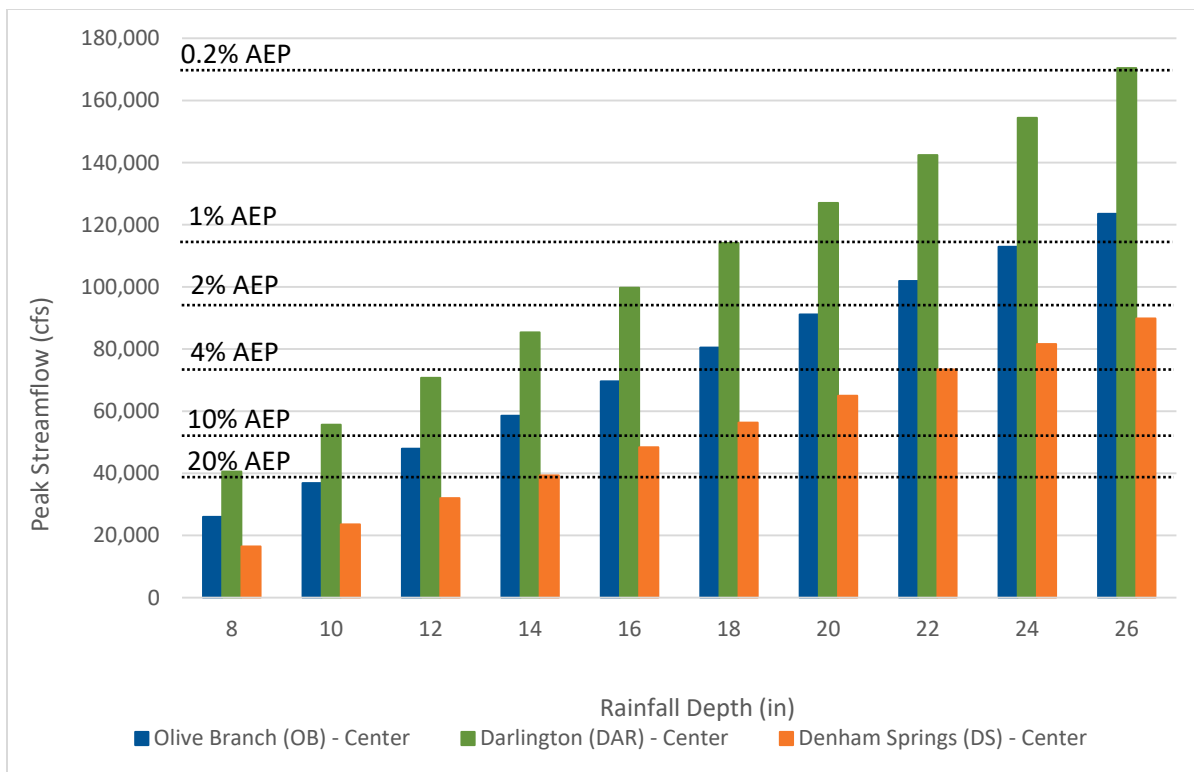


Figure 65: Design Storm Flows on the Amite River at Darlington with Multiple Storm Centers

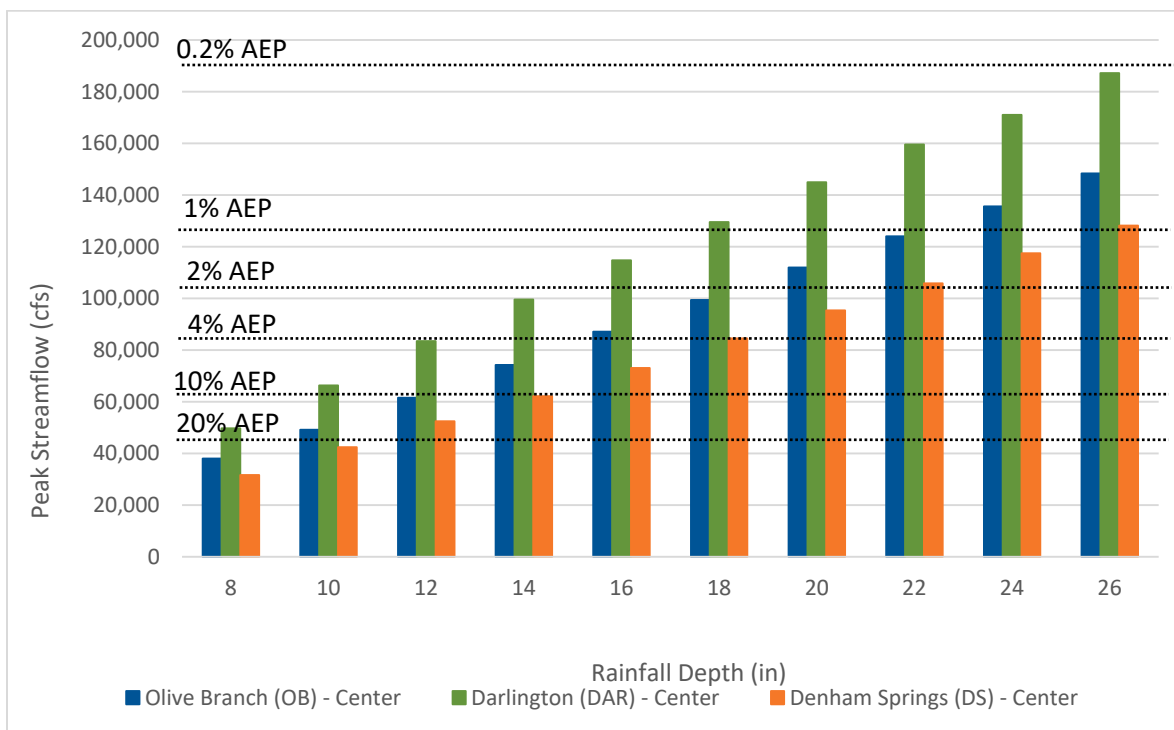


Figure 66: Design Storm Flows on the Amite River at Magnolia with Multiple Storm Centers

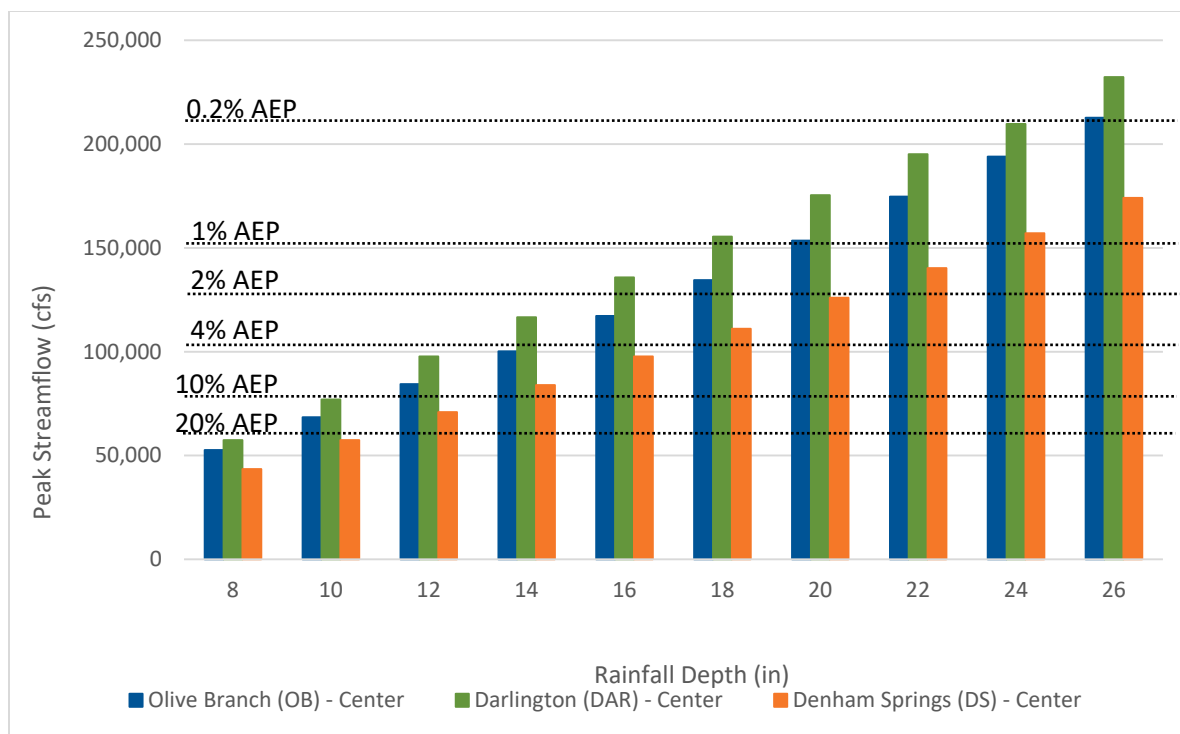


Figure 67: Design Storm Flows on the Amite River at Denham Springs with Multiple Storm Centers

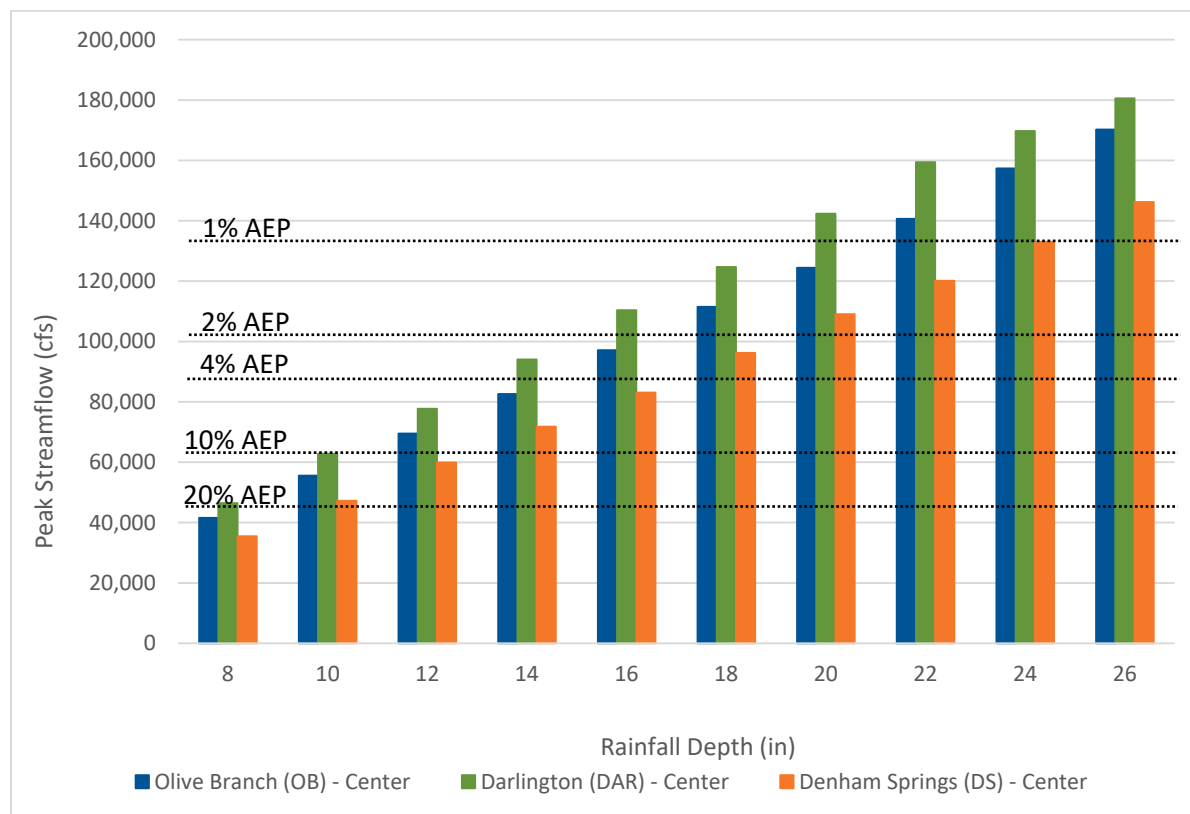


Figure 68: Design Storm Flows on the Amite River at Port Vincent with Multiple Storm Centers

Boundary Conditions

One of the hydraulic model inputs that can influence simulation results significantly is the choice of boundary conditions that are used. The term “boundary conditions” refers to the behavior that is prescribed by the user to define what is to occur at the edges or boundaries of the area to be modeled (i.e., the model domain) throughout the model simulation; boundary conditions can include, depending on what model is used, water levels, water velocities and direction, flows, and wind speed and direction. While simulations of historic floods are relatively simple since observed boundary conditions can be used, the combined probability of coastal and riverine flooding requires careful selection of appropriate boundaries when developing design boundary conditions.

The boundary conditions that are applicable for the HEC-RAS modeling of the Amite River system are flows and water surface elevations. At the upstream end of the ARB model domain, the boundary conditions used are flow hydrographs produced by the HEC-HMS hydrologic model. A water surface elevation hydrograph boundary condition is appropriate at the downstream end of the ARB model domain due to the backwater effects caused by Lake Maurepas. The lake is also influenced by diurnal tidal fluctuations and experiences periodic water surface elevation changes due to its connection with the Gulf of Mexico, through the Lake Pontchartrain basin estuary.

The purpose of this section is to give the users a suite of boundary conditions with supporting research to make an informed decision on which conditions to use. Note that the project management team will need to decide which (if any) of the conditions presented herein is applicable for their application of the model. For example, using a downstream boundary condition water surface elevation hydrograph for a specific historical event might be preferred over any of those presented herein. **Appendix 4** presents more details of the analysis and research contained within this section including sources of data that might be used to obtain data for other boundary conditions.

After analysis of historical data from the USACE, USGS, and NOAA, water surface elevation boundary conditions were developed for the downstream end of the Amite River where it meets Lake Maurepas for the following conditions:

- Average or “typical” conditions,
- Wind and storm surge influenced conditions,
- “Typical” flood conditions, and
- Period of record peak flood conditions.

Tabular data for each of these four conditions are presented in the following sections as well as in the digital project delivery in Excel format to simplify the application of this data for future users.

Average or “Typical” Conditions

Daily and hourly stage data from the USACE’s Pass Manchac near Pontchatoula station were used to develop the “typical” or average downstream boundary condition for the Amite River Basin hydraulic model. Daily values were used to determine the long-term average water surface elevation and hourly data were used to develop the average diurnal tidal pattern in Lake Maurepas. The boundary conditions for average conditions for a 72-hr period are given in **Table 28** and can be copied and duplicated as necessary to fill out the desired simulation period in the HEC-RAS flow file.

Table 28: Average or “typical” conditions downstream boundary condition water surface elevation hydrograph.		
Hour	Date / Time	Elevation (ft, NAVD 88)
0	1/1/18 12:00	0.83
1	1/1/18 13:00	0.81
2	1/1/18 14:00	0.79
3	1/1/18 15:00	0.76
4	1/1/18 16:00	0.73
5	1/1/18 17:00	0.70
6	1/1/18 18:00	0.67
7	1/1/18 19:00	0.64
8	1/1/18 20:00	0.62
9	1/1/18 21:00	0.61
10	1/1/18 22:00	0.61
11	1/1/18 23:00	0.61
12	1/2/18 0:00	0.63
13	1/2/18 1:00	0.65
14	1/2/18 2:00	0.67
15	1/2/18 3:00	0.70
16	1/2/18 4:00	0.73
17	1/2/18 5:00	0.76

Table 28: Average or “typical” conditions downstream boundary condition water surface elevation hydrograph.

Hour	Date / Time	Elevation (ft, NAVD 88)
18	1/2/18 6:00	0.79
19	1/2/18 7:00	0.81
20	1/2/18 8:00	0.83
21	1/2/18 9:00	0.85
22	1/2/18 10:00	0.85
23	1/2/18 11:00	0.85

Wind and Storm Surge Influenced Conditions

The 10 largest daily average wind speeds recorded at the New Orleans Airport (NOAA station USW00012916) from January 1984 through June 2018 are presented in **Table 29**. The top nine recorded values occurred during tropical storms that developed in August through October during the peak of the northern Atlantic Hurricane season. The average wind speed during Hurricane Isaac is the largest on record and resulted in a powerful storm surge that resulted in the water surface elevation of record in Lake Maurepas. However, wind speed alone is not the only factor contributing to high water surface elevations in Lake Maurepas. Other factors such as storm intensity, forward speed, size, and angle of approach to the coast can affect storm surge intensity and drive the water surface elevation. This is evident by the fact that similar wind speeds resulted in substantially different water surface elevations in Lake Maurepas during other events.

Table 29: Average Daily Wind Speed vs. Measured Lake Maurepas water surface elevation.

Date	Storm Name	USW00012916 Average Daily Wind Speed (mph)	Pass Manchac 10-day Maximum water surface elevation (ft., NAVD88)
8/29/2012	Hurricane Isaac	35.34	6.54
9/1/2008	Hurricane Gustav	29.53	NR
9/27/1998	Hurricane Georges	26.40	2.86
8/26/1992	Hurricane Andrew	25.50	2.81
9/24/2005	Hurricane Katrina	24.38	NA
9/12/2008	Hurricane Ike	24.38	NA
10/27/1985	Hurricane Juan	24.16	4.91
9/25/2002	Hurricane Isidore	22.82	4.45
9/15/2004	Hurricane Ivan	22.59	2.82
3/13/1993	1993 Storm of Century	22.15	1.22

One possible alternative for developing a boundary condition from these data is to use the statistics from the 10-day maximum water surface elevation values to generate an average scenario. Using this approach, the wind-induced water elevation stage boundary condition would be equal to a constant 3.66 ft., NAVD88 water elevation boundary condition.

“Typical” Flood Conditions

The 15 largest discharge measurements from 1985-2018 at the USGS Amite River at Port Vincent (07380120) gage are listed in **Table 30**. Lake Maurepas water surface elevation values measured at the USACE’s Pass Manchac station are also reported for the same day as the measured peak flow along with the maximum stage recorded during the 5 day window around the peak flow date. The worst-case boundary condition for Lake Maurepas would be a constant elevation of +4.91 ft., NAVD88. The mean of all the 5 day peak values is 2.15 ft., NAVD88 which could be used to represent an average constant flood water elevation boundary condition.

Table 30: Amite River Peak Discharges vs. Measured Lake Maurepas water surface elevation.

Date	Port Vincent Discharge (cfs)	Value Code1	Pass Manchac	
			Peak Discharge Water Surface Elevation2 (ft., NAVD88)	5-day Maximum Water Surface Elevation (ft., NAVD88)
8/15/2016	199,000	P	1.30	1.72
1/28/1990	69,500	P	0.73	1.02
1/23/1993	48,400	P	1.79	1.93
4/30/1997	45,300	P	1.08	2.02
4/13/1995	44,700	P	1.92	2.48
3/8/1992	43,100	P	1.05	2.03
11/1/1985	42,200	P	3.62	4.91
2/24/2003	42,100	P	0.95	1.59
1/9/1998	41,000	P	N/A	1.84
3/14/2016	41,700	A	2.59	3.03
4/4/1988	38,300	P	2.29	2.69
1/13/2013	35,200	P	2.05	2.18
3/17/1999	33,900	P	0.72	0.83
2/28/1997	31,800	A	1.33	1.88
5/18/2004	31,400	P	2.09	2.09
P=Peak Value / A=Average Daily Value. N/A = Not Available.				

Period of Record Peak Flood Conditions

The water surface elevation of record in Lake Maurepas measured at the Pass Manchac station occurred on August 30, 2012. On this date the water surface elevation at Pass Manchac reached 6.54 ft., NAVD88, at the same time that Hurricane Isaac made landfall along the Louisiana-Mississippi coast southeast of Lake Maurepas. The time series boundary conditions for the record water surface elevation are given in **Table 31** and can be copied to the HEC-RAS flow file.

Table 31: Period of record flood conditions downstream boundary condition water surface elevation hydrograph.

Hour	Date / Time	Elevation (ft, NAVD 88)
0	1/1/18 12:00	1.21
1	1/1/18 13:00	1.21
2	1/1/18 14:00	1.21
3	1/1/18 15:00	1.21
4	1/1/18 16:00	1.21
5	1/1/18 17:00	1.20
6	1/1/18 18:00	1.20
7	1/1/18 19:00	1.20
8	1/1/18 20:00	1.20
9	1/1/18 21:00	1.20
10	1/1/18 22:00	1.20
11	1/1/18 23:00	1.20
12	1/2/18 0:00	1.20
13	1/2/18 1:00	1.19
14	1/2/18 2:00	1.19
15	1/2/18 3:00	1.19
16	1/2/18 4:00	1.19
17	1/2/18 5:00	1.19
18	1/2/18 6:00	1.19
19	1/2/18 7:00	1.19
20	1/2/18 8:00	1.19
21	1/2/18 9:00	1.18
22	1/2/18 10:00	1.18

Table 31: Period of record flood conditions downstream boundary condition water surface elevation hydrograph.

Hour	Date / Time	Elevation (ft, NAVD 88)
23	1/2/18 11:00	1.18
24	1/2/18 12:00	1.18
25	1/2/18 13:00	1.23
26	1/2/18 14:00	1.28
27	1/2/18 15:00	1.33
28	1/2/18 16:00	1.37
29	1/2/18 17:00	1.42
30	1/2/18 18:00	1.47
31	1/2/18 19:00	1.52
32	1/2/18 20:00	1.57
33	1/2/18 21:00	1.62
34	1/2/18 22:00	1.66
35	1/2/18 23:00	1.71
36	1/3/18 0:00	1.76
37	1/3/18 1:00	1.81
38	1/3/18 2:00	1.86
39	1/3/18 3:00	1.91
40	1/3/18 4:00	1.95
41	1/3/18 5:00	2.00
42	1/3/18 6:00	2.05
43	1/3/18 7:00	2.10
44	1/3/18 8:00	2.15
45	1/3/18 9:00	2.20

Table 31: Period of record flood conditions downstream boundary condition water surface elevation hydrograph.

Hour	Date / Time	Elevation (ft, NAVD 88)
46	1/3/18 10:00	2.24
47	1/3/18 11:00	2.29
48	1/3/18 12:00	2.34
49	1/3/18 13:00	2.52
50	1/3/18 14:00	2.69
51	1/3/18 15:00	2.87
52	1/3/18 16:00	3.04
53	1/3/18 17:00	3.22
54	1/3/18 18:00	3.39
55	1/3/18 19:00	3.57
56	1/3/18 20:00	3.74
57	1/3/18 21:00	3.92
58	1/3/18 22:00	4.09
59	1/3/18 23:00	4.27
60	1/4/18 0:00	4.44
61	1/4/18 1:00	4.62
62	1/4/18 2:00	4.79
63	1/4/18 3:00	4.97
64	1/4/18 4:00	5.14
65	1/4/18 5:00	5.32
66	1/4/18 6:00	5.49
67	1/4/18 7:00	5.67
68	1/4/18 8:00	5.84

Table 31: Period of record flood conditions downstream boundary condition water surface elevation hydrograph.

Hour	Date / Time	Elevation (ft, NAVD 88)
69	1/4/18 9:00	6.02
70	1/4/18 10:00	6.19
71	1/4/18 11:00	6.37
72	1/4/18 12:00	6.54
73	1/4/18 13:00	6.51
74	1/4/18 14:00	6.47
75	1/4/18 15:00	6.44
76	1/4/18 16:00	6.41
77	1/4/18 17:00	6.37
78	1/4/18 18:00	6.34
79	1/4/18 19:00	6.31
80	1/4/18 20:00	6.27
81	1/4/18 21:00	6.24
82	1/4/18 22:00	6.21
83	1/4/18 23:00	6.17
84	1/5/18 0:00	6.14
85	1/5/18 1:00	6.11
86	1/5/18 2:00	6.07
87	1/5/18 3:00	6.04
88	1/5/18 4:00	6.01
89	1/5/18 5:00	5.97
90	1/5/18 6:00	5.94
91	1/5/18 7:00	5.91

Table 31: Period of record flood conditions downstream boundary condition water surface elevation hydrograph.

Hour	Date / Time	Elevation (ft, NAVD 88)
92	1/5/18 8:00	5.87
93	1/5/18 9:00	5.84
94	1/5/18 10:00	5.81
95	1/5/18 11:00	5.77
96	1/5/18 12:00	5.74
97	1/5/18 13:00	5.70
98	1/5/18 14:00	5.67
99	1/5/18 15:00	5.63
100	1/5/18 16:00	5.60
101	1/5/18 17:00	5.56
102	1/5/18 18:00	5.53
103	1/5/18 19:00	5.49
104	1/5/18 20:00	5.46
105	1/5/18 21:00	5.42
106	1/5/18 22:00	5.39
107	1/5/18 23:00	5.35
108	1/6/18 0:00	5.32
109	1/6/18 1:00	5.28
110	1/6/18 2:00	5.24
111	1/6/18 3:00	5.21
112	1/6/18 4:00	5.17
113	1/6/18 5:00	5.14
114	1/6/18 6:00	5.10

Table 31: Period of record flood conditions downstream boundary condition water surface elevation hydrograph.

Hour	Date / Time	Elevation (ft, NAVD 88)
115	1/6/18 7:00	5.07
116	1/6/18 8:00	5.03
117	1/6/18 9:00	5.00
118	1/6/18 10:00	4.96
119	1/6/18 11:00	4.93
120	1/6/18 12:00	4.89
121	1/6/18 13:00	4.86
122	1/6/18 14:00	4.83
123	1/6/18 15:00	4.80
124	1/6/18 16:00	4.77
125	1/6/18 17:00	4.74
126	1/6/18 18:00	4.72
127	1/6/18 19:00	4.69
128	1/6/18 20:00	4.66
129	1/6/18 21:00	4.63
130	1/6/18 22:00	4.60
131	1/6/18 23:00	4.57
132	1/7/18 0:00	4.54
133	1/7/18 1:00	4.51
134	1/7/18 2:00	4.48
135	1/7/18 3:00	4.45
136	1/7/18 4:00	4.42
137	1/7/18 5:00	4.39

Table 31: Period of record flood conditions downstream boundary condition water surface elevation hydrograph.

Hour	Date / Time	Elevation (ft, NAVD 88)
138	1/7/18 6:00	4.37
139	1/7/18 7:00	4.34
140	1/7/18 8:00	4.31
141	1/7/18 9:00	4.28
142	1/7/18 10:00	4.25
143	1/7/18 11:00	4.22
144	1/7/18 12:00	4.19
145	1/7/18 13:00	4.16
146	1/7/18 14:00	4.13
147	1/7/18 15:00	4.10
148	1/7/18 16:00	4.07
149	1/7/18 17:00	4.04
150	1/7/18 18:00	4.01
151	1/7/18 19:00	3.97
152	1/7/18 20:00	3.94
153	1/7/18 21:00	3.91
154	1/7/18 22:00	3.88
155	1/7/18 23:00	3.85
156	1/8/18 0:00	3.82
157	1/8/18 1:00	3.79
158	1/8/18 2:00	3.76
159	1/8/18 3:00	3.73
160	1/8/18 4:00	3.70

Table 31: Period of record flood conditions downstream boundary condition water surface elevation hydrograph.

Hour	Date / Time	Elevation (ft, NAVD 88)
161	1/8/18 5:00	3.67
162	1/8/18 6:00	3.64
163	1/8/18 7:00	3.60
164	1/8/18 8:00	3.57
165	1/8/18 9:00	3.54
166	1/8/18 10:00	3.51
167	1/8/18 11:00	3.48
168	1/8/18 12:00	3.45
169	1/8/18 13:00	3.42
170	1/8/18 14:00	3.39
171	1/8/18 15:00	3.36
172	1/8/18 16:00	3.34
173	1/8/18 17:00	3.31
174	1/8/18 18:00	3.28
175	1/8/18 19:00	3.25
176	1/8/18 20:00	3.22
177	1/8/18 21:00	3.19
178	1/8/18 22:00	3.16
179	1/8/18 23:00	3.13
180	1/9/18 0:00	3.11
181	1/9/18 1:00	3.08
182	1/9/18 2:00	3.05
183	1/9/18 3:00	3.02

Table 31: Period of record flood conditions downstream boundary condition water surface elevation hydrograph.

Hour	Date / Time	Elevation (ft, NAVD 88)
184	1/9/18 4:00	2.99
185	1/9/18 5:00	2.96
186	1/9/18 6:00	2.93
187	1/9/18 7:00	2.90
188	1/9/18 8:00	2.88
189	1/9/18 9:00	2.85
190	1/9/18 10:00	2.82
191	1/9/18 11:00	2.79
192	1/9/18 12:00	2.76
193	1/9/18 13:00	2.74
194	1/9/18 14:00	2.71
195	1/9/18 15:00	2.69
196	1/9/18 16:00	2.67
197	1/9/18 17:00	2.64
198	1/9/18 18:00	2.62
199	1/9/18 19:00	2.60
200	1/9/18 20:00	2.57
201	1/9/18 21:00	2.55
202	1/9/18 22:00	2.53
203	1/9/18 23:00	2.50
204	1/10/18 0:00	2.48
205	1/10/18 1:00	2.46
206	1/10/18 2:00	2.43

Table 31: Period of record flood conditions downstream boundary condition water surface elevation hydrograph.

Hour	Date / Time	Elevation (ft, NAVD 88)
207	1/10/18 3:00	2.41
208	1/10/18 4:00	2.39
209	1/10/18 5:00	2.36
210	1/10/18 6:00	2.34
211	1/10/18 7:00	2.32
212	1/10/18 8:00	2.29
213	1/10/18 9:00	2.27
214	1/10/18 10:00	2.25
215	1/10/18 11:00	2.22
216	1/10/18 12:00	2.20
217	1/10/18 13:00	2.19
218	1/10/18 14:00	2.17
219	1/10/18 15:00	2.16
220	1/10/18 16:00	2.14
221	1/10/18 17:00	2.13
222	1/10/18 18:00	2.11
223	1/10/18 19:00	2.10
224	1/10/18 20:00	2.08
225	1/10/18 21:00	2.07
226	1/10/18 22:00	2.05
227	1/10/18 23:00	2.04
228	1/11/18 0:00	2.03
229	1/11/18 1:00	2.01

Table 31: Period of record flood conditions downstream boundary condition water surface elevation hydrograph.

Hour	Date / Time	Elevation (ft, NAVD 88)
230	1/11/18 2:00	2.00
231	1/11/18 3:00	1.98
232	1/11/18 4:00	1.97
233	1/11/18 5:00	1.95
234	1/11/18 6:00	1.94
235	1/11/18 7:00	1.92
236	1/11/18 8:00	1.91
237	1/11/18 9:00	1.89
238	1/11/18 10:00	1.88
239	1/11/18 11:00	1.86
240	1/11/18 12:00	1.85
241	1/11/18 13:00	1.85
242	1/11/18 14:00	1.86
243	1/11/18 15:00	1.86
244	1/11/18 16:00	1.87
245	1/11/18 17:00	1.87
246	1/11/18 18:00	1.87
247	1/11/18 19:00	1.88
248	1/11/18 20:00	1.88
249	1/11/18 21:00	1.88
250	1/11/18 22:00	1.89
251	1/11/18 23:00	1.89
252	1/12/18 0:00	1.90

Table 31: Period of record flood conditions downstream boundary condition water surface elevation hydrograph.

Hour	Date / Time	Elevation (ft, NAVD 88)
253	1/12/18 1:00	1.90
254	1/12/18 2:00	1.90
255	1/12/18 3:00	1.91
256	1/12/18 4:00	1.91
257	1/12/18 5:00	1.91
258	1/12/18 6:00	1.92
259	1/12/18 7:00	1.92
260	1/12/18 8:00	1.93
261	1/12/18 9:00	1.93
262	1/12/18 10:00	1.93
263	1/12/18 11:00	1.94
264	1/12/18 12:00	1.94
265	1/12/18 13:00	1.94
266	1/12/18 14:00	1.94
267	1/12/18 15:00	1.94
268	1/12/18 16:00	1.94
269	1/12/18 17:00	1.94
270	1/12/18 18:00	1.94
271	1/12/18 19:00	1.94
272	1/12/18 20:00	1.94
273	1/12/18 21:00	1.94
274	1/12/18 22:00	1.94
275	1/12/18 23:00	1.94

Table 31: Period of record flood conditions downstream boundary condition water surface elevation hydrograph.

Hour	Date / Time	Elevation (ft, NAVD 88)
276	1/13/18 0:00	1.94
277	1/13/18 1:00	1.93
278	1/13/18 2:00	1.93
279	1/13/18 3:00	1.93
280	1/13/18 4:00	1.93
281	1/13/18 5:00	1.93
282	1/13/18 6:00	1.93
283	1/13/18 7:00	1.93
284	1/13/18 8:00	1.93
285	1/13/18 9:00	1.93
286	1/13/18 10:00	1.93
287	1/13/18 11:00	1.93
288	1/13/18 12:00	1.93
289	1/13/18 13:00	1.92
290	1/13/18 14:00	1.90
291	1/13/18 15:00	1.89
292	1/13/18 16:00	1.88
293	1/13/18 17:00	1.86
294	1/13/18 18:00	1.85
295	1/13/18 19:00	1.84
296	1/13/18 20:00	1.82
297	1/13/18 21:00	1.81
298	1/13/18 22:00	1.80

Table 31: Period of record flood conditions downstream boundary condition water surface elevation hydrograph.

Hour	Date / Time	Elevation (ft, NAVD 88)
299	1/13/18 23:00	1.78
300	1/14/18 0:00	1.77
301	1/14/18 1:00	1.76
302	1/14/18 2:00	1.74
303	1/14/18 3:00	1.73
304	1/14/18 4:00	1.72
305	1/14/18 5:00	1.70
306	1/14/18 6:00	1.69
307	1/14/18 7:00	1.68
308	1/14/18 8:00	1.66
309	1/14/18 9:00	1.65
310	1/14/18 10:00	1.64
311	1/14/18 11:00	1.62
312	1/14/18 12:00	1.61
313	1/14/18 13:00	1.61
314	1/14/18 14:00	1.61
315	1/14/18 15:00	1.60
316	1/14/18 16:00	1.60
317	1/14/18 17:00	1.60
318	1/14/18 18:00	1.60
319	1/14/18 19:00	1.59
320	1/14/18 20:00	1.59
321	1/14/18 21:00	1.59

Table 31: Period of record flood conditions downstream boundary condition water surface elevation hydrograph.

Hour	Date / Time	Elevation (ft, NAVD 88)
322	1/14/18 22:00	1.59
323	1/14/18 23:00	1.58
324	1/15/18 0:00	1.58
325	1/15/18 1:00	1.58
326	1/15/18 2:00	1.58
327	1/15/18 3:00	1.57
328	1/15/18 4:00	1.57
329	1/15/18 5:00	1.57
330	1/15/18 6:00	1.57
331	1/15/18 7:00	1.56
332	1/15/18 8:00	1.56
333	1/15/18 9:00	1.56
334	1/15/18 10:00	1.56
335	1/15/18 11:00	1.55
336	1/15/18 12:00	1.55
337	1/15/18 13:00	1.55
338	1/15/18 14:00	1.54
339	1/15/18 15:00	1.54
340	1/15/18 16:00	1.53
341	1/15/18 17:00	1.53
342	1/15/18 18:00	1.52
343	1/15/18 19:00	1.52
344	1/15/18 20:00	1.51

Table 31: Period of record flood conditions downstream boundary condition water surface elevation hydrograph.

Hour	Date / Time	Elevation (ft, NAVD 88)
345	1/15/18 21:00	1.51
346	1/15/18 22:00	1.50
347	1/15/18 23:00	1.50
348	1/16/18 0:00	1.49
349	1/16/18 1:00	1.49
350	1/16/18 2:00	1.48
351	1/16/18 3:00	1.48
352	1/16/18 4:00	1.47
353	1/16/18 5:00	1.47
354	1/16/18 6:00	1.46
355	1/16/18 7:00	1.46
356	1/16/18 8:00	1.45
357	1/16/18 9:00	1.45
358	1/16/18 10:00	1.44
359	1/16/18 11:00	1.44

Stationarity Analysis of Historic Precipitation and Flow

In 2016, the United States Army Corps of Engineers (USACE) issued Engineering and Construction Bulletin No. 2016-25 (ECB 2016-25), which stipulated that climate change should be considered for all Federally funded projects in planning stages. A qualitative analysis of historical climate trends as well as an assessment of future projections was provisioned by ECB 2016-25. Even if climate change does not appear to be an impact for a particular region of interest, the formal analysis outlined in ECB 2016-25 results in better informed planning and engineering decisions. For example, an increase in impervious area can often result in higher streamflow, even with no trend in heavy rainfall.

Although this study did not fall under the requirements of ECB 2016-25, future applications of the model to assess the feasibility of project alternatives likely would fall under this requirement if Federal funds are used for planning and implementation. To provide future users of the ARBNM with an insight into the potential vulnerability of the watershed, stationarity tests were performed on long-record precipitation and streamflow gages to assess whether non-stationarity needs to be factored in for future planning projects. These tests were performed through water year 2016.

The full stationarity study is included in **Appendix 5**.

Summary of Stationarity Assessment

The Flood of August 2016 significantly increased the estimated 1% Annual Exceedance Probability flows for the lower reaches of Amite and Comite Rivers. The 1% AEP is still considerably lower than the flows recorded during that event.

The stationarity tests show positive trends in both precipitation and streamflow. For precipitation gages, regional-scale changes in Annual Maximum Series, Peaks-Over-Threshold and the 99th percentile of daily rainfall all suggest an upward increase in heavy rainfall magnitude and intensity. For streamflow, increases were found at 3 of the 6 tested gages (with no significant changes at the other sites): the Comite River near Olive Branch, Comite River near Comite and Amite River near Denham Springs. For the Olive Branch site, only two of the four trend tests found significant results, making it difficult to definitively confirm that non-stationarity was present. The two other sites had more convincing evidence of increased streamflow over time, though it is difficult to determine if this is due to changes in precipitation or impervious cover owing to a marked increase in the number of residential structures being built around the time of the changes in streamflow.

CONSEQUENCE MODEL

Version 1.0 of the February 2019 Amite River Basin (ARB) consequence model was developed in HEC-FIA Version 3.0.1 and covered the entire ARB. The model was developed to operate both standalone by reading in HEC-RAS gridded outputs from RAS Mapper as well as seamlessly integrating within HEC-WAT to develop on-the-fly consequence assessments from the ARB HEC-RAS model results. HEC-FIA calculates economic losses (structure, content, etc.), agriculture losses, and expected life loss.

Base Input Data

As illustrated in **Figure 69**, the HEC-FIA model included:

- 230,382 structures derived from the 2018 LA DOTD LiDAR point cloud
- HUC8 boundary for the ARB
- 6 Parish boundaries within the ARB
- 2016 Agriculture data derived from the USDA National Agricultural Statistics Service CropScope and Cropland Data Layer (NASS CDL).

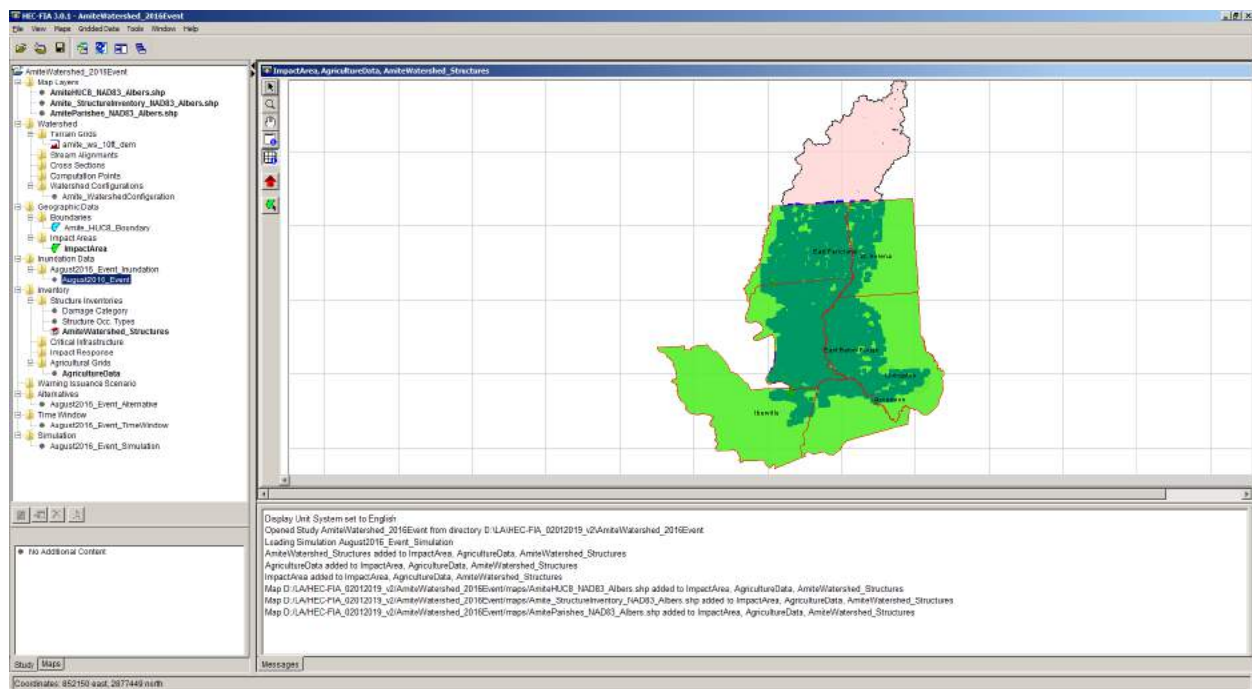


Figure 69: ARB HEC-FIA Consequence Model Overview

HEC-FIA required an array of inputs as listed in **Table 32**. In order to produce the necessary structure inventory input for the HEC-FIA model, Dewberry initially investigated utilizing parish assessor and Hazus data; however, it was quickly determined that the necessary input fields for HEC-FIA were either incomplete or not present in these datasets. In an effort to refine this data, Dewberry acquired the National Structure Inventory (NSI) from FEMA through the public website:

https://data.fema.com/DR4277_Severe_Storms_Flooding_LA/Structure_Data/.

The NSI is based on FEMA's Hazus database, but has been enhanced with the NLCD database to identify areas that are urbanized. This was performed by the USACE who is understood to have converted the Hazus database to point-based structures that contain consistent attributes throughout the entire United States. Investigation of the NSI data showed that, while this dataset was more robust than the Hazus and assessor data, structure locations were not accurately represented as illustrated in **Figure 70**. This identified a need to develop more accurate structure inventory for the ARB HEC-FIA model.

Table 32: HEC-FIA Structure Inventory inputs for HEC-FIA	
Damage Category	Number of Cars
Occupancy Type	Population 5pm Over 65
Replacement Value	Population 5pm Under 65
Construction Type	Population Day Over 65
Content Value	Population Day Under 65
Foundation Height	Population Night Over 65
Foundation Type	Population Night Under 65
Number of Stories	Number of Years in Service

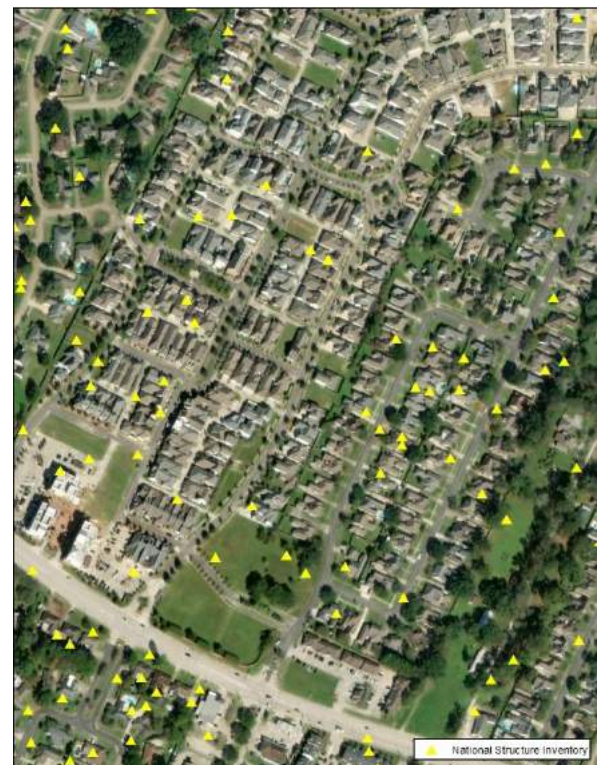


Figure 70: Example of the NSI (yellow triangles) in East Baton Rouge Parish.

Building Footprint Development

To overcome the limitations of NSI data and meet the needs of the ARB HEC-FIA model, Dewberry developed approximate building footprints for the entire ARB using point cloud information from the 2018 LA DOTD LiDAR. A high level cleaning was performed on the building footprints to remove artifacts and minor ancillary structures (i.e. bridges, overpasses, boats, sheds etc.). If multiple structures were located within a single parcel (where parcel information was acquired), then the structure with the largest area was kept, and remaining structures were removed being assumed to represent ancillary structures of minimal economic value such as pet houses and small storage sheds. However, upon review of parcels with 4 or more sizable structures, it was generally determined that these represented either industrial locations or locations where new housing developments have occurred and the parcel data does not represent the subdivided lots. Therefore these buildings were preserved and assumed to be valid structure of significant economic value. **Figure 71** shows a comparison between the LiDAR derived structures and the NSI.



Figure 71: Comparison of LiDAR derived structures (red squares) and the NSI (yellow triangles) in East Baton Rouge parish.

With the building footprints completed, information listed in **Table 32** was populated for each structure. Ascension, East Baton Rouge, and Livingston parishes supplied parcel data, which contained information regarding the replacement value of the structure, but no other information. No parcel information was obtained from East Feliciana, Iberville, nor St. Helena parishes. To conflate the necessary fields to the building footprints, a spatial query was done, where the information from the closest NSI point was assigned to the LiDAR derived structure. Replacement values for Ascension, East Baton Rouge, and Livingston structures were assigned from the parcel dataset, and content value was assumed to be 50% of the replacement value. All other fields were conflated from the NSI data. For East Feliciana, Iberville, and St. Helena parishes, all fields were conflated from the NSI data, and attributes populated for all points.

Agricultural Grid

Agricultural information was determined from the USDA NASS CDL grid which can be downloaded from <https://nassgeodata.gmu.edu/CropScape/>. This indicated that there are eight crops within the ARB: corn, other hays, rice, soybeans, sorghum, sugar cane, sweet potatoes, and winter wheat.

In the ARB, agriculture data makes up only 0.0047% of the total land area; however, as demonstrated below, HEC-FIA is able to compute agricultural damage based on depth and duration of flooding. For future basin studies, this will likely become more significant with an example being north Louisiana, where there are large areas of sweet potato and other crops.

Inundation Grids

HEC-FIA accepts inundation information in several formats. For ARB HEC-FIA model, the hydraulic data type is assumed to utilize grids only since the ARB HEC-RAS model is fully spatially referenced and grids can be automatically exported from RAS Mapper in HEC-FIA ready TIF formats. **Figure 72** illustrates the input grids necessary for this model.

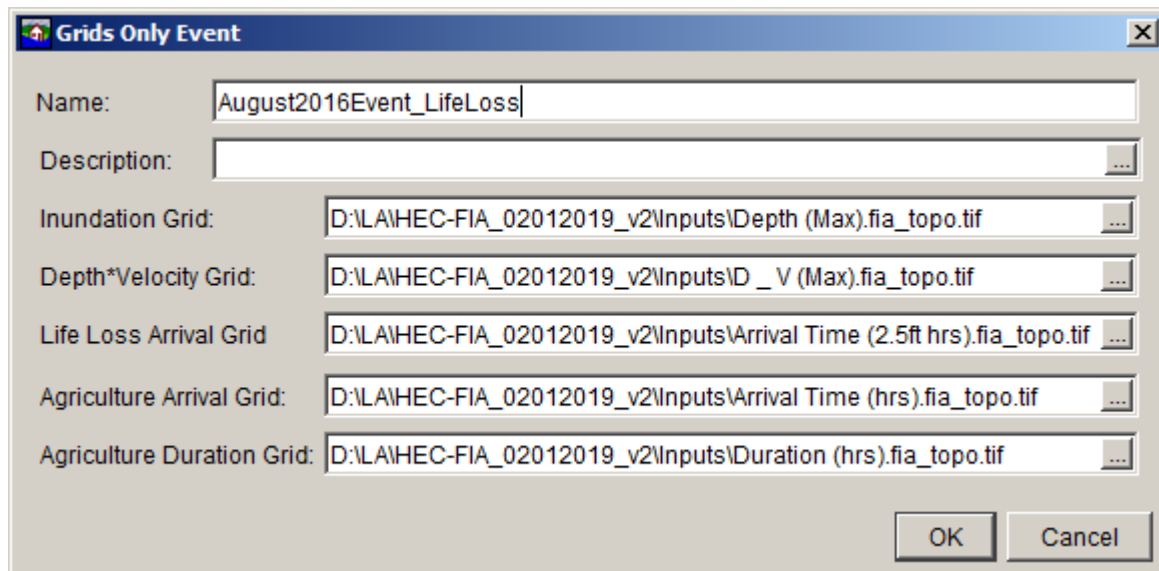


Figure 72: HEC-FIA grids only event set-up.

Model Parameters

Economic Losses

As previously described, the input structures into the HEC-FIA model have multiple fields to determine both the economic losses as well as the life-loss computations. The most critical parameter for structure and content value loss calculations are the structure occupancy type (inputted as the damage category). HEC-FIA accepts 36 structure occupancy types, which associates the structure with a predetermined depth-damage curve within HEC-FIA. **Table 33** shows the structure occupancy type, description, and number of structures in the ARB determined from the building information developed specifically for this project.

Table 33: Occupancy Type and Count Estimated for the ARB		
Structure Occupancy Type	Description	Number of Structures
Agricultural	Average Agricultural	446
Commercial	Retail, Wholesale, Personal & Repair Services, Professional/Tech Services, Bank, Hospital, Medical Office, Entertainment/recreation, Theater	12,697
Educational	School, College/University	852
Government	Government Services, Emergency Response	562
Industrial	Heavy Industrial, Light Industrial, Food/Drug/Chemical, Metals/Minerals Processing, High Technology, Construction	3,321
Religious	Church	2,043
Residential	1, 2, or 3 Story, Split Level, Condominium with living area on multiple floors, Mobile Home, Hotel & Motel, Institutional Dormitory, Nursing Home	210,461
Total:		230,382

Examples of the depth damage curves utilized by HEC-FIA to estimate economic losses are presented in **Figure 73** and **Figure 74**. These depth-damage functions are default values within the HEC-FIA software. The depth-damage relationships closely follows nationally accepted values present in FEMA's Hazus software.

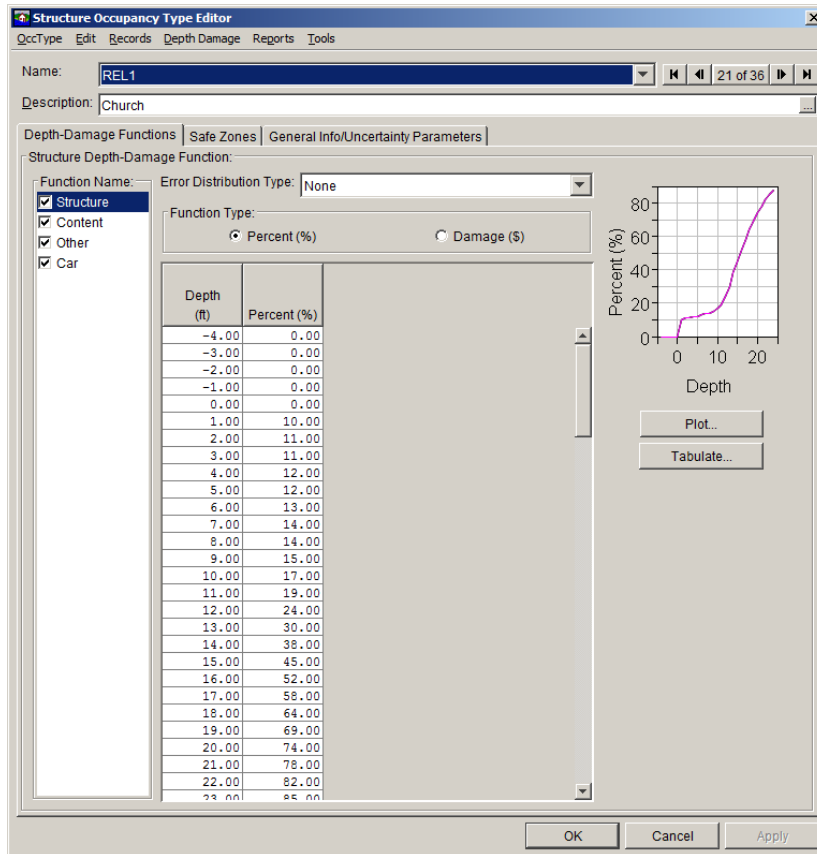


Figure 73: Depth-damage curve associated with structure occupancy type REL 1, Church.

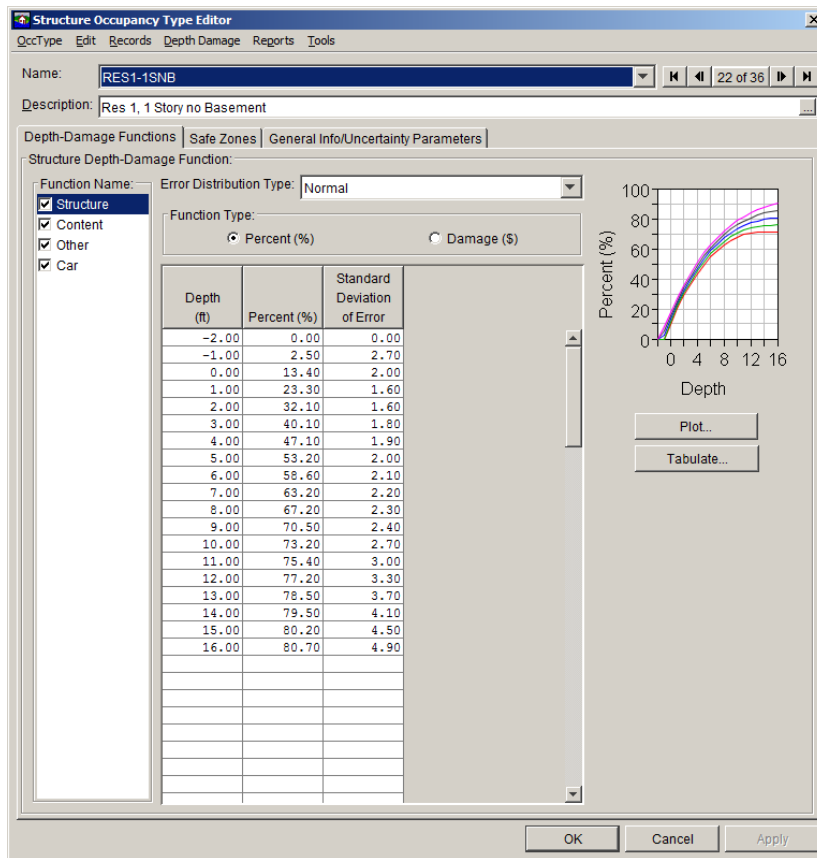


Figure 74: Depth-damage curve associated with structure occupancy type RES1-1SNB, Residential one story with no basement.

Agricultural Data

As previously discussed, HEC-FIA can also compute the agriculture loss for flooding events. The USDA NASS CDL grid is imported into HEC-FIA. Within the ARB, there were eight unique crops identified: corn, other hays, rice, soybeans, sorghum, sugar cane, sweet potatoes, and winter wheat. For each unique crop type, several factors were determined including the fixed planting cost, typical harvest date, cost to harvest, yield, and unit price. These values were determined by investigating reports from various entities, including the USDA 'Field Crops – Usual Planting and Harvesting Dates' and the 2016 Crop Budgets from the LSU Agriculture Center.

HEC-FIA also requires the duration versus percent crop loss to compute crop loss information. **Figure 75** shows how this information is inputted into HEC-FIA and can be customized per crop.

Crop Loss Editor

Crop: Corn 1 of 8

	Date (DDMMM)	Jan	Feb	Mar	Apr	May	Jun	Jul	Aug	Sep	Oct	Nov	Dec
Fixed Cost		\$39.39	\$39.39	\$39.39	\$39.39	\$39.39	\$39.39	\$39.39	\$39.39	\$39.39	\$39.39	\$39.39	\$39.39
Variable Cost First Pla...	01Mar	0.00	0.00	0.00	0.00	0.00	0.00	0.00	0.00	0.00	0.00	0.00	0.00
Variable Cost Last Pla...	01Apr	0.00	0.00	0.00	0.00	0.00	0.00	0.00	0.00	0.00	0.00	0.00	0.00

Substitute Crop:

Harvest Date	Harvest Cost	Yield	Unit	Unit Price	% Loss from Late Plant
01Aug	\$40.70	165.0	BU	\$3.70	0.0

Number of Days	Jan	Feb	Mar	Apr	May	Jun	Jul	Aug	Sep	Oct	Nov	Dec
1.0	5.0	5.0	5.0	5.0	5.0	5.0	5.0	5.0	5.0	5.0	5.0	5.0
2.0	15.0	15.0	15.0	15.0	15.0	15.0	15.0	15.0	15.0	15.0	15.0	15.0
3.0	25.0	25.0	25.0	25.0	25.0	25.0	25.0	25.0	25.0	25.0	25.0	25.0
7.0	50.0	50.0	50.0	50.0	50.0	50.0	50.0	50.0	50.0	50.0	50.0	50.0

Add Duration

Plot Tabulate OK Cancel

Figure 75: Crop loss editor table in HEC-FIA.

Life-Loss

HEC-FIA has the ability to model the life-loss for flooding events utilizing a simplified version of the LIFESim methodology (Utah State University, 2005). The key difference between the full version of LIFESim methodology used in HEC-LifeSim and the simplified HEC-LifeSim is the evacuation modeling simulations. Further discussion of the evacuation definition will be discussed in the Alternatives section below.

Life-Loss simulations for the ARB requires user defined information regarding the structure stability under flooding conditions, impact areas, and warning issuance scenarios; as well as outputs from the ARB HEC-RAS model, including depth times velocity grid and arrival time of the flooding.

The structure occupancy type also informs HEC-FIA Life-Loss simulations the “safe zone” within each structure. The safe zone refers to the depth of water necessary to deem a structure unsafe during a flooding event. **Figure 76** and **Figure 77** show examples of different stories and the variance of the safe zone. Safe zones are computed differently based on age of occupants, and are categorized as over 65 and under 65.

Structure Occupancy Type Editor

QccType Edit Records Reports Tools

Name: **RES1-1SNB** 22 of 36

Description: Res 1, 1 Story no Basement

Depth-Damage Functions Safe Zones General Info/Uncertainty Parameters

Structure Height Information:
Number of Stories: 1

Structure Zone Height Information:

	Under 65	Over 65
Chance Zone		
Chance Zone Start (ft):	15.0	6.0
Compromised Zone		
Compromised Zone Start (ft):	13.0	4.0
Safe Zone		

Depth * Velocity Thresholds

	Partial Damage	Total Damage
Wood Frame - Anchored (ft2):	32.3	75.3
Wood Frame - Unanchored (ft2):	21.5	32.3
Masonry, Concrete, and Steel (ft2):	32.3	75.3

OK Cancel Apply

Figure 76: Safe zone parameters for structure occupancy type RES1-1SNB, Residential one story with no basement

Structure Occupancy Type Editor

QccType Edit Records Reports Tools

Name: RES1-2SNB 24 of 36

Description: Res 1, 2 Story no Basement

Depth-Damage Functions Safe Zones General Info/Uncertainty Parameters

Structure Height Information:
Number of Stories: 2

Structure Zone Height Information:

	Under 65	Over 65
Chance Zone		
Chance Zone Start (ft):	24.0	15.0
Compromised Zone		
Compromised Zone Start (ft):	22.0	13.0
Safe Zone		

Depth * Velocity Thresholds

	Partial Damage	Total Damage
Wood Frame - Anchored (ft2):	32.3	75.3
Wood Frame - Unanchored (ft2):	21.5	32.3
Masonry, Concrete, and Steel (ft2):	32.3	75.3

OK Cancel Apply

Figure 77: Safe zone parameters for structure occupancy type RES1-2SNB, Residential two story with no basement.

Impact Area Parameters and Warning Issuance Scenario

The impact parameters in HEC-FIA allows the user to input the effectiveness of the warning system as related to the flooding event. The warning system was assumed to be “EAS, sirens, and auto-dial telephones,” and the default values for timing and effectiveness were utilized as illustrated in **Figure 78**.

Impact Area Editor

Impact Area Name: Ascension

Impact Area Description:

Life Loss Parameters | Population Adjustment | Adjusted Price Index

☐ Apply to all impact areas.

Warning System:

Mobilization:

Error Distribution Type:

k: 30 Min Limit:
 a1: Release Rate:
 a2:

Time (minutes)	% War... (Day)	% War... (Night)
0	0.00	0.00
1	11.68	11.97
2	22.32	22.81

% Warned

Minutes

Day Night

Effectiveness by Activity Type

Home...	Indoors	Outdo...	In Tra...	Worki...	Watch...	Listen...
95.0	97.0	90.0	90.0	85.0	100.0	100.0

Time (minutes)	% Mobilized
0.0	0.0
15.0	50.0
60.0	75.0
120.0	85.0
240.0	98.0

% Mobilized

Minutes

Additional Parameters

OK Cancel Apply

Figure 78: Impact area editor showing the default values chosen for the ARB.

“Additional parameters” were selected to allow the life-loss calculations to perform the calculations with uncertainty. The default values for the three zones (safe zone [sz], compromised zone [cz], and chance zone [chz]), as well as the non-evacuation depth of 2 ft., and the activity type distribution were utilized as illustrated in **Figure 79**.

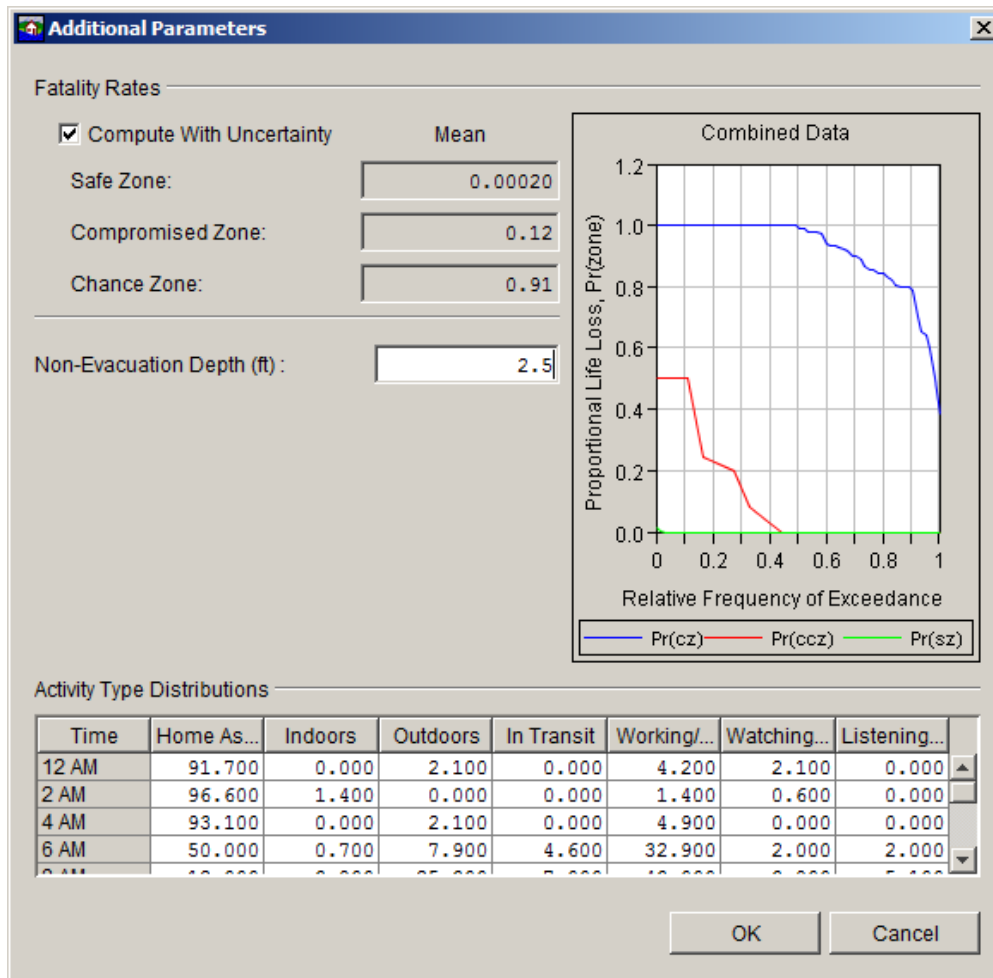


Figure 79: “Additional Parameters” editor for computing life-loss with uncertainty.

The final parameter for life-loss calculations is the Warning Issuance Scenario, which defines the timing of when the warning is issued relative to the start of the flooding event. For the ARB HEC-FIA model, the issuance scenario was set to “12 hrs” relative to start time (i.e. the warnings were issued 12 hrs after the perceived start of the flooding event) as illustrated in **Figure 80**. For the ARB hydraulics, precipitation began falling on August 10th at noon. **Figure 81** details the actual timing of watches and warnings issued by the NWS within the ARB for the August 2016 event which was used to develop the 12 hour assumption.

All Structures	Hours Relative to Start Time	Error Distribution Type	Most Likely Offset (Minutes)	Standard Deviation	Log 10 Standard Deviation	Minimum Value	Maximum Value
All Structur...	12.0	None	0.0				

Figure 80: Warning issuance scenario for the August 2016 flooding event.

- Mon 1014a - Hydrologic Outlook (ESFLIX) issued headlining Heavy Rainfall May Produce Elevated River Levels in Coming Days mentioning a flood watch may be posted at a later time
- Mon 359p - First email sent to emergency managers talking about heavy rainfall potential later in the week
- Mon 451p - First graphic posted to social media and website showing potential for heavy rainfall later in the week.
- Tues 139p - Flood Watch issued for St. Tammany and MS Coastal Counties
- Tues 200p - First webinar briefing held for emergency managers to talk about heavy rainfall potential
- Wed 951a - Flood Watch expanded to include north shore and southern Tangipahoa Parishes
- Thur 432a - Flood Watch replaced with Flash Flood Watch and expanded to include all of SE LA and S MS Thursday morning (first issuance for BTR area)
- Thur 854a - First Flash Flood Warning issued for parts of coastal MS
- Thur 928a - First Flash Flood Warning issued for parts of LA River Parishes
- Thur 1019a - First Flood Warning issued for Amite/Comite Rivers
- Thur 516p - First Flash Flood Warning issued for part of SW MS
- Fri 209a - First Flash Flood Warning issued for parishes north of Baton Rouge
- Fri 423a - First Flash Flood Warning issued for Baton Rouge and surrounding areas
- Fri 618a - First Flash Flood Emergency issued for part of SW MS
- Fri 621a - First Flash Flood Emergency issued for parts of SE LA north of Baton Rouge
- Fri 1005a - First Flash Flood Emergency issued for parts of Baton Rouge metro

Figure 81: Timeline of watches and warnings issued by the NWS for Louisiana.

Source: Ken Graham, Meteorologist in Charge, National Weather Service for New Orleans and Baton Rouge

Alternatives

The Alternatives input in HEC-FIA informs HEC-FIA what datasets to use in modeling the economic damages, agricultural damages, and life-loss as illustrated in **Figure 82**.

The simplified HEC-LifeSim requires users to input the evacuation information in one of four ways:

- Let HEC-FIA Compute. The user inputs the Impact Area and a nominal evacuation velocity. The distance from each structure is subsequently computed using a straight line from the structure to the edge of the impact area, and the evacuation velocity determines the amount of time to arrive at the impact area boundary
- All Structures. The evacuation time for all structures within the study are assigned a nominal evacuation time.
- Impact Areas. The evacuation time for all structures within a specific impact area will be assigned the same nominal evacuation time.

- Individual structures. Each structure within the study area can be assigned an evacuation time based on the user input.

The screenshot shows the 'Edit Alternative' dialog box with the following fields and options:

- Name:** Alt_LifeLoss
- Description:** (empty text box)
- Impact Area Set:** ImpactArea
- Inundation Configuration:** August2016Event_LifeLoss
- Structure Inventory:** AmiteWatershed_Structures
- Critical Infrastructure:** (empty dropdown)
- Impact Response:** (empty dropdown)
- Agriculture Inventory:** AgriculturalGrid
- Warning Issuance:** WarningIssuance

Below these fields are tabs for **Life Loss**, **Agriculture**, **Uncertainty**, **ECAM**, and **Output**. The **Life Loss** tab is active and contains:

- ☒ **Compute Life Loss**
- ☒ **Compute Life Loss for Relative Times** with a **Choose Times** button
- Evacuation Information** section:
 - Define Time By:** Let HEC-FIA Compute
 - Select Hazard Area Shapefile:** AmiteParishes_NAD83_Albers.shp
 - Nominal Evacuation Velocity(mph):** 25.0

At the bottom are **OK** and **Cancel** buttons.

Figure 82: Alternative editing GUI

Results and Validation

To ensure that the ARB HEC-FIA model produces reasonable results for economic and life loss estimates, the August 2016 flood was used to validate results against documented damages and reported fatalities.

Economic losses and life-loss for this event were summarized in the report “The Economic Impact of the August 2016 Floods in the State of Louisiana,” a report commissioned by Louisiana Economic Development (LED). The report estimates the number of structures damaged, economic losses from flooding, and life-loss as a result of the flooding.

Economic Damages

Table 34 summarizes the economic damages computed in the HEC-FIA simulation of the August 2016 event.

Table 34: Summary of HEC-FIA Computed Economic Damages Estimated for the August 2016 Flood				
Parish	Structure Damage (\$1000)	Content Damage (\$1000)	Car Damage (\$1000)	Total (\$1000)
Ascension	102,303.07	38,023.41	9,895.57	150,222.05
East Baton Rouge	1,499,495.04	706,891.26	112,432.77	2,318,818.82
East Feliciana	9,994.10	5,534.93	1,588.50	17,117.52
Iberville	8,018.76	3,921.36	45.95	11,986.07
Livingston	1,134,989.06	514,080.80	58,352.05	1,707,421.82
St. Helena	2,772.98	1,148.95	782.31	4,704.24
Total	2,757,573.12	1,269,600.64	183,097.14	4,210,270.98

Per the LED report, the total structure damage for the entire event (consisting of 20 counties), was estimated at \$4.439 billion dollars, while the total content damage was estimated at \$1.541 billion dollars. Note that the LED report does not break down the damage numbers by parish, however, this would suggest that the HEC-FIA results are reasonable and as expected are less than the values reported by LED which was not limited to the ARB.

Number of Structures

Table 35 compares the number of structures damaged from the HEC-FIA model versus the number estimated from the LED report for the 6 parishes in the ARB for the August 2016 flood. Note, that the LED numbers are parish-wide.

Table 35: Summary of HEC-FIA Computed Damaged Structures Counts Estimated for the August 2016 Flood			
Parish	HEC-FIA	LED Estimate	LED Weighted ¹
Ascension	3,969	13,100	2,096
East Baton Rouge	47,181	41,000	30,750
East Feliciana	317	300	246
Iberville	270	100	7
Livingston	19,431	38,300	18,845
St. Helena	67	400	132
Total	71,235	93,200	52,076

¹ The LED weighted values were determined assuming an even distribution of the structures for the portion of the parish within the ARB.

Life-Loss

HEC-FIA Life-Loss Detailed Report provides information about how the life-loss was calculated for the study area. The report aggregates the data to explain how life loss was computed. **Table 36** summarizes the documented and HEC-FIA simulated life loss estimates for the ARB. The documented life loss was obtained from online media sources which included the location of the fatality enabling life loss within the ARB to be isolated. It is important to note that HEC-FIA is unable to consider all local variables that may have life safety impacts. This may include variables such as the ownership of boats and large trucks with high ground clearance and four wheel drive. Within the ARB, there is visible evidence that boat and truck ownership is likely significantly higher than the national average. Additionally, the Cajun Navy, an informal ad-hoc volunteer group comprising of boat owners responded to the august 2016 flood to assist in evacuations which likely reduced life loss. Testing of the HEC-FIA life loss simulations indicated that it was highly sensitive to the amount of warning time given.

Table 36: Summary of observed and HEC-FIA simulated life loss for the August 2016 Flood for the ARB				
Parish	Documented Life Loss ¹		HEC-FIA Modeled Life Loss	
	Under 65	Over 65	Under 65	Over 65
Ascension	0	0	0	0
East Baton Rouge	4	1	5	12
East Feliciana	0	0	0	0
Iberville	0	0	0	0
Livingston ²	1	1	5	7
St. Helena	0	0	0	0
Total	5	2	10	19
¹ Information obtained from https://www.nola.com/weather/2016/08/la_flood_victims_black_and_white.html ² A total of 2 deaths were reported, but the age of one was not identified and was assumed to be under 65				

While there is considerable uncertainty when estimating life loss and HEC-FIA clearly over estimated life loss during the August 2016 flood, it does provide a good foundation for assessing project alternatives and performing an apples to apples comparison of the potential benefits.

The ARB HEC-FIA model provides a reliable platform for futures users to further refine the model and perform economic and life loss assessments to quantify and evaluate the potential consequences of both structural and non-structural measures on both a project and regional planning level.

HEC-WAT IMPLEMENTATION AND DEMONSTRATION PROJECTS

HEC-WAT is a relatively new tool developed by the USACE HEC with the goal to provide an integrated modeling framework that promotes the building, editing, and running of models commonly applied by multi-disciplinary teams including the saving and displaying of data and results in a coordinated fashion. More simply, HEC-WAT is an interface that streamlines and integrates a water resources study using software commonly applied by multi-disciplinary teams. Many tools within the HEC suite of software are implemented within HEC-WAT, thus allowing a study team to perform many of the necessary hydrologic, hydraulic, and planning/consequence analyses from a single interface. The ARB HEC-WAT model integrates the ARB HEC-HMS, HEC-RAS and HEC-FIA models as illustrated in **Figure 83**.

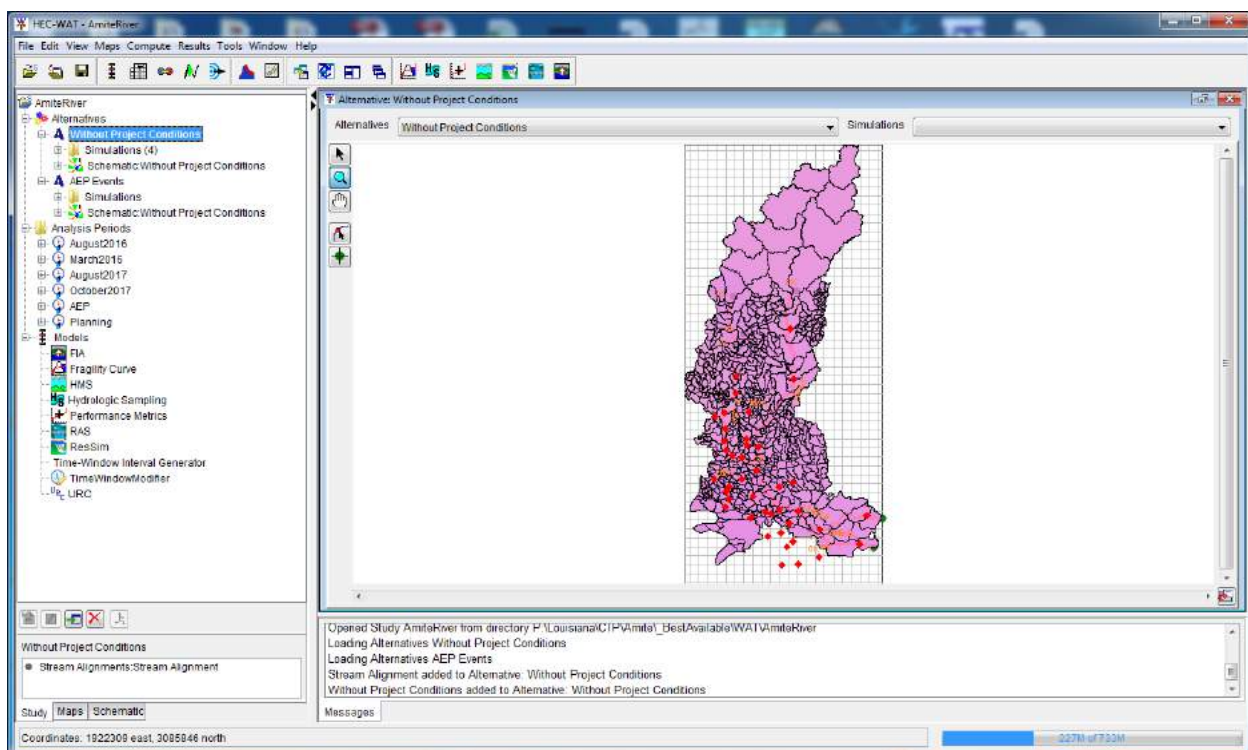


Figure 83: ARB HEC-WAT Model

HEC-WAT does not replace existing software but instead the framework allows them to work together. The model integration of the individual pieces of software within the HEC-WAT framework is achieved through the concept of a "plug-in". The plug-in is what allows the individual pieces of software to integrate without requiring special code in HEC-WAT to support the individual pieces of software. While the 400+ HEC-HMS inflow boundary conditions for ARB HEC-RAS model were manually linked, HEC-WAT allows for a streamlined process via a user interface to dynamically link the models together. As the ARBNM is improved with more detail in the future, HEC-WAT demonstrates the potential to be a valuable tool.

Additionally, model simulations can be linked as well. HEC-WAT allows the user to run the HEC-HMS and HEC-RAS models simultaneously. Traditionally, the HEC-HMS model is opened and run first with the HEC-HMS results potentially being copied over to the HEC-RAS model directory. Then, the HEC-RAS model is opened and run. **Figure 84** shows how HEC-HMS and HEC-RAS can be dynamically linked. The “Location” column represents the HEC-RAS boundary conditions and the “Location/Parameter” column represents the HEC-HMS element where flow is to be delivered from. **Figure 85** shows how models can be linked together. As previously mentioned, the ARB HEC-WAT model included the ARB HEC-HMS, HEC-RAS, and HEC-FIA models.

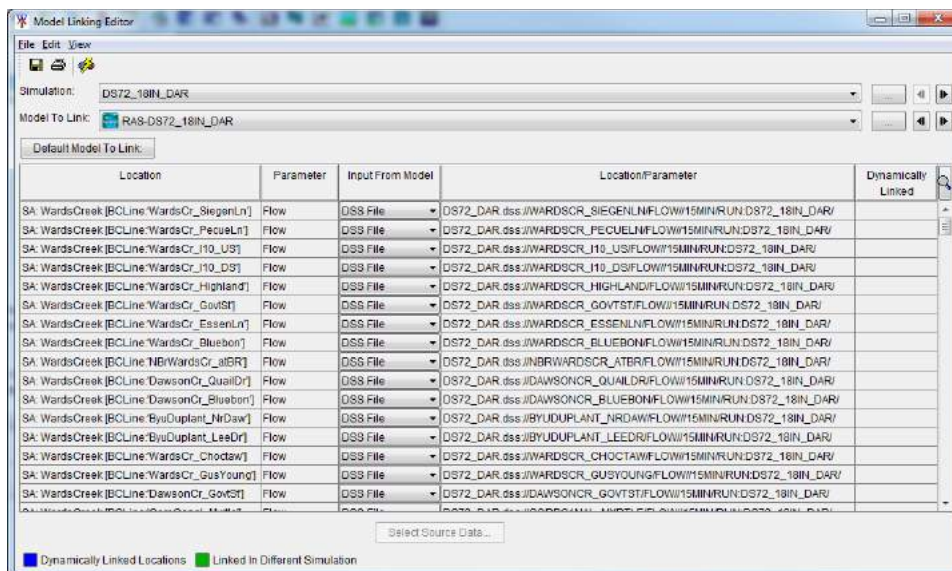


Figure 84: HEC-WAT Model Linking Editor

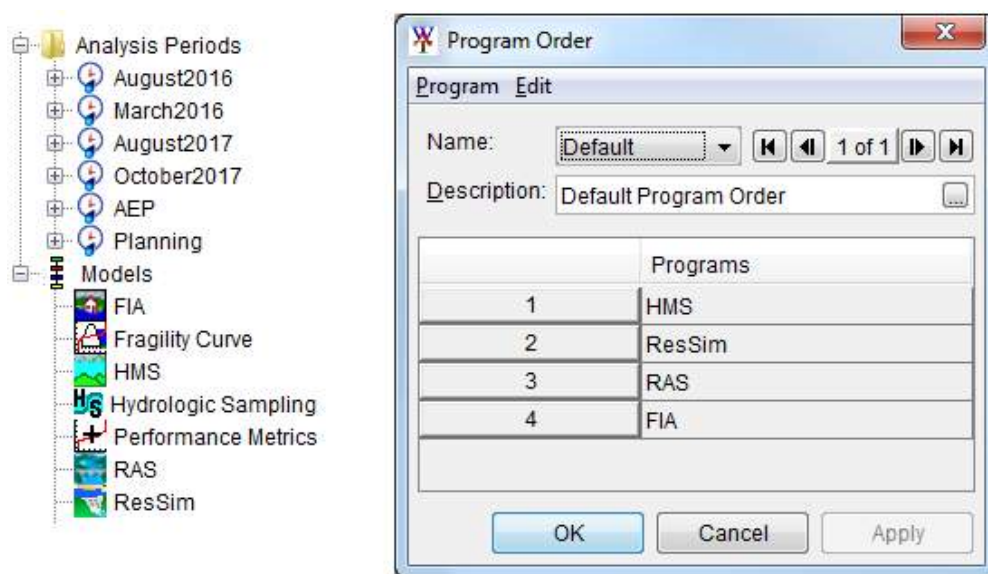


Figure 85: Software Linking in HEC-WAT

Through the Flood Risk Analysis (FRA) compute option HEC-WAT supports risk analysis on a systems approach for the analysis of complex riverine systems while implementing flood risk and uncertainty and systems analysis requirements. The HEC-WAT software also allows a user to perform plan comparisons or system performance analyses while incorporating risk analysis methods.

HEC-WAT was implemented to test its potential application for the ARBNM and Louisiana Watershed Initiative (LWI). This included integration of the HEC-HMS, HEC-RAS and HEC-FIA models which were used to demonstrate several project alternatives. A potential alternative can be seen below in **Figure 86**. In this example, the 18 in. design storm centered over Darlington is being modeled. Notice how the HEC-HMS and HEC-RAS model runs are selected for this alternative.

Program	Alternative	Simulation Time Window	Time Window Adjustment	Needs To Compute
HMS	(RUN)DS72_18IN_DAR	Simulation Window	Edit...	<input type="checkbox"/>
ResSim		Simulation Window	N/A	<input type="checkbox"/>
RAS	DS72_18IN_DAR	Simulation Window	Edit...	<input type="checkbox"/>
FIA		Simulation Window	N/A	<input type="checkbox"/>

Figure 86: Create a new HEC-WAT Alternative Simulation.

At face value, the alternative above is no different than what was previously modeled other than being self-contained within one interface. However, HEC-WAT creates a localized copy of the HEC-RAS geometry which allows the user to test “What If” scenarios such as bridges being obstructed or the incorporation of structural flood protection measures without affecting the base, or original model geometry. The user can then run HEC-FIA to compare economic damages of selected alternatives.

While HEC-WAT demonstrated strong potential for future applications, particularly for advanced users to perform complex flood risk assessments for major flood control projects, due to the nature of provisional releases, numerous undocumented bugs were found making the software somewhat challenging to use in the interim. Additionally, HEC-WAT version 1.0 did not support HEC-RAS Version 5.0.6 indicating that it lagged the current releases of HEC-RAS.

SUMMARY AND RECOMMENDATIONS

The ARBNM was demonstrated through the simulation of historical flood events to reasonably replicate observed results for an array of events. While complex due to the size of the ARB, it was possible to create AEP design floods using the HMR 52 procedures to create a catalog of design floods with a varying magnitude of cumulative precipitation to support design. Additionally the development of the ARB Consequence Model showed through the analysis of the August 2016 flood that it can reasonably estimate economic and life safety consequences using the results of the ARB HEC-RAS model. The ARBNM provides users with a without project conditions model that will enable apples to apples comparisons of project alternatives. The following recommendations are made for improvements to the ARBNM and for the LWI.

Recommendations for Improvements to the ARBNM

1. **Future HEC-RAS Release Finite Volume 1D Computation Engine:** It is recommended that upon formal or beta release of the future Finite Volume 1D computation engine for HEC-RAS 1D that LA DOTD perform thorough testing to ensure that it creates results that reasonably match those of the current ARBNM. The new Finite Volume Method engine is expected to provide improved stability and run times when compared to the existing finite difference 1D computation engine and will therefore make the ARBNM more efficient to utilize.
2. **Future HEC-RAS Release Supporting Modeling of Bridges in 2D Flow Areas:** It is understood that HEC-RAS Version 5.1 will enable users to code bridges within 2D Storage Area Connections. Currently HEC-RAS does not support the modeling of bridges within 2D Flow Areas and therefore Version 1.0 of the ARBNM simulates bridges within 2D Flow Areas as either multiple culverts representing bridge spans or slotted weirs within 2D Storage Area Connections. It is recommended that upon release of this feature within HEC-RAS that LA DOTD update the ARBNM to more accurately model bridges within 2D Flow Areas eliminating the need to model bridges as multiple culverts or slotted weirs.
3. **Rain-on-Grid Hydrology:** HEC-RAS version 5.0.6 supports rain-on-grid simulations within 2D Flow Areas, however, its capabilities are limited to applying only net runoff uniformly within a 2D Flow Area. Therefore it does not model infiltration losses as flow moves over the 2D mesh. It is understood that future releases of HEC-RAS will incorporate hydrologic processes into the HEC-RAS 2D Flow Area mesh enabling distributed losses to be performed. At this time, it is not recommended that rain-on-grid methodologies be used for the ARBNM, however, upon formal or beta release of improved rain-on-grid methodologies within HEC-RAS, it is recommended that LA DOTD perform testing of the methodology to determine its suitability for both the ARB and LWI. It is expected that rain-on-grid could provide significant value for urban modeling where watershed boundaries are complicated and subjective due to the unconfined nature of flooding. Example basins would include Bayou Manchac, Wards Creek, Clay Cut Bayou and Jones Creek to name a few.

4. **Stormwater and Flood Control Design Criteria for Local Communities:** While the ARBNM provides a catalog of storms suitable for analysis of flooding directly related to the Amite and Comite River's, it is recommended that that LA DOTD perform outreach to all local communities within the ARB to determine local design criteria for hydrologic and hydraulic design to better support their needs for assessing projects on smaller tributaries of the ARB. This may require utilizing the HEC-MetVue models to develop additional storms including the 4% AEP (25-year), 24-hr storm which is frequency used by local communities. Currently, when modeling tributaries independently, the 72-hr duration design storms will likely provide lower intensities than desired since the model has been optimized for the large Amite and Comite Rivers.
5. **Additional Storm Durations for Comite River:** It is recommended that additional storm durations be developed for the Comite River to represents its relatively shorter time of concentration. This has resulted in large precipitation depths to be required to achieve major floods along the Comite River. Storm durations of 24- and 48-hrs would likely provide added value.
6. **Updating of Hydrologic and Hydraulic Models with NLCD 2016 Data:** The 2016 NLCD is anticipated to be released sometime in 2019. This data will provide an improved representation of land use that can be used to refine HEC-HMS hydrologic parameters in addition to refining the application of HEC-RAS Manning's N values in 2D Flow Areas.
7. **Refinement of Models for Future Adoption by FEMA:** It is recommended to utilize the Cooperating Technical Partner (CTP) program funded by FEMA at LA DOTD to upgrade the ARBNM to enable the current flood risk to be mapped throughout the ARB through the future adoption of the models by FEMA. While the models likely represent a higher quality analysis than the effective models, additional detail and features specific to FEMA Guidelines and Specifications will enable them to be incorporated. This may include:
 - a) **Development of Regulatory Floodways for the Amite River and Comite River main channels:** It is recommended that through the Cooperating Technical Partner (CTP) program, LA DOTD coordinate with FEMA Region VI to define technical procedures acceptable to FEMA for the development of unsteady 1D and 2D floodplains within the ARB. Implementation of these procedures to develop a floodway will enable FEMA to adopt the ARBNM in areas where a regulatory floodway is already established, providing improved quality mapping for the local communities and additional stakeholders.
 - b) **Refined Detail in Medium Detail 2D Study Areas:** It is recommended that major tributaries to the Amite and Comite River's mapped by FEMA as a Zone AE flooding sources be upgraded to enable future adoption of the models by FEMA. While the models likely represent a higher quality analysis than the effective models, additional detail will enable them to meet FEMA Guidelines and Specifications. This may include:

- Refining land use polygons to include channel polygons allowing the N values to be refined to the channel portion
 - Development of floodway simulations using previously
 - Full detail survey of hydraulic structures to include survey grade elevations and incorporation into the HEC-RAS model.
 - Incorporation of channel survey into the 2D mesh to enable true channel geometry to be simulated within HEC-RAS. This will be critical for the detailed modeling of culverts as 2D Storage Area Connections which require inverts to be higher than the adjacent 2D cells.
 - Modeling of accredited levees that can be certified to show risk reduction from the 1% AEP flood event.
8. **HEC-FIA Structure Information:** While the current ARB Consequence Model produced reasonable estimations on the economic and life safety consequences for the August 2016 flood, further information should be researched and gathered for the existing structure attributes. The various components of the structures was gleaned from the NSI; however, this data has inherent issues given the source of the data. At the very least, information regarding the occupancy type and foundation height for each structure should be further investigated, as these attributes directly influence the building damage computation, critical in both the economic and life-loss simulations. Other attributes, such as building and content value, building height, and building occupancy are other critical attributes that can be improved with better information from parcel information.
9. **HEC-FIA Evacuation Information:** Currently national assumptions pertaining to evacuations are used for the ARB consequence model. Information such as warning times for evacuation have proven to have a high sensitivity for life loss estimated when using the ARB HEC-FIA consequence model. While often the release of this data is restricted, the collection and analysis of local Emergency Action Plans and Emergency Operation Plans from the local communities in the ARB would enable the national assumptions to be updated with more refined local data.
10. **HEC-LifeSim:** HEC-LifeSim is a relatively new program that provides a more advanced assessment of life safety than HEC-FIA. A key enhancements is the ability to simulate the evacuation of a population during a flood events. Documentation indicates that HEC-FIA models can be easily imported to HEC-LifeSim to enable the more advanced functions to be realized. It is recommended that HEC-LifeSim be considered as a future pilot study for the ARBNM to determine whether it would add value by providing local communities with a tool that can be used to inform flood response and evacuation plans.

REFERENCES

Berg, R. (2013). Tropical Cyclone Report – Hurricane Isaac (AL092012). National Hurricane Center. January 28, 2013.

Estimating Hydraulic Roughness Coefficients, Cowan, Agricultural Engineering, Vol. 37, no. 7, pp 473-475, July 1956

Fort Bend County, TX, Drainage Criteria Manual, Section 2.0 Hydrology, Online Source (as of February 2019) <https://www.fortbendcountytexas.gov/government/departments/county-services/drainage-district/drainage-criteria-manual>

"Global Historical Climatology Network (GHCN)." National Climatic Data Center. NOAA, n.d. Web. 01 Aug. 2017.

Kocin, P., Schumacher, P., Morales, R., and Uccellini, L. (1994). Overview of the 12-14 March 1993 Superstorm. National Weather Service.

National Climatic Data Center. 2017. URL:
<http://www.ncdc.noaa.gov/nexradinv/chooseday.jsp?id=khn>

NOAA, Hydro Meteorological Report No. 52, Application of Probably Maximum Precipitation Estimates – United States East of the 105th Meridian, August 1982

NOAA. (2018). National Oceanic and Atmospheric Administration Tides and Currents -Station 8761927. Retrieved from: <https://tidesandcurrents.noaa.gov/stationhome.html?id=8761927> [Accessed July 2018].

NOAA. Stage IV gridded precipitation data UCAR data server
<https://data.eol.ucar.edu/dataset/113.003>

Nonstationarity Detection Tool. Vers. 1.1. Washington, D.C.: U.S. Army Corps of Engineers (USACE), Climate Preparedness and Resilience Community of Practice, 2017. Computer software.

Open-Channel Hydraulic, V.T. Chow, McGraw-Hill, 1959

Peak FQ. Vers. 7.1. Reston, VA: U.S. Geological Survey (USGS), Office of Surface Water, 2014. Computer software.

R Core Team (2013). R: A language and environment for statistical computing. R Foundation for Statistical Computing, Vienna, Austria. URL <http://www.R-project.org/>.

SSURGO (Soil Survey Geographic database) Natural Resources Conservation Service (NRCS) - National Cartography and Geospatial Center (NCGC)

Subcommittee on Hydrology of the Advisory Committee on Water Information, 2016. "Bulletin 17C, Guidelines for Determining Flood Flow Frequency".

U.S. Geological Survey 2001. The National Flood Frequency Program – Methods for Estimating Flood Magnitude and Frequency in Rural Areas in Louisiana, 2001.

U.S. Geological Survey, 2012, The StreamStats program, URL <http://streamstats.usgs.gov>.

University Corporation for Atmospheric Research data server
(<https://data.eol.ucar.edu/dataset/113.003>)

URS. (2006). Mississippi River Reintroduction into Maurepas Swamp Project (PO-29). Volume IV of VII – Hydrologic Data. June 29, 2006.

USACE HEC_FIA Flood Impact Assessment, Version 3.1 Provisional, Computer software downloaded from https://www.hec.usace.army.mil/software/hec-fia/3.0_downloads.aspx

USACE HEC-DSSVue, Data Storage System, Version 2.0.1, Computer software downloaded from <https://www.hec.usace.army.mil/software/hec-dssvue/downloads.aspx>

USACE HEC-HMS Hydrologic Modeling System, Version 4.2.1, Computer software downloaded from <https://www.hec.usace.army.mil/software/hec-hms/downloads.aspx>

USACE HEC-RAS River Analysis System, Version 5.0.6, Computer software downloaded from <https://www.hec.usace.army.mil/software/hec-ras/downloads.aspx>

USACE HEC-SSP Statistical Software Package. Vers. 2.1.1, Computer software downloaded from <https://www.hec.usace.army.mil/software/hec-ssp/download.aspx>

USACE HEC-WAT Watershed Assessment Tool, Version 1.0 Provisional, Computer software downloaded from <https://www.hec.usace.army.mil/software/hec-wat>

USACE, 2016. Engineering and Construction Bulletin No. 2016-25

USACE, HEC-GeoHMS, Version 10.0 for ArcGIS, Computer Software Downloaded from <https://www.hec.usace.army.mil/software/hec-geohms/downloads.aspx>

USACE, HEC-HMS Hydrologic Modeling System, Technical Reference Manual, March 2000.

USACE, HEC-HMS Hydrologic Modeling System, User's Manual, Version 4.2, August 2016

USACE, HEC-RAS River Analysis System, 2D Modeling User's Manual, Version 5.0, February 2016.

USACE, HEC-RAS River Analysis System, Hydraulic Reference Manual, Version 5.0, February 2016

USACE, HEC-RAS River Analysis System, Supplemental to HEC-RAS Version 5.0, User's Manual, Version 5.0.4, April 2018

USACE, HEC-RAS River Analysis System, User's Manual, Version 5.0, February 2016

USACE, HMR52 Probable Maximum Storm (Eastern United States) User's Manual. March 1984, Updated April 1987

USGS, Guidelines for Determining Flood Flow Frequencies, Bulletin #17B of the Hydrology Sub Committee, Revised September 1981

USGS, Guidelines for Determining Flood Flow Frequencies, Bulletin #17C, 2018

USGS, The National Flood-Frequency Program, Methods for Estimating Flood Magnitude and Frequency in Rural Areas in Louisiana, 2001

Utah State University, LIFESim: A model for estimating dam failure life loss, 2005

Wang, S. Y. S., Zhao, L., & Gillies, R. R. (2016). Synoptic and quantitative attributions of the extreme precipitation leading to the August 2016 Louisiana flood. *Geophysical Research Letters*, 43(22).

Woody L. Cowen, Estimating Hydraulic Roughness Coefficients, *Agricultural Engineering*, Volume 37, no. 7, pp 473-475, July 1956

APPENDIX 1: HEC-HMS MODEL PARAMETER SUMMARY

HEC-HMS Model Parameter Summary

Table A1-1: HEC-HMS Model Parameter Summary

HEC-HMS Subbasin	Green and Ampt Loss Parameters								Mod Clark Transform Parameters	
	Drainage Area (sq mi)	Initial Content	Saturated Content	Suction (in)	Conductivity (in/hr)	Impervious % 2011 NLCD	Impervious % 2030 ICLUS	Impervious % 2050 ICLUS	Time of Concentration (hr)	Storage Coefficient (hr)
AllenByu_HWY1032	2.5	0.24	0.34	6.55	0.042	9.3	15.0	15.0	3.2	9.1
AlligatorT_Bluff	3.5	0.25	0.35	6.99	0.034	17.3	19.0	24.9	2.0	5.5
AmiteDivCnl_C01	18.5	0.21	0.29	11.09	0.008	0.0	0.1	0.1	0.1	73.0
AmiteDivCnl_C02	8.3	0.19	0.26	10.59	0.012	0.1	0.1	0.1	0.1	36.8
AmiteDivC_HWY22	11.1	0.19	0.27	8.42	0.026	2.0	2.5	2.7	2.1	18.9
AmiteRT34_HWY16	0.4	0.23	0.32	6.12	0.048	15.3	15.3	19.3	1.8	3.9
AmiteR_BarbByu	19.8	0.24	0.34	7.59	0.037	0.4	0.4	0.4	3.1	16.8
AmiteR_BeaverCrk	9.2	0.24	0.33	6.45	0.043	0.1	0.1	0.1	7.4	9.4
AmiteR_BluffCrk	7.0	0.22	0.31	7.29	0.082	0.5	0.5	0.5	6.3	6.8
AmiteR_ChaneyBr	1.1	0.27	0.38	8.4	0.018	1.8	1.8	1.8	3.5	4.7
AmiteR_ChinqCan	7.4	0.24	0.33	8.23	0.027	1.5	1.7	2.1	4.6	24.5
AmiteR_ClearCrk	5.9	0.24	0.34	5.51	0.056	0.5	0.5	0.5	6.0	5.6
AmiteR_ColBay	1.8	0.2	0.29	6.96	0.025	1.0	1.2	1.4	2.1	7.0
AmiteR_C01	4.5	0.23	0.32	6.31	0.041	0.3	0.4	0.5	3.4	12.9
AmiteR_C02	4.5	0.21	0.3	5.91	0.038	1.3	1.6	1.9	3.5	11.2

Table A1-1: HEC-HMS Model Parameter Summary

AmiteR_C03	4.5	0.23	0.32	6.22	0.046	0.4	0.5	0.6	7.3	15.9
AmiteR_C04	2.4	0.22	0.32	6.18	0.039	3.6	4.7	5.7	2.8	3.9
AmiteR_C05	3.4	0.23	0.32	6.25	0.047	3.8	5.4	7.3	6.4	14.9
AmiteR_C06	1.2	0.23	0.33	6.76	0.032	6.7	13.5	16.2	2.9	4.2
AmiteR_C07	0.8	0.23	0.32	6.32	0.041	4.3	5.6	6.8	1.9	3.3
AmiteR_C08	1.1	0.23	0.33	6.31	0.041	16.7	23.4	30.1	2.4	3.0
AmiteR_C09	1.6	0.23	0.32	6.31	0.054	2.1	2.6	2.7	3.1	5.0
AmiteR_C10	2.2	0.23	0.32	6.3	0.041	8.3	10.0	11.7	2.8	4.4
AmiteR_C11	2.8	0.25	0.35	7.42	0.03	9.3	11.8	16.3	3.4	12.0
AmiteR_C12	2.9	0.23	0.32	6.43	0.041	9.5	9.5	15.5	3.0	4.6
AmiteR_C13	3.1	0.22	0.31	6.21	0.04	2.9	4.2	4.9	4.4	7.2
AmiteR_C14	3.8	0.23	0.32	6.31	0.053	0.6	0.7	0.9	3.9	6.9
AmiteR_C15	4.2	0.24	0.34	7.04	0.029	1.7	2.0	2.6	4.6	9.6
AmiteR_DarlingCrk	13.2	0.24	0.33	6.45	0.049	0.4	0.4	0.4	7.7	8.3
AmiteR_HendByu	1.2	0.16	0.22	8.77	0.02	3.7	5.0	5.8	2.5	6.6
AmiteR_HWY16	6.0	0.21	0.3	9.06	0.021	1.4	1.5	1.5	3.3	24.1
AmiteR_HWY22	12.1	0.25	0.35	8.87	0.027	0.6	0.7	0.7	1.8	32.6
AmiteR_KingGBYu	18.7	0.24	0.34	8.88	0.027	0.9	1.0	1.0	4.4	48.6

Table A1-1: HEC-HMS Model Parameter Summary

AmiteR_L03	0.8	0.24	0.34	6.37	0.041	21.7	31.6	34.0	1.3	1.6
AmiteR_Magnolia	1.9	0.24	0.34	7.03	0.06	8.4	10.3	13.0	2.6	3.7
AmiteR_Maurepas	12.0	0.26	0.36	10.43	0.016	0.7	0.7	0.7	2.5	65.7
AmiteR_PigeonCrk	16.9	0.21	0.3	7.73	0.06	0.4	0.4	0.4	8.2	12.0
AmiteR_PtVincent	5.6	0.21	0.29	6.27	0.033	2.0	2.4	2.4	3.0	16.6
AmiteR_RockyCrk	23.6	0.21	0.3	7.45	0.055	0.3	0.3	0.3	7.9	9.6
AmiteR_R03	1.4	0.26	0.36	6.85	0.039	25.7	36.2	36.2	1.7	2.8
AmiteR_StateHwy10	14.6	0.21	0.3	6.58	0.047	0.3	0.3	0.3	6.6	6.5
AmiteR_StateHwy37	15.0	0.2	0.28	7.2	0.06	0.5	0.5	0.5	7.9	9.8
AmiteR_StateHwy432	2.5	0.22	0.31	6.58	0.041	0.2	0.2	0.2	3.9	2.6
AmiteR_US_Div	0.4	0.04	0.05	3.77	0.004	1.7	2.0	2.0	14.5	52.8
AmiteR_WhittenCrk	16.7	0.23	0.32	7.2	0.052	0.5	0.5	0.5	7.5	10.7
AmiteR_17	3.4	0.24	0.34	6.86	0.06	0.8	0.9	0.9	5.2	7.2
AmiteR_18	1.9	0.26	0.37	7.4	0.033	0.6	0.7	0.7	4.1	5.3
AntiochC_LeeMrtn	4.0	0.25	0.35	6.56	0.042	0.6	0.7	0.9	3.1	8.2
BeaverBr_CnMkt	0.7	0.23	0.32	6.55	0.042	8.3	8.4	9.1	3.0	7.7
BeaverBr_DuffRd	2.4	0.23	0.32	6.55	0.042	2.2	3.5	4.0	2.4	7.9
BeaverBr_RR	3.3	0.23	0.32	6.55	0.042	3.9	5.3	6.2	2.9	6.0

Table A1-1: HEC-HMS Model Parameter Summary

BeaverByuNP_Hoop	1.3	0.23	0.33	6.53	0.041	11.0	12.8	14.4	3.4	7.8
BeaverByuNP_US	0.4	0.22	0.31	6.56	0.042	8.3	18.6	18.6	2.4	4.8
BeaverByu_Denham	1.2	0.22	0.31	6.56	0.041	1.3	1.3	1.5	4.0	7.3
BeaverByu_French	0.8	0.25	0.35	6.94	0.036	6.8	8.4	9.4	3.4	5.0
BeaverByu_GrnSp	1.8	0.24	0.33	6.51	0.04	16.4	16.4	16.4	2.4	4.9
BeaverByu_Hooper	4.3	0.22	0.31	6.52	0.041	3.5	4.5	5.6	3.1	7.8
BeaverByu_US_LOC	0.6	0.23	0.32	6.57	0.041	1.3	1.5	1.6	2.4	5.5
BeaverByu_Wax	2.2	0.23	0.32	6.55	0.039	7.0	8.1	8.7	2.3	7.6
BeaverCrk_01	39.2	0.28	0.39	6.12	0.049	0.9	0.9	0.9	8.0	10.8
BeaverCrk_02	44.8	0.27	0.38	6.18	0.048	0.3	0.3	0.3	8.2	10.8
BeaverCrk_03	16.7	0.27	0.38	5.98	0.05	0.2	0.2	0.2	7.3	8.9
BeaverCrk_04	2.9	0.26	0.37	6.21	0.046	0.2	0.2	0.2	4.1	2.9
BeaverCrk_05	3.0	0.24	0.34	6.12	0.047	0.2	0.2	0.2	3.7	2.6
BeaverCrk_06	0.5	0.22	0.3	6.21	0.041	0.1	0.1	0.1	3.5	2.7
BeaverCrk_07	0.6	0.22	0.31	6.35	0.041	0.2	0.2	0.2	2.7	7.3
BeaverC2_CnMkt	2.5	0.22	0.32	6.55	0.042	7.5	7.5	8.6	2.8	7.7
BeaverC2_ForeRd	0.7	0.22	0.32	6.57	0.042	4.3	6.1	6.1	2.6	7.3
BeaverC2_HWY16	1.3	0.23	0.32	6.44	0.043	13.0	16.8	19.1	2.6	4.2

Table A1-1: HEC-HMS Model Parameter Summary

BeaverC2_Magnol	0.7	0.23	0.33	6.47	0.043	16.8	16.8	23.2	1.7	1.9
BeaverC2_Sprgflld	1.2	0.23	0.32	6.56	0.042	18.0	25.5	29.0	1.9	4.7
BeaverC3_DS_Pear	1.1	0.22	0.31	7.22	0.041	0.4	0.5	0.5	2.8	5.4
BeaverC3_Jackson	1.0	0.25	0.36	7.31	0.042	0.7	0.8	0.8	2.4	2.6
BeaverC3_LSandy	2.0	0.23	0.32	7.02	0.042	0.1	0.2	0.2	3.7	5.9
BeaverC3_Milldal	2.1	0.25	0.35	6.75	0.042	0.5	0.6	0.6	3.1	4.6
BeaverC3_Peairs	2.0	0.23	0.32	6.85	0.042	0.3	0.3	0.4	4.4	8.1
BeaverC3_US_LOC	0.2	0.25	0.35	7.03	0.042	1.0	1.0	1.0	1.7	1.9
BeaverPondByu_DS	1.9	0.23	0.32	6.44	0.039	0.2	0.2	0.2	4.6	9.5
BeaverPondByu_US	4.4	0.25	0.35	6.56	0.041	0.1	0.2	0.2	4.9	8.3
BFountainNP	0.8	0.23	0.33	6.79	0.039	21.4	21.4	23.4	1.4	1.7
BFountNBr_Boyd	0.2	0.3	0.42	11.83	0.011	60.8	60.8	60.8	0.4	0.3
BFountNBr_Lee	0.5	0.24	0.33	11.34	0.015	25.6	27.2	29.2	0.9	3.2
BFountSBr_BF	0.8	0.2	0.29	12.02	0.009	9.9	11.4	11.4	2.3	2.4
BFountSBr_Gour	0.4	0.23	0.32	12.27	0.008	23.1	23.5	24.0	2.1	1.8
BFountSBr_US	0.2	0.31	0.44	10.21	0.02	42.9	44.4	45.1	1.1	1.3
BFountT1_DS	1.1	0.22	0.32	7.22	0.035	11.8	14.2	19.6	1.8	2.7
BFountT1_Highlnd	1.0	0.24	0.34	6.66	0.041	31.7	31.9	35.4	1.0	1.5

Table A1-1: HEC-HMS Model Parameter Summary

BFount_BFSBr	0.3	0.2	0.28	12.41	0.007	39.9	39.9	39.9	1.3	2.4
BFount_Bluebon	4.0	0.21	0.29	8.42	0.034	23.6	25.8	27.9	2.0	7.5
BFount_Burbank	0.2	0.27	0.39	12.14	0.009	24.9	30.3	32.6	1.1	1.5
BFount_BurbankDr	4.2	0.22	0.31	7.58	0.034	27.5	32.2	32.9	2.2	4.7
BFount_ByuManch	2.0	0.19	0.26	11.15	0.015	4.6	5.8	6.8	2.1	17.7
BFount_ElbowByu	1.8	0.17	0.23	11.01	0.016	19.6	26.7	30.4	4.1	9.0
BFount_Nich_DS	0.8	0.15	0.22	12.2	0.01	23.0	27.2	27.2	1.8	6.8
BFount_Nich_US	0.3	0.34	0.48	11.96	0.01	62.6	62.6	62.6	0.4	0.3
BFount_US_Trib	9.0	0.17	0.23	10.49	0.02	3.7	5.1	6.4	5.5	14.7
BirchCrk_01	1.0	0.25	0.35	4.72	0.069	1.2	1.2	1.2	2.3	1.1
BlackCrk_01	0.4	0.25	0.35	4.93	0.066	0.0	0.1	0.1	2.4	1.6
BlackCrk_02	0.3	0.2	0.29	6.39	0.048	0.2	0.2	0.2	1.9	1.1
BlackCrk_03	0.7	0.25	0.35	5.18	0.062	0.5	0.5	0.5	2.2	1.2
BlackCrk_04	0.9	0.25	0.35	4.94	0.065	0.8	0.8	0.8	2.6	1.7
BlackCrk_05	0.7	0.23	0.32	5.6	0.057	0.1	0.1	0.1	2.5	1.6
BlackCrk_06	0.2	0.21	0.3	6.62	0.043	0.4	0.4	0.4	2.1	1.1
BlackCrk_07	1.0	0.21	0.29	6.42	0.046	0.1	0.1	0.1	3.3	2.3
BlackCrk_08	0.2	0.24	0.33	6.04	0.05	1.7	1.7	1.7	1.5	0.7

Table A1-1: HEC-HMS Model Parameter Summary

BlackCrk_09	1.3	0.24	0.33	5.71	0.058	1.0	1.0	1.0	3.2	2.0
BLACKCR_CMB	0.2	0.26	0.37	6.45	0.041	0.1	0.1	0.1	2.0	2.7
BLACKCR_HWY412	2.8	0.26	0.36	6.55	0.042	0.1	0.1	0.1	4.5	7.8
BlackwtrBT1_BB	3.5	0.23	0.33	6.55	0.042	7.0	8.3	9.4	3.5	9.8
BlackwtrBT1_Core	1.3	0.23	0.32	6.57	0.042	1.5	2.4	2.4	2.3	4.1
BlackwtrBT1_Mcul	0.9	0.22	0.31	6.55	0.041	1.2	1.6	1.6	2.0	5.0
BlackwtrBT2_BB	0.8	0.23	0.32	6.53	0.042	1.7	2.1	2.1	2.3	6.7
BlackwtrBT2_DW	0.6	0.23	0.32	6.56	0.042	1.3	1.3	1.5	2.1	5.2
BlackwtrBT3_US	0.8	0.23	0.32	6.46	0.043	1.6	2.1	2.1	2.4	5.8
BlackwtrB_BBT1	1.7	0.23	0.32	6.59	0.041	1.3	1.8	1.9	3.1	5.8
BlackwtrB_BBT2	1.4	0.22	0.31	6.56	0.042	1.3	1.3	1.5	2.9	6.9
BlackwtrB_Comite	2.1	0.23	0.33	6.57	0.041	10.0	11.9	12.7	3.1	4.8
BlackwtrB_McCull	0.7	0.22	0.31	6.56	0.042	0.8	1.0	1.0	2.4	4.8
BlackwtrB_US	0.6	0.22	0.31	6.48	0.041	0.3	0.3	0.4	2.5	5.2
BlackwtrT3_DS	0.3	0.22	0.31	6.53	0.043	1.7	2.1	2.1	2.0	4.1
BluffCrk_AmiteR	1.8	0.23	0.32	6.54	0.044	0.3	0.3	0.3	5.3	5.3
BluffCrk_01	1.2	0.24	0.33	6.85	0.039	0.3	0.3	0.3	2.4	1.5
BluffCrk_02	1.4	0.22	0.31	7.15	0.037	0.2	0.2	0.2	2.9	2.0

Table A1-1: HEC-HMS Model Parameter Summary

BluffCrk_03	1.6	0.19	0.27	7.63	0.033	0.3	0.3	0.3	3.6	2.7
BluffCrk_04	2.1	0.2	0.28	7.43	0.035	0.1	0.1	0.1	4.2	3.8
BluffCrk_05	2.9	0.2	0.28	7.41	0.035	0.1	0.1	0.1	4.3	3.9
BluffCrk_06	5.0	0.2	0.28	7.36	0.035	0.3	0.3	0.3	5.8	6.6
BluffCrk_07	5.8	0.21	0.3	7.22	0.036	0.3	0.3	0.3	5.1	5.7
BluffSwamp_Gage	0.7	0.23	0.32	7.92	0.027	22.6	35.8	35.8	1.7	2.3
ByuBraud_HWY30	2.3	0.13	0.19	10.83	0.019	12.5	12.5	12.5	2.5	4.3
ByuBraud_HWY74	3.4	0.11	0.15	12.24	0.01	11.9	11.9	11.9	4.2	10.1
ByuBraud_US_LOC	9.6	0.18	0.25	10.15	0.029	6.1	6.1	6.1	5.4	14.4
ByuDuplant_LeeDr	0.7	0.28	0.39	8.81	0.025	18.3	20.4	22.7	1.3	1.4
ByuDuplant_NrDaw	2.4	0.26	0.37	8.13	0.03	16.6	21.6	23.5	1.8	3.9
ByuManch_Airline	1.0	0.21	0.3	6.76	0.038	24.3	26.0	43.5	1.6	2.7
ByuManch_BFount	0.0	0.19	0.27	9.48	0.022	6.3	7.8	9.0	1.0	1.0
ByuManch_Cotton	2.0	0.22	0.32	6.44	0.039	2.8	3.7	4.5	2.5	4.1
ByuManch_Gator	0.1	0.19	0.27	10.69	0.029	7.8	9.1	9.7	2.8	15.4
ByuManch_NrAmite	1.2	0.22	0.31	6.85	0.04	4.3	4.3	4.3	2.9	5.8
ByuManch_NrLiPra	1.8	0.23	0.32	6.46	0.04	2.2	2.9	3.5	3.2	7.1
ByuManch_NrMSRiv	1.4	0.2	0.28	8.28	0.034	11.1	12.9	12.9	3.3	5.3

Table A1-1: HEC-HMS Model Parameter Summary

ByuManch_Perkins	1.5	0.23	0.32	6.43	0.036	22.7	31.3	35.9	1.6	2.1
ByuManch_Welsh	2.0	0.21	0.3	6.41	0.039	18.4	20.9	23.9	2.2	3.6
ByuPaul_HWY30	1.4	0.18	0.25	10.75	0.034	1.3	1.3	1.3	3.2	4.1
ByuPaul_US_HWY30	3.7	0.16	0.23	10.67	0.028	2.3	2.3	2.3	5.2	11.1
ByuPaul_US_LOC	4.3	0.16	0.23	11.38	0.023	2.2	2.2	2.2	3.0	10.4
CampCreek_HWY42	7.4	0.24	0.34	6.69	0.042	0.5	0.5	0.6	1.9	10.3
ChaneyBr_HWY16	1.9	0.23	0.32	6.49	0.041	1.1	1.1	1.1	3.7	9.2
ChinqCan_C01	12.1	0.26	0.37	10.85	0.015	0.4	0.4	0.4	1.8	42.3
ChinqCan_C02	14.0	0.25	0.35	9.94	0.018	2.2	2.2	2.2	3.5	18.0
ClayCut_Airline	1.2	0.3	0.43	9.34	0.025	55.6	60.1	74.4	0.5	0.7
ClayCut_AntiochR	2.5	0.24	0.33	6.9	0.041	32.4	39.7	41.6	1.3	1.8
ClayCut_CalRd	0.6	0.26	0.37	7.56	0.036	38.2	39.5	41.5	0.7	1.0
ClayCut_Inns	0.2	0.24	0.34	6.64	0.041	41.2	66.4	66.4	0.5	0.5
ClayCut_JacksB	1.3	0.27	0.38	7.92	0.034	38.4	43.3	49.4	0.9	1.4
ClayCut_NrAmite	3.1	0.23	0.33	6.4	0.041	4.2	6.0	8.1	2.8	5.3
ClayCut_Siegen	0.6	0.28	0.4	8.36	0.031	53.8	78.3	87.8	0.6	0.6
ClayCut_US_Tiger	4.7	0.24	0.34	6.85	0.041	14.0	14.0	15.6	2.7	4.7
ClaytonByuT1	0.5	0.23	0.32	6.54	0.043	2.1	3.3	4.0	2.3	2.8

Table A1-1: HEC-HMS Model Parameter Summary

ClaytonByu_Bend	0.8	0.22	0.31	6.4	0.044	7.6	7.6	10.4	3.0	3.9
ClearCrkT1_01	0.4	0.25	0.35	6.56	0.042	0.2	0.2	0.2	1.3	0.5
ClearCrkT1_02	1.0	0.25	0.34	6.55	0.042	0.0	0.1	0.1	3.2	2.1
ClearCrk_01	1.7	0.25	0.36	6.32	0.046	0.2	0.2	0.2	3.2	1.9
ClearCrk_02	2.4	0.25	0.35	6.39	0.044	0.4	0.4	0.4	3.8	2.7
ClearCrk_03	0.7	0.23	0.32	6.54	0.04	0.8	0.8	0.8	2.6	1.3
ClearCrk_04	1.8	0.24	0.34	6.55	0.042	0.3	0.3	0.3	4.4	3.3
ClintonAllenLat	2.7	0.23	0.32	6.54	0.042	5.2	6.8	8.7	3.5	7.4
ClyellCrkNP	1.9	0.24	0.34	6.54	0.042	0.3	0.4	0.5	2.4	7.6
ClyellT9_DS_FL	0.7	0.26	0.36	6.57	0.042	1.1	1.4	1.6	1.6	3.5
ClyellT9_FL	1.2	0.26	0.36	6.56	0.042	1.4	1.8	2.3	1.9	7.1
Clyell_CB	5.3	0.24	0.34	7.03	0.039	0.9	1.1	1.3	2.2	11.7
Clyell_DS_I12	2.8	0.25	0.35	6.55	0.042	1.1	1.4	1.6	2.0	5.8
Clyell_DS_LigoLn	2.7	0.22	0.31	6.51	0.043	0.9	1.3	1.5	2.6	8.7
Clyell_FLBlvd	3.6	0.25	0.35	6.56	0.042	1.0	1.5	2.0	2.4	7.1
Clyell_I12	2.1	0.24	0.34	6.56	0.042	1.3	1.8	2.4	2.3	4.5
Clyell_JoelWatts	5.3	0.24	0.34	6.56	0.042	0.7	0.9	1.0	2.9	7.8
Clyell_LigoLn	4.5	0.24	0.34	6.54	0.042	0.7	0.9	1.1	2.5	8.9

Table A1-1: HEC-HMS Model Parameter Summary

Clyell_LilClyell	2.1	0.24	0.34	6.57	0.042	0.6	0.6	0.7	2.2	4.6
Clyell_LodStafrd	4.5	0.23	0.33	6.48	0.041	0.6	0.7	0.9	3.0	8.3
Clyell_US_LOC	1.1	0.24	0.33	6.57	0.042	0.5	0.6	0.6	1.8	4.4
Clyell_W_Hood	4.2	0.24	0.34	6.57	0.042	0.7	0.7	0.8	3.1	10.6
ColtonCrk_HWY16	3.8	0.23	0.32	6.39	0.041	11.9	13.6	16.0	3.2	5.7
ColyellBay	8.1	0.24	0.33	7.41	0.037	0.9	1.1	1.2	2.7	22.3
COMITE_atComite	2.5	0.22	0.31	7	0.088	0.9	1.1	1.1	3.8	7.0
COMITE_Baker	8.0	0.23	0.33	6.76	0.071	1.4	1.5	1.7	4.6	10.0
COMITE_DenhamSpr	2.2	0.25	0.34	6.47	0.055	9.5	11.6	12.0	3.0	5.2
COMITE_dsJOORRD	0.5	0.25	0.35	7.17	0.036	2.4	2.4	2.4	1.7	1.3
COMITE_dsLA37	1.6	0.23	0.32	6.43	0.044	10.4	11.8	13.8	2.6	3.7
COMITE_DS_OB	0.2	0.22	0.31	5.98	0.084	3.6	3.6	3.6	1.8	1.2
COMITE_HooperRd	2.2	0.24	0.34	6.76	0.058	7.7	9.6	9.6	4.0	5.8
COMITE_Hurricane	1.0	0.23	0.32	6.55	0.039	6.7	8.0	9.5	2.4	3.0
COMITE_nrComite	1.3	0.26	0.37	7.74	0.053	2.9	3.2	3.3	4.2	5.4
COMITE_RR	2.2	0.23	0.32	6.43	0.055	1.9	2.6	3.7	3.7	5.4
COMITE_usLA37	1.4	0.25	0.36	7.23	0.032	9.5	11.2	14.1	2.3	2.7
COMITE_US_OB	0.2	0.22	0.3	6.17	0.039	0.9	0.9	0.9	1.4	0.7

Table A1-1: HEC-HMS Model Parameter Summary

COMITE_Zachary	5.7	0.23	0.32	6.48	0.056	1.0	1.1	1.2	4.6	9.2
CooperMillB_BC	0.9	0.26	0.36	6.5	0.041	0.6	0.6	0.6	2.9	4.1
CooperMillB_Midw	0.4	0.24	0.34	6.55	0.042	2.7	2.7	2.7	1.9	2.5
CooperMillB_UWB	0.6	0.22	0.31	6.07	0.038	0.3	0.4	0.6	2.4	4.8
CorpCanalNP	0.6	0.3	0.42	10.32	0.018	47.2	47.2	47.2	1.2	1.6
CorpCanal_Myrtle	0.8	0.32	0.45	9.55	0.023	61.2	76.1	76.1	0.5	0.6
CorpCanal_Stanford	0.6	0.34	0.48	10.42	0.013	39.2	41.6	44.5	0.8	0.9
CorpCanal_State	1.0	0.33	0.46	10.23	0.017	48.4	51.7	51.7	0.9	1.0
DarlingCrk_AmiteR	3.5	0.2	0.29	7.95	0.041	0.6	0.6	0.6	4.7	5.9
DarlingCrk_01	1.3	0.25	0.35	5.29	0.062	0.4	0.4	0.4	3.3	2.5
DarlingCrk_02	0.8	0.25	0.34	4.84	0.066	0.3	0.3	0.3	2.2	1.3
DarlingCrk_03	0.5	0.25	0.35	4.89	0.066	0.5	0.5	0.5	1.9	0.8
DarlingCrk_04	0.2	0.24	0.34	5.42	0.059	0.2	0.2	0.2	1.6	0.6
DarlingCrk_05	0.5	0.24	0.34	5.44	0.058	0.4	0.4	0.4	2.2	1.2
DarlingCrk_06	1.0	0.24	0.34	6.25	0.059	0.2	0.2	0.2	3.7	2.5
DarlingCrk_07	10.1	0.24	0.34	5.23	0.063	0.3	0.3	0.3	5.8	6.3
DarlingCrk_08	3.3	0.23	0.33	5.45	0.059	0.4	0.4	0.4	3.9	2.6
DarlingCrk_09	2.0	0.22	0.3	5.81	0.054	0.7	0.7	0.7	3.8	2.8

Table A1-1: HEC-HMS Model Parameter Summary

DarlingCrk_10	1.2	0.23	0.33	5.5	0.057	0.8	0.8	0.8	4.0	3.4
DarlingCrk_11	0.8	0.19	0.27	7.02	0.043	0.4	0.4	0.4	2.4	1.5
DarlingCrk_12	0.8	0.19	0.26	8.12	0.036	0.3	0.3	0.3	2.6	1.8
DarlingCrk_13	0.8	0.2	0.28	7.58	0.041	1.2	1.2	1.2	3.2	2.7
DawsonCr_Bluebon	2.6	0.27	0.38	7.97	0.032	32.6	35.6	38.0	1.5	2.8
DawsonCr_College	1.5	0.3	0.42	9.13	0.026	36.1	39.2	41.7	0.9	0.9
DawsonCr_GovtSt	1.3	0.3	0.42	9.04	0.027	49.4	51.0	54.2	0.7	1.0
DawsonCr_Hund_DS	0.9	0.28	0.4	8.35	0.03	27.3	29.5	31.9	1.3	1.5
DawsonCr_QuailDr	1.4	0.27	0.38	8.23	0.032	30.7	35.3	37.4	1.2	1.7
DawsonCr_WardCr	1.0	0.28	0.4	8.49	0.03	41.5	46.8	57.5	1.1	1.6
DraughnsC_French	2.5	0.24	0.34	6.57	0.037	7.1	9.2	10.1	3.0	4.9
DraughnsC_GrnSpr	2.4	0.23	0.32	6.55	0.041	8.1	9.4	12.2	2.4	5.4
DraughnsC_MagBr	1.0	0.22	0.32	6.56	0.041	10.6	11.1	11.7	2.7	8.3
DuffByu_Jackson	1.5	0.23	0.33	6.64	0.042	1.1	1.1	1.5	3.3	4.0
DuffByu_PtHud	0.5	0.26	0.36	6.58	0.042	0.0	0.1	0.1	2.1	2.0
DuffB_DS_Jack	0.4	0.24	0.33	6.58	0.04	0.5	0.6	0.6	1.8	1.8
DumplinC_DS_RR	0.5	0.24	0.34	6.57	0.042	22.4	29.8	38.7	0.9	1.4
DumplinC_I12	1.1	0.23	0.33	6.46	0.041	13.9	13.9	20.6	1.6	2.7

Table A1-1: HEC-HMS Model Parameter Summary

DumplinC_RR	0.8	0.22	0.31	6.53	0.042	7.7	12.6	15.2	1.7	3.9
DumplinC_US_LOC	1.0	0.22	0.31	6.55	0.042	6.9	13.4	15.0	1.6	4.8
DunnCrk_01	0.6	0.26	0.36	6.65	0.043	0.0	0.1	0.1	1.7	0.9
DunnCrk_02	0.8	0.23	0.32	6.9	0.041	0.0	0.1	0.1	2.4	1.5
DunnCrk_03	1.8	0.26	0.36	5.59	0.055	0.5	0.5	0.5	3.7	2.7
DunnCrk_04	0.5	0.25	0.36	5.57	0.055	0.2	0.2	0.2	3.5	2.1
EastForkAmite_01	38.9	0.25	0.35	6.43	0.043	0.6	0.6	0.6	8.9	16.5
EastForkAmite_02	46.8	0.27	0.38	6.16	0.048	0.5	0.5	0.5	9.6	14.8
EastForkAmite_03	95.7	0.26	0.37	5.83	0.053	0.4	0.4	0.4	11.7	19.7
EastForkAmite_04	55.2	0.26	0.37	5.87	0.051	0.3	0.3	0.3	11.5	18.3
EFDumplin_Corbin	0.2	0.22	0.31	6.55	0.042	1.3	1.7	2.5	1.0	3.5
EFDumplin_RR	0.9	0.23	0.32	6.52	0.042	13.0	16.9	21.3	1.6	3.6
ELatCypB_Lavey	0.4	0.26	0.37	6.57	0.042	20.7	24.3	30.6	1.1	1.7
ELatCypB_LCB	0.8	0.23	0.33	6.63	0.041	16.3	16.3	19.6	2.0	3.1
ElbowBayou	6.1	0.14	0.2	10.91	0.015	3.6	3.6	4.8	4.6	13.7
ElbowByu_Burbank	5.7	0.18	0.25	10.33	0.022	3.0	4.1	5.9	2.6	16.9
ENGINEERDEPOT_DS	1.4	0.25	0.35	6.73	0.041	27.2	27.3	29.5	1.8	3.3
ENGINEERDEPOT_US	0.8	0.28	0.39	7.8	0.034	41.3	54.2	54.2	1.0	1.7

Table A1-1: HEC-HMS Model Parameter Summary

FeldersB_BrownRd	0.6	0.25	0.35	6.57	0.042	0.8	0.9	1.3	1.9	6.0
FeldersB_DSJMay	0.9	0.24	0.34	6.6	0.042	3.2	4.5	6.3	1.4	2.5
FeldersB_WC	1.1	0.23	0.33	7.18	0.042	8.8	8.8	11.4	1.7	3.8
FlanaganByu_SC	0.5	0.24	0.33	6.62	0.042	0.4	0.4	0.5	2.2	2.9
FlanaganByu_01	2.0	0.24	0.34	7.33	0.041	0.1	0.1	0.1	2.6	2.5
FlatLake	4.0	0.15	0.22	9.86	0.014	0.7	0.8	0.9	3.5	20.6
GatorByu_Gage	0.2	0.17	0.24	9.64	0.019	2.3	3.3	4.9	2.8	5.2
GatorByu_USGage	36.0	0.14	0.2	11.21	0.015	4.0	4.5	5.5	6.7	27.7
GraysCrkBr_BMcD	0.4	0.25	0.36	6.55	0.042	21.0	21.0	24.3	1.2	2.4
GraysCrkBr_Dunn	0.4	0.24	0.34	6.3	0.046	14.5	16.5	16.5	1.2	1.8
GraysCrkBr_I12	0.8	0.24	0.33	6.57	0.042	5.0	5.1	6.3	1.9	6.1
GraysCrkBr_RR	0.5	0.25	0.36	6.45	0.041	16.7	20.9	25.2	1.1	2.4
GraysCrkBr_USI12	0.6	0.24	0.34	6.57	0.042	11.5	13.8	19.5	1.9	3.9
GraysCrkLat_RR	0.7	0.23	0.33	6.45	0.043	24.4	31.7	39.5	1.4	2.6
GraysCrk_Hwy1033	4.7	0.24	0.34	6.49	0.043	2.6	3.5	4.1	3.3	11.1
GraysCrk_HWY16	1.6	0.25	0.35	6.52	0.042	8.5	13.3	14.9	2.7	6.7
GraysCrk_I12	1.2	0.24	0.34	6.57	0.042	18.6	18.9	26.1	2.0	5.0
GraysCrk_Julban	2.1	0.22	0.31	5.83	0.037	10.0	12.5	14.4	2.5	8.8

Table A1-1: HEC-HMS Model Parameter Summary

GraysCrk_NrAmite	5.5	0.24	0.34	6.53	0.042	1.8	2.4	2.4	4.0	12.0
GraysCrk_RR	0.7	0.24	0.34	6.56	0.042	21.0	21.0	23.5	1.6	3.2
GraysCrk_US	0.4	0.25	0.35	6.55	0.042	24.2	31.2	37.5	0.9	1.1
GraysCrk_WaxD	0.7	0.24	0.33	6.57	0.042	17.5	18.2	23.4	1.5	2.6
HannaC_PrideBar	1.5	0.21	0.3	7.19	0.037	0.1	0.1	0.1	3.0	3.1
HareLat_Airline	0.9	0.26	0.37	7.5	0.036	39.1	43.8	46.5	0.8	1.1
HareLat_OldHmd	0.3	0.26	0.37	7.32	0.034	41.5	45.6	47.4	0.5	0.4
HendByu_DSptVinc	3.8	0.24	0.34	6.82	0.032	3.6	4.9	5.7	2.8	10.8
HendByu_HWY431	4.2	0.22	0.31	7.93	0.029	2.4	2.6	3.2	2.6	8.4
HendByu_Joboy	0.4	0.24	0.33	6.57	0.042	19.6	25.6	25.6	1.0	2.3
HendByu_NrPtVinc	3.4	0.24	0.34	6.52	0.039	10.5	10.8	11.8	2.0	9.8
HendByu_US_Timbr	1.7	0.24	0.34	6.57	0.036	9.1	9.5	12.0	1.9	4.7
HogBayou_BC	1.0	0.26	0.37	6.53	0.042	0.0	0.1	0.1	3.6	7.0
HoneyCut_East	1.1	0.26	0.37	7.02	0.039	38.3	40.2	44.8	1.0	1.9
HoneyCut_NrAmite	1.5	0.26	0.37	7.12	0.038	23.0	26.8	32.7	1.7	2.3
HoneyCut_West	0.4	0.27	0.38	6.95	0.04	38.0	39.8	40.6	0.6	0.9
HornsbyCrk_CnMkt	1.1	0.24	0.34	6.52	0.042	0.5	0.5	0.5	2.4	4.4
HornsbyCrk_DSCan	1.8	0.25	0.35	6.56	0.042	0.7	0.9	1.2	2.3	4.6

Table A1-1: HEC-HMS Model Parameter Summary

HornsbyCrk_FLBd	5.2	0.24	0.34	6.55	0.042	2.6	3.1	3.4	3.4	12.3
HornsbyCrk_HCT1	0.6	0.23	0.32	6.48	0.043	0.8	1.0	1.1	1.4	2.7
HornsbyCrk_HCT3	1.4	0.23	0.32	6.55	0.042	0.6	0.7	0.7	2.1	5.2
HornsbyCT1_Corbn	1.6	0.23	0.32	6.53	0.042	0.8	0.8	1.0	2.3	6.2
HornsbyCT3_Corbn	1.5	0.22	0.31	6.49	0.043	0.5	0.8	0.8	2.0	5.1
HornsbyCT3_HC	0.9	0.22	0.31	6.53	0.042	0.7	0.7	0.9	1.9	5.2
HornsbyC_I12	2.9	0.24	0.34	6.5	0.041	2.7	3.3	3.8	2.7	6.9
HubByu_DS_GS_PH	1.7	0.22	0.31	6.53	0.041	1.0	1.1	1.4	2.9	7.1
HubByu_GrnwelSpr	3.0	0.22	0.31	6.52	0.042	1.1	1.4	1.5	4.6	9.2
HubByu_GS_PtHud	1.1	0.23	0.32	6.56	0.041	1.2	1.2	1.3	2.5	5.8
HubByu_Peairs	0.3	0.22	0.31	6.47	0.043	0.0	0.1	0.1	2.1	5.0
HunterByu_01	0.5	0.2	0.28	7.58	0.034	0.0	0.1	0.1	2.1	1.3
HunterByu_02	1.0	0.2	0.28	7.46	0.034	0.1	0.1	0.1	2.8	2.0
HunterByu_03	0.7	0.22	0.31	6.96	0.04	0.0	0.1	0.1	2.4	1.4
HunterByu_04	0.9	0.21	0.29	7.41	0.034	0.3	0.3	0.3	2.4	1.3
HunterByu_05	1.5	0.21	0.29	7.25	0.036	0.2	0.2	0.2	3.8	3.0
HURRICANE_dsJOOR	1.4	0.25	0.36	7.2	0.038	34.1	37.2	38.2	1.3	1.9
HURRICANE_HOWELL	2.0	0.28	0.39	7.77	0.035	33.4	34.8	37.2	1.5	3.6

Table A1-1: HEC-HMS Model Parameter Summary

HURRICANE_Joor	2.7	0.27	0.38	8.02	0.034	28.0	32.7	35.9	2.2	4.7
HURRICANE_Presct	0.6	0.26	0.36	7.19	0.039	31.9	35.0	35.9	0.8	0.9
HURRICANE_Wildwd	0.5	0.27	0.37	7.66	0.036	41.6	43.3	45.2	0.6	1.4
IndianByu_PtHud	1.4	0.25	0.35	7.5	0.042	0.5	0.6	0.6	2.9	3.7
IndianByu_UWB	1.9	0.24	0.34	7.54	0.042	0.5	0.6	0.6	3.2	4.1
JacksB_Claycut	1.0	0.25	0.35	6.73	0.041	43.9	44.6	49.7	0.7	0.8
JacksB_ParkFor	0.4	0.3	0.42	8.4	0.031	46.1	48.0	51.5	0.6	0.6
JoinerCrk_01	0.4	0.19	0.26	6.46	0.048	0.5	0.5	0.5	1.7	0.9
JoinerCrk_02	0.8	0.25	0.35	4.83	0.067	0.1	0.1	0.1	2.9	2.0
JoinerCrk_03	0.9	0.24	0.34	4.84	0.067	0.6	0.6	0.6	2.8	1.7
JoinerCrk_04	1.7	0.25	0.35	4.7	0.069	0.8	0.8	0.8	3.2	2.2
JoinerCrk_05	1.1	0.23	0.32	5.47	0.059	0.3	0.3	0.3	3.1	2.3
JoinerCrk_06	0.7	0.22	0.31	6.11	0.054	0.6	0.6	0.6	2.6	1.5
JonesBayou	1.0	0.24	0.34	7.59	0.041	2.7	2.9	3.8	3.0	5.3
JonesCr_Airline	0.8	0.34	0.48	10.81	0.017	60.5	67.3	74.0	0.6	1.1
JonesCr_FLBlvd	2.1	0.28	0.39	8.35	0.032	43.0	47.0	51.2	0.9	1.9
JonesCr_Mont	2.0	0.28	0.4	8.71	0.029	47.3	62.7	68.8	1.0	1.9
JonesCr_NrAmite	2.6	0.23	0.33	6.34	0.036	23.7	25.7	28.0	2.5	5.6

Table A1-1: HEC-HMS Model Parameter Summary

JonesCr_OldHamd	2.6	0.27	0.38	7.51	0.036	35.9	38.3	41.5	1.2	2.0
JonesCr_ONealLn	1.9	0.25	0.36	6.89	0.035	32.2	36.4	40.5	1.1	1.2
JonesCr_WeinerCr	2.4	0.27	0.39	7.73	0.034	37.3	42.3	43.0	1.3	2.1
KnoxBr_Firewood	0.5	0.26	0.37	7.07	0.036	43.4	52.5	63.1	0.5	1.3
KnoxBr_ONealLn	0.8	0.24	0.34	6.47	0.041	29.2	30.8	32.5	1.3	1.8
LCypByu_Comite	2.2	0.25	0.35	7.11	0.039	11.3	11.3	12.0	3.0	5.2
LCypByu_DS_Lavey	0.4	0.21	0.3	6.9	0.039	6.1	6.6	9.4	3.0	3.5
LCypByu_GBL	1.7	0.27	0.38	8.58	0.033	22.0	22.9	26.8	2.0	3.6
LCypByu_Hooper	1.7	0.23	0.33	7.48	0.041	9.6	11.1	13.8	3.0	4.5
LCypByu_Lavey	0.9	0.24	0.34	7.21	0.04	15.4	17.5	17.5	1.9	2.2
LCypByu_Thomas	0.4	0.24	0.33	7.3	0.041	6.0	6.0	6.0	2.0	2.5
LCypByu_US_SL	2.0	0.25	0.35	7.02	0.041	12.7	13.9	15.8	2.3	3.2
LilClyell_DS_I12	3.5	0.24	0.34	7.68	0.039	3.8	5.3	6.5	3.1	14.1
LilClyell_I12	2.9	0.24	0.33	6.51	0.042	3.3	4.7	6.9	2.5	7.9
LilClyell_L01	0.6	0.25	0.36	6.53	0.043	3.2	7.2	7.2	1.8	3.9
LilClyell_Prloux	2.3	0.22	0.31	8.22	0.042	4.6	5.8	7.2	2.4	7.9
LilClyell_Range	0.9	0.23	0.33	6.53	0.043	14.6	14.8	18.0	1.3	4.0
LilClyell_RangLn	4.3	0.24	0.33	7.35	0.042	1.2	1.4	1.6	2.3	9.9

Table A1-1: HEC-HMS Model Parameter Summary

LilClyell_Satsu	1.2	0.24	0.34	6.89	0.042	1.8	1.9	2.0	1.8	4.5
LilSndyC2_DS_Jac	0.5	0.22	0.31	7.32	0.041	0.6	0.6	0.6	2.3	2.2
LilSndyC2_DS_Mil	0.2	0.23	0.32	6.64	0.041	1.9	2.4	2.8	2.2	2.0
LilSndyC2_DS_Per	0.1	0.23	0.32	6.46	0.041	1.0	1.0	1.3	2.2	1.9
LilSndyC2_Jack	0.9	0.23	0.32	6.62	0.041	0.3	0.3	0.3	2.6	2.8
LilSndyC2_Lib	0.7	0.23	0.32	6.33	0.044	0.4	0.5	0.5	2.5	2.6
LilSndyC2_MilId	0.8	0.22	0.31	6.68	0.042	0.5	0.5	0.5	2.2	3.7
LilSndyC2_Peairs	0.8	0.23	0.32	6.59	0.041	0.3	0.3	0.3	4.6	5.5
LilSndyC2_US_Jac	1.8	0.23	0.33	6.89	0.041	0.4	0.5	0.5	3.6	3.9
LilSndyC2_US_LOC	4.2	0.21	0.3	7.32	0.036	0.3	0.3	0.3	4.3	4.4
LilSndyC2_Wind	0.5	0.23	0.32	6.48	0.043	0.2	0.2	0.3	1.9	2.9
LittleSandyCrk_01	0.5	0.2	0.28	7.42	0.035	0.2	0.2	0.2	2.1	1.3
LittleSandyCrk_02	0.8	0.2	0.29	7.33	0.035	0.5	0.5	0.5	2.5	1.8
LittleSandyCrk_03	1.4	0.19	0.27	7.57	0.033	0.4	0.4	0.4	2.9	2.0
LittleSandyCrk_04	2.3	0.2	0.28	7.53	0.034	0.2	0.2	0.2	3.7	3.1
LittleSandyCrk_05	2.4	0.2	0.28	7.46	0.035	0.2	0.2	0.2	4.2	3.9
LittleSandyCrk_06	2.8	0.21	0.29	7.14	0.037	0.2	0.2	0.2	4.2	3.8
LivelyBT_FL	0.9	0.29	0.41	8.32	0.032	48.7	51.6	53.8	0.6	0.9

Table A1-1: HEC-HMS Model Parameter Summary

LivelyBT_LB	0.9	0.27	0.38	7.21	0.039	43.8	43.8	43.8	1.2	2.0
LivelyB_FLBlvd	1.5	0.28	0.39	7.72	0.035	32.0	38.5	43.1	1.3	2.2
LivelyB_HoneyCut	0.8	0.28	0.39	7.6	0.036	35.9	38.7	39.5	0.9	1.5
LivelyB_LBT	0.4	0.26	0.37	7.36	0.037	45.8	46.8	46.8	0.7	0.9
LivelyB_Pvt	0.7	0.25	0.36	6.57	0.042	7.3	13.0	19.7	1.8	3.9
LongSlashBranch	0.7	0.24	0.34	6.32	0.046	33.3	37.4	39.7	1.2	2.3
LSU_NP_MaySt	0.8	0.25	0.35	7.15	0.029	28.5	30.7	30.7	1.1	1.3
LSU_NP_Stanfrd	0.8	0.16	0.22	4.76	0.019	12.5	13.2	14.6	2.6	3.6
LWhiteByu_Comite	4.4	0.25	0.35	7.25	0.041	12.5	15.4	16.5	4.8	12.1
LWhiteByu_Pettit	2.5	0.23	0.33	7.57	0.041	4.7	5.2	6.5	3.1	8.9
LWhiteByu_US_Pet	3.5	0.24	0.34	7.77	0.041	7.0	8.7	9.4	5.1	32.9
MidClyellT3	0.3	0.23	0.32	6.57	0.042	2.1	2.1	2.7	1.6	4.6
MidClyellT5_CnMk	0.9	0.23	0.32	6.52	0.042	3.9	3.9	4.7	2.0	6.0
MidClyellT5_MC	1.3	0.23	0.33	6.55	0.042	2.1	2.7	3.4	2.5	6.2
MidClyellT5_Sprg	0.6	0.22	0.31	6.53	0.042	1.1	1.2	1.6	1.9	4.3
MidClyellT6_GalG	0.4	0.24	0.33	6.55	0.042	9.1	9.1	9.1	1.7	4.8
MidClyellT6_MC	1.5	0.22	0.31	6.54	0.042	1.5	2.1	2.5	2.6	5.4
MidClyell_CB	7.9	0.25	0.35	6.94	0.04	0.9	0.9	1.0	3.8	10.3

Table A1-1: HEC-HMS Model Parameter Summary

MidClyell_CnMkt	2.2	0.24	0.33	6.5	0.043	0.9	1.0	1.1	2.3	5.6
MidClyell_FLBlvd	1.2	0.23	0.32	6.57	0.042	3.3	4.6	5.5	2.2	3.8
MidClyell_HoodRd	3.8	0.24	0.34	6.56	0.042	0.6	0.7	0.8	2.8	10.2
MidClyell_I12	3.5	0.24	0.34	6.59	0.041	4.4	6.4	6.6	2.8	8.0
MidClyell_MCT1	2.0	0.23	0.32	6.5	0.043	1.0	1.1	1.4	2.2	6.7
MidClyell_MCT3	1.7	0.23	0.32	6.57	0.042	0.9	1.2	1.3	2.4	5.3
MidClyell_MCT5	0.5	0.24	0.34	6.56	0.042	2.9	3.8	5.3	1.8	3.0
MidClyell_MCT6	0.9	0.23	0.32	6.55	0.042	2.9	3.6	4.4	2.0	4.3
MidClyell_TylrBy	5.1	0.24	0.34	6.55	0.042	1.8	2.1	2.5	2.6	6.9
MidClyell_US_LOC	3.9	0.21	0.29	7.25	0.04	0.6	0.6	0.6	5.2	9.4
MidClyell_WeissR	1.7	0.23	0.32	6.54	0.042	0.2	0.2	0.3	2.6	10.3
MillCrk_CarsonRd	0.2	0.23	0.32	6.51	0.041	1.3	1.3	1.3	1.7	1.8
MillCrk_MahoneyRd	6.5	0.2	0.28	7.47	0.034	0.1	0.1	0.1	6.3	7.9
MillCrk_PrideBar	0.6	0.22	0.31	6.36	0.039	0.3	0.3	0.3	1.8	1.8
MillC_SandyC	0.7	0.23	0.32	6.57	0.042	0.3	0.4	0.5	2.3	3.5
MillersCT_I12	0.1	0.24	0.34	6.57	0.042	10.4	22.0	28.7	1.2	2.5
MillersCT_MC	1.0	0.24	0.33	6.45	0.041	28.2	35.7	42.2	2.3	3.5
MillersCT_UnT	0.7	0.24	0.34	6.55	0.043	36.5	55.9	79.7	1.0	2.3

Table A1-1: HEC-HMS Model Parameter Summary

MillersC_Julban	1.7	0.25	0.35	6.54	0.042	8.8	11.4	13.3	2.5	5.7
MolerB_CnMkt	1.9	0.22	0.31	6.56	0.042	1.7	1.9	2.0	1.7	7.3
MolerB_Springfld	1.0	0.22	0.31	6.55	0.042	3.7	5.0	5.6	1.7	4.2
MolerB_WC	0.4	0.21	0.3	6.5	0.041	3.8	4.8	5.6	1.4	3.0
MuddyCrk_Henry	0.6	0.25	0.35	6.65	0.041	23.8	38.6	48.5	1.1	3.0
MuddyCrk_HWY42	2.1	0.24	0.34	6.6	0.04	11.2	13.4	18.2	1.8	9.9
MuddyCrk_LilPra	1.0	0.25	0.35	6.52	0.039	17.5	18.5	25.2	1.5	3.0
MuddyCrk_NrManch	0.9	0.25	0.35	6.71	0.038	9.8	11.7	12.5	1.8	2.7
MuddyCrk_NrOakGr	1.0	0.25	0.36	6.57	0.037	12.8	17.6	17.6	1.5	5.8
NBrWardsCr_atBR	2.9	0.28	0.39	8.14	0.032	40.2	42.3	48.4	1.3	2.1
NBrWardsCr_FL	0.7	0.33	0.46	10.08	0.021	55.4	89.3	89.3	0.7	1.5
NBrWardsCr_Hare	1.0	0.31	0.43	9.44	0.025	52.6	86.4	86.5	0.7	1.1
NBrWardsCr_I10	1.4	0.28	0.39	8.07	0.033	40.3	53.0	56.2	1.1	1.4
NewR_Maurepas	9.0	0.29	0.41	11.78	0.006	0.0	0.1	0.1	0.1	122.0
ROBERTCN_dsJOOR	0.5	0.23	0.32	6.88	0.041	9.2	9.2	9.8	1.9	2.1
ROBERTCN_Grnwell	2.0	0.25	0.35	7.49	0.037	32.1	33.9	36.1	1.5	3.3
ROBERTCN_Joor	1.0	0.23	0.32	6.87	0.042	8.8	10.3	12.1	2.5	4.1
ROBERTCN_T	0.4	0.24	0.33	6.74	0.041	27.2	27.2	29.9	1.2	1.8

Table A1-1: HEC-HMS Model Parameter Summary

ROBERTCN_US_LOC	0.6	0.26	0.36	7.06	0.039	24.0	24.0	26.7	1.6	2.7
RobertsByu_01	0.5	0.2	0.28	7.54	0.033	0.9	0.9	0.9	1.5	0.7
RobertsByu_02	0.3	0.19	0.27	7.62	0.032	0.2	0.2	0.2	1.4	0.6
RobertsByu_03	0.8	0.2	0.27	7.58	0.033	0.2	0.2	0.2	2.1	1.2
RobertsByu_04	0.5	0.2	0.28	7.25	0.036	0.3	0.3	0.3	2.4	1.3
SandyCrk_01	0.2	0.24	0.34	6.78	0.04	0.5	0.5	0.5	1.9	1.4
SandyCrk_02	0.6	0.24	0.33	6.77	0.039	1.1	1.1	1.1	1.9	1.2
SandyCrk_03	1.7	0.22	0.3	7.05	0.036	0.1	0.1	0.1	2.8	2.0
SandyCrk_04	1.4	0.25	0.35	6.55	0.042	0.1	0.1	0.1	2.7	1.7
SandyCrk_05	1.3	0.25	0.35	6.55	0.042	0.3	0.3	0.3	2.6	1.6
SandyCrk_06	2.2	0.24	0.33	6.64	0.041	0.3	0.3	0.3	3.0	2.2
SandyCrk_07	1.2	0.25	0.34	6.31	0.044	0.5	0.5	0.5	2.7	1.6
SandyCrk_08	2.0	0.23	0.33	6.58	0.04	0.5	0.5	0.5	3.0	1.9
SandyCrk_09	1.0	0.24	0.34	6.52	0.043	0.0	0.1	0.1	3.5	2.6
SandyCrk_10	0.7	0.21	0.3	6.37	0.041	0.4	0.4	0.4	2.9	1.8
SandyCrk_11	1.6	0.25	0.35	6.47	0.043	0.0	0.1	0.1	3.7	2.5
SandyCrk_12	0.1	0.22	0.31	6.62	0.041	0.7	0.7	0.7	1.8	1.1
SandyCrk_13	1.4	0.22	0.31	6.89	0.041	0.3	0.3	0.3	4.8	4.1

Table A1-1: HEC-HMS Model Parameter Summary

SandyCrk_14	1.9	0.21	0.29	7.41	0.036	0.3	0.3	0.3	4.4	3.9
SandyCrk_15	0.7	0.21	0.3	7.84	0.039	0.1	0.1	0.1	3.4	2.7
SandyCrk_16	1.3	0.2	0.28	7.43	0.035	0.1	0.1	0.1	3.9	3.6
SandyCrk_17	1.7	0.22	0.31	6.79	0.04	0.1	0.1	0.1	4.5	5.0
SandyCrk_18	0.7	0.22	0.31	6.61	0.042	0.4	0.4	0.4	4.5	5.9
SandyCrk_19	2.2	0.21	0.3	7.08	0.038	0.2	0.2	0.2	4.4	4.6
SandyCrk_20	1.2	0.22	0.31	7	0.039	0.3	0.3	0.3	4.7	8.4
SandyC_AlphonFor	0.8	0.22	0.3	5.87	0.05	0.1	0.1	0.1	3.0	4.8
SandyC_BeaverPnd	0.7	0.23	0.33	6.5	0.04	0.7	0.8	0.8	3.4	5.4
SandyC_FB	0.3	0.24	0.34	6.48	0.043	0.1	0.1	0.1	2.2	2.9
SandyC_GrnwelSpr	2.8	0.23	0.32	6.37	0.043	0.7	0.9	0.9	3.8	6.4
SandyC_MillC	0.7	0.23	0.33	6.51	0.042	0.3	0.3	0.4	3.7	6.6
SandyC_PrideBay	0.8	0.23	0.33	6.44	0.041	0.8	1.0	1.0	2.0	2.0
SandyC_StnyPtBur	0.6	0.23	0.32	6.47	0.041	0.4	0.4	0.6	2.4	2.1
SandyC_UN3SC	3.1	0.25	0.35	6.51	0.043	0.1	0.1	0.1	4.0	6.2
SandyRun_01	0.5	0.25	0.35	4.78	0.068	0.4	0.4	0.4	1.6	0.7
SandyRun_02	1.0	0.24	0.34	5.07	0.064	0.4	0.4	0.4	2.5	1.3
SandyRun_03	0.3	0.22	0.31	5.77	0.055	0.4	0.4	0.4	1.7	0.7

Table A1-1: HEC-HMS Model Parameter Summary

SandyRun_04	0.5	0.19	0.27	6.41	0.048	0.4	0.4	0.4	2.1	0.9
SandyRun_05	0.9	0.2	0.29	6.28	0.05	0.4	0.4	0.4	2.5	1.5
SandyRun_06	1.2	0.2	0.28	6.47	0.048	0.4	0.4	0.4	2.7	1.6
SandyRun_07	1.2	0.24	0.33	5.55	0.06	0.1	0.1	0.1	2.6	1.2
SandyRun_08	0.5	0.22	0.31	6.74	0.045	0.1	0.1	0.1	1.9	0.9
ScalousCr	4.2	0.21	0.29	7.46	0.036	0.1	0.1	0.1	5.3	6.0
SCanal_Dyer	1.0	0.23	0.32	8.61	0.042	1.9	2.4	3.1	3.3	7.0
SCanal_Plank	1.1	0.24	0.34	7.4	0.041	0.2	0.3	0.3	2.7	4.9
ShoeCT1_SC	0.3	0.24	0.34	6.56	0.042	21.3	21.3	23.5	1.3	2.1
ShoeCT1_US_LOC	0.4	0.25	0.35	7.09	0.039	20.3	20.3	20.3	1.4	2.0
ShoeC_Comite	1.5	0.24	0.34	6.57	0.037	8.1	9.4	9.6	2.8	4.3
ShoeC_DS_Hooper	0.6	0.23	0.32	6.52	0.042	10.9	13.6	16.6	1.6	2.1
ShoeC_Gurney	0.2	0.25	0.35	6.49	0.041	5.5	6.6	7.5	1.4	2.3
ShoeC_Hooper	0.2	0.26	0.36	7.24	0.038	11.5	13.4	13.9	1.8	4.2
ShoeC_Pecos	1.7	0.24	0.34	6.59	0.039	11.1	12.8	16.4	2.5	3.5
ShoeC_SCT1	1.2	0.23	0.32	6.73	0.041	6.8	7.9	7.9	2.4	3.9
SouthCanal_Div	2.7	0.23	0.33	8.5	0.04	5.9	11.6	11.6	3.5	13.1
SouthCanal_HWY19	0.3	0.24	0.33	9.11	0.039	7.6	7.6	9.1	1.5	1.4

Table A1-1: HEC-HMS Model Parameter Summary

SOUTHLATERAL	0.7	0.25	0.35	6.72	0.042	19.8	21.2	23.7	1.7	2.5
SouthSandyRun_01	0.2	0.25	0.35	4.64	0.069	0.0	0.1	0.1	1.5	0.6
SouthSandyRun_02	0.4	0.25	0.35	5.14	0.062	0.1	0.1	0.1	2.0	0.9
SouthSandyRun_03	0.9	0.25	0.35	5.02	0.064	0.5	0.5	0.5	2.9	2.0
SouthSandyRun_04	0.5	0.25	0.35	5.04	0.064	0.9	0.9	0.9	2.1	1.1
SpillersCT2_	0.7	0.25	0.35	7.33	0.037	0.3	0.4	0.4	2.8	7.6
SpillersCT2_SC	1.0	0.23	0.32	6.52	0.038	0.9	1.0	1.1	2.9	7.4
SpillersCT2_Wei	1.1	0.23	0.33	6.92	0.039	1.5	1.7	1.9	2.3	5.6
SpillersCT2_3	0.2	0.22	0.31	6.3	0.048	2.6	2.8	3.1	3.9	18.3
SpillersC_DS_Sim	0.4	0.22	0.31	6.55	0.042	0.6	0.7	0.8	2.6	6.7
SpillersC_Hess	0.5	0.21	0.3	5.91	0.051	1.5	2.1	2.1	2.1	4.8
SpillersC_HWY16	1.1	0.23	0.33	6.38	0.043	5.0	6.1	6.1	3.2	5.1
SpillersC_Sims	0.8	0.21	0.3	6.13	0.048	0.4	0.4	0.6	2.5	5.0
SpillersC_WeissRd	1.5	0.22	0.3	6.18	0.048	0.3	0.4	0.5	3.2	10.9
StoneByu_01	0.3	0.23	0.32	6.12	0.039	1.1	1.1	1.1	1.8	1.1
StoneByu_02	0.2	0.25	0.35	6.53	0.042	1.4	1.4	1.4	1.5	0.6
StoneByu_03	0.9	0.23	0.32	6.84	0.039	1.0	1.0	1.0	2.2	1.3
StoneByu_04	0.6	0.2	0.29	7.41	0.035	0.0	0.1	0.1	2.6	1.7

Table A1-1: HEC-HMS Model Parameter Summary

StoneByu_05	1.3	0.19	0.26	6.99	0.032	0.2	0.2	0.2	3.5	2.7
SUB_BLACKCRK_01	0.8	0.23	0.33	6.39	0.041	0.4	0.4	0.4	2.5	1.8
SUB_BLACKCRK_02	1.8	0.24	0.34	6.4	0.041	0.8	0.8	0.8	3.6	3.2
SUB_BLACKCRK_03	2.5	0.25	0.35	6.54	0.042	0.1	0.1	0.1	4.0	3.9
SUB_BLACKCRK_04	3.2	0.25	0.35	6.5	0.041	0.2	0.2	0.2	4.7	5.0
SUB_BLACKCRK_05	1.4	0.26	0.36	6.52	0.042	0.3	0.3	0.3	3.9	4.5
SUB_COMITENP_01	0.5	0.26	0.37	6.57	0.042	1.2	1.4	1.4	2.0	1.8
SUB_COMITENP_02	0.4	0.25	0.35	6.41	0.049	1.7	2.0	2.4	2.3	2.0
SUB_COMITE_01	24.6	0.26	0.37	6.64	0.046	0.8	0.9	0.9	8.1	10.4
SUB_COMITE_02	1.3	0.21	0.3	6.98	0.037	0.1	0.1	0.1	4.1	3.1
SUB_COMITE_03	12.8	0.23	0.32	6.69	0.041	0.1	0.1	0.1	7.4	9.1
SUB_COMITE_04	3.1	0.23	0.33	6.58	0.043	0.0	0.1	0.1	3.6	2.5
SUB_COMITE_05	4.5	0.24	0.34	6.56	0.042	0.2	0.2	0.2	5.3	4.9
SUB_COMITE_06	3.1	0.22	0.31	6.98	0.039	0.1	0.1	0.1	4.9	4.2
SUB_COMITE_07	6.8	0.21	0.29	7.21	0.036	0.0	0.1	0.1	6.3	7.4
SUB_COMITE_09	9.1	0.21	0.29	7.05	0.036	0.3	0.3	0.3	6.3	7.4
SUB_COMITE_10	1.1	0.23	0.32	6.58	0.043	0.2	0.2	0.2	9.8	26.1
SUB_COMITE_12	0.4	0.2	0.29	6.38	0.037	0.0	0.1	0.1	3.7	2.9

Table A1-1: HEC-HMS Model Parameter Summary

SUB_COMITE_13	3.6	0.22	0.31	6.95	0.038	0.8	0.8	0.8	4.9	4.2
SUB_COMITE_14	2.6	0.22	0.31	6.87	0.039	1.1	1.1	1.1	5.0	4.4
SUB_COMITE_15	4.1	0.21	0.3	6.94	0.037	0.3	0.3	0.3	3.7	2.8
SUB_COMITE_18	2.2	0.22	0.3	6.4	0.039	0.2	0.2	0.2	5.2	5.7
SUB_COMITE_19	2.2	0.23	0.33	6.63	0.041	0.2	0.2	0.2	5.8	5.5
SUB_COMITE_21	2.7	0.22	0.31	6.58	0.055	0.3	0.3	0.3	3.8	6.8
SUB_COMITE_22	8.5	0.22	0.31	6.84	0.05	0.3	0.3	0.3	7.5	10.4
SUB_COMITE_23	3.5	0.24	0.34	6.22	0.085	0.4	0.5	0.5	4.9	5.8
SUB_COMITE_25	0.6	0.23	0.32	6.19	0.148	0.4	0.4	0.4	2.7	3.4
SUB_COMITE_26	0.8	0.23	0.33	6.44	0.111	0.5	0.5	0.5	3.1	4.2
SUB_DOYLEBAYOU_01	1.2	0.25	0.35	6.57	0.042	0.5	0.5	0.5	3.3	3.1
SUB_DOYLEBAYOU_02	1.7	0.24	0.34	6.55	0.042	0.1	0.1	0.1	3.8	5.4
SUB_DOYLEBAYOU_03	2.3	0.26	0.36	6.56	0.042	0.4	0.4	0.4	4.5	8.3
SUB_DOYLEBAYOU_05	0.6	0.25	0.35	6.57	0.042	0.2	0.3	0.4	3.6	6.4
SUB_DOYLEBAYOU_06	0.9	0.24	0.34	7.17	0.041	0.3	0.3	0.4	3.2	6.3
SUB_DOYLEBAYOU_07	0.5	0.25	0.35	6.5	0.04	0.4	0.6	0.6	2.5	2.1
SUB_DOYLEBAYOU_08	1.8	0.25	0.35	6.81	0.041	0.7	0.9	1.0	3.9	4.6
SUB_DOYLENP1_01	0.9	0.25	0.36	6.56	0.042	7.6	8.9	8.9	2.5	3.3

Table A1-1: HEC-HMS Model Parameter Summary

SUB_DOYLENP1_02	0.2	0.25	0.35	6.52	0.042	0.5	0.7	0.7	1.8	1.5
SUB_FISHERBAYOU_01	0.7	0.2	0.29	7.44	0.034	0.1	0.1	0.1	2.5	2.0
SUB_FISHERBAYOU_02	1.1	0.2	0.28	7.43	0.034	0.2	0.2	0.2	3.5	2.9
SUB_FISHERBAYOU_03	2.9	0.2	0.29	7.38	0.034	0.1	0.1	0.1	4.3	3.6
SUB_HOGBAYOU_01	0.9	0.25	0.35	6.53	0.042	0.1	0.1	0.1	2.9	2.5
SUB_HOGBAYOU_02	1.2	0.25	0.35	6.55	0.042	0.1	0.1	0.1	3.1	2.9
SUB_IRONBAYOU_01	0.5	0.24	0.34	6.56	0.042	0.4	0.4	0.4	2.5	1.9
SUB_IRONBAYOU_02	0.8	0.24	0.34	6.55	0.042	0.3	0.3	0.3	2.3	1.5
SUB_IRONBAYOU_03	1.0	0.26	0.36	6.53	0.042	0.6	0.6	0.6	3.2	3.2
SUB_IRONBAYOU_04	0.9	0.26	0.36	6.54	0.042	0.5	0.5	0.5	4.0	6.7
SUB_KNIGHTONBAYOU_01	0.3	0.2	0.28	7.38	0.035	0.2	0.2	0.2	2.1	1.2
SUB_KNIGHTONBAYOU_02	1.6	0.2	0.28	7.35	0.036	0.0	0.1	0.1	3.5	2.7
SUB_KNIGHTONBAYOU_03	2.4	0.2	0.28	7.45	0.034	0.1	0.1	0.1	3.4	2.6
SUB_KNIGHTONBAYOU_04	1.5	0.22	0.3	6.78	0.04	0.0	0.1	0.1	4.9	5.2
SUB_LEWISCRK_01	0.8	0.21	0.3	7.09	0.037	5.1	5.1	5.1	2.1	1.0
SUB_LEWISCRK_02	0.3	0.21	0.3	7.05	0.039	5.6	5.6	5.6	2.2	1.3
SUB_LEWISCRK_03	0.2	0.21	0.3	6.82	0.039	0.3	0.3	0.3	2.2	1.4
SUB_LITCOMITE_01	10.9	0.23	0.32	7.99	0.042	0.5	0.5	0.5	5.9	6.3

Table A1-1: HEC-HMS Model Parameter Summary

SUB_LITCOMITE_02	1.3	0.23	0.32	6.78	0.041	0.0	0.1	0.1	2.8	1.7
SUB_LITCOMITE_03	3.6	0.24	0.34	6.63	0.041	0.5	0.5	0.5	5.8	6.3
SUB_LITREDWOOD_01	0.8	0.22	0.31	6.12	0.039	1.0	1.0	1.0	3.2	2.3
SUB_LITREDWOOD_02	1.1	0.24	0.33	6.49	0.041	0.2	0.2	0.2	3.7	3.2
SUB_LITREDWOOD_03	1.9	0.24	0.33	6.66	0.041	0.2	0.2	0.2	3.7	3.1
SUB_LITREDWOOD_04	1.3	0.22	0.3	6.83	0.039	0.2	0.2	0.2	4.6	4.2
SUB_LITREDWOOD_05	2.4	0.2	0.28	7.45	0.034	0.2	0.2	0.2	4.0	3.3
SUB_MONAHANBAYOU_01	1.2	0.2	0.28	7.5	0.033	0.5	0.5	0.5	2.7	1.9
SUB_MONAHANBAYOU_02	2.5	0.2	0.28	7.29	0.034	0.2	0.2	0.2	4.7	4.6
SUB_PRETTYCRK_01	1.3	0.23	0.32	7	0.039	0.2	0.2	0.2	2.5	1.6
SUB_PRETTYCRK_02	2.2	0.22	0.31	7.04	0.039	0.2	0.2	0.2	3.3	2.6
SUB_PRETTYCRK_03	2.3	0.22	0.31	7.01	0.037	0.2	0.2	0.2	3.0	1.9
SUB_PRETTYCRK_04	4.5	0.2	0.28	7.48	0.034	0.0	0.1	0.1	5.0	4.9
SUB_PRETTYCRK_05	3.6	0.24	0.34	6.37	0.046	0.7	0.7	0.7	4.4	3.9
SUB_PRETTYCRK_06	4.5	0.21	0.29	7.1	0.036	0.2	0.2	0.2	5.6	5.7
SUB_PRETTYCRK_07	3.1	0.22	0.31	6.99	0.039	0.5	0.5	0.5	4.7	4.5
SUB_PRETTYCRK_08	1.7	0.23	0.32	6.46	0.041	6.1	6.1	6.1	4.0	3.1
SUB_PRETTYCRK_09	0.0	0.21	0.29	5.86	0.038	0.0	0.1	0.1	1.1	0.9

Table A1-1: HEC-HMS Model Parameter Summary

SUB_REDWOODCRK_01	0.7	0.19	0.27	7.61	0.032	0.7	0.7	0.7	2.3	1.4
SUB_REDWOODCRK_02	1.2	0.21	0.29	7.05	0.036	1.2	1.2	1.2	2.5	1.4
SUB_REDWOODCRK_03	2.9	0.21	0.3	7.25	0.036	0.5	0.5	0.5	3.4	2.6
SUB_REDWOODCRK_04	3.0	0.22	0.31	6.82	0.039	0.1	0.1	0.1	4.5	3.8
SUB_REDWOODCRK_05	1.8	0.24	0.34	6.56	0.042	0.1	0.1	0.1	4.7	5.2
SUB_REDWOODCRK_06	3.8	0.22	0.32	6.93	0.038	1.1	1.1	1.1	4.4	3.8
SUB_REDWOODCRK_08	1.9	0.23	0.32	6.63	0.04	0.2	0.2	0.2	5.0	5.0
SUB_REDWOODCRK_09	3.5	0.2	0.28	7.39	0.034	0.4	0.4	0.4	5.0	4.5
SUB_REDWOODCRK_10	1.1	0.23	0.32	6.85	0.039	0.3	0.3	0.3	4.0	3.7
SUB_REDWOODCRK_11	2.6	0.25	0.35	6.59	0.041	0.5	0.5	0.5	5.3	7.2
SUB_REDWOODCRK_12	1.3	0.23	0.32	6.94	0.038	0.2	0.2	0.2	3.7	3.4
SUB_REDWOODCRK_13	2.7	0.24	0.33	6.55	0.042	0.1	0.1	0.1	4.6	4.7
SUB_REDWOODCRK_14	1.2	0.24	0.34	6.55	0.042	0.2	0.2	0.2	4.4	5.1
SUB_REDWOODCRK_15	0.4	0.25	0.35	6.77	0.041	0.1	0.1	0.2	2.5	2.9
SUB_REDWOODCRK_16	0.4	0.24	0.34	6.49	0.042	0.0	0.1	0.1	2.3	3.0
SUB_REDWOODCRK_17	0.7	0.25	0.35	6.88	0.041	0.2	0.2	0.2	4.0	6.1
SUB_REDWOODCRK_18	0.1	0.24	0.34	6.47	0.042	1.0	1.0	1.3	1.4	1.0
SUB_REDWOODNP	0.5	0.25	0.35	6.55	0.042	0.0	0.1	0.1	3.0	3.4

Table A1-1: HEC-HMS Model Parameter Summary

SUB_SCHLEIBAYOU_01	0.5	0.2	0.29	7.47	0.034	1.1	1.1	1.1	2.6	1.8
SUB_SCHLEIBAYOU_02	1.1	0.21	0.3	7.21	0.036	0.5	0.5	0.5	2.9	2.3
SUB_SCHLEIBAYOU_03	1.3	0.21	0.29	7.11	0.037	0.5	0.5	0.5	3.8	3.7
SUB_SESSIONSBAYOU_NP	1.5	0.2	0.28	7.54	0.034	0.1	0.1	0.1	3.8	3.1
SUB_SESSIONSBAYOU_01	0.6	0.2	0.28	7.42	0.034	0.0	0.1	0.1	1.9	1.1
SUB_SESSIONSBAYOU_02	0.8	0.21	0.29	7.25	0.037	0.2	0.2	0.2	2.9	2.0
SUB_SESSIONSBAYOU_03	1.5	0.21	0.29	7.11	0.037	0.1	0.1	0.1	3.5	2.7
SUB_SESSIONSBAYOU_04	0.6	0.22	0.31	6.49	0.043	0.2	0.2	0.2	3.1	2.1
SUB_UNT_LEWISCRK	0.4	0.2	0.28	7.49	0.034	4.1	4.1	4.1	2.3	1.1
SUB_UNT3_REDWOOD_1	0.4	0.26	0.37	6.57	0.042	2.2	2.7	2.7	2.0	2.3
SUB_UNT3_REDWOOD_2	0.3	0.26	0.36	6.57	0.042	0.0	0.1	0.1	2.1	2.2
SUB_UN_UN3_REDWOOD	0.3	0.26	0.37	6.57	0.042	1.8	2.3	2.3	1.7	1.4
SUB_UN_UN4_REDWOOD_1	2.9	0.25	0.35	6.56	0.042	0.1	0.1	0.1	4.0	4.0
SUB_UN_UN4_REDWOOD_2	0.4	0.25	0.36	6.56	0.042	0.1	0.1	0.2	2.5	2.3
SUB_UN_UN4_REDWOOD_3	0.0	0.24	0.33	6.5	0.043	0.0	0.1	0.2	0.8	0.2
SUB_UN3_REDWOOD_02	0.2	0.25	0.35	6.96	0.041	0.6	0.6	0.6	1.8	1.2
SUB_UN4_REDWOOD_01	0.5	0.25	0.36	6.57	0.042	0.2	0.2	0.2	2.6	2.6
SUB_UN4_REDWOOD_02	0.2	0.25	0.35	6.49	0.042	0.2	0.2	0.3	1.7	1.2

Table A1-1: HEC-HMS Model Parameter Summary

SUB_WALNUTBR_01	0.7	0.25	0.35	6.56	0.042	0.1	0.1	0.1	2.3	1.3
SUB_WALNUTBR_02	1.6	0.25	0.35	6.56	0.042	0.1	0.1	0.1	3.2	2.3
SUB_WALNUTBR_03	1.9	0.24	0.34	6.38	0.043	0.2	0.2	0.2	3.6	2.4
SUB_WFRKLITCOMITE_01	4.4	0.22	0.3	8.29	0.042	0.2	0.2	0.2	4.7	3.9
SUB_WFRKLITCOMITE_02	1.1	0.22	0.31	6.99	0.04	0.2	0.2	0.2	3.3	2.3
SUB_WHITEBAYOU_01	0.6	0.25	0.35	6.57	0.042	0.0	0.1	0.1	2.4	1.9
SUB_WHITEBAYOU_02	1.3	0.25	0.35	6.51	0.041	0.0	0.1	0.1	3.1	3.2
SUB_WHITEBAYOU_03	2.4	0.26	0.36	6.53	0.042	0.3	0.3	0.3	4.7	6.4
SUB_WHITEBAYOU_04	1.3	0.26	0.36	6.56	0.042	0.4	0.4	0.4	3.6	5.8
SUB_WHITEBAYOU_05	1.6	0.26	0.37	6.56	0.042	0.2	0.2	0.2	3.0	4.2
SUB_WHITEBAYOU_06	2.9	0.25	0.35	6.51	0.041	0.2	0.2	0.2	4.7	6.1
TaberC_CarsonRd	1.4	0.23	0.32	6.54	0.041	0.3	0.3	0.3	3.4	4.2
TaberC_HannaC	3.1	0.23	0.32	6.84	0.04	0.4	0.4	0.4	3.6	3.6
TaylorByu_DS_I12	2.5	0.24	0.34	6.58	0.041	6.4	8.0	10.2	2.6	7.8
TaylorByu_FL	0.3	0.23	0.32	6.57	0.042	26.3	31.7	41.1	0.7	1.3
TaylorByu_I12	1.7	0.23	0.32	6.51	0.041	19.3	21.6	37.5	1.9	6.1
TaylorByu_RR	0.3	0.23	0.32	6.55	0.042	11.9	19.8	22.6	1.0	2.9
UnDuffByu_DS	0.3	0.22	0.31	7.3	0.041	0.0	0.1	0.1	1.9	1.6

Table A1-1: HEC-HMS Model Parameter Summary

UnDuffByu_US	0.2	0.24	0.34	6.67	0.042	11.3	11.3	11.3	1.6	1.5
UnT_GreenwellSp	1.1	0.23	0.32	6.55	0.041	0.3	0.3	0.4	2.9	5.6
UNT1ADarlingCrk_01	0.5	0.25	0.35	4.71	0.069	0.3	0.3	0.3	2.2	1.3
UNT1BlackCrk_01	0.6	0.25	0.35	5.06	0.064	0.2	0.2	0.2	2.0	1.2
UNT1BluffCrk_01	3.5	0.22	0.3	7.15	0.036	0.2	0.2	0.2	5.1	4.5
UNT1DarlingCrk_01	0.7	0.2	0.28	6.2	0.051	0.3	0.3	0.3	2.1	1.0
UNT1DarlingCrk_02	0.6	0.24	0.33	4.76	0.064	0.3	0.3	0.3	1.6	0.7
UNT1DarlingCrk_03	0.6	0.24	0.33	5.92	0.059	0.2	0.2	0.2	2.4	1.3
UNT1DunnCrk_01	1.6	0.2	0.28	7.32	0.036	0.4	0.4	0.4	3.4	2.4
UNT1SouthSandyRun_01	0.5	0.23	0.33	5.19	0.061	0.5	0.5	0.5	1.7	0.9
UNT1WoodlandCrk_01	3.4	0.25	0.35	6.38	0.044	0.4	0.4	0.4	3.8	2.9
UNT2ASSandyRun	0.1	0.24	0.34	4.49	0.068	0.8	0.8	0.8	1.2	0.5
UNT2BlackCrk_01	0.8	0.24	0.34	5	0.065	1.1	1.1	1.1	2.9	1.8
UNT2BluffCrk_01	3.3	0.2	0.28	7.54	0.034	0.2	0.2	0.2	4.5	4.0
UNT2DarlingCrk_01	0.4	0.25	0.35	4.9	0.066	0.5	0.5	0.5	1.9	1.0
UNT2DarlingCrk_02	0.5	0.25	0.35	4.71	0.068	0.5	0.5	0.5	1.9	0.9
UNT2DarlingCrk_03	0.6	0.25	0.35	4.93	0.065	0.4	0.4	0.4	2.2	1.0
UNT2SouthSandyRun_01	0.1	0.25	0.35	4.61	0.07	0.0	0.1	0.1	1.2	0.4

Table A1-1: HEC-HMS Model Parameter Summary

UNT2SouthSandyRun_02	0.5	0.24	0.34	4.92	0.064	0.2	0.2	0.2	1.8	0.8
UNT3ADarlingCrk_01	0.6	0.24	0.34	5.19	0.062	0.1	0.1	0.1	2.5	1.3
UNT3BlackCrk_01	1.7	0.23	0.33	5.35	0.061	0.3	0.3	0.3	3.8	3.2
UNT3DarlingCrk_01	6.1	0.24	0.34	5.09	0.065	0.4	0.4	0.4	4.5	3.7
UNT3DarlingCrk_02	0.3	0.23	0.32	5.75	0.055	0.2	0.2	0.2	2.1	1.5
UNT3DarlingCrk_03	0.6	0.23	0.32	5.83	0.054	0.5	0.5	0.5	1.9	0.8
UNT3DarlingCrk_04	0.8	0.21	0.3	6.15	0.05	0.2	0.2	0.2	2.1	1.2
UnT3SandyC_Librt1	0.2	0.24	0.34	6.48	0.041	0.7	0.7	0.7	1.5	2.8
UnT3SandyC_Librt2	0.4	0.23	0.33	6.49	0.043	0.7	0.7	0.7	1.9	2.5
UNT3SouthSandyRun_01	0.5	0.25	0.35	4.63	0.07	0.1	0.1	0.1	1.9	1.0
UNT3SouthSandyRun_02	0.7	0.25	0.35	4.69	0.069	0.6	0.6	0.6	1.9	0.9
UNT3SouthSandyRun_03	0.7	0.25	0.35	4.78	0.067	0.4	0.4	0.4	2.0	0.9
UNT4ADarlingCrk_01	0.2	0.25	0.35	5.19	0.062	0.2	0.2	0.2	1.4	0.5
UNT4ADarlingCrk_02	0.1	0.25	0.35	5.57	0.056	0.3	0.3	0.3	1.2	0.4
UNT4DarlingCrk_01	2.2	0.25	0.36	5.15	0.064	0.1	0.1	0.1	3.7	3.0
UNT4DarlingCrk_02	0.2	0.25	0.34	5.37	0.06	0.0	0.1	0.1	2.0	1.0
UNT4DarlingCrk_03	0.2	0.23	0.33	6.24	0.048	0.0	0.1	0.1	1.6	0.6
Un_UpperWhiteByu	1.3	0.23	0.32	5.95	0.038	0.1	0.1	0.1	2.4	9.7

Table A1-1: HEC-HMS Model Parameter Summary

Un1LilSndyC2_DS	1.2	0.23	0.33	7.1	0.042	1.0	1.1	1.2	3.2	3.5
Un1LilSndyC2_US	0.2	0.25	0.35	6.57	0.042	0.5	0.5	0.5	1.7	1.1
Un1MilIC_PrideB	0.5	0.22	0.31	6.59	0.042	0.2	0.2	0.2	2.3	1.9
Un1MilIC_US_LOC	0.2	0.22	0.31	6.57	0.042	0.3	0.3	0.3	1.5	1.6
Un1SandyC	0.8	0.23	0.32	6.89	0.041	0.0	0.1	0.1	3.4	3.5
Un2LilSndyC2_DS	0.6	0.23	0.32	6.62	0.041	0.2	0.2	0.2	2.3	2.1
Un2LilSndyC2_US	0.4	0.23	0.33	6.99	0.041	0.7	0.8	1.0	1.6	1.4
Un2_NBrWards_DS	0.6	0.24	0.34	6.73	0.041	39.4	39.4	45.1	0.8	0.9
Un2_NBrWards_US	0.8	0.28	0.39	8.09	0.033	35.5	36.9	41.1	1.0	1.6
Un3LilSndyC2_DS	0.7	0.23	0.33	6.57	0.042	0.5	0.5	0.5	2.2	2.6
Un3LilSndyC2_US	0.3	0.24	0.34	6.55	0.041	1.3	1.9	1.9	1.4	1.3
Un4LilSndyC2	0.7	0.23	0.32	6.53	0.041	0.7	0.7	1.1	2.4	4.0
Un4SandyC_DS	0.3	0.24	0.34	6.24	0.041	0.4	0.4	0.5	1.9	3.0
Un4SandyC_US	0.3	0.23	0.32	6.55	0.04	1.1	1.5	1.5	1.6	1.5
UpperWhiteByu_DS	0.5	0.25	0.35	7.62	0.042	1.5	1.9	2.3	2.6	2.9
UpperWhiteByu_US	0.5	0.25	0.36	7.43	0.042	2.0	2.4	2.5	1.9	1.7
UWhiteByu_Div	0.2	0.25	0.35	6.57	0.04	0.0	0.2	0.2	2.3	2.5
UWhiteByu_DW	0.9	0.25	0.36	6.55	0.042	0.5	0.5	0.6	2.4	3.1

Table A1-1: HEC-HMS Model Parameter Summary

UWhiteByu_Hudson	3.1	0.25	0.35	6.62	0.042	1.5	2.0	2.5	3.6	5.9
UWhiteByu_HWY64	3.5	0.25	0.35	6.75	0.042	5.4	6.2	7.0	4.0	5.4
UWhiteByu_LowZac	0.9	0.25	0.35	7.08	0.041	9.3	11.0	16.4	2.2	2.4
UWhiteByu_US_Div	0.6	0.24	0.34	6.61	0.041	0.2	0.3	0.3	2.3	3.8
UWhiteByu_UT	3.5	0.25	0.36	6.87	0.042	0.8	1.1	1.3	3.9	6.3
WardsCr_Bluebon	0.8	0.32	0.45	9.69	0.023	43.6	54.5	66.9	1.0	1.1
WardsCr_Choctaw	1.0	0.28	0.4	8.21	0.032	43.5	43.5	44.1	0.6	1.8
WardsCr_College	1.0	0.26	0.37	7.71	0.035	22.1	25.2	26.3	1.1	1.1
WardsCr_EssenLn	1.9	0.27	0.38	7.96	0.035	28.5	36.4	36.4	1.6	2.8
WardsCr_GovtSt	2.9	0.29	0.42	8.92	0.028	44.0	44.3	48.8	1.2	2.3
WardsCr_GusYoung	0.8	0.25	0.36	7.07	0.038	45.5	48.1	50.7	0.7	1.3
WardsCr_Highland	3.6	0.24	0.33	7.03	0.039	21.0	24.5	28.9	2.0	2.7
WardsCr_I10_DS	1.2	0.23	0.32	7.84	0.039	28.9	29.4	36.4	1.8	3.0
WardsCr_I10_US	1.4	0.27	0.38	7.79	0.035	30.8	37.0	40.6	1.0	1.1
WardsCr_Manchac	1.8	0.24	0.34	7.47	0.037	28.7	28.7	31.0	1.6	2.7
WardsCr_PecueLn	2.0	0.25	0.35	7.78	0.034	39.8	39.8	43.9	1.2	1.9
WardsCr_SiegenLn	3.3	0.26	0.36	7.34	0.036	40.2	43.7	50.2	1.0	1.3
WaxDitch	0.7	0.24	0.34	6.57	0.042	25.7	35.2	40.3	1.3	2.6

Table A1-1: HEC-HMS Model Parameter Summary

WClyellT1_DS_Spr	0.5	0.22	0.3	6.54	0.042	3.3	4.2	4.2	1.8	4.2
WClyellT1_Pvt	1.4	0.23	0.32	6.37	0.045	0.7	0.9	0.9	2.0	4.1
WClyellT1_SprfdR	2.5	0.22	0.31	6.54	0.042	0.6	0.7	0.8	1.7	9.8
WClyell_ArnoldR	2.4	0.23	0.32	6.56	0.042	0.6	0.7	0.7	2.3	5.4
WClyell_CnMkt	1.4	0.22	0.31	6.57	0.042	0.5	0.6	0.7	2.7	6.9
WClyell_DS_Arnld	3.2	0.23	0.32	6.54	0.042	6.3	6.5	7.4	2.4	6.5
WClyell_DS_I12	3.7	0.24	0.34	6.51	0.041	6.1	7.9	9.0	2.5	7.2
WClyell_DS_Spr	0.3	0.22	0.32	6.56	0.042	0.9	1.2	1.2	1.5	2.9
WClyell_HoodRd	2.6	0.24	0.34	6.61	0.042	2.0	2.4	3.2	2.6	7.9
WClyell_I12	3.8	0.23	0.33	6.49	0.041	9.5	12.0	12.6	2.1	4.3
WClyell_JoeMayR	3.6	0.24	0.34	6.56	0.042	6.9	8.7	12.3	2.6	7.0
WClyell_NanWes	0.7	0.21	0.3	5.96	0.05	5.0	6.9	6.9	1.8	5.0
WClyell_RR	2.1	0.23	0.33	6.51	0.042	9.4	12.7	15.7	2.5	5.3
WClyell_SprgfdR	2.2	0.22	0.31	6.55	0.042	0.6	0.9	1.0	2.2	7.8
WeinerCr_DS	1.7	0.28	0.39	8.06	0.031	50.1	55.5	55.5	0.8	1.1
WeinerCr_I12	0.2	0.31	0.44	9.15	0.027	54.6	60.8	67.7	0.7	1.1
WeinerCr_US	0.5	0.31	0.43	9.02	0.027	51.4	52.2	58.2	0.6	0.6
WelshGullyT1	0.3	0.26	0.37	6.57	0.039	9.3	10.0	11.6	1.6	1.9

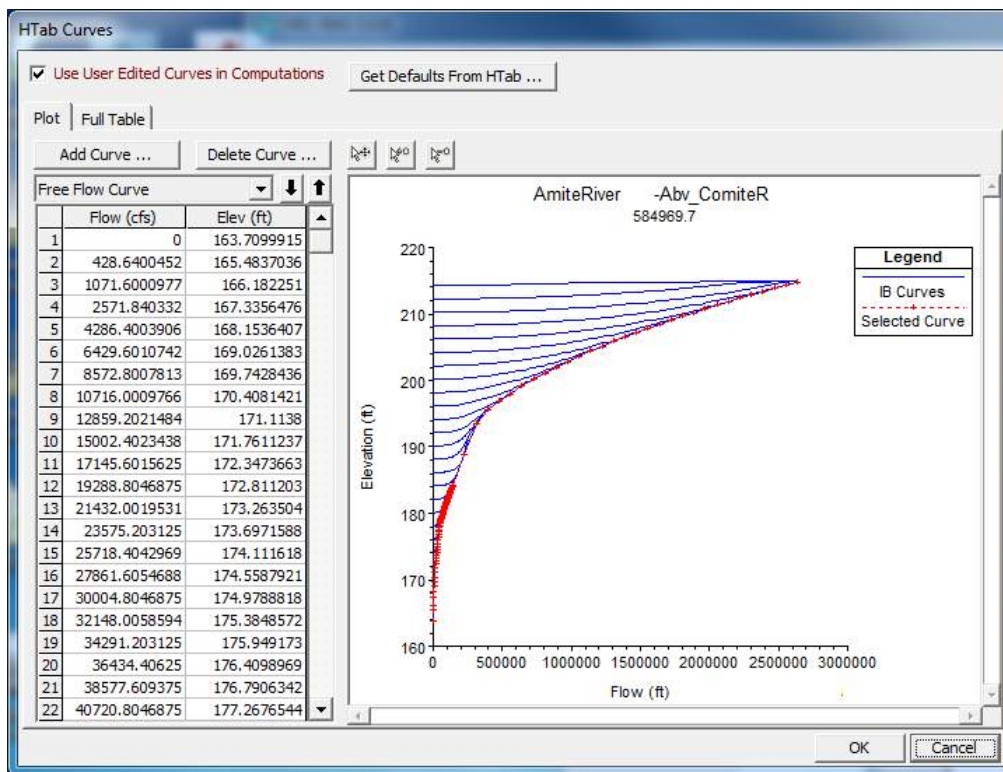
Table A1-1: HEC-HMS Model Parameter Summary

WelshGul_Manchac	0.4	0.21	0.3	6.96	0.041	3.9	3.9	3.9	2.0	2.0
WelshGul_NrPrair	1.5	0.26	0.36	6.57	0.039	25.1	29.9	32.9	1.7	3.6
WestForkAmite_01	33.1	0.27	0.38	6.27	0.046	0.6	0.6	0.6	8.0	11.6
WestForkAmite_02	64.2	0.27	0.37	5.88	0.052	0.3	0.3	0.3	12.6	22.2
WestForkAmite_03	53.6	0.27	0.38	5.87	0.052	0.7	0.7	0.7	9.2	12.6
WestForkAmite_04	38.6	0.26	0.37	5.91	0.05	0.3	0.3	0.3	11.7	18.0
WFrkBeaverC2_Spr	0.9	0.23	0.32	6.44	0.043	16.5	19.0	23.4	2.1	5.0
WFrkBeaverC2_US	0.3	0.22	0.3	5.88	0.048	14.9	14.9	14.9	1.6	3.8
WindByu_Jackson	0.5	0.23	0.32	6.57	0.042	0.6	0.8	1.0	1.9	2.5
WindByu_LSC2	0.7	0.23	0.33	6.48	0.043	0.5	0.5	0.7	2.9	3.5
WindByu_Milldale	1.1	0.24	0.34	6.55	0.042	0.4	0.4	0.4	2.5	4.2
WindByu_PeairsRd	0.7	0.23	0.32	6.52	0.041	0.9	1.2	1.2	1.9	1.8
WLatCypB_ScotZac	1.9	0.25	0.36	7.91	0.038	16.2	20.4	26.4	2.6	7.2
WLatCypB_US_LOC	0.3	0.24	0.34	7.96	0.041	0.1	0.1	0.2	2.1	4.7
WoodlandCrk_01	0.2	0.25	0.35	6.5	0.041	0.8	0.8	0.8	1.6	0.9
WoodlandCrk_02	1.8	0.25	0.35	6.32	0.044	0.2	0.2	0.2	3.0	2.0
WoodlandCrk_03	0.6	0.23	0.32	6.92	0.04	0.1	0.1	0.1	2.6	1.5
WoodlandCrk_04	0.4	0.23	0.32	6.99	0.039	0.4	0.4	0.4	2.1	1.0

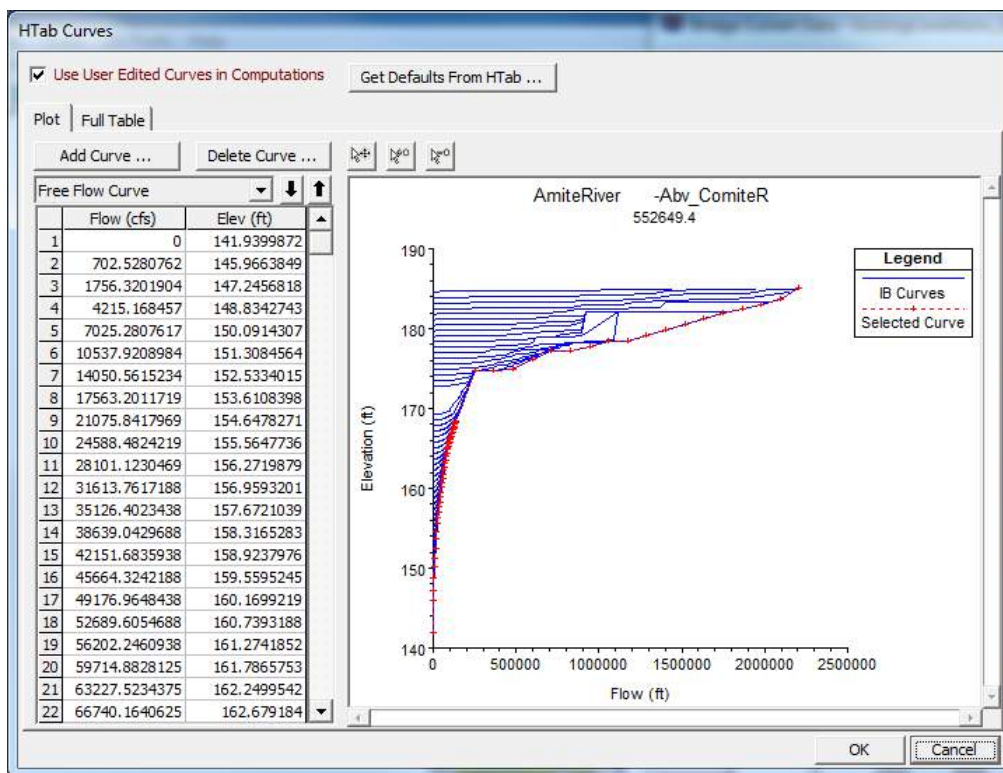
Table A1-1: HEC-HMS Model Parameter Summary										
WoodlandCrk_05	2.1	0.25	0.35	6.57	0.042	0.2	0.2	0.2	2.9	1.7
WoodlandCrk_06	1.4	0.24	0.34	6.6	0.042	0.0	0.1	0.1	3.3	2.0
WoodlandCrk_07	1.1	0.22	0.3	6.69	0.041	0.0	0.1	0.1	4.0	3.6

APPENDIX 2: HTAB CURVES FOR BRIDGES IN THE DYNAMIC ARB HEC-RAS MODEL

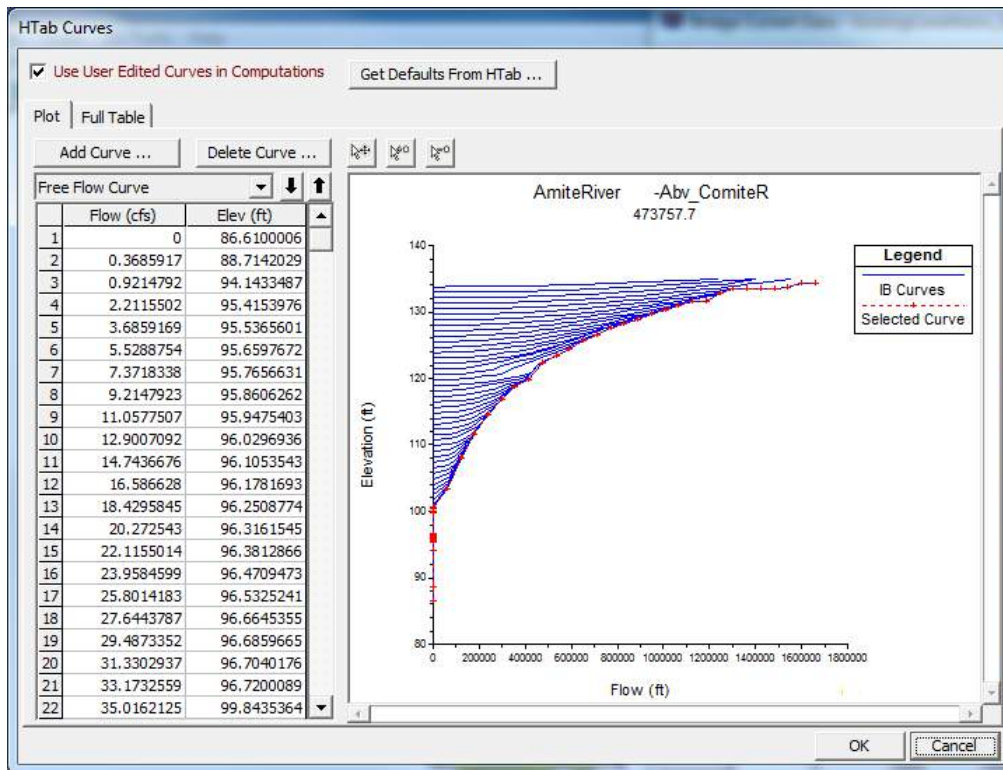
HTab Curves for Bridges in the Dynamic ARB HEC-RAS Model



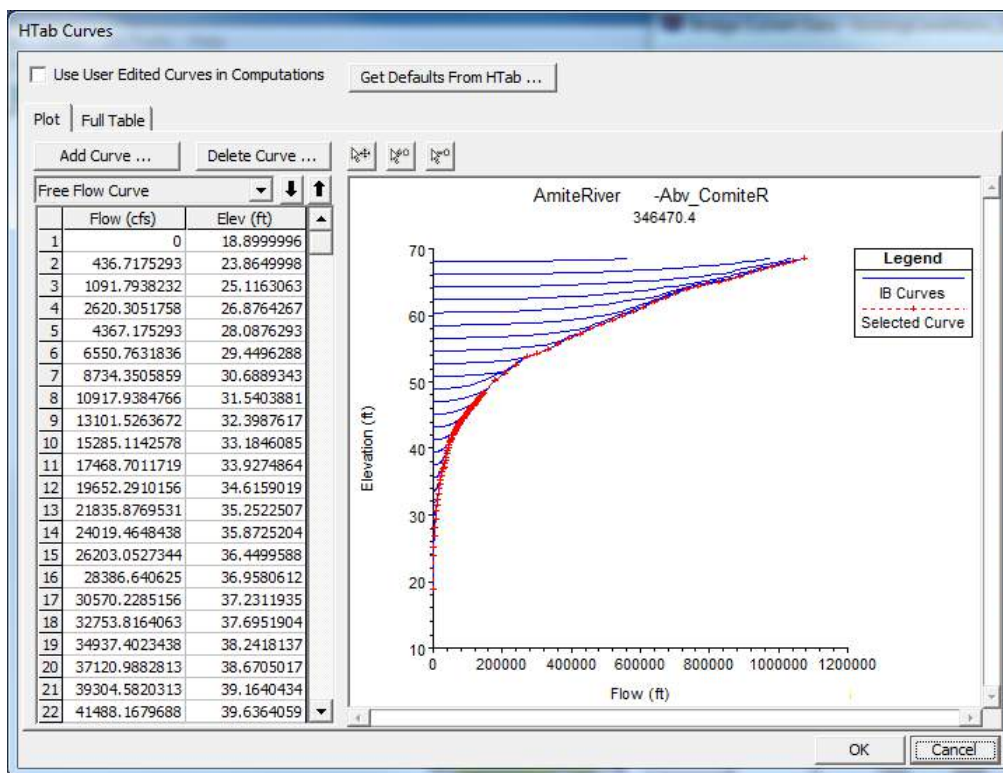
Highway 432, Amite River, Abv_ComiteR, Sta: 584969.7



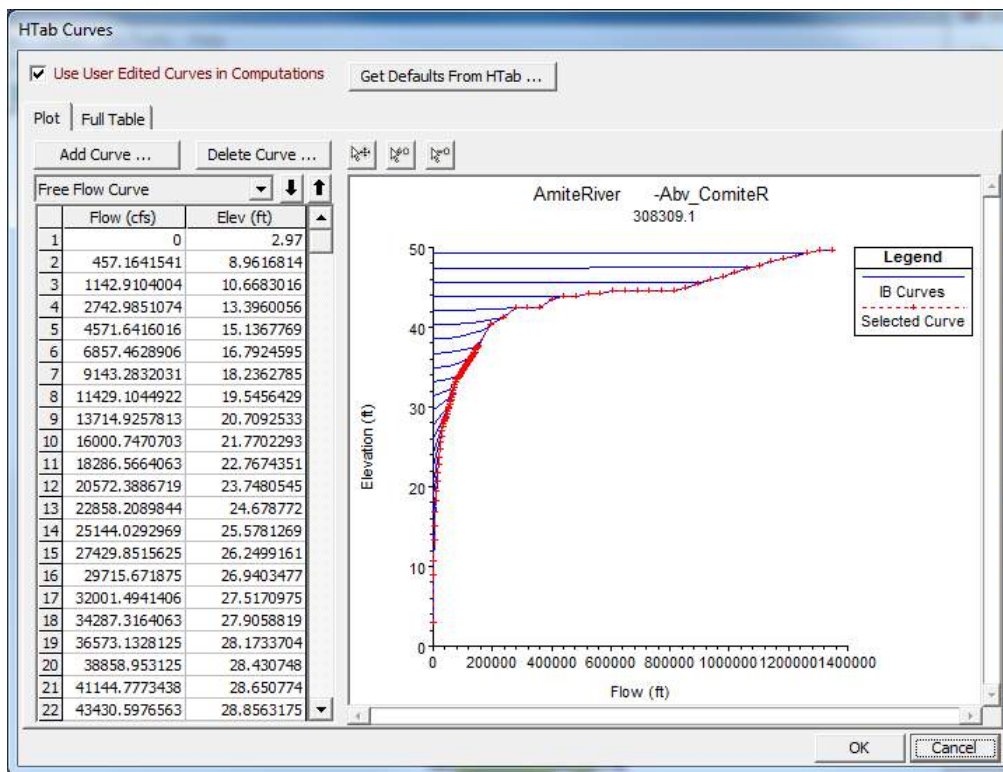
Highway 10, Amite River, Abv_ComiteR, Sta: 552649.4



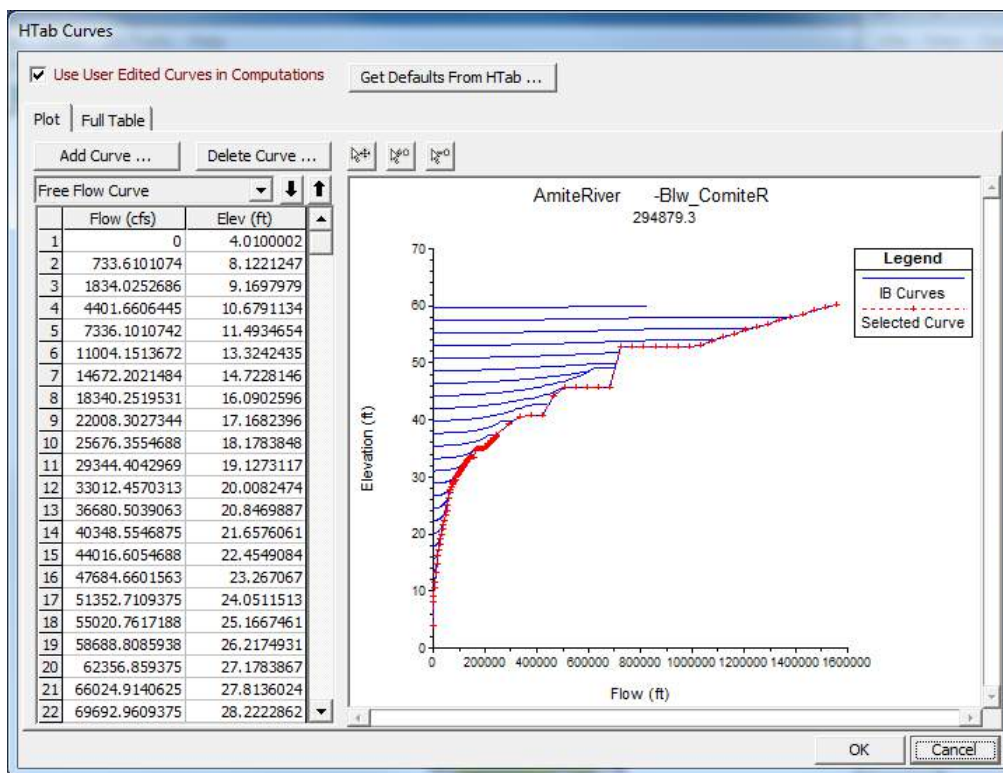
Highway 37/63, Amite River, Abv_ComiteR, Sta: 473757.7



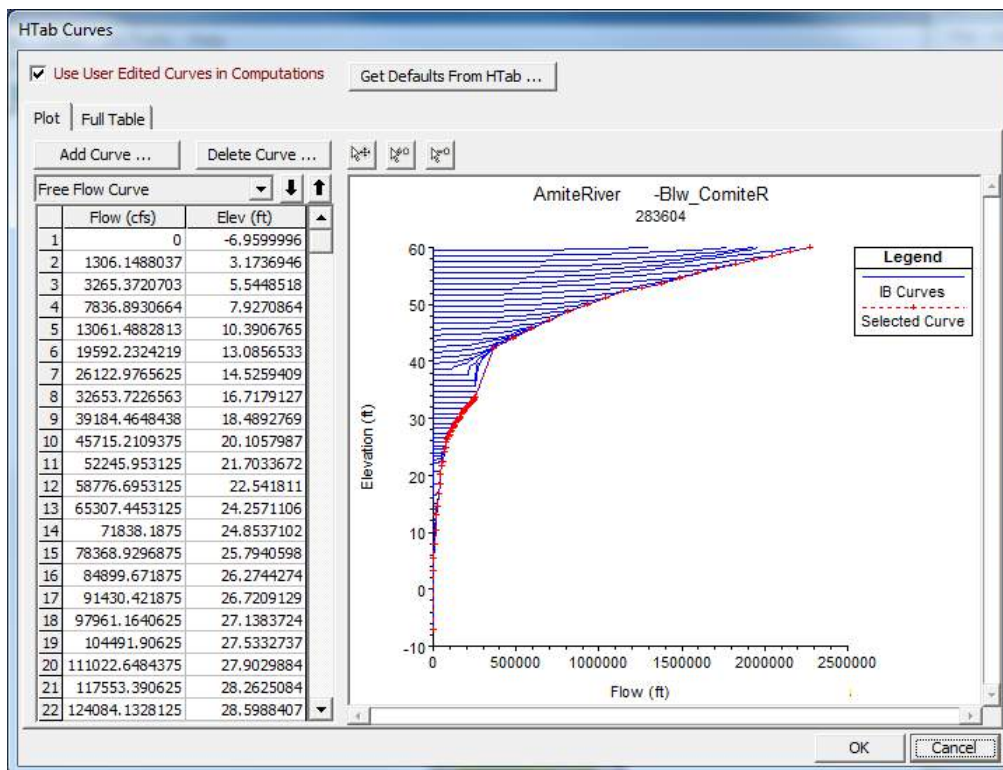
Magnolia Bridge Road, Amite River, Abv_ComiteR, Sta: 346470.4



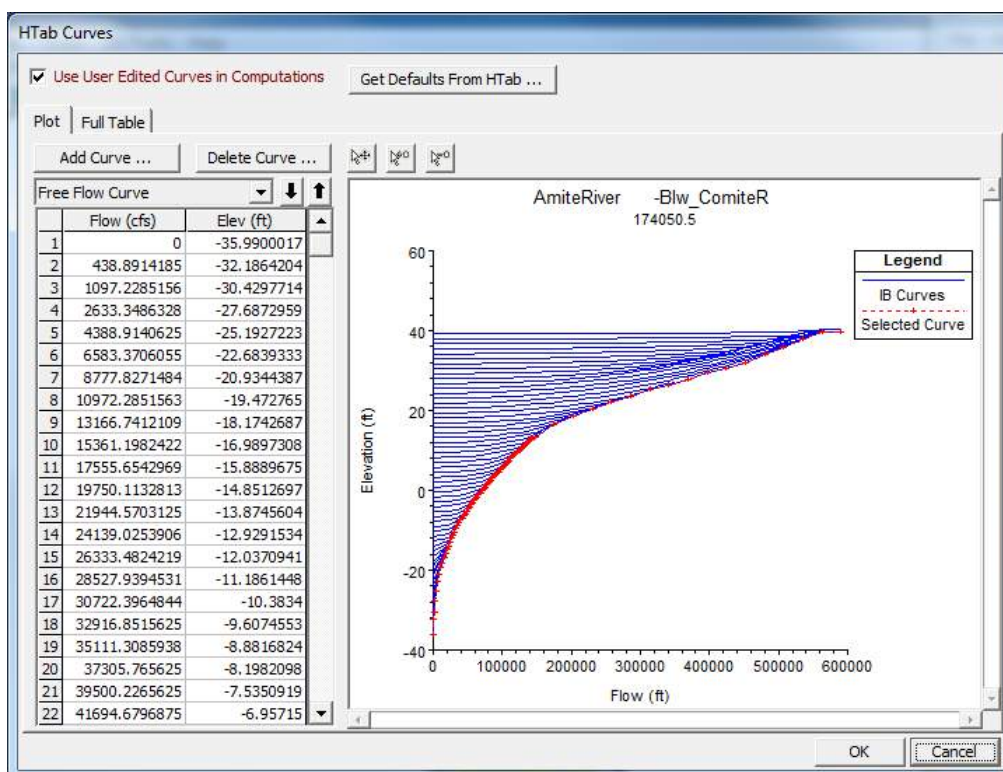
Railroad, Amite River, Abv_ComiteR, Sta: 308309.1



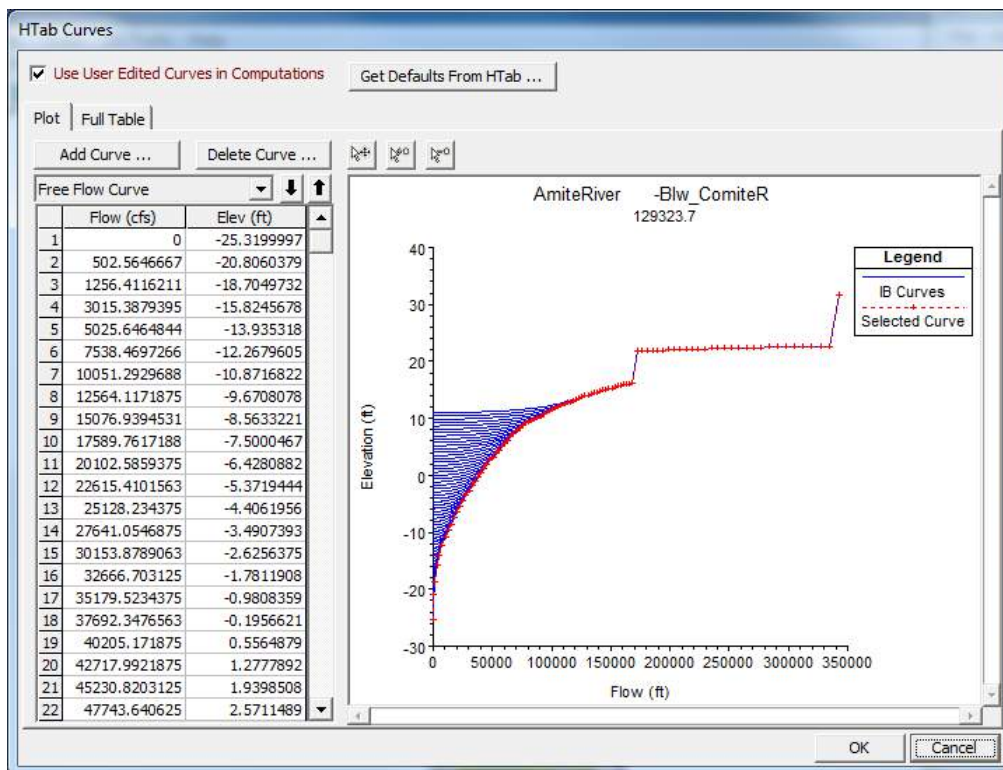
Florida Blvd/Ave, Amite River, Blw_ComiteR, Sta: 294879.3



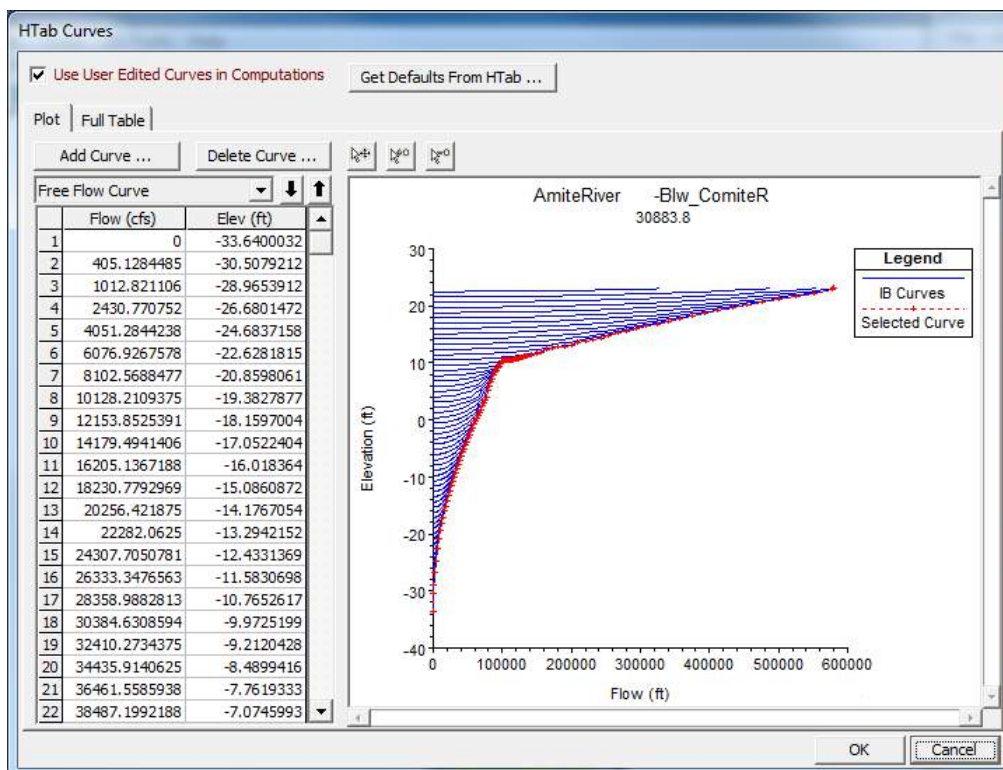
Interstate 12, Amite River, Blw_ComiteR, Sta: 283604



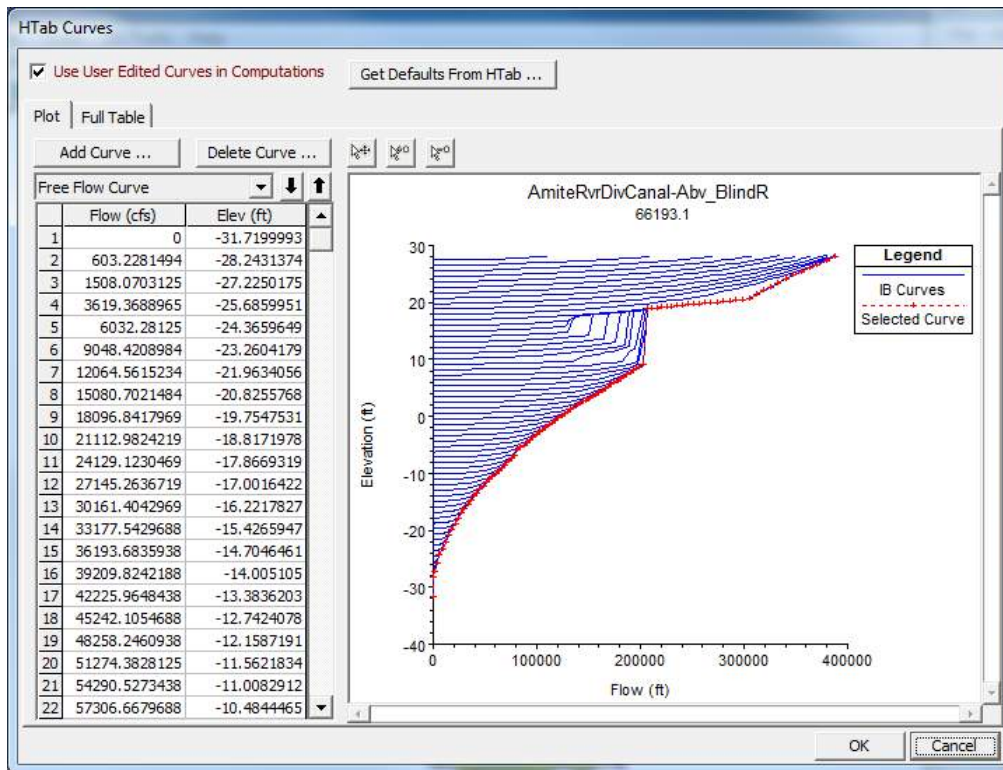
Highway 42, Amite River, Blw_ComiteR, Sta: 174050.5



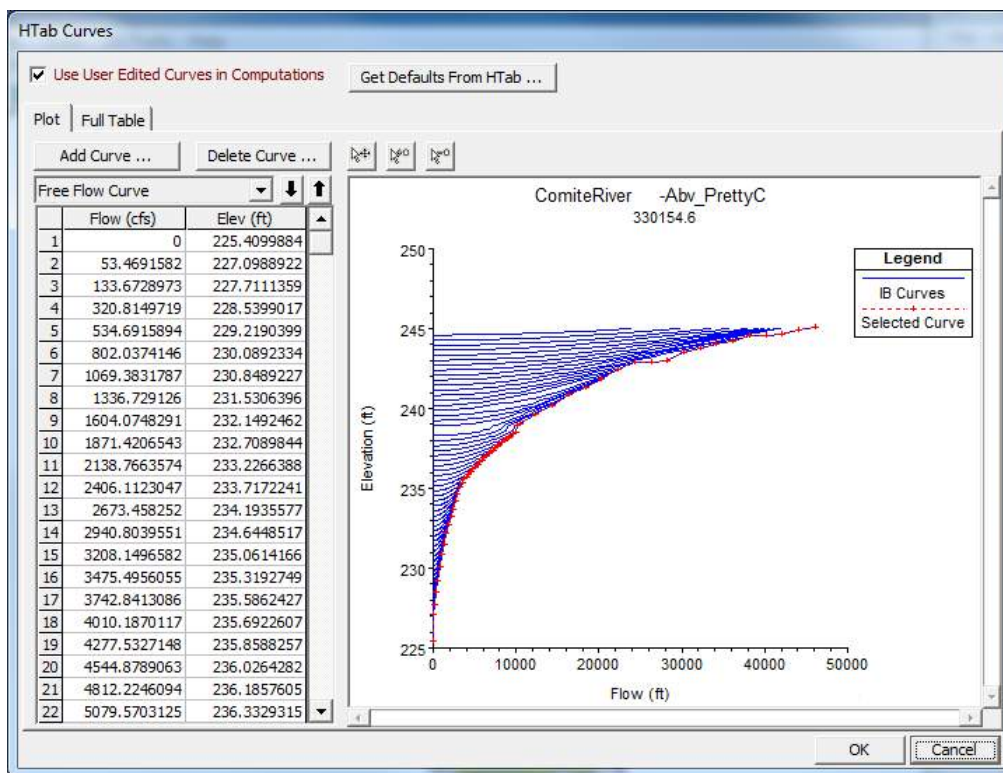
Highway 16, Amite River, Blw_ComiteR, Sta: 129323.7



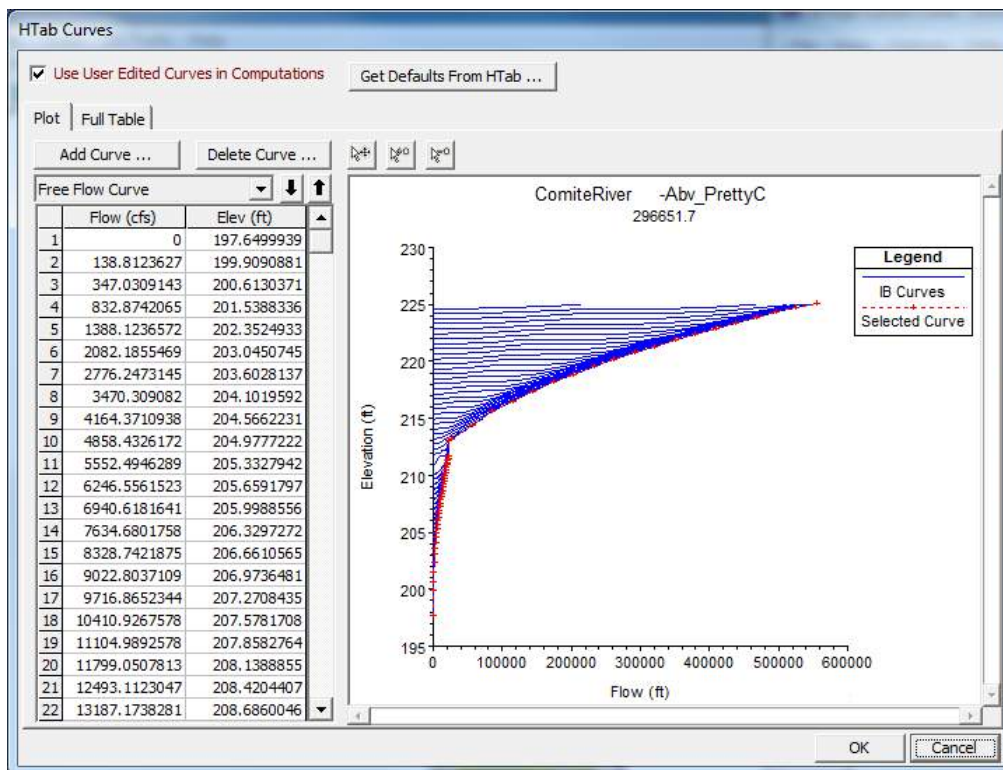
Highway 22, Amite River, Blw_ComiteR, Sta: 30883.8



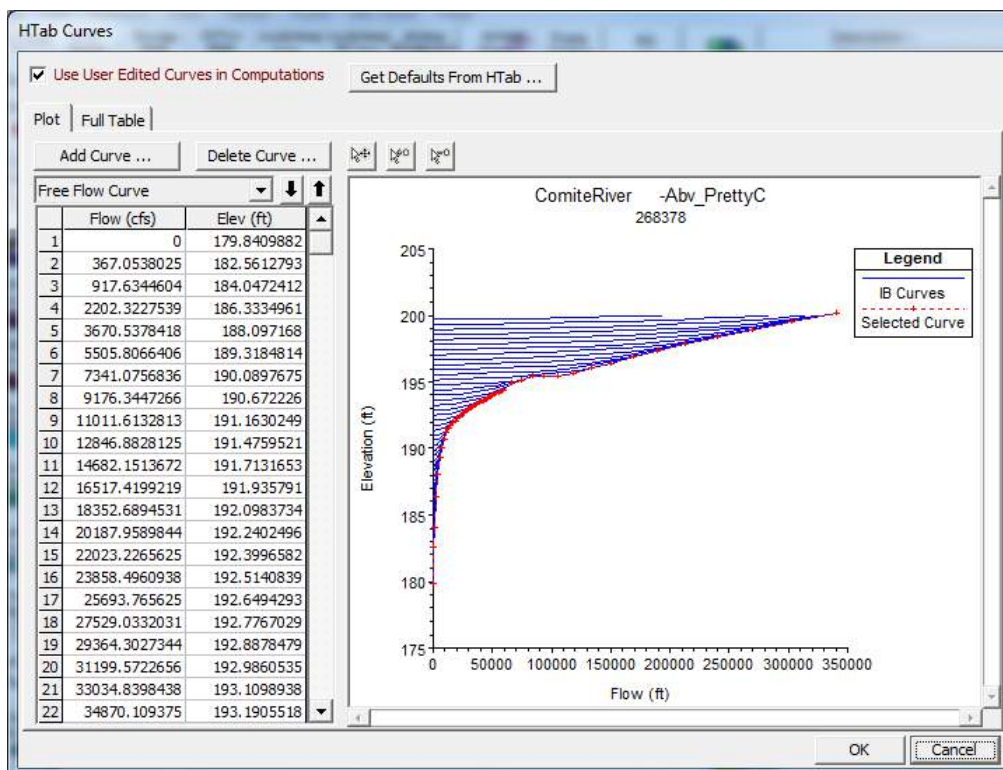
Highway 22, AmiteRvrDivCanal, Abv_BlindR, Sta: 66193.1



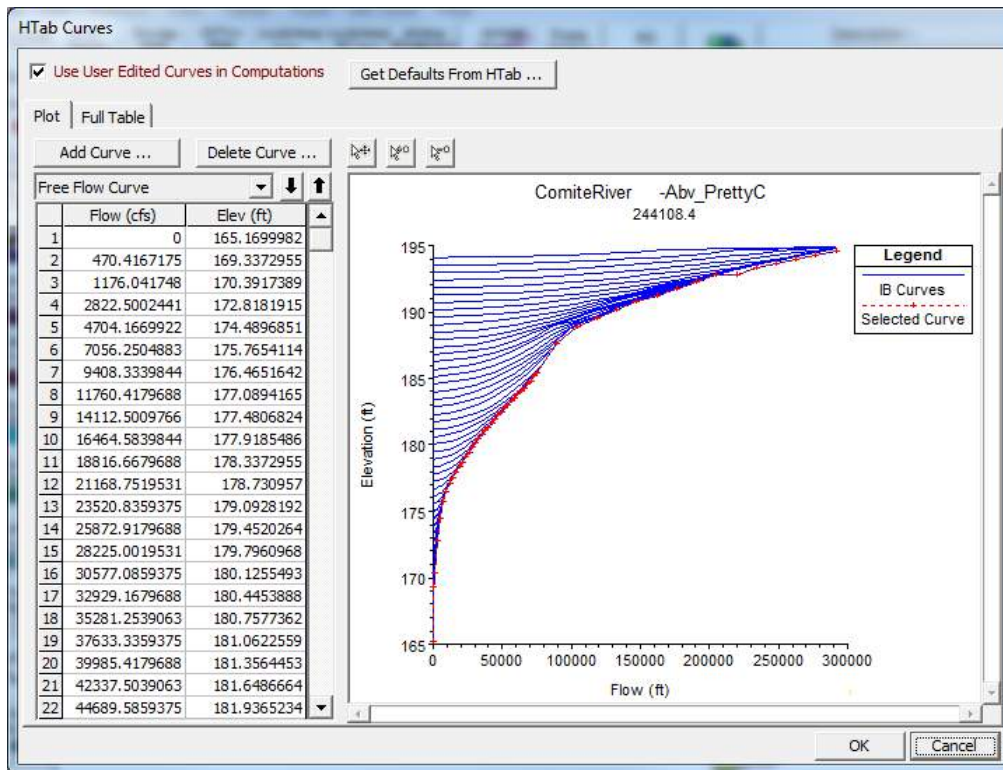
Highway 422 Azalea Street, Comite River, Abv_PrettyC, Sta: 330154.6



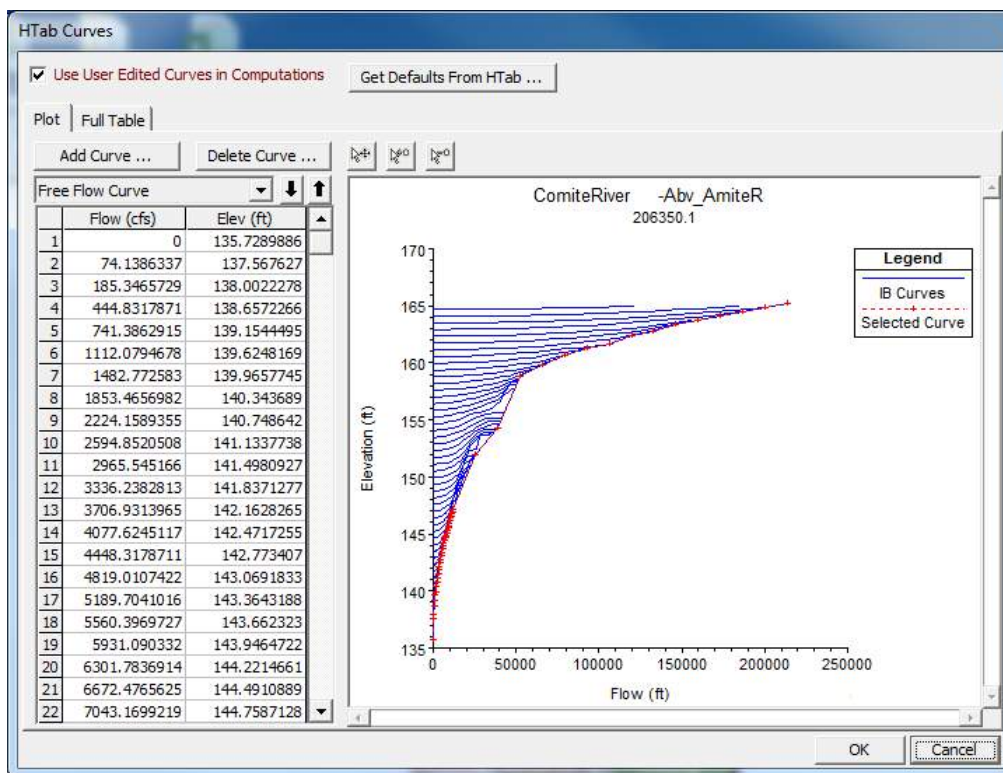
Carruth Road, Comite River, Abv_PrettyC, Sta: 296651.7



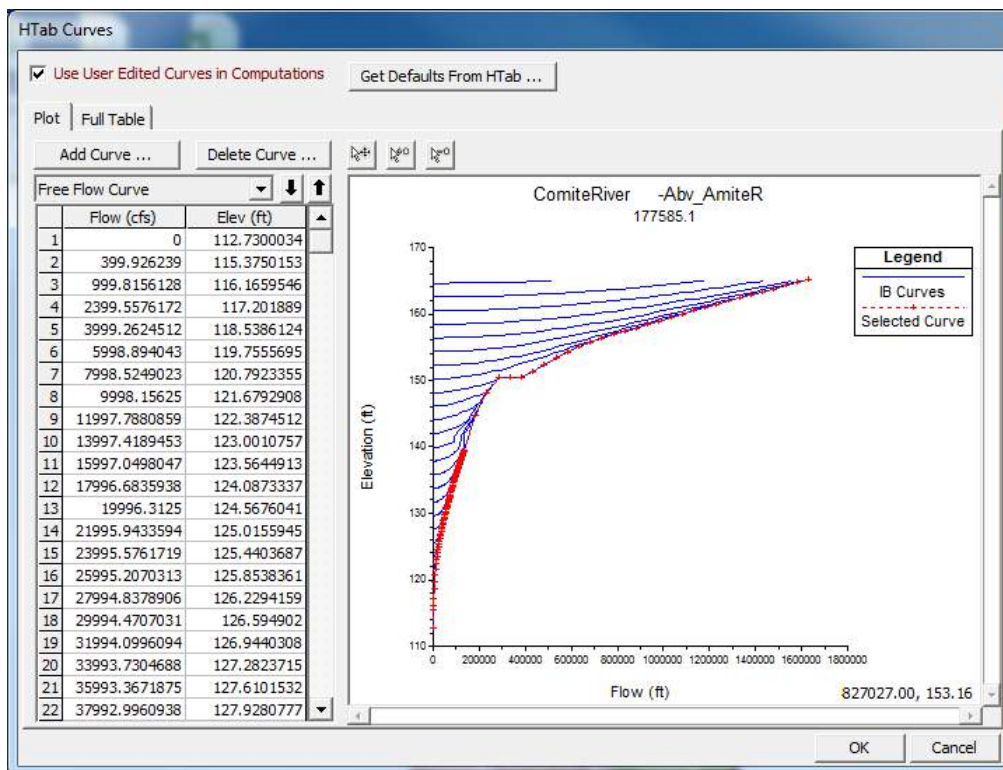
Wilson-Clinton Road, Comite River, Abv_PrettyC, Sta: 268378



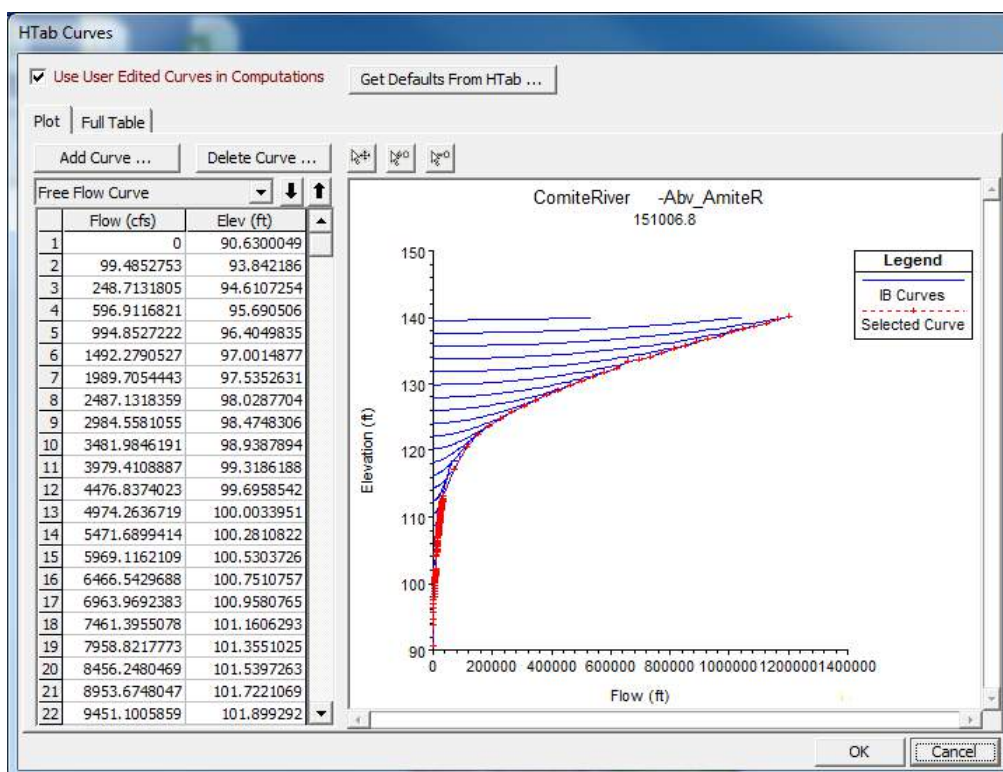
Highway 10, Comite River, Abv_PrettyC, Sta: 244108.4



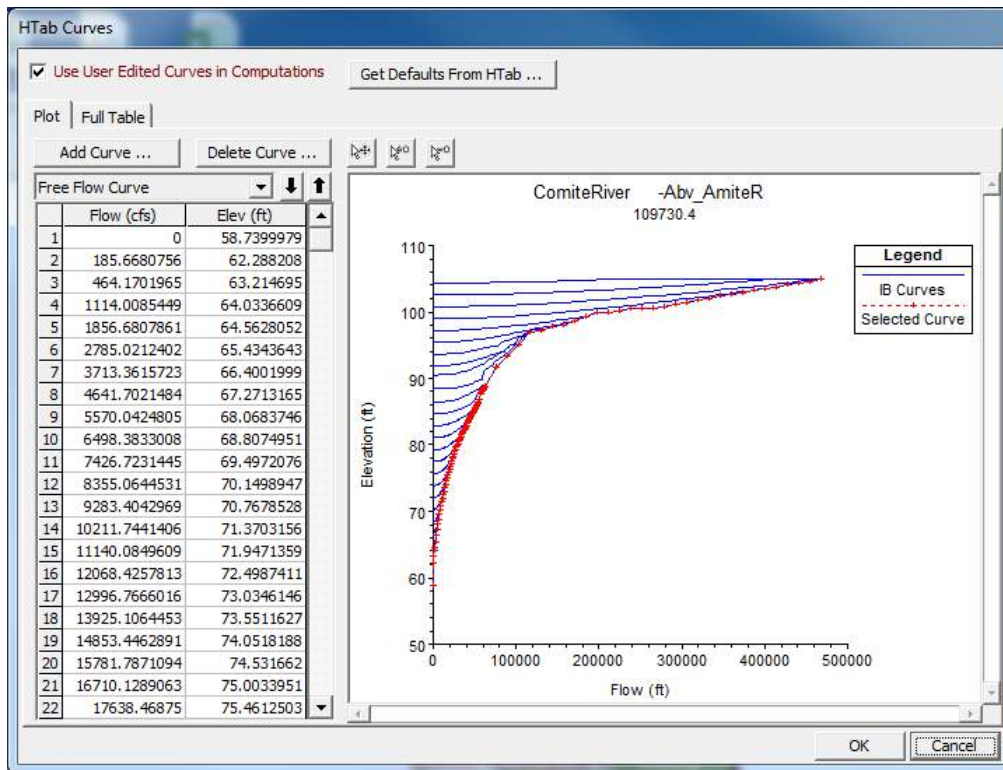
Overton Ford Road, Comite River, Abv_AmiteR, Sta: 206350.1



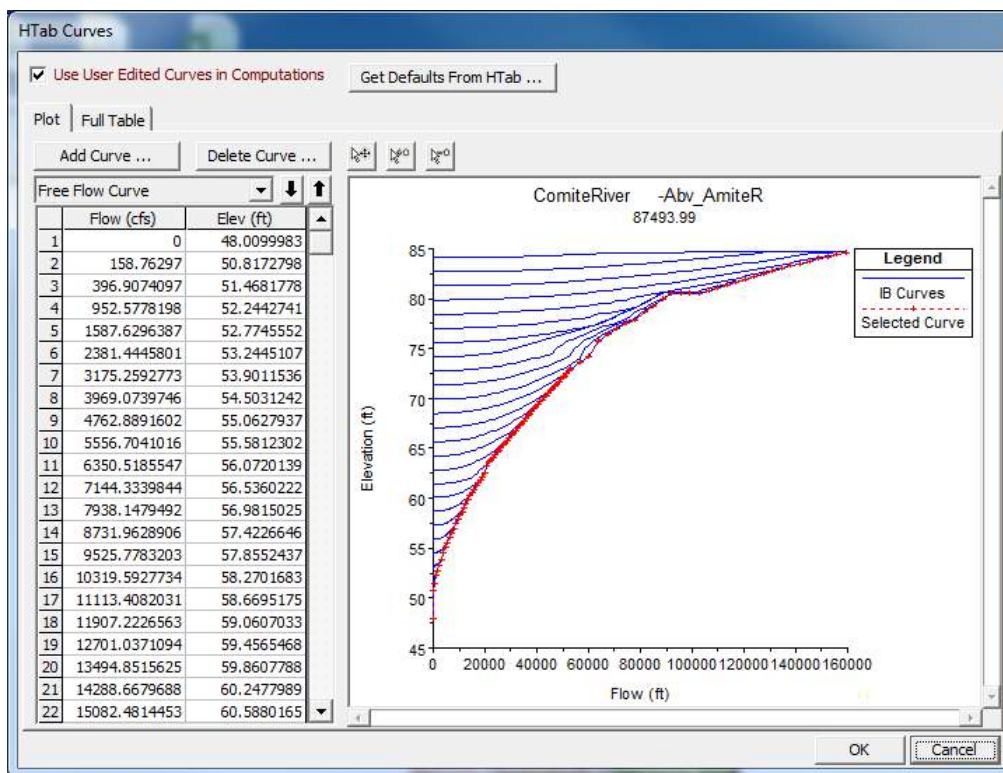
Highway 67, Comite River, Abv_AmiteR, Sta: 177585.1



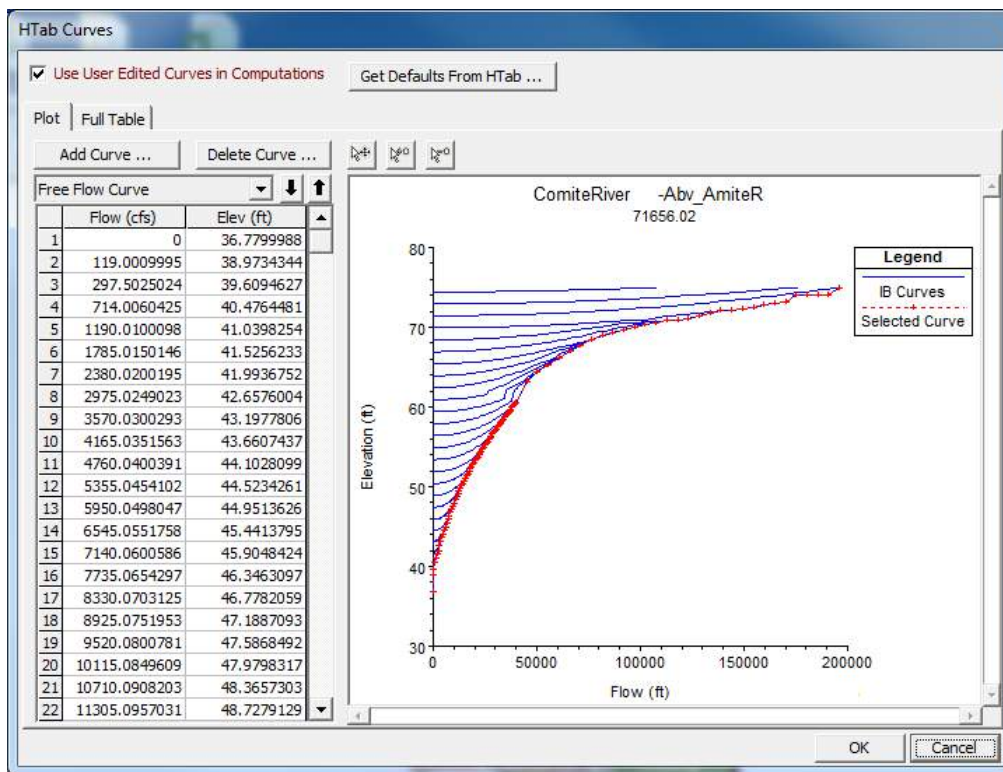
Port Hudson Pride Road, Comite River, Abv_AmiteR, Sta: 151006.8



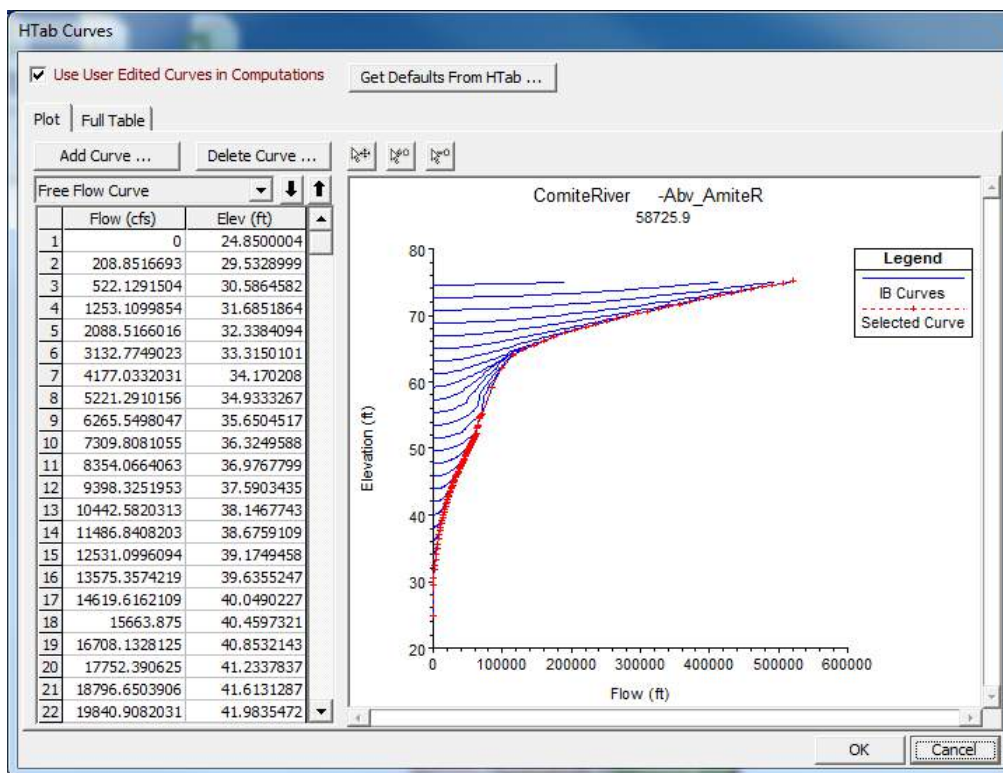
Zachary Deerford Road, Comite River, Abv_AmiteR, Sta: 109730.4



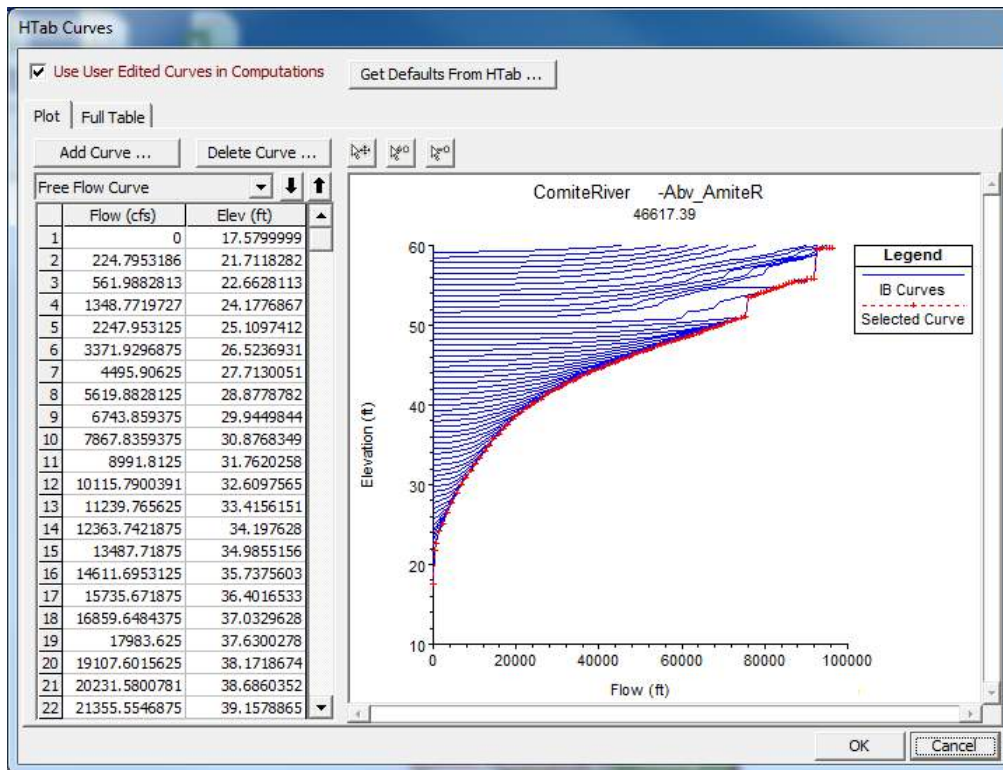
Dyer Road, Comite River, Abv_AmiteR, Sta: 87493.99



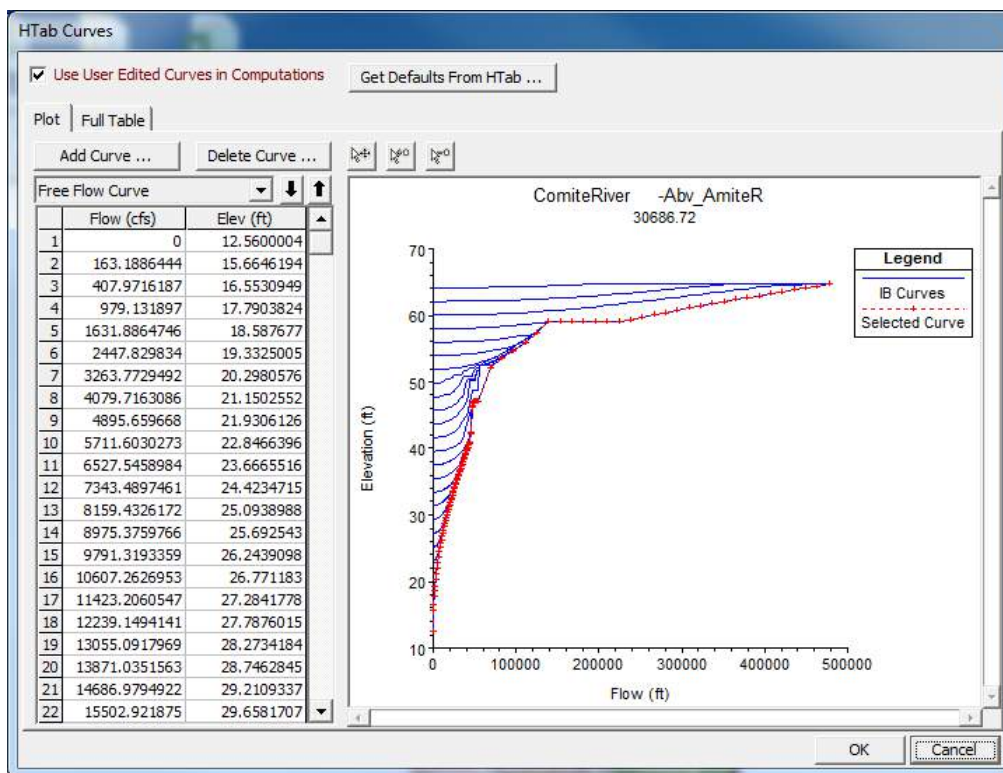
Comite Drive, Comite River, Abv_AmiteR, Sta: 71656.02



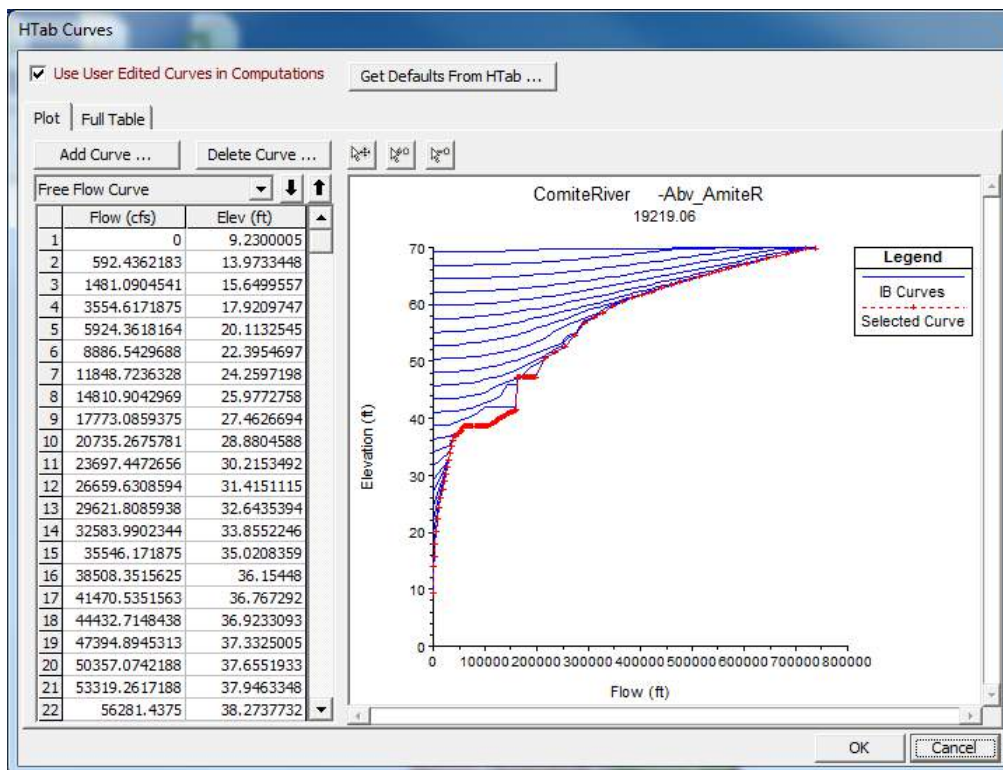
Highway 408 Hooper Street, Comite River, Abv_AmiteR, Sta: 58725.9



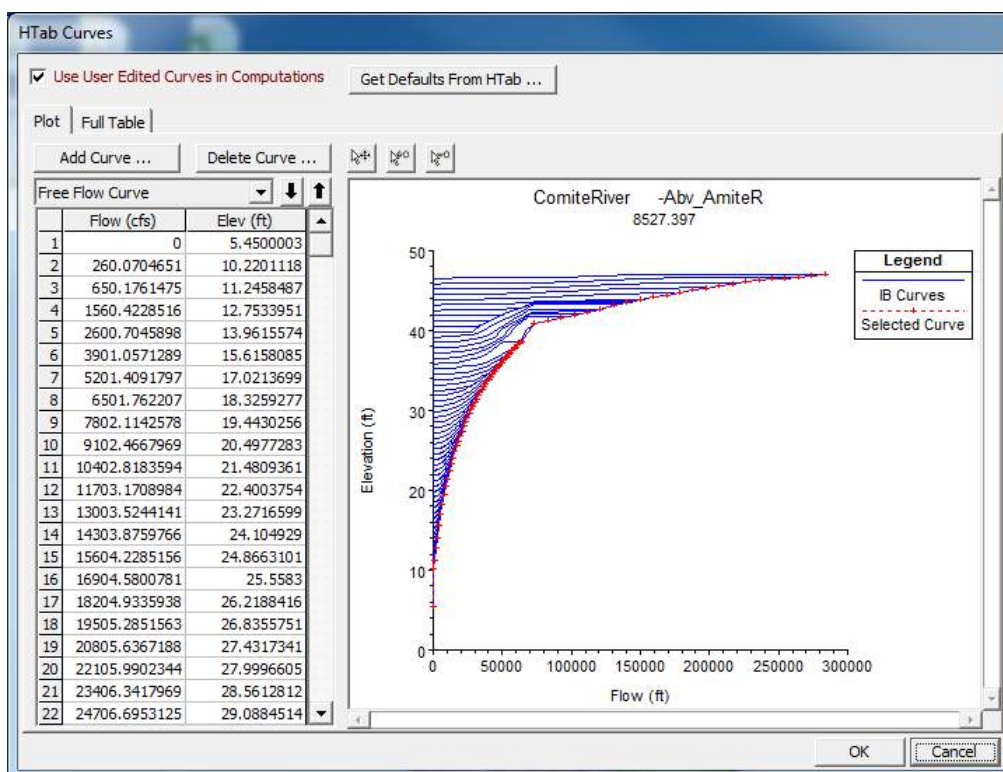
Highway 946 Joor Road, Comite River, Abv_AmiteR, Sta: 46617.39



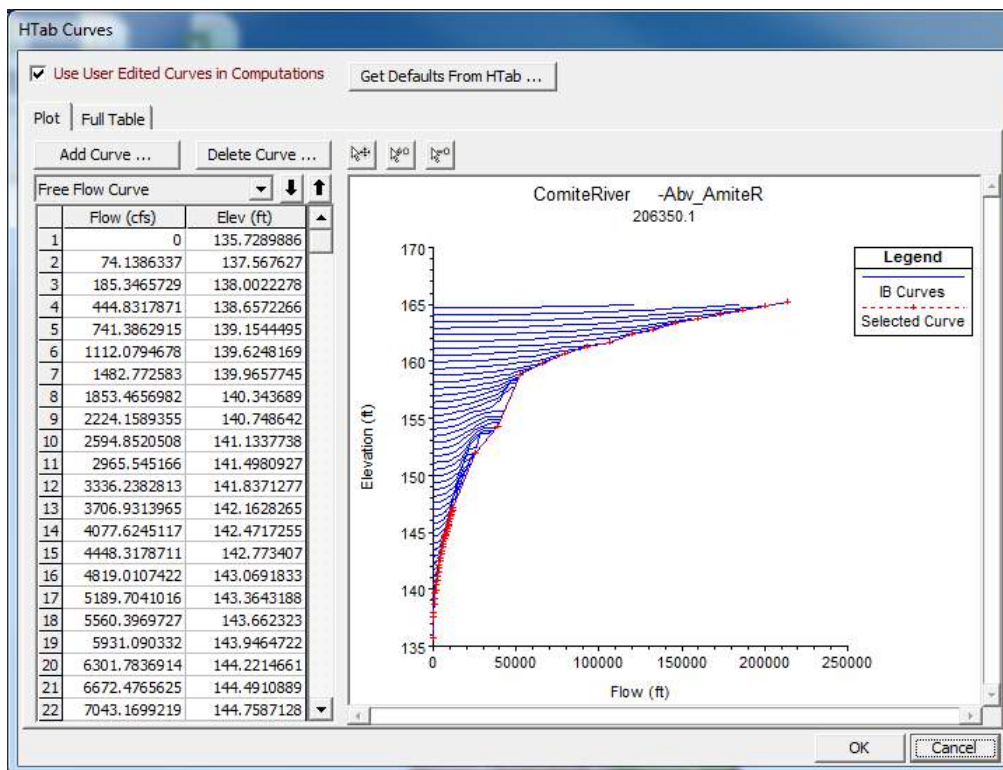
Highway 37 Greenwell Springs Road, Comite River, Abv_AmiteR, Sta: 30686.72



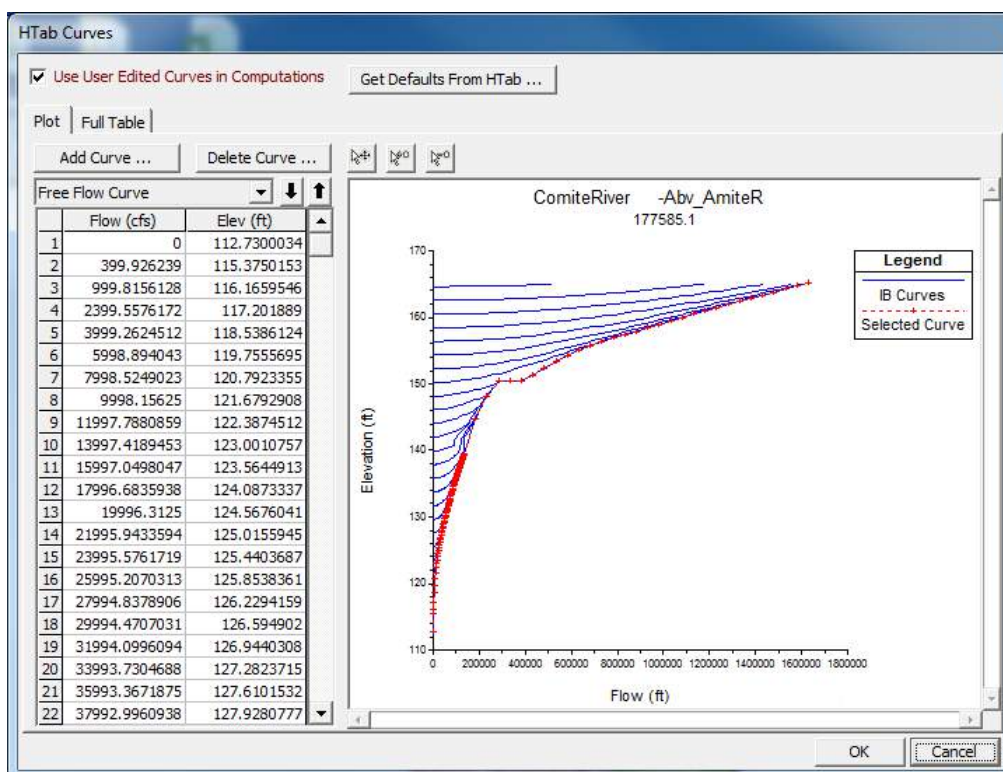
Central Throughway, Comite River, Abv_AmiteR, Sta: 19219.06



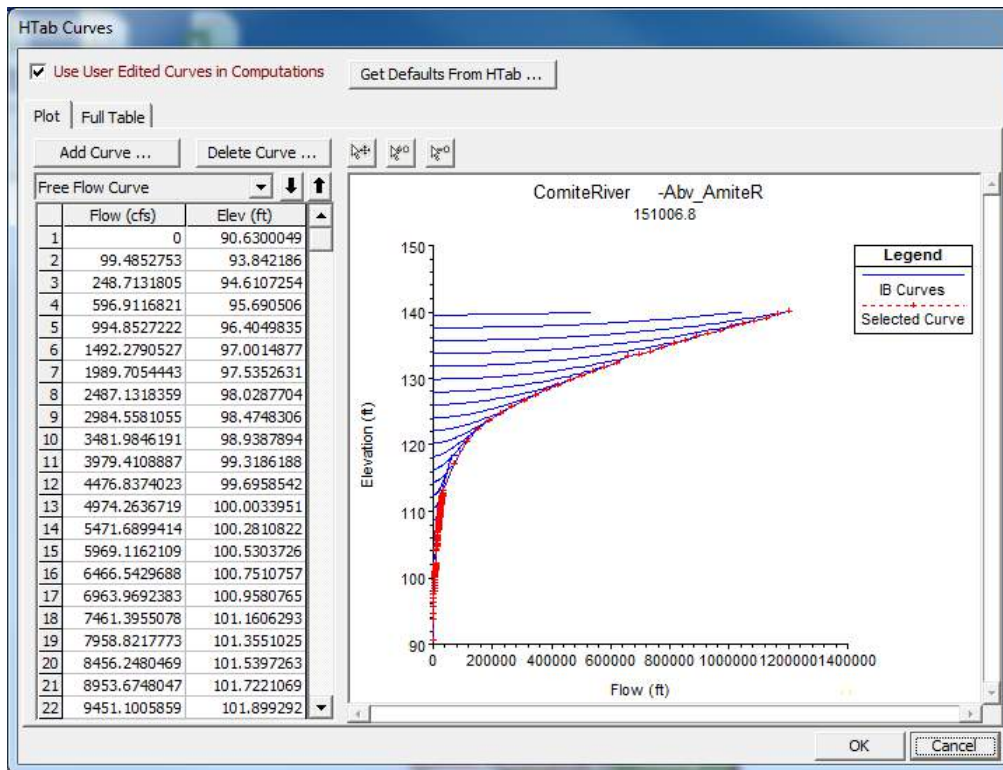
Railroad, Comite River, Abv_AmiteR, Sta: 8527.397



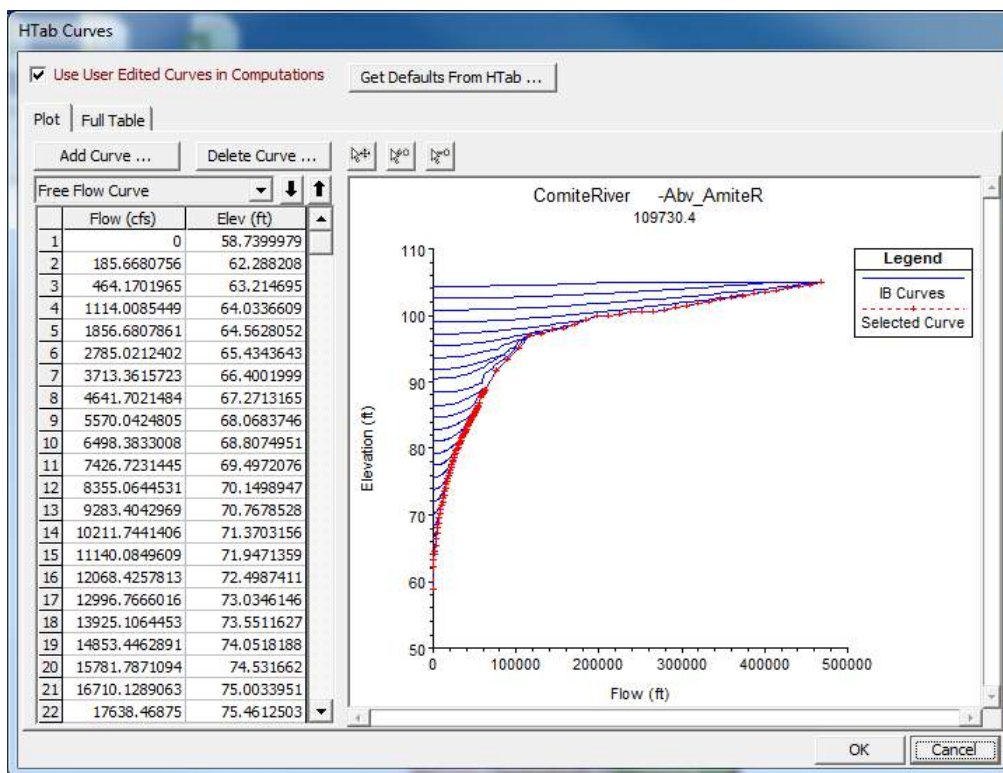
Overton Ford Road, Comite River, Abv_AmiteR, Sta: 206350.1



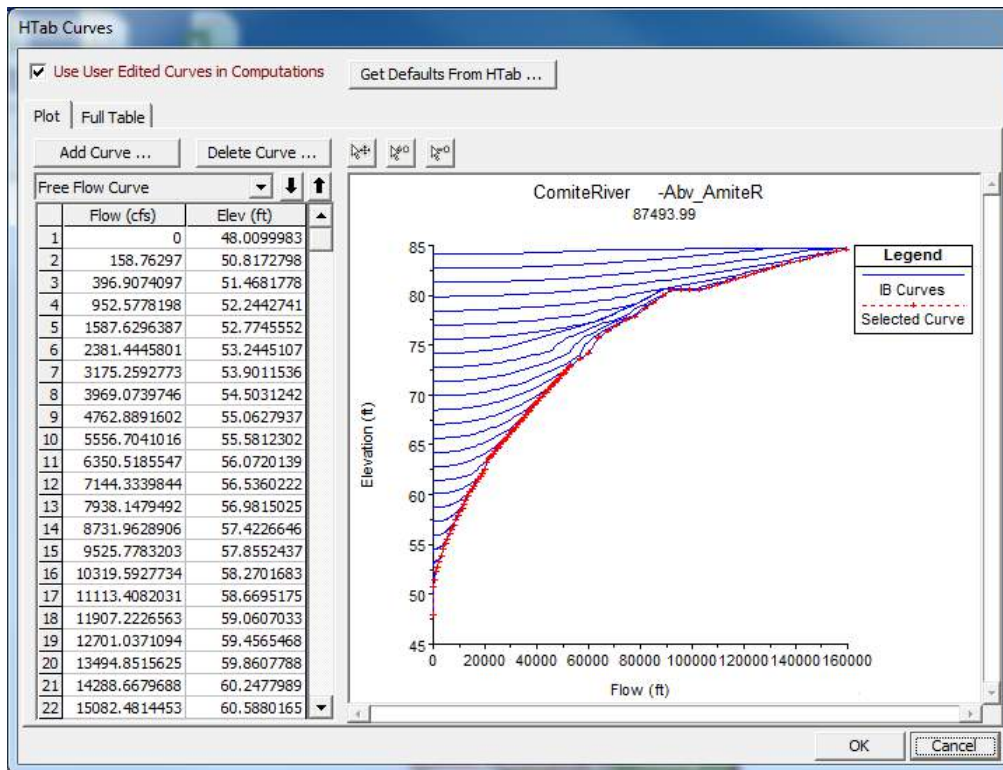
Highway 67, Comite River, Abv_AmiteR, Sta: 177585.1



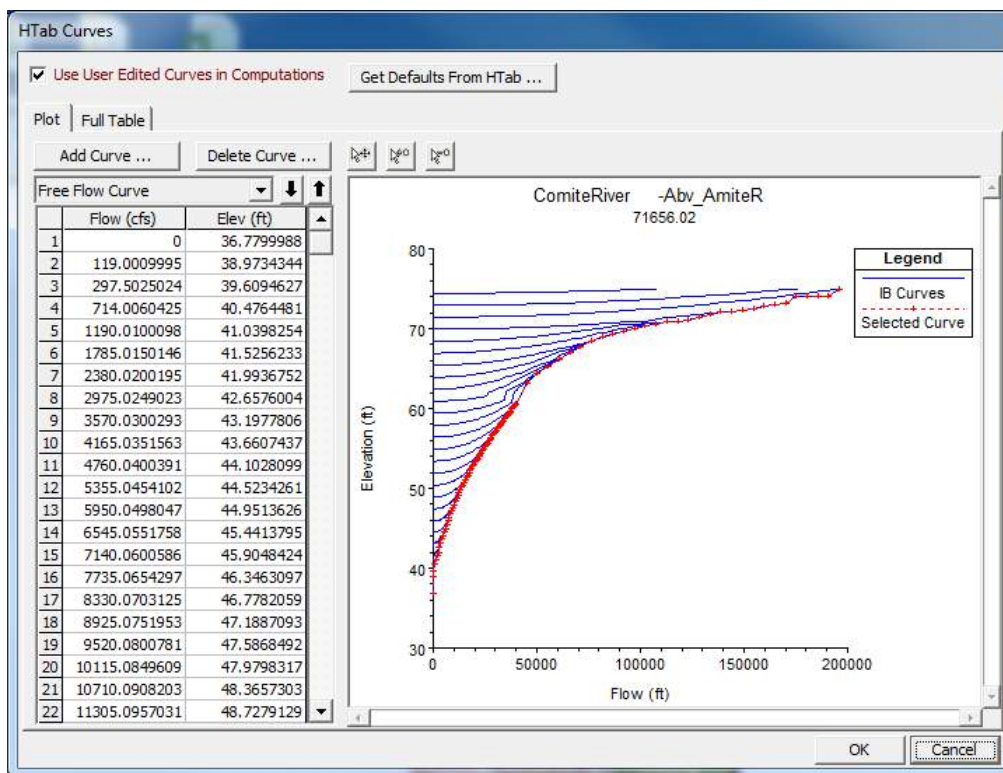
Port Hudson Pride Road, Comite River, Abv_AmiteR, Sta: 151006.8



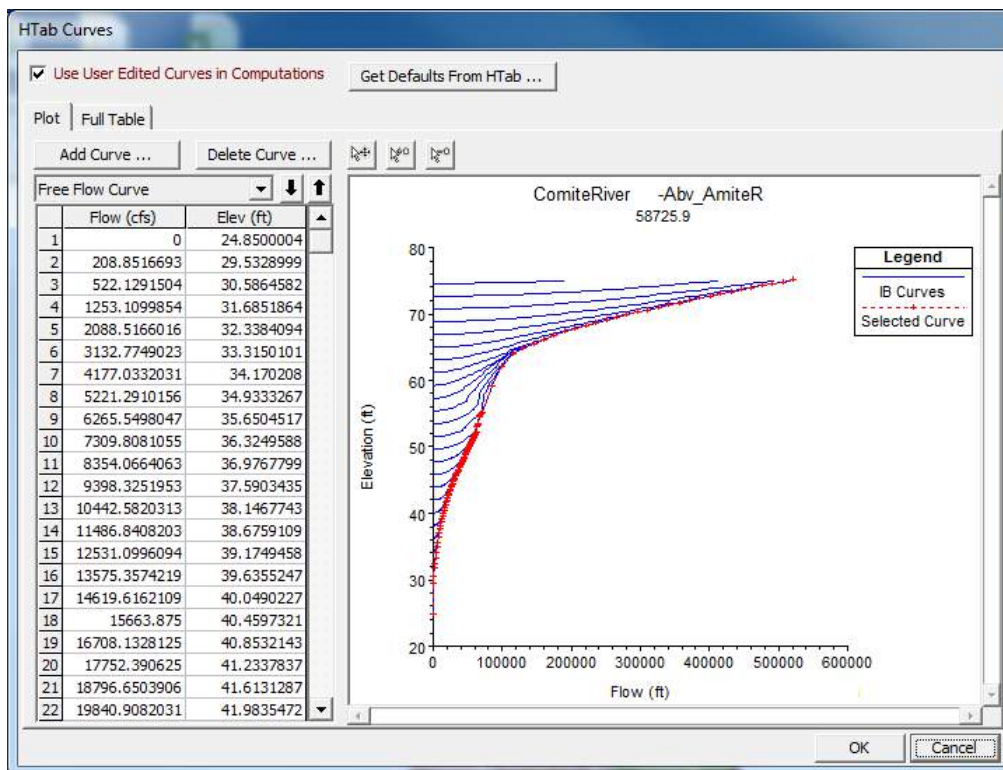
Zachary Deerford Road, Comite River, Abv_AmiteR, Sta: 109730.4



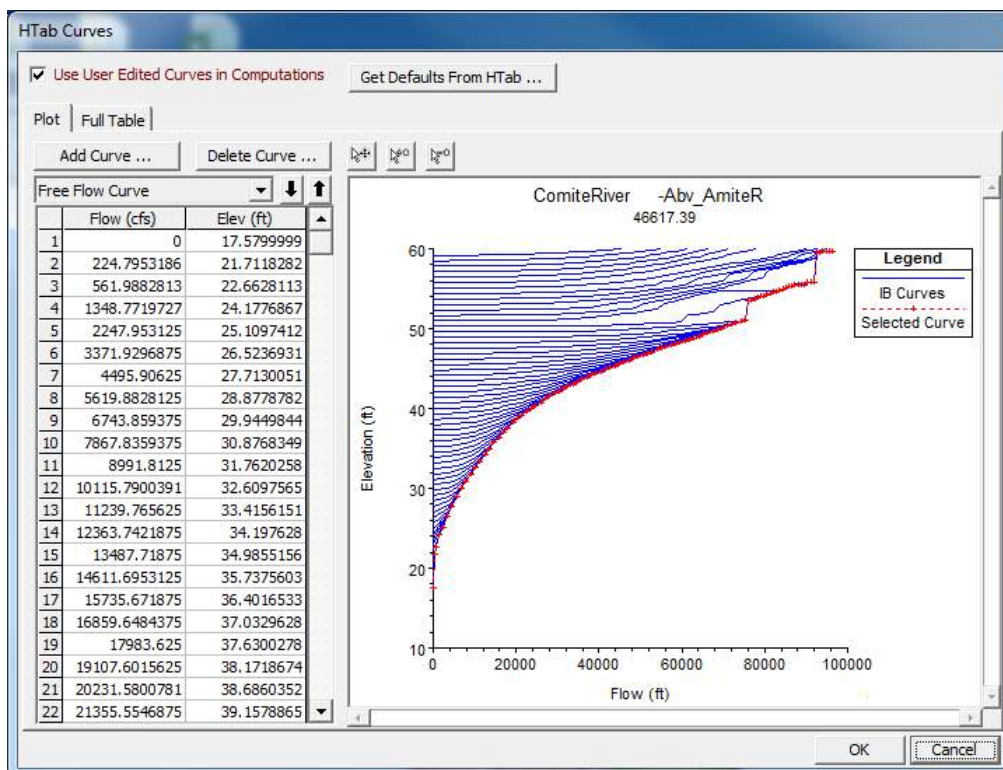
Dyer Road, Comite River, Abv_AmiteR, Sta: 87493.99



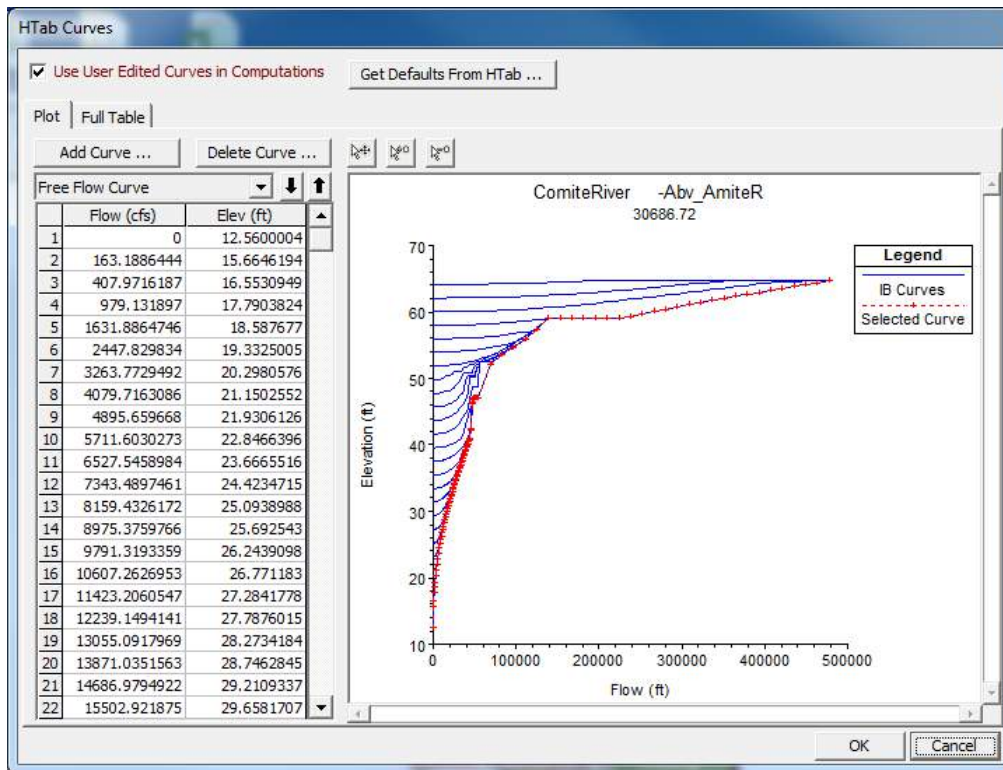
Comite Drive, Comite River, Abv_AmiteR, Sta: 71656.02



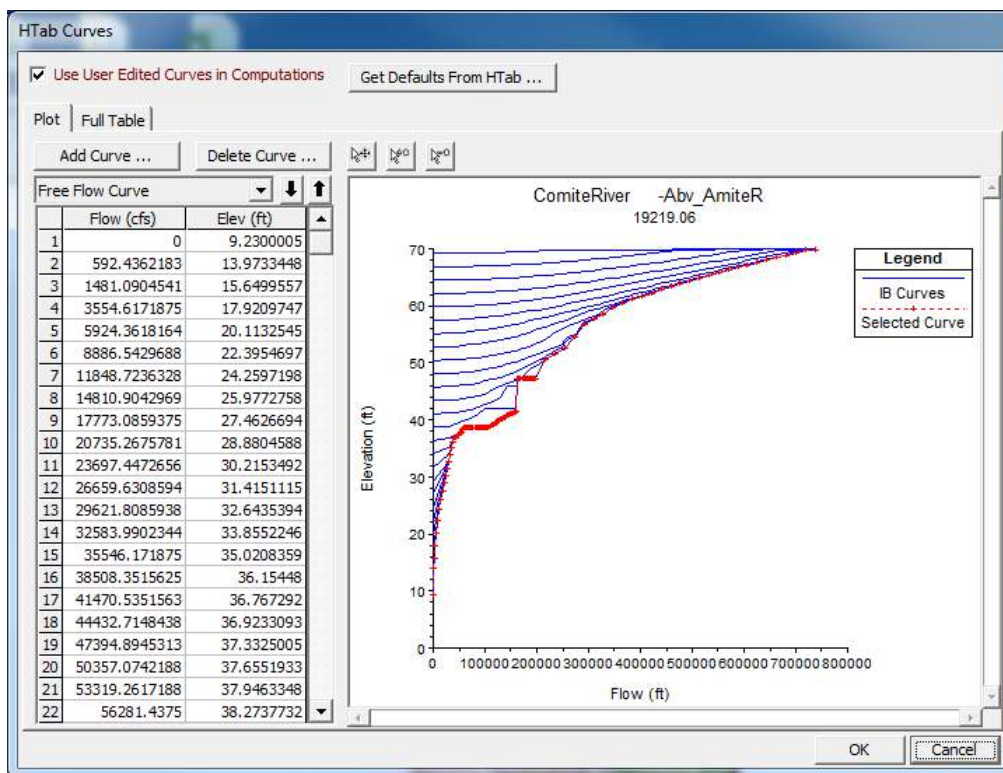
Highway 408 Hooper Street, Comite River, Abv_AmiteR, Sta: 58725.9



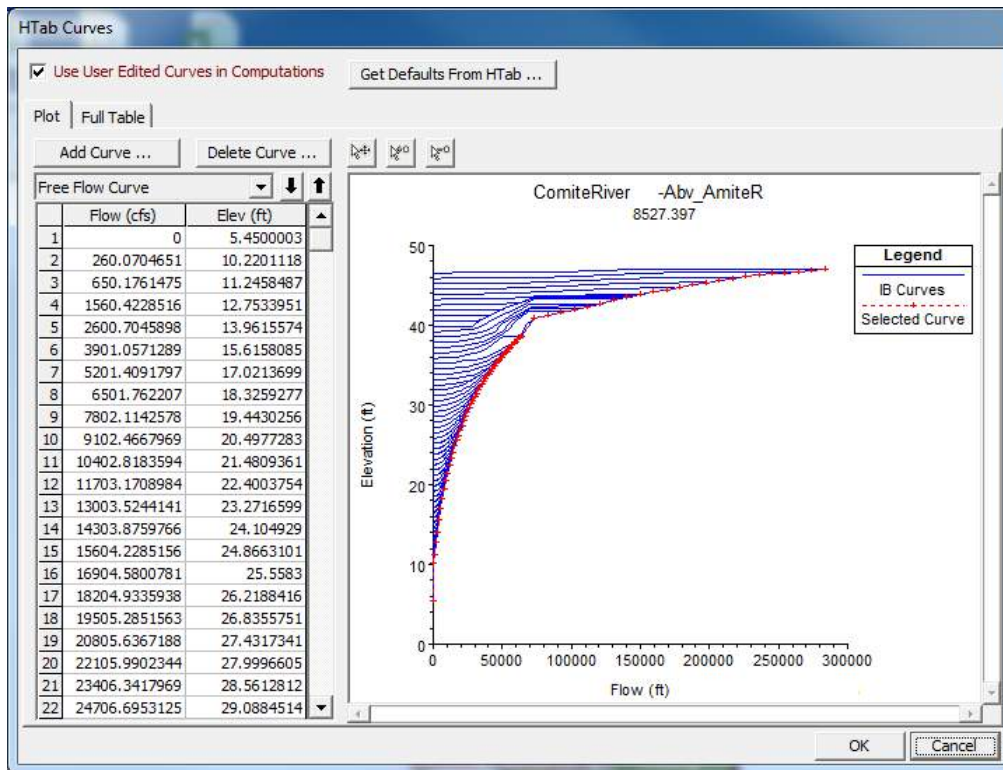
Highway 946 Joor Road, Comite River, Abv_AmiteR, Sta: 46617.39



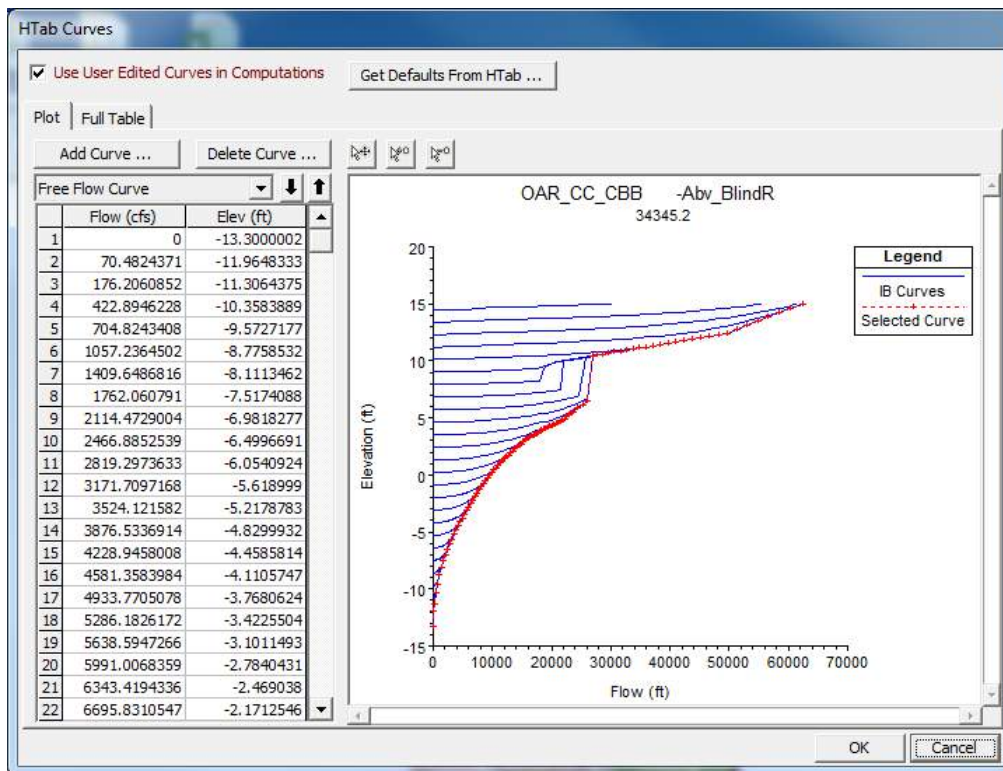
Highway 37 Greenwell Springs Road, Comite River, Abv_AmiteR, Sta: 30686.72



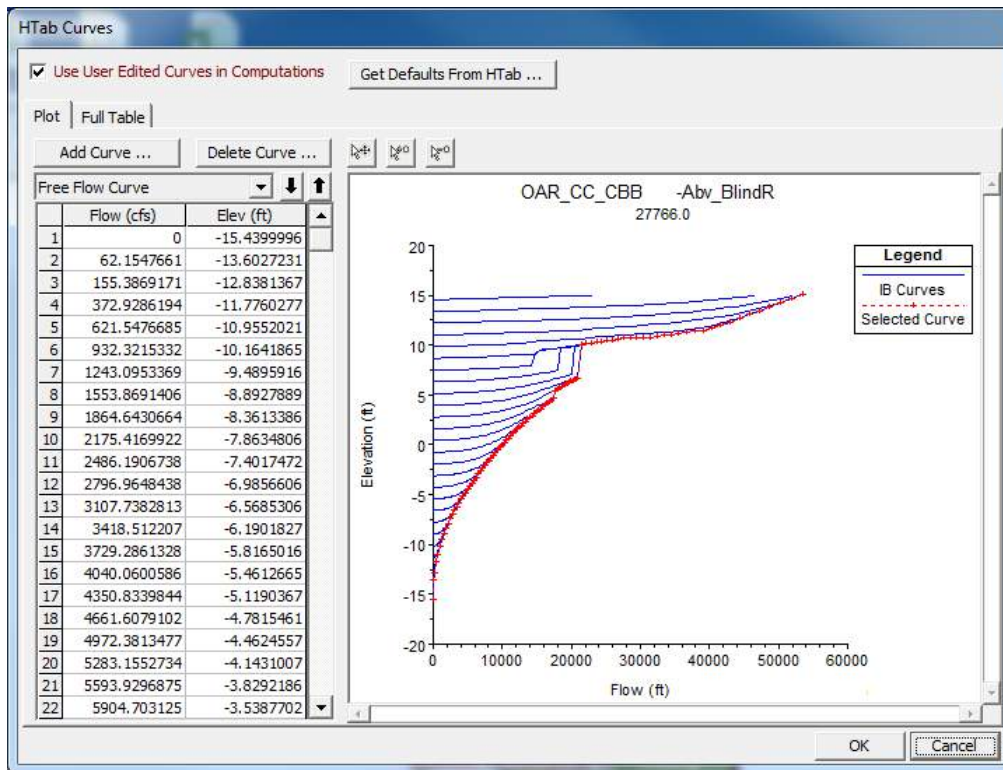
Central Throughway, Comite River, Abv_AmiteR, Sta: 19219.06



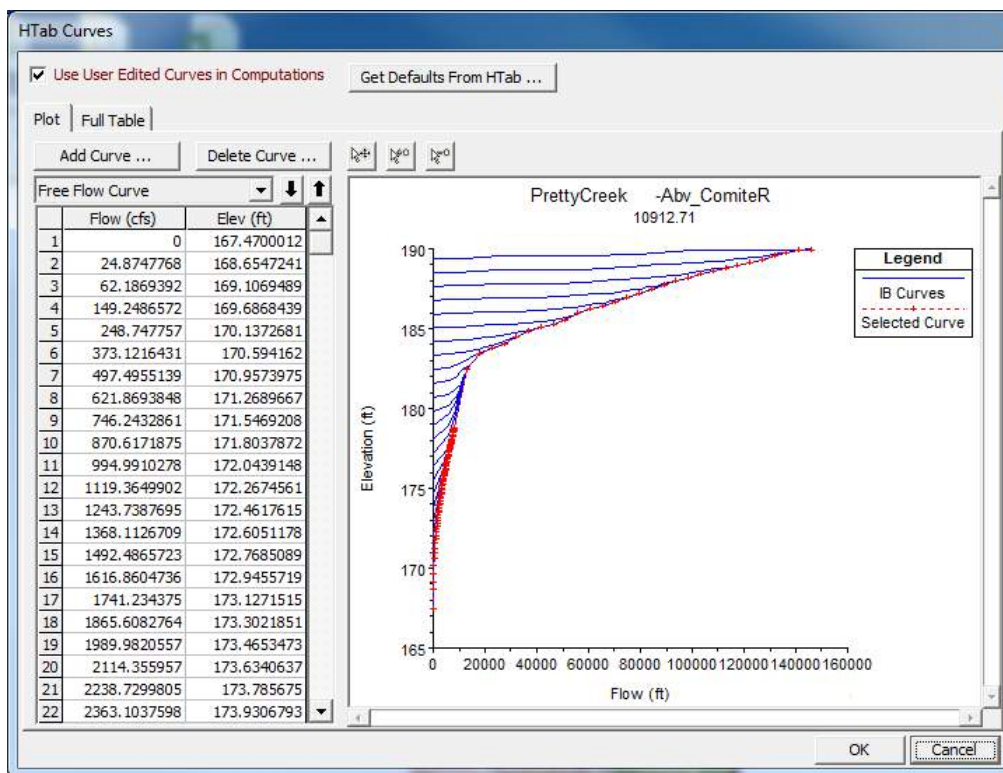
Railroad, Comite River, Abv_AmiteR, Sta: 8527.397



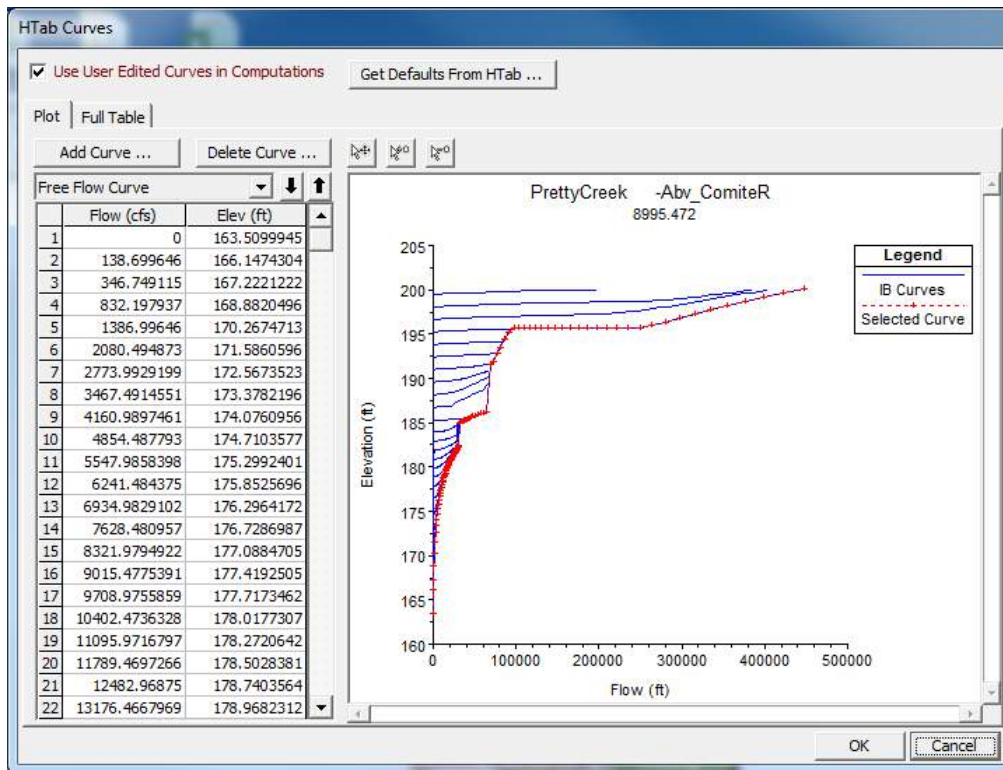
Bridge, OAR_CC_CBB, Abv_BlindR, Sta: 34345.2



Highway 22, OAR_CC_CBB, Abv_BlindR, Sta: 27766.0



Woodville Street, Pretty Creek, Abv_ComiteR, Sta: 10912.71



Highway 10, Pretty Creek, Abv_ComiteR, Sta: 8995.472

APPENDIX 3: HEC-SSP STATISTICAL ANALYSIS REPORTS

HEC-SSP Statistical Analysis Reports

USGS 07376679 East Amite R near Peoria, MS

Regional Skew: 0.037

Regional Skew MSE: 0.3025

Plotting Position Type: Hirsch-Stedinger

Upper Confidence Level: 0.1

Lower Confidence Level: 0.9

Use non-standard frequencies

Frequency: 0.2

Frequency: 0.5

Frequency: 1.0

Frequency: 2.0

Frequency: 4.0

Frequency: 10.0

Frequency: 20.0

Frequency: 50.0

Frequency: 80.0

Frequency: 90.0

Frequency: 95.0

Frequency: 99.0

Display ordinate values using 1 digits in fraction part of value

--- End of Input Data ---

<< EMA Representation of Data >>

EAST FORK AMITE RIVER-PEORIA, MS-FLOW-ANNUAL PEAK

		Value			Threshold		
Year	Peak	Low	High		Low	High	
Type							

---	-----				-----		
1990	34,000.0	34,000.0	34,000.0	4,700.0	1.0E99	Hist	
1991	---	1.0E-99	34,000.0	34,000.0	1.0E99	Cens	
1992	---	1.0E-99	34,000.0	34,000.0	1.0E99	Cens	
1993	---	1.0E-99	34,000.0	34,000.0	1.0E99	Cens	
1994	---	1.0E-99	34,000.0	34,000.0	1.0E99	Cens	
1995	---	1.0E-99	34,000.0	34,000.0	1.0E99	Cens	
1996	---	1.0E-99	34,000.0	34,000.0	1.0E99	Cens	
1997	---	1.0E-99	34,000.0	34,000.0	1.0E99	Cens	
1998	16,000.0	16,000.0	16,000.0	4,700.0	1.0E99	Syst	
1999	9,500.0	9,500.0	9,500.0	4,700.0	1.0E99	Syst	
2000	1,500.0	1.0E-6	4,700.0	4,700.0	1.0E99	Syst	
2001	8,580.0	8,580.0	8,580.0	4,700.0	1.0E99	Syst	
2002	15,700.0	15,700.0	15,700.0	4,700.0	1.0E99	Syst	
2003	23,300.0	23,300.0	23,300.0	4,700.0	1.0E99	Syst	

2004	13,400.0	13,400.0	13,400.0	4,700.0	1.0E99	Syst
2005	15,600.0	15,600.0	15,600.0	4,700.0	1.0E99	Syst
2006	1,450.0	1.0E-6	4,700.0	4,700.0	1.0E99	Syst
2007	9,360.0	9,360.0	9,360.0	4,700.0	1.0E99	Syst
2008	6,890.0	6,890.0	6,890.0	4,700.0	1.0E99	Syst
2009	13,300.0	13,300.0	13,300.0	4,700.0	1.0E99	Syst
2010	4,700.0	4,700.0	4,700.0	4,700.0	1.0E99	Syst
2011	9,010.0	9,010.0	9,010.0	4,700.0	1.0E99	Syst
2012	12,400.0	12,400.0	12,400.0	4,700.0	1.0E99	Syst
2013	12,200.0	12,200.0	12,200.0	4,700.0	1.0E99	Syst
2014	13,800.0	13,800.0	13,800.0	4,700.0	1.0E99	Syst
2015	5,450.0	5,450.0	5,450.0	4,700.0	1.0E99	Syst
2016	18,100.0	18,100.0	18,100.0	4,700.0	1.0E99	Syst
2017	5,800.0	5,800.0	5,800.0	4,700.0	1.0E99	Syst

 ---|-----|

Fitted log10 Moments			Mean	Variance
Std Dev	Skew			
EMA at-site data w/o regional info			4.007546	
0.068810	0.262317	-0.321387		
EMA w/ regional info and B17b MSE(G)			4.008400	
0.066101	0.257100	-0.116642		
EMA w/ regional info and specified MSE(G)			4.008400	
0.066101	0.257100	-0.116642		

EMA Estimate of MSE[G at-site]	0.205469
MSE[G at-site systematic]	0.274092
Effective Record Length [G at-site]	26.679629
Grubbs-Beck Critical Value	4,700.000000

--- Final Results ---

<< Plotting Positions >>

EAST FORK AMITE RIVER-PEORIA, MS-FLOW-ANNUAL PEAK

Events Analyzed				Ordered Events			
Day	Mon	Year	FLOW CFS	Rank	Water Year	FLOW CFS	H-S Plot Pos
25	Jan	1990	34,000.0	1	1990	34,000.0	1.79
01	Jan	1991	---	2	2003	23,300.0	8.14
01	Jan	1992	---	3	2016	18,100.0	12.71
01	Jan	1993	---	4	1998	16,000.0	17.27

01 Jan 1994	---	5	2002	15,700.0	21.84	
01 Jan 1995	---	6	2005	15,600.0	26.41	
01 Jan 1996	---	7	2014	13,800.0	30.98	
01 Jan 1997	---	8	2004	13,400.0	35.55	
07 Jan 1998	16,000.0	9	2009	13,300.0	40.11	
14 Mar 1999	9,500.0	10	2012	12,400.0	44.68	
03 Apr 2000	1,500.0	11	2013	12,200.0	49.25	
03 Mar 2001	8,580.0	12	1999	9,500.0	53.82	
26 Sep 2002	15,700.0	13	2007	9,360.0	58.38	
22 Feb 2003	23,300.0	14	2011	9,010.0	62.95	
05 Feb 2004	13,400.0	15	2001	8,580.0	67.52	
01 Apr 2005	15,600.0	16	2008	6,890.0	72.09	
16 Dec 2005	1,450.0	17	2017	5,800.0	76.65	
28 Oct 2006	9,360.0	18	2015	5,450.0	81.22	
03 Sep 2008	6,890.0	19	2010	4,700.0*	85.79	
28 Mar 2009	13,300.0	20	2000	1,500.0*	92.06	
19 Dec 2009	4,700.0	21	2006	1,450.0*	96.73	
09 Mar 2011	9,010.0	22	1997	---	---	
31 Aug 2012	12,400.0	23	1996	---	---	
12 Feb 2013	12,200.0	24	1995	---	---	
21 Feb 2014	13,800.0	25	1994	---	---	
10 Mar 2015	5,450.0	26	1993	---	---	
11 Mar 2016	18,100.0	27	1992	---	---	
04 Apr 2017	5,800.0	28	1991	---	---	
----- -----						

* Outlier

* Low outlier plotting positions are computed using Median parameters.

<< Frequency Curve >>

EAST FORK AMITE RIVER-PEORIA, MS-FLOW-ANNUAL PEAK

Computed	Variance	Percent	Confidence Limits
Curve	Log (EMA)	Chance	0.10 0.90
FLOW, CFS		Exceedance	FLOW, CFS
----- -----			
51,531.9	0.01985	0.200	90,681.0 36,831.0
43,900.6	0.01469	0.500	70,568.1 32,681.4
38,403.5	0.01147	1.000	57,870.9 29,427.8
33,128.5	0.00882	2.000	46,989.1 26,069.5
28,055.4	0.00672	4.000	37,646.2 22,602.4
21,602.8	0.00472	10.000	27,230.0 17,846.9
16,831.0	0.00375	20.000	20,476.1 14,095.7
10,313.3	0.00335	50.000	12,262.8 8,600.5
6,217.3	0.00511	80.000	7,452.6 4,627.7
4,741.0	0.00780	90.000	5,799.1 3,116.1
3,777.1	0.01165	95.000	4,767.0 2,191.1
2,445.3	0.02511	99.000	3,399.8 1,078.4
----- -----			

<< Systematic Statistics >>
 EAST FORK AMITE RIVER-PEORIA, MS-FLOW-ANNUAL PEAK

Log Transform: FLOW, CFS		Number of Events	
Mean	4.008	Historic Events	1
Standard Dev	0.257	High Outliers	0
Station Skew	-0.321	Low Outliers	2
Regional Skew	0.037	Zero Events	0
Weighted Skew	-0.117	Missing Events	7
Adopted Skew	-0.117	Systematic Events	20
		Historic Period	28

--- End of Analytical Frequency Curve ---

USGS 07377000 Amite River near Darlington, LA

Regional Skew: 0.038
 Regional Skew MSE: 0.302

Plotting Position Type: Hirsch-Stedinger

Upper Confidence Level: 0.1
 Lower Confidence Level: 0.9

Use non-standard frequencies

Frequency: 0.2
 Frequency: 0.5
 Frequency: 1.0
 Frequency: 2.0
 Frequency: 4.0
 Frequency: 10.0
 Frequency: 20.0
 Frequency: 50.0
 Frequency: 80.0
 Frequency: 90.0
 Frequency: 95.0
 Frequency: 99.0

Display ordinate values using 1 digits in fraction part of value

--- End of Input Data ---

<< EMA Representation of Data >>
 AmDarling2019-Darlington, LA-FLOW-ANNUAL PEAK

		Value				Threshold	
Year	Peak	Low	High	Low	High		
Type							
----- ----- ----- ----- ----- ----- ----- -----							
---	-----						
1949	20,000.0		20,000.0	20,000.0		12,300.0	1.0E99 Syst
1950	43,400.0		43,400.0	43,400.0		12,300.0	1.0E99 Syst
1951	31,600.0		31,600.0	31,600.0		12,300.0	1.0E99 Syst
1952	3,180.0		1.0E-6	12,300.0		12,300.0	1.0E99 Syst
1953	18,900.0		18,900.0	18,900.0		12,300.0	1.0E99 Syst
1954	3,280.0		1.0E-6	12,300.0		12,300.0	1.0E99 Syst
1955	55,700.0		55,700.0	55,700.0		12,300.0	1.0E99 Syst
1956	20,400.0		20,400.0	20,400.0		12,300.0	1.0E99 Syst
1957	20,200.0		20,200.0	20,200.0		12,300.0	1.0E99 Syst
1958	22,400.0		22,400.0	22,400.0		12,300.0	1.0E99 Syst
1959	6,900.0		1.0E-6	12,300.0		12,300.0	1.0E99 Syst
1960	9,800.0		1.0E-6	12,300.0		12,300.0	1.0E99 Syst
1961	37,900.0		37,900.0	37,900.0		12,300.0	1.0E99 Syst
1962	15,400.0		15,400.0	15,400.0		12,300.0	1.0E99 Syst
1963	4,530.0		1.0E-6	12,300.0		12,300.0	1.0E99 Syst
1964	44,500.0		44,500.0	44,500.0		12,300.0	1.0E99 Syst
1965	44,500.0		44,500.0	44,500.0		12,300.0	1.0E99 Syst
1966	20,000.0		20,000.0	20,000.0		12,300.0	1.0E99 Syst
1967	39,300.0		39,300.0	39,300.0		12,300.0	1.0E99 Syst
1968	8,000.0		1.0E-6	12,300.0		12,300.0	1.0E99 Syst
1969	8,600.0		1.0E-6	12,300.0		12,300.0	1.0E99 Syst
1970	3,630.0		1.0E-6	12,300.0		12,300.0	1.0E99 Syst
1971	10,100.0		1.0E-6	12,300.0		12,300.0	1.0E99 Syst
1972	45,500.0		45,500.0	45,500.0		12,300.0	1.0E99 Syst
1973	62,100.0		62,100.0	62,100.0		12,300.0	1.0E99 Syst
1974	22,400.0		22,400.0	22,400.0		12,300.0	1.0E99 Syst
1975	40,700.0		40,700.0	40,700.0		12,300.0	1.0E99 Syst
1976	7,660.0		1.0E-6	12,300.0		12,300.0	1.0E99 Syst
1977	76,400.0		76,400.0	76,400.0		12,300.0	1.0E99 Syst
1978	30,500.0		30,500.0	30,500.0		12,300.0	1.0E99 Syst
1979	43,400.0		43,400.0	43,400.0		12,300.0	1.0E99 Syst
1980	47,500.0		47,500.0	47,500.0		12,300.0	1.0E99 Syst
1981	8,320.0		1.0E-6	12,300.0		12,300.0	1.0E99 Syst
1982	18,100.0		18,100.0	18,100.0		12,300.0	1.0E99 Syst
1983	63,300.0		63,300.0	63,300.0		12,300.0	1.0E99 Syst
1984	13,000.0		13,000.0	13,000.0		12,300.0	1.0E99 Syst
1985	8,970.0		1.0E-6	12,300.0		12,300.0	1.0E99 Syst
1986	17,500.0		17,500.0	17,500.0		12,300.0	1.0E99 Syst
1987	21,200.0		21,200.0	21,200.0		12,300.0	1.0E99 Syst
1988	22,000.0		22,000.0	22,000.0		12,300.0	1.0E99 Syst
1989	16,000.0		16,000.0	16,000.0		12,300.0	1.0E99 Syst
1990	104,000.0		104,000.0	104,000.0		12,300.0	1.0E99 Syst
1991	19,500.0		19,500.0	19,500.0		12,300.0	1.0E99 Syst
1992	26,900.0		26,900.0	26,900.0		12,300.0	1.0E99 Syst
1993	19,400.0		19,400.0	19,400.0		12,300.0	1.0E99 Syst
1994	60,800.0		60,800.0	60,800.0		12,300.0	1.0E99 Syst
1995	23,300.0		23,300.0	23,300.0		12,300.0	1.0E99 Syst
1996	16,200.0		16,200.0	16,200.0		12,300.0	1.0E99 Syst
1997	39,300.0		39,300.0	39,300.0		12,300.0	1.0E99 Syst
1998	27,800.0		27,800.0	27,800.0		12,300.0	1.0E99 Syst
1999	24,100.0		24,100.0	24,100.0		12,300.0	1.0E99 Syst
2000	3,010.0		1.0E-6	12,300.0		12,300.0	1.0E99 Syst
2001	29,600.0		29,600.0	29,600.0		12,300.0	1.0E99 Syst
2002	9,890.0		1.0E-6	12,300.0		12,300.0	1.0E99 Syst
2003	37,600.0		37,600.0	37,600.0		12,300.0	1.0E99 Syst
2004	16,800.0		16,800.0	16,800.0		12,300.0	1.0E99 Syst

2005	5,740.0		1.0E-6	12,300.0		12,300.0	1.0E99	Syst	
2006	2,860.0		1.0E-6	12,300.0		12,300.0	1.0E99	Syst	
2007	10,000.0		1.0E-6	12,300.0		12,300.0	1.0E99	Syst	
2008	33,400.0		33,400.0	33,400.0		12,300.0	1.0E99	Syst	
2009	33,000.0		33,000.0	33,000.0		12,300.0	1.0E99	Syst	
2010	9,990.0		1.0E-6	12,300.0		12,300.0	1.0E99	Syst	
2011	15,300.0		15,300.0	15,300.0		12,300.0	1.0E99	Syst	
2012	19,600.0		19,600.0	19,600.0		12,300.0	1.0E99	Syst	
2013	31,100.0		31,100.0	31,100.0		12,300.0	1.0E99	Syst	
2014	20,900.0		20,900.0	20,900.0		12,300.0	1.0E99	Syst	
2015	12,300.0		12,300.0	12,300.0		12,300.0	1.0E99	Syst	
2016	116,000.0		116,000.0	116,000.0		12,300.0	1.0E99	Syst	
2017	10,040.0		1.0E-6	12,300.0		12,300.0	1.0E99	Syst	
----- ----- ----- -----									

```
-----
Fitted log10 Moments                                Mean      Variance
Std Dev      Skew
-----
```

```
-----
EMA at-site data w/o regional info                4.295143
0.127939      0.357685      -0.336054
EMA w/ regional info and B17b MSE(G)              4.302085
0.118987      0.344945      -0.141502
EMA w/ regional info and specified MSE(G)          4.302085
0.118987      0.344945      -0.141502
-----
```

```
-----
EMA Estimate of MSE[G at-site]                    0.095865
MSE[G at-site systematic]                         0.095865
Effective Record Length [G at-site]               69.000000
Grubbs-Beck Critical Value                        12,300.000000
-----
```

--- Final Results ---

<< Plotting Positions >>

AmDarling2019-Darlington, LA-FLOW-ANNUAL PEAK

Events Analyzed				Ordered Events			
				Water	FLOW	H-S	
Day	Mon	Year	CFS	Year	CFS	Plot	Pos
----- ----- ----- -----							
28	Feb	1949	20,000.0	1	2016	116,000.0	1.42
07	Jan	1950	43,400.0	2	1990	104,000.0	2.84
30	Mar	1951	31,600.0	3	1977	76,400.0	4.26
21	Dec	1951	3,180.0	4	1983	63,300.0	5.68
20	May	1953	18,900.0	5	1973	62,100.0	7.10
16	Jan	1954	3,280.0	6	1994	60,800.0	8.53

	13 Apr 1955	55,700.0		7	1955	55,700.0	9.95	
	12 Mar 1956	20,400.0		8	1980	47,500.0	11.37	
	29 Jun 1957	20,200.0		9	1972	45,500.0	12.79	
	23 Sep 1958	22,400.0		10	1965	44,500.0	14.21	
	03 Feb 1959	6,900.0		11	1964	44,500.0	15.63	
	19 Dec 1959	9,800.0		12	1979	43,400.0	17.05	
	18 Mar 1961	37,900.0		13	1950	43,400.0	18.47	
	28 Apr 1962	15,400.0		14	1975	40,700.0	19.89	
	21 Jan 1963	4,530.0		15	1997	39,300.0	21.31	
	03 Mar 1964	44,500.0		16	1967	39,300.0	22.73	
	05 Oct 1964	44,500.0		17	1961	37,900.0	24.15	
	13 Feb 1966	20,000.0		18	2003	37,600.0	25.58	
	15 Apr 1967	39,300.0		19	2008	33,400.0	27.00	
	17 Dec 1967	8,000.0		20	2009	33,000.0	28.42	
	14 Apr 1969	8,600.0		21	1951	31,600.0	29.84	
	21 Mar 1970	3,630.0		22	2013	31,100.0	31.26	
	18 Sep 1971	10,100.0		23	1978	30,500.0	32.68	
	07 Dec 1971	45,500.0		24	2001	29,600.0	34.10	
	25 Mar 1973	62,100.0		25	1998	27,800.0	35.52	
	14 Apr 1974	22,400.0		26	1992	26,900.0	36.94	
	09 Jun 1975	40,700.0		27	1999	24,100.0	38.36	
	01 Apr 1976	7,660.0		28	1995	23,300.0	39.78	
	22 Apr 1977	76,400.0		29	1974	22,400.0	41.20	
	30 Nov 1977	30,500.0		30	1958	22,400.0	42.63	
	23 Apr 1979	43,400.0		31	1988	22,000.0	44.05	
	28 Mar 1980	47,500.0		32	1987	21,200.0	45.47	
	11 Dec 1980	8,320.0		33	2014	20,900.0	46.89	
	17 Feb 1982	18,100.0		34	1956	20,400.0	48.31	
	07 Apr 1983	63,300.0		35	1957	20,200.0	49.73	
	14 Feb 1984	13,000.0		36	1966	20,000.0	51.15	
	27 Feb 1985	8,970.0		37	1949	20,000.0	52.57	
	30 Oct 1985	17,500.0		38	2012	19,600.0	53.99	
	01 Mar 1987	21,200.0		39	1991	19,500.0	55.41	
	03 Apr 1988	22,000.0		40	1993	19,400.0	56.83	
	20 May 1989	16,000.0		41	1953	18,900.0	58.26	
	25 Jan 1990	104,000.0		42	1982	18,100.0	59.68	
	01 May 1991	19,500.0		43	1986	17,500.0	61.10	
	06 Mar 1992	26,900.0		44	2004	16,800.0	62.52	
	21 Jan 1993	19,400.0		45	1996	16,200.0	63.94	
	28 Jan 1994	60,800.0		46	1989	16,000.0	65.36	
	12 Apr 1995	23,300.0		47	1962	15,400.0	66.78	
	19 Dec 1995	16,200.0		48	2011	15,300.0	68.20	
	28 Apr 1997	39,300.0		49	1984	13,000.0	69.62	
	08 Jan 1998	27,800.0		50	2015	12,300.0*	71.04	
	14 Mar 1999	24,100.0		51	1971	10,100.0*	73.05	
	04 Apr 2000	3,010.0		52	2017	10,040.0*	74.50	
	08 Jun 2001	29,600.0		53	2007	10,000.0*	75.94	
	28 Sep 2002	9,890.0		54	2010	9,990.0*	77.38	
	23 Feb 2003	37,600.0		55	2002	9,890.0*	78.82	
	13 Feb 2004	16,800.0		56	1960	9,800.0*	80.26	
	02 Feb 2005	5,740.0		57	1985	8,970.0*	81.70	
	03 Feb 2006	2,860.0		58	1969	8,600.0*	83.14	

28 Oct 2006	10,000.0	59	1981	8,320.0*	84.58	
03 Sep 2008	33,400.0	60	1968	8,000.0*	86.02	
29 Mar 2009	33,000.0	61	1976	7,660.0*	87.46	
16 Oct 2009	9,990.0	62	1959	6,900.0*	88.90	
10 Mar 2011	15,300.0	63	2005	5,740.0*	90.35	
01 Sep 2012	19,600.0	64	1963	4,530.0*	91.79	
13 Feb 2013	31,100.0	65	1970	3,630.0*	93.23	
22 Feb 2014	20,900.0	66	1954	3,280.0*	94.67	
03 Mar 2015	12,300.0	67	1952	3,180.0*	96.11	
12 Aug 2016	116,000.0	68	2000	3,010.0*	97.55	
04 Apr 2017	10,040.0	69	2006	2,860.0*	98.99	
----- -----						

* Outlier

* Low outlier plotting positions are computed using Median parameters.

<< Frequency Curve >>

AmDarling2019-Darlington, LA-FLOW-ANNUAL PEAK

Computed		Variance	Percent	Confidence Limits	
Curve		Log (EMA)	Chance	0.10	0.90
FLOW, CFS			Exceedance	FLOW, CFS	
-----			-----	-----	
172,128.8	0.01633		0.200	280,835.0	126,187.6
139,554.5	0.01149		0.500	208,265.6	107,007.2
117,083.4	0.00859		1.000	164,208.5	92,674.1
96,399.2	0.00629		2.000	127,783.8	78,556.1
77,419.7	0.00456		4.000	97,671.0	64,732.1
54,776.6	0.00300		10.000	65,554.8	47,087.5
39,311.1	0.00226		20.000	45,687.1	34,341.0
20,427.6	0.00197		50.000	23,235.7	17,713.3
10,337.1	0.00468		80.000	12,069.2	7,615.0
7,163.5	0.00910		90.000	8,816.3	4,607.1
5,262.2	0.01556		95.000	6,905.5	2,971.3
2,910.2	0.03839		99.000	4,501.0	1,221.9
-----			-----	-----	

<< Systematic Statistics >>

AmDarling2019-Darlington, LA-FLOW-ANNUAL PEAK

Log Transform:		Number of Events	
FLOW, CFS			
Mean	4.302	Historic Events	0
Standard Dev	0.345	High Outliers	0
Station Skew	-0.336	Low Outliers	19
Regional Skew	0.038	Zero Events	0
Weighted Skew	-0.142	Missing Events	0
Adopted Skew	-0.142	Systematic Events	69

USGS 07377300 Amite River at Magnolia, LA

Regional Skew: 0.038

Regional Skew MSE: 0.302

Plotting Position Type: Hirsch-Stedinger

Upper Confidence Level: 0.1

Lower Confidence Level: 0.9

Use non-standard frequencies

Frequency: 0.2

Frequency: 0.5

Frequency: 1.0

Frequency: 2.0

Frequency: 4.0

Frequency: 10.0

Frequency: 20.0

Frequency: 50.0

Frequency: 80.0

Frequency: 90.0

Frequency: 95.0

Frequency: 99.0

Display ordinate values using 1 digits in fraction part of value

--- End of Input Data ---

<< EMA Representation of Data >>

AmDarling2019-Magnolia, LA-FLOW-ANNUAL PEAK

		Value		Threshold		Type
Year	Peak	Low	High	Low	High	
1949	23,800.0	23,800.0	23,800.0	1.0E-99	1.0E99	Syst
1950	35,100.0	35,100.0	35,100.0	1.0E-99	1.0E99	Syst
1951	31,500.0	31,500.0	31,500.0	1.0E-99	1.0E99	Syst
1952	10,300.0	10,300.0	10,300.0	1.0E-99	1.0E99	Syst
1953	48,400.0	48,400.0	48,400.0	1.0E-99	1.0E99	Syst
1954	10,800.0	10,800.0	10,800.0	1.0E-99	1.0E99	Syst
1955	53,700.0	53,700.0	53,700.0	1.0E-99	1.0E99	Syst
1956	22,800.0	22,800.0	22,800.0	1.0E-99	1.0E99	Syst
1957	12,500.0	12,500.0	12,500.0	1.0E-99	1.0E99	Syst
1958	13,800.0	13,800.0	13,800.0	1.0E-99	1.0E99	Syst
1959	15,800.0	15,800.0	15,800.0	1.0E-99	1.0E99	Syst
1960	17,900.0	17,900.0	17,900.0	1.0E-99	1.0E99	Syst
1961	42,900.0	42,900.0	42,900.0	1.0E-99	1.0E99	Syst
1962	35,300.0	35,300.0	35,300.0	1.0E-99	1.0E99	Syst
1963	12,100.0	12,100.0	12,100.0	1.0E-99	1.0E99	Syst
1964	29,300.0	29,300.0	29,300.0	1.0E-99	1.0E99	Syst
1965	39,200.0	39,200.0	39,200.0	1.0E-99	1.0E99	Syst
1966	30,000.0	30,000.0	30,000.0	1.0E-99	1.0E99	Syst
1967	40,400.0	40,400.0	40,400.0	1.0E-99	1.0E99	Syst
1968	12,100.0	12,100.0	12,100.0	1.0E-99	1.0E99	Syst

1969	18,600.0		18,600.0	18,600.0		1.0E-99	1.0E99		Syst	
1970	15,200.0		15,200.0	15,200.0		1.0E-99	1.0E99		Syst	
1971	12,100.0		12,100.0	12,100.0		1.0E-99	1.0E99		Syst	
1972	42,100.0		42,100.0	42,100.0		1.0E-99	1.0E99		Syst	
1973	51,900.0		51,900.0	51,900.0		1.0E-99	1.0E99		Syst	
1974	22,200.0		22,200.0	22,200.0		1.0E-99	1.0E99		Syst	
1975	30,100.0		30,100.0	30,100.0		1.0E-99	1.0E99		Syst	
1976	14,000.0		14,000.0	14,000.0		1.0E-99	1.0E99		Syst	
1977	85,100.0		85,100.0	85,100.0		1.0E-99	1.0E99		Syst	
1978	25,800.0		25,800.0	25,800.0		1.0E-99	1.0E99		Syst	
1979	42,600.0		42,600.0	42,600.0		1.0E-99	1.0E99		Syst	
1980	43,400.0		43,400.0	43,400.0		1.0E-99	1.0E99		Syst	
1981	14,300.0		14,300.0	14,300.0		1.0E-99	1.0E99		Syst	
1982	17,700.0		17,700.0	17,700.0		1.0E-99	1.0E99		Syst	
1983	75,700.0		75,700.0	75,700.0		1.0E-99	1.0E99		Syst	
1993	59,600.0		59,600.0	59,600.0		1.0E-99	1.0E99		Syst	
1994	54,700.0		54,700.0	54,700.0		1.0E-99	1.0E99		Syst	
1995	44,100.0		44,100.0	44,100.0		1.0E-99	1.0E99		Syst	
1996	32,200.0		32,200.0	32,200.0		1.0E-99	1.0E99		Syst	
1997	44,000.0		44,000.0	44,000.0		1.0E-99	1.0E99		Syst	
1998	36,200.0		36,200.0	36,200.0		1.0E-99	1.0E99		Syst	
1999	31,700.0		31,700.0	31,700.0		1.0E-99	1.0E99		Syst	
2001	51,300.0		51,300.0	51,300.0		1.0E-99	1.0E99		Syst	
2002	20,500.0		20,500.0	20,500.0		1.0E-99	1.0E99		Syst	
2003	44,000.0		44,000.0	44,000.0		1.0E-99	1.0E99		Syst	
2004	27,900.0		27,900.0	27,900.0		1.0E-99	1.0E99		Syst	
2005	21,400.0		21,400.0	21,400.0		1.0E-99	1.0E99		Syst	
2006	7,380.0		7,380.0	7,380.0		1.0E-99	1.0E99		Syst	
2008	44,600.0		44,600.0	44,600.0		1.0E-99	1.0E99		Syst	
2009	33,500.0		33,500.0	33,500.0		1.0E-99	1.0E99		Syst	
2010	21,800.0		21,800.0	21,800.0		1.0E-99	1.0E99		Syst	
2011	24,100.0		24,100.0	24,100.0		1.0E-99	1.0E99		Syst	
2012	24,800.0		24,800.0	24,800.0		1.0E-99	1.0E99		Syst	
2013	28,900.0		28,900.0	28,900.0		1.0E-99	1.0E99		Syst	
2014	26,100.0		26,100.0	26,100.0		1.0E-99	1.0E99		Syst	
2015	22,000.0		22,000.0	22,000.0		1.0E-99	1.0E99		Syst	
2016	202,000.0		202,000.0	202,000.0		1.0E-99	1.0E99		Syst	
2017	21,360.0		21,360.0	21,360.0		1.0E-99	1.0E99		Syst	
----- ----- ----- ----- -----										

Fitted log10 Moments				Mean	Variance
Std Dev Skew					

EMA at-site data w/o regional info				4.447842	
0.067418	0.259649	0.349190			
EMA w/ regional info and B17b MSE(G)				4.447842	
0.067418	0.259649	0.264946			
EMA w/ regional info and specified MSE(G)				4.447842	
0.067418	0.259649	0.264946			

EMA Estimate of MSE[G at-site]	0.112105
MSE[G at-site systematic]	0.112105

Effective Record Length [G at-site]
Grubbs-Beck Critical Value

58.000000
0.000000

--- Final Results ---

<< Plotting Positions >>

AmDarling2019-Magnolia, LA-FLOW-ANNUAL PEAK

Events Analyzed				Ordered Events			
			FLOW			FLOW	H-S
Day	Mon	Year	CFS	Rank	Water Year	CFS	Plot Pos
04	May	1949	23,800.0	1	2016	202,000.0	1.69
09	Jan	1950	35,100.0	2	1977	85,100.0	3.39
01	Apr	1951	31,500.0	3	1983	75,700.0	5.08
05	Apr	1952	10,300.0	4	1993	59,600.0	6.78
20	May	1953	48,400.0	5	1994	54,700.0	8.47
11	Dec	1953	10,800.0	6	1955	53,700.0	10.17
15	Apr	1955	53,700.0	7	1973	51,900.0	11.86
14	Mar	1956	22,800.0	8	2001	51,300.0	13.56
01	Jul	1957	12,500.0	9	1953	48,400.0	15.25
25	Sep	1958	13,800.0	10	2008	44,600.0	16.95
04	Feb	1959	15,800.0	11	1995	44,100.0	18.64
19	Dec	1959	17,900.0	12	2003	44,000.0	20.34
18	Mar	1961	42,900.0	13	1997	44,000.0	22.03
29	Apr	1962	35,300.0	14	1980	43,400.0	23.73
30	Nov	1962	12,100.0	15	1961	42,900.0	25.42
03	Mar	1964	29,300.0	16	1979	42,600.0	27.12
06	Oct	1964	39,200.0	17	1972	42,100.0	28.81
17	Feb	1966	30,000.0	18	1967	40,400.0	30.51
15	Apr	1967	40,400.0	19	1965	39,200.0	32.20
30	Nov	1967	12,100.0	20	1998	36,200.0	33.90
13	Apr	1969	18,600.0	21	1962	35,300.0	35.59
08	Oct	1969	15,200.0	22	1950	35,100.0	37.29
30	Nov	1970	12,100.0	23	2009	33,500.0	38.98
06	Dec	1971	42,100.0	24	1996	32,200.0	40.68
27	Mar	1973	51,900.0	25	1999	31,700.0	42.37
15	Apr	1974	22,200.0	26	1951	31,500.0	44.07
10	Jan	1975	30,100.0	27	1975	30,100.0	45.76
30	Nov	1975	14,000.0	28	1966	30,000.0	47.46
23	Apr	1977	85,100.0	29	1964	29,300.0	49.15
01	Dec	1977	25,800.0	30	2013	28,900.0	50.85
23	Apr	1979	42,600.0	31	2004	27,900.0	52.54
14	Apr	1980	43,400.0	32	2014	26,100.0	54.24
30	Nov	1980	14,300.0	33	1978	25,800.0	55.93
30	Nov	1981	17,700.0	34	2012	24,800.0	57.63
08	Apr	1983	75,700.0	35	2011	24,100.0	59.32
01	Jan	1984	---	36	1949	23,800.0	61.02
01	Jan	1985	---	37	1956	22,800.0	62.71
01	Jan	1986	---	38	1974	22,200.0	64.41

01 Jan 1987	---	39	2015	22,000.0	66.10	
01 Jan 1988	---	40	2010	21,800.0	67.80	
01 Jan 1989	---	41	2005	21,400.0	69.49	
01 Jan 1990	---	42	2017	21,360.0	71.19	
01 Jan 1991	---	43	2002	20,500.0	72.88	
01 Jan 1992	---	44	1969	18,600.0	74.58	
21 Jan 1993	59,600.0	45	1960	17,900.0	76.27	
29 Jan 1994	54,700.0	46	1982	17,700.0	77.97	
12 Apr 1995	44,100.0	47	1959	15,800.0	79.66	
19 Dec 1995	32,200.0	48	1970	15,200.0	81.36	
29 Apr 1997	44,000.0	49	1981	14,300.0	83.05	
09 Jan 1998	36,200.0	50	1976	14,000.0	84.75	
15 Mar 1999	31,700.0	51	1958	13,800.0	86.44	
05 Apr 2000	---	52	1957	12,500.0	88.14	
09 Jun 2001	51,300.0	53	1971	12,100.0	89.83	
10 Apr 2002	20,500.0	54	1968	12,100.0	91.53	
04 Feb 2003	44,000.0	55	1963	12,100.0	93.22	
17 May 2004	27,900.0	56	1954	10,800.0	94.92	
02 Feb 2005	21,400.0	57	1952	10,300.0	96.61	
03 Feb 2006	7,380.0	58	2006	7,380.0	98.31	
01 Jan 2007	---	59	2000	---	---	
04 Sep 2008	44,600.0	60	2007	---	---	
30 Mar 2009	33,500.0	61	1992	---	---	
19 Dec 2009	21,800.0	62	1991	---	---	
10 Mar 2011	24,100.0	63	1990	---	---	
02 Sep 2012	24,800.0	64	1989	---	---	
14 Feb 2013	28,900.0	65	1988	---	---	
23 Feb 2014	26,100.0	66	1987	---	---	
04 Mar 2015	22,000.0	67	1986	---	---	
13 Aug 2016	202,000.0	68	1985	---	---	
04 Apr 2017	21,360.0	69	1984	---	---	

* Low outlier plotting positions are computed using Median parameters.

<< Frequency Curve >>

AmDarling2019-Magnolia, LA-FLOW-ANNUAL PEAK

Computed	Variance	Percent	Confidence Limits	
Curve	Log (EMA)	Chance	0.10	0.90
FLOW, CFS		Exceedance	FLOW, CFS	

190,091.2	0.01767	0.200	325,531.6	139,159.3
151,714.9	0.01243	0.500	236,478.7	116,385.7
126,449.2	0.00919	1.000	184,007.7	100,337.7
104,044.8	0.00656	2.000	141,767.3	85,233.4
84,175.4	0.00452	4.000	107,855.3	71,000.3
61,247.6	0.00265	10.000	73,145.1	53,376.9
45,957.9	0.00181	20.000	52,747.0	40,791.9
27,314.2	0.00130	50.000	30,452.3	24,550.3
16,851.9	0.00135	80.000	18,749.3	15,036.0

13,283.7	0.00170	90.000	14,894.8	11,601.8
10,994.8	0.00234	95.000	12,504.7	9,312.1
7,848.2	0.00506	99.000	9,412.8	6,099.6

<< Systematic Statistics >>

AmDarling2019-Magnolia, LA-FLOW-ANNUAL PEAK

Log Transform:		Number of Events	
FLOW, CFS			
Mean	4.448	Historic Events	0
Standard Dev	0.260	High Outliers	0
Station Skew	0.349	Low Outliers	0
Regional Skew	0.038	Zero Events	0
Weighted Skew	0.265	Missing Events	11
Adopted Skew	0.265	Systematic Events	58
		Historic Period	69

--- End of Analytical Frequency Curve ---

USGS 07378500 Amite River near Denham Springs, LA

Regional Skew: 0.032

Regional Skew MSE: 0.302

Plotting Position Type: Hirsch-Stedinger

Upper Confidence Level: 0.1

Lower Confidence Level: 0.9

Use non-standard frequencies

Frequency: 0.2

Frequency: 0.5

Frequency: 1.0

Frequency: 2.0

Frequency: 4.0

Frequency: 10.0

Frequency: 20.0

Frequency: 50.0

Frequency: 80.0

Frequency: 90.0

Frequency: 95.0

Frequency: 99.0

Display ordinate values using 1 digits in fraction part of value

--- End of Input Data ---

<< EMA Representation of Data >>

AmDarling2019-Denham Springs, LA-FLOW-ANNUAL PEAK

Year	Peak	Value		Threshold		Type
		Low	High	Low	High	
1921	93,000.0	93,000.0	93,000.0	1.0E-99	1.0E99	Hist
1922	---	1.0E-99	93,000.0	93,000.0	1.0E99	Cens
1923	---	1.0E-99	93,000.0	93,000.0	1.0E99	Cens
1924	---	1.0E-99	93,000.0	93,000.0	1.0E99	Cens
1925	---	1.0E-99	93,000.0	93,000.0	1.0E99	Cens
1926	---	1.0E-99	93,000.0	93,000.0	1.0E99	Cens
1927	---	1.0E-99	93,000.0	93,000.0	1.0E99	Cens
1928	---	1.0E-99	93,000.0	93,000.0	1.0E99	Cens
1929	---	1.0E-99	93,000.0	93,000.0	1.0E99	Cens
1930	---	1.0E-99	93,000.0	93,000.0	1.0E99	Cens
1931	---	1.0E-99	93,000.0	93,000.0	1.0E99	Cens
1932	---	1.0E-99	93,000.0	93,000.0	1.0E99	Cens
1933	---	1.0E-99	93,000.0	93,000.0	1.0E99	Cens
1934	---	1.0E-99	93,000.0	93,000.0	1.0E99	Cens
1935	---	1.0E-99	93,000.0	93,000.0	1.0E99	Cens
1936	---	1.0E-99	93,000.0	93,000.0	1.0E99	Cens
1937	---	1.0E-99	93,000.0	93,000.0	1.0E99	Cens
1938	---	1.0E-99	93,000.0	93,000.0	1.0E99	Cens
1939	12,100.0	12,100.0	12,100.0	1.0E-99	1.0E99	Syst
1940	16,000.0	16,000.0	16,000.0	1.0E-99	1.0E99	Syst
1941	20,800.0	20,800.0	20,800.0	1.0E-99	1.0E99	Syst
1942	12,200.0	12,200.0	12,200.0	1.0E-99	1.0E99	Syst
1943	40,200.0	40,200.0	40,200.0	1.0E-99	1.0E99	Syst
1944	11,000.0	11,000.0	11,000.0	1.0E-99	1.0E99	Syst
1945	11,600.0	11,600.0	11,600.0	1.0E-99	1.0E99	Syst
1946	15,500.0	15,500.0	15,500.0	1.0E-99	1.0E99	Syst
1947	27,800.0	27,800.0	27,800.0	1.0E-99	1.0E99	Syst
1948	45,100.0	45,100.0	45,100.0	1.0E-99	1.0E99	Syst
1949	28,800.0	28,800.0	28,800.0	1.0E-99	1.0E99	Syst
1950	40,800.0	40,800.0	40,800.0	1.0E-99	1.0E99	Syst
1951	36,900.0	36,900.0	36,900.0	1.0E-99	1.0E99	Syst
1952	8,230.0	8,230.0	8,230.0	1.0E-99	1.0E99	Syst
1953	67,000.0	67,000.0	67,000.0	1.0E-99	1.0E99	Syst
1954	15,200.0	15,200.0	15,200.0	1.0E-99	1.0E99	Syst
1955	54,300.0	54,300.0	54,300.0	1.0E-99	1.0E99	Syst
1956	23,400.0	23,400.0	23,400.0	1.0E-99	1.0E99	Syst
1957	12,300.0	12,300.0	12,300.0	1.0E-99	1.0E99	Syst
1958	14,700.0	14,700.0	14,700.0	1.0E-99	1.0E99	Syst
1959	19,100.0	19,100.0	19,100.0	1.0E-99	1.0E99	Syst
1960	18,800.0	18,800.0	18,800.0	1.0E-99	1.0E99	Syst
1961	49,100.0	49,100.0	49,100.0	1.0E-99	1.0E99	Syst
1962	49,700.0	49,700.0	49,700.0	1.0E-99	1.0E99	Syst
1963	5,150.0	5,150.0	5,150.0	1.0E-99	1.0E99	Syst
1964	40,500.0	40,500.0	40,500.0	1.0E-99	1.0E99	Syst
1965	49,900.0	49,900.0	49,900.0	1.0E-99	1.0E99	Syst
1966	39,700.0	39,700.0	39,700.0	1.0E-99	1.0E99	Syst
1967	47,800.0	47,800.0	47,800.0	1.0E-99	1.0E99	Syst
1968	6,290.0	6,290.0	6,290.0	1.0E-99	1.0E99	Syst
1969	23,000.0	23,000.0	23,000.0	1.0E-99	1.0E99	Syst
1970	21,700.0	21,700.0	21,700.0	1.0E-99	1.0E99	Syst
1971	12,600.0	12,600.0	12,600.0	1.0E-99	1.0E99	Syst
1972	51,800.0	51,800.0	51,800.0	1.0E-99	1.0E99	Syst
1973	61,800.0	61,800.0	61,800.0	1.0E-99	1.0E99	Syst

1974	21,300.0		21,300.0	21,300.0		1.0E-99	1.0E99		Syst	
1975	29,900.0		29,900.0	29,900.0		1.0E-99	1.0E99		Syst	
1976	16,100.0		16,100.0	16,100.0		1.0E-99	1.0E99		Syst	
1977	110,000.0		110,000.0	110,000.0		1.0E-99	1.0E99		Syst	
1978	31,300.0		31,300.0	31,300.0		1.0E-99	1.0E99		Syst	
1979	68,600.0		68,600.0	68,600.0		1.0E-99	1.0E99		Syst	
1980	64,200.0		64,200.0	64,200.0		1.0E-99	1.0E99		Syst	
1981	11,300.0		11,300.0	11,300.0		1.0E-99	1.0E99		Syst	
1982	23,900.0		23,900.0	23,900.0		1.0E-99	1.0E99		Syst	
1983	112,000.0		112,000.0	112,000.0		1.0E-99	1.0E99		Syst	
1984	23,600.0		23,600.0	23,600.0		1.0E-99	1.0E99		Syst	
1985	26,400.0		26,400.0	26,400.0		1.0E-99	1.0E99		Syst	
1986	43,900.0		43,900.0	43,900.0		1.0E-99	1.0E99		Syst	
1987	31,300.0		31,300.0	31,300.0		1.0E-99	1.0E99		Syst	
1988	41,300.0		41,300.0	41,300.0		1.0E-99	1.0E99		Syst	
1989	29,400.0		29,400.0	29,400.0		1.0E-99	1.0E99		Syst	
1990	96,700.0		96,700.0	96,700.0		1.0E-99	1.0E99		Syst	
1991	37,700.0		37,700.0	37,700.0		1.0E-99	1.0E99		Syst	
1992	48,600.0		48,600.0	48,600.0		1.0E-99	1.0E99		Syst	
1993	81,900.0		81,900.0	81,900.0		1.0E-99	1.0E99		Syst	
1994	66,500.0		66,500.0	66,500.0		1.0E-99	1.0E99		Syst	
1995	65,300.0		65,300.0	65,300.0		1.0E-99	1.0E99		Syst	
1996	49,000.0		49,000.0	49,000.0		1.0E-99	1.0E99		Syst	
1997	59,300.0		59,300.0	59,300.0		1.0E-99	1.0E99		Syst	
1998	50,200.0		50,200.0	50,200.0		1.0E-99	1.0E99		Syst	
1999	38,900.0		38,900.0	38,900.0		1.0E-99	1.0E99		Syst	
2000	7,730.0		7,730.0	7,730.0		1.0E-99	1.0E99		Syst	
2001	83,500.0		83,500.0	83,500.0		1.0E-99	1.0E99		Syst	
2002	23,300.0		23,300.0	23,300.0		1.0E-99	1.0E99		Syst	
2003	54,000.0		54,000.0	54,000.0		1.0E-99	1.0E99		Syst	
2004	41,100.0		41,100.0	41,100.0		1.0E-99	1.0E99		Syst	
2005	27,400.0		27,400.0	27,400.0		1.0E-99	1.0E99		Syst	
2006	5,260.0		5,260.0	5,260.0		1.0E-99	1.0E99		Syst	
2007	37,300.0		37,300.0	37,300.0		1.0E-99	1.0E99		Syst	
2008	67,400.0		67,400.0	67,400.0		1.0E-99	1.0E99		Syst	
2009	43,100.0		43,100.0	43,100.0		1.0E-99	1.0E99		Syst	
2010	27,200.0		27,200.0	27,200.0		1.0E-99	1.0E99		Syst	
2011	31,600.0		31,600.0	31,600.0		1.0E-99	1.0E99		Syst	
2012	35,500.0		35,500.0	35,500.0		1.0E-99	1.0E99		Syst	
2013	37,800.0		37,800.0	37,800.0		1.0E-99	1.0E99		Syst	
2014	29,300.0		29,300.0	29,300.0		1.0E-99	1.0E99		Syst	
2015	27,900.0		27,900.0	27,900.0		1.0E-99	1.0E99		Syst	
2016	266,000.0		266,000.0	266,000.0		1.0E-99	1.0E99		Syst	
2017	26,500.0		26,500.0	26,500.0		1.0E-99	1.0E99		Syst	
----- ----- ----- -----										

Fitted log10 Moments			Mean	Variance
Std Dev	Skew			
EMA at-site data w/o regional info			4.488804	
0.099412	0.315296	-0.251113		
EMA w/ regional info and B17b MSE (G)			4.488490	
0.099205	0.314969	-0.193677		
EMA w/ regional info and specified MSE (G)			4.488463	
0.099187	0.314940	-0.188676		

```

-----
EMA Estimate of MSE[G at-site]                0.074645
MSE[G at-site systematic]                     0.080339
Effective Record Length [G at-site]           85.026078
Grubbs-Beck Critical Value                    0.000000

```

--- Final Results ---

<< Plotting Positions >>

AmDarling2019-Denham Springs, LA-FLOW-ANNUAL PEAK

Events Analyzed				Ordered Events			
			FLOW	Water		FLOW	H-S
Day	Mon	Year	CFS	Rank	Year	CFS	Plot Pos
15	Mar	1921	93,000.0	1	2016	266,000.0	0.86
01	Jan	1922	---	2	1983	112,000.0	1.72
01	Jan	1923	---	3	1977	110,000.0	2.58
01	Jan	1924	---	4	1990	96,700.0	3.44
01	Jan	1925	---	5	1921	93,000.0	4.30
01	Jan	1926	---	6	2001	83,500.0	6.40
01	Jan	1927	---	7	1993	81,900.0	7.65
01	Jan	1928	---	8	1979	68,600.0	8.90
01	Jan	1929	---	9	2008	67,400.0	10.15
01	Jan	1930	---	10	1953	67,000.0	11.39
01	Jan	1931	---	11	1994	66,500.0	12.64
01	Jan	1932	---	12	1995	65,300.0	13.89
01	Jan	1933	---	13	1980	64,200.0	15.14
01	Jan	1934	---	14	1973	61,800.0	16.39
01	Jan	1935	---	15	1997	59,300.0	17.63
01	Jan	1936	---	16	1955	54,300.0	18.88
01	Jan	1937	---	17	2003	54,000.0	20.13
01	Jan	1938	---	18	1972	51,800.0	21.38
06	Jun	1939	12,100.0	19	1998	50,200.0	22.63
07	Jul	1940	16,000.0	20	1965	49,900.0	23.87
17	Dec	1940	20,800.0	21	1962	49,700.0	25.12
19	Sep	1942	12,200.0	22	1961	49,100.0	26.37
23	Mar	1943	40,200.0	23	1996	49,000.0	27.62
23	Mar	1944	11,000.0	24	1992	48,600.0	28.87
10	Jan	1945	11,600.0	25	1967	47,800.0	30.11
07	Jul	1946	15,500.0	26	1948	45,100.0	31.36
14	Mar	1947	27,800.0	27	1986	43,900.0	32.61
05	Mar	1948	45,100.0	28	2009	43,100.0	33.86
24	Mar	1949	28,800.0	29	1988	41,300.0	35.11
09	Jan	1950	40,800.0	30	2004	41,100.0	36.35
01	Apr	1951	36,900.0	31	1950	40,800.0	37.60
06	Apr	1952	8,230.0	32	1964	40,500.0	38.85

	20 May 1953	67,000.0		33	1943	40,200.0	40.10	
	11 Dec 1953	15,200.0		34	1966	39,700.0	41.35	
	15 Apr 1955	54,300.0		35	1999	38,900.0	42.59	
	14 Mar 1956	23,400.0		36	2013	37,800.0	43.84	
	01 Jul 1957	12,300.0		37	1991	37,700.0	45.09	
	17 Nov 1957	14,700.0		38	2007	37,300.0	46.34	
	04 Feb 1959	19,100.0		39	1951	36,900.0	47.59	
	19 Dec 1959	18,800.0		40	2012	35,500.0	48.83	
	20 Mar 1961	49,100.0		41	2011	31,600.0	50.08	
	29 Apr 1962	49,700.0		42	1987	31,300.0	51.33	
	22 Jan 1963	5,150.0		43	1978	31,300.0	52.58	
	04 Mar 1964	40,500.0		44	1975	29,900.0	53.83	
	07 Oct 1964	49,900.0		45	1989	29,400.0	55.07	
	13 Feb 1966	39,700.0		46	2014	29,300.0	56.32	
	17 Apr 1967	47,800.0		47	1949	28,800.0	57.57	
	13 May 1968	6,290.0		48	2015	27,900.0	58.82	
	14 Apr 1969	23,000.0		49	1947	27,800.0	60.07	
	08 Oct 1969	21,700.0		50	2005	27,400.0	61.31	
	20 Sep 1971	12,600.0		51	2010	27,200.0	62.56	
	08 Dec 1971	51,800.0		52	2017	26,500.0	63.81	
	27 Mar 1973	61,800.0		53	1985	26,400.0	65.06	
	27 Dec 1973	21,300.0		54	1982	23,900.0	66.30	
	10 May 1975	29,900.0		55	1984	23,600.0	67.55	
	27 Mar 1976	16,100.0		56	1956	23,400.0	68.80	
	23 Apr 1977	110,000.0		57	2002	23,300.0	70.05	
	02 Dec 1977	31,300.0		58	1969	23,000.0	71.30	
	24 Apr 1979	68,600.0		59	1970	21,700.0	72.54	
	30 Mar 1980	64,200.0		60	1974	21,300.0	73.79	
	12 Dec 1980	11,300.0		61	1941	20,800.0	75.04	
	18 Feb 1982	23,900.0		62	1959	19,100.0	76.29	
	08 Apr 1983	112,000.0		63	1960	18,800.0	77.54	
	12 Dec 1983	23,600.0		64	1976	16,100.0	78.78	
	24 Oct 1984	26,400.0		65	1940	16,000.0	80.03	
	31 Oct 1985	43,900.0		66	1946	15,500.0	81.28	
	20 Jan 1987	31,300.0		67	1954	15,200.0	82.53	
	04 Apr 1988	41,300.0		68	1958	14,700.0	83.78	
	21 May 1989	29,400.0		69	1971	12,600.0	85.02	
	27 Jan 1990	96,700.0		70	1957	12,300.0	86.27	
	22 Feb 1991	37,700.0		71	1942	12,200.0	87.52	
	07 Mar 1992	48,600.0		72	1939	12,100.0	88.77	
	22 Jan 1993	81,900.0		73	1945	11,600.0	90.02	
	30 Jan 1994	66,500.0		74	1981	11,300.0	91.26	
	12 Apr 1995	65,300.0		75	1944	11,000.0	92.51	
	20 Dec 1995	49,000.0		76	1952	8,230.0	93.76	
	29 Apr 1997	59,300.0		77	2000	7,730.0	95.01	
	09 Jan 1998	50,200.0		78	1968	6,290.0	96.26	
	15 Mar 1999	38,900.0		79	2006	5,260.0	97.50	
	06 May 2000	7,730.0		80	1963	5,150.0	98.75	
	09 Jun 2001	83,500.0		81	1938	---*	---	
	10 Apr 2002	23,300.0		82	1937	---*	---	
	24 Feb 2003	54,000.0		83	1936	---*	---	
	17 May 2004	41,100.0		84	1935	---*	---	

02 Feb 2005	27,400.0	85	1934	----	*	----	
30 Apr 2006	5,260.0	86	1933	----	*	----	
29 Oct 2006	37,300.0	87	1932	----	*	----	
05 Sep 2008	67,400.0	88	1931	----	*	----	
30 Mar 2009	43,100.0	89	1930	----	*	----	
19 Dec 2009	27,200.0	90	1929	----	*	----	
10 Mar 2011	31,600.0	91	1928	----	*	----	
20 Feb 2012	35,500.0	92	1927	----	*	----	
11 Jan 2013	37,800.0	93	1926	----	*	----	
23 Feb 2014	29,300.0	94	1925	----	*	----	
04 Mar 2015	27,900.0	95	1924	----	*	----	
14 Aug 2016	266,000.0	96	1923	----	*	----	
22 Jan 2017	26,500.0	97	1922	----	*	----	
----- -----							

* Low outlier plotting positions are computed using Median parameters.

<< Frequency Curve >>

AmDarling2019-Denham Springs, LA-FLOW-ANNUAL PEAK

Computed Curve	Variance Log (EMA)	Percent Chance	Confidence Limits	
FLOW, CFS		Exceedance	0.10 FLOW, CFS	0.90 FLOW, CFS
210,449.8	0.01008	0.200	298,903.3	162,547.4
175,336.3	0.00703	0.500	234,865.6	141,176.0
150,376.4	0.00518	1.000	193,017.8	124,692.3
126,759.5	0.00371	2.000	156,210.8	107,937.1
104,435.8	0.00261	4.000	123,932.9	90,934.4
76,768.0	0.00170	10.000	87,449.2	68,238.4
57,016.0	0.00138	20.000	63,787.3	51,100.5
31,503.7	0.00136	50.000	35,116.8	28,197.5
16,853.9	0.00185	80.000	19,042.3	14,713.2
11,995.7	0.00268	90.000	13,820.2	10,099.7
8,997.0	0.00402	95.000	10,633.1	7,216.1
5,157.4	0.00933	99.000	6,562.4	3,603.5

<< Systematic Statistics >>

AmDarling2019-Denham Springs, LA-FLOW-ANNUAL PEAK

Log Transform:		Number of Events	
FLOW, CFS			
Mean	4.488	Historic Events	1
Standard Dev	0.315	High Outliers	0
Station Skew	-0.251	Low Outliers	0
Regional Skew	0.032	Zero Events	0
Weighted Skew	-0.189	Missing Events	17
Adopted Skew	-0.189	Systematic Events	79

	Historic Period	97
--	-----------------	----

--- End of Analytical Frequency Curve ---

USGS 07380120 Amite River at Port Vincent, LA

Regional Skew: 0.047

Regional Skew MSE: 0.302

Plotting Position Type: Hirsch-Stedinger

Upper Confidence Level: 0.05

Lower Confidence Level: 0.95

Use non-standard frequencies

Frequency: 0.2

Frequency: 0.5

Frequency: 1.0

Frequency: 2.0

Frequency: 4.0

Frequency: 10.0

Frequency: 20.0

Frequency: 50.0

Frequency: 80.0

Frequency: 90.0

Frequency: 95.0

Frequency: 99.0

Display ordinate values using 1 digits in fraction part of value

--- End of Input Data ---

<< EMA Representation of Data >>

Amite Pt Vincent-Port Vincent, LA-FLOW-ANNUAL PEAK

Year	Peak	Value		Threshold		Type
		Low	High	Low	High	
1985	30,000.0	30,000.0	30,000.0	1.0E-99	1.0E99	Syst
1986	42,200.0	42,200.0	42,200.0	1.0E-99	1.0E99	Syst
1987	30,000.0	30,000.0	30,000.0	1.0E-99	1.0E99	Syst
1988	38,300.0	38,300.0	38,300.0	1.0E-99	1.0E99	Syst
1989	28,400.0	28,400.0	28,400.0	1.0E-99	1.0E99	Syst
1990	69,500.0	69,500.0	69,500.0	1.0E-99	1.0E99	Syst
1991	22,900.0	22,900.0	22,900.0	1.0E-99	1.0E99	Syst
1992	43,100.0	43,100.0	43,100.0	1.0E-99	1.0E99	Syst
1993	48,400.0	48,400.0	48,400.0	1.0E-99	1.0E99	Syst
1994	27,900.0	27,900.0	27,900.0	1.0E-99	1.0E99	Syst
1995	44,700.0	44,700.0	44,700.0	1.0E-99	1.0E99	Syst
1996	8,620.0	8,620.0	8,620.0	1.0E-99	1.0E99	Syst

1997	45,300.0		45,300.0	45,300.0		1.0E-99	1.0E99		Syst	
1998	41,000.0		41,000.0	41,000.0		1.0E-99	1.0E99		Syst	
1999	33,900.0		33,900.0	33,900.0		1.0E-99	1.0E99		Syst	
2000	12,600.0		12,600.0	12,600.0		1.0E-99	1.0E99		Syst	
2001	12,600.0		12,600.0	12,600.0		1.0E-99	1.0E99		Syst	
2002	12,300.0		12,300.0	12,300.0		1.0E-99	1.0E99		Syst	
2003	42,100.0		42,100.0	42,100.0		1.0E-99	1.0E99		Syst	
2004	31,400.0		31,400.0	31,400.0		1.0E-99	1.0E99		Syst	
2005	20,500.0		20,500.0	20,500.0		1.0E-99	1.0E99		Syst	
2006	11,700.0		11,700.0	11,700.0		1.0E-99	1.0E99		Syst	
2007	22,800.0		22,800.0	22,800.0		1.0E-99	1.0E99		Syst	
2008	22,800.0		22,800.0	22,800.0		1.0E-99	1.0E99		Syst	
2009	29,000.0		29,000.0	29,000.0		1.0E-99	1.0E99		Syst	
2010	20,800.0		20,800.0	20,800.0		1.0E-99	1.0E99		Syst	
2011	20,300.0		20,300.0	20,300.0		1.0E-99	1.0E99		Syst	
2012	24,100.0		24,100.0	24,100.0		1.0E-99	1.0E99		Syst	
2013	35,200.0		35,200.0	35,200.0		1.0E-99	1.0E99		Syst	
2014	20,300.0		20,300.0	20,300.0		1.0E-99	1.0E99		Syst	
2015	17,100.0		17,100.0	17,100.0		1.0E-99	1.0E99		Syst	
2016	199,000.0		199,000.0	199,000.0		1.0E-99	1.0E99		Syst	
2017	20,400.0		20,400.0	20,400.0		1.0E-99	1.0E99		Syst	
----- ----- ----- -----										

```
-----
-----
Fitted log10 Moments                                Mean      Variance
Std Dev      Skew
```

```
-----
EMA at-site data w/o regional info                4.443663
0.066496      0.257869      0.808860
EMA w/ regional info and B17b MSE(G)              4.443663
0.066496      0.257869      0.481797
EMA w/ regional info and specified MSE(G)          4.443663
0.066496      0.257869      0.481797
-----
-----
```

```
EMA Estimate of MSE[G at-site]                    0.227170
MSE[G at-site systematic]                          0.227170
Effective Record Length [G at-site]                33.000000
Grubbs-Beck Critical Value                         0.000000
```

--- Final Results ---

<< Plotting Positions >>

Amite Pt Vincent-Port Vincent, LA-FLOW-ANNUAL PEAK

Events Analyzed			Ordered Events			
			Water	FLOW	H-S	
Day	Mon	Year	CFS	Rank	Year	CFS Plot Pos
----- ----- ----- -----						

	28 Feb 1985	30,000.0		1	2016	199,000.0	2.94	
	01 Nov 1985	42,200.0		2	1990	69,500.0	5.88	
	20 Jan 1987	30,000.0		3	1993	48,400.0	8.82	
	04 Apr 1988	38,300.0		4	1997	45,300.0	11.76	
	22 May 1989	28,400.0		5	1995	44,700.0	14.71	
	28 Jan 1990	69,500.0		6	1992	43,100.0	17.65	
	24 Feb 1991	22,900.0		7	1986	42,200.0	20.59	
	08 Mar 1992	43,100.0		8	2003	42,100.0	23.53	
	23 Jan 1993	48,400.0		9	1998	41,000.0	26.47	
	01 Feb 1994	27,900.0		10	1988	38,300.0	29.41	
	13 Apr 1995	44,700.0		11	2013	35,200.0	32.35	
	15 Apr 1996	8,620.0		12	1999	33,900.0	35.29	
	30 Apr 1997	45,300.0		13	2004	31,400.0	38.24	
	09 Jan 1998	41,000.0		14	1987	30,000.0	41.18	
	17 Mar 1999	33,900.0		15	1985	30,000.0	44.12	
	06 May 2000	12,600.0		16	2009	29,000.0	47.06	
	19 Nov 2000	12,600.0		17	1989	28,400.0	50.00	
	30 Sep 2002	12,300.0		18	1994	27,900.0	52.94	
	24 Feb 2003	42,100.0		19	2012	24,100.0	55.88	
	18 May 2004	31,400.0		20	1991	22,900.0	58.82	
	04 Feb 2005	20,500.0		21	2008	22,800.0	61.76	
	30 Apr 2006	11,700.0		22	2007	22,800.0	64.71	
	30 Oct 2006	22,800.0		23	2010	20,800.0	67.65	
	04 Sep 2008	22,800.0		24	2005	20,500.0	70.59	
	31 Mar 2009	29,000.0		25	2017	20,400.0	73.53	
	20 Dec 2009	20,800.0		26	2014	20,300.0	76.47	
	12 Mar 2011	20,300.0		27	2011	20,300.0	79.41	
	21 Feb 2012	24,100.0		28	2015	17,100.0	82.35	
	13 Jan 2013	35,200.0		29	2001	12,600.0	85.29	
	24 Feb 2014	20,300.0		30	2000	12,600.0	88.24	
	05 Mar 2015	17,100.0		31	2002	12,300.0	91.18	
	15 Aug 2016	199,000.0		32	2006	11,700.0	94.12	
	24 Jan 2017	20,400.0		33	1996	8,620.0	97.06	
	----- ----- ----- -----							

* Low outlier plotting positions are computed using Median parameters.

<< Frequency Curve >>

Amite Pt Vincent-Port Vincent, LA-FLOW-ANNUAL PEAK

	Computed	Variance		Percent		Confidence Limits	
	Curve	Log (EMA)		Chance		0.05 0.95	
	FLOW, CFS			Exceedance		FLOW, CFS	
	----- ----- ----- -----						
	217,391.0	0.03454		0.200		734,936.7 131,022.4	
	167,317.2	0.02444		0.500		450,916.3 108,317.7	
	135,813.6	0.01817		1.000		310,646.3 92,595.1	
	108,956.3	0.01305		2.000		213,346.9 78,023.3	
	86,073.4	0.00903		4.000		145,992.6 64,509.0	
	60,892.9	0.00527		10.000		87,729.6 48,095.9	
	44,925.1	0.00349		20.000		58,878.5 36,616.3	

	26,486.8	0.00222		50.000		32,072.8	22,190.2	
	16,704.9	0.00203		80.000		19,835.2	13,885.3	
	13,468.8	0.00242		90.000		16,019.5	10,768.6	
	11,419.1	0.00322		95.000		13,764.0	8,665.4	
	8,631.8	0.00672		99.000		11,151.9	5,732.6	
	-----	-----		-----		-----	-----	

<< Systematic Statistics >>

Amite Pt Vincent-Port Vincent, LA-FLOW-ANNUAL PEAK

Log Transform:		Number of Events	
FLOW, CFS			
Mean	4.444	Historic Events	0
Standard Dev	0.258	High Outliers	0
Station Skew	0.809	Low Outliers	0
Regional Skew	0.047	Zero Events	0
Weighted Skew	0.482	Missing Events	0
Adopted Skew	0.482	Systematic Events	33

--- End of Analytical Frequency Curve ---

USGS 07377500 Comite River near Olive Branch, LA

Regional Skew: 0.187

Regional Skew MSE: 0.302

Plotting Position Type: Hirsch-Stedinger

Upper Confidence Level: 0.1

Lower Confidence Level: 0.9

Use non-standard frequencies

Frequency: 0.2

Frequency: 0.5

Frequency: 1.0

Frequency: 2.0

Frequency: 4.0

Frequency: 10.0

Frequency: 20.0

Frequency: 50.0

Frequency: 80.0

Frequency: 90.0

Frequency: 95.0

Frequency: 99.0

Display ordinate values using 1 digits in fraction part of value

--- End of Input Data ---

<< EMA Representation of Data >>

AmDarling2019-Olive Branch, LA-FLOW-ANNUAL PEAK

Year	Peak	Value		Threshold		Type
		Low	High	Low	High	
1943	12,400.0	12,400.0	12,400.0	1.0E-99	1.0E99	Syst
1944	3,110.0	3,110.0	3,110.0	1.0E-99	1.0E99	Syst
1945	3,460.0	3,460.0	3,460.0	1.0E-99	1.0E99	Syst
1946	2,870.0	2,870.0	2,870.0	1.0E-99	1.0E99	Syst
1947	5,240.0	5,240.0	5,240.0	1.0E-99	1.0E99	Syst
1948	9,900.0	9,900.0	9,900.0	1.0E-99	1.0E99	Syst
1949	11,300.0	11,300.0	11,300.0	1.0E-99	1.0E99	Syst
1950	11,300.0	11,300.0	11,300.0	1.0E-99	1.0E99	Syst
1951	9,900.0	9,900.0	9,900.0	1.0E-99	1.0E99	Syst
1952	1,530.0	1,530.0	1,530.0	1.0E-99	1.0E99	Syst
1953	13,300.0	13,300.0	13,300.0	1.0E-99	1.0E99	Syst
1954	1,780.0	1,780.0	1,780.0	1.0E-99	1.0E99	Syst
1955	14,400.0	14,400.0	14,400.0	1.0E-99	1.0E99	Syst
1956	8,140.0	8,140.0	8,140.0	1.0E-99	1.0E99	Syst
1957	4,270.0	4,270.0	4,270.0	1.0E-99	1.0E99	Syst
1958	3,510.0	3,510.0	3,510.0	1.0E-99	1.0E99	Syst
1959	3,100.0	3,100.0	3,100.0	1.0E-99	1.0E99	Syst
1960	4,450.0	4,450.0	4,450.0	1.0E-99	1.0E99	Syst
1961	19,900.0	19,900.0	19,900.0	1.0E-99	1.0E99	Syst
1962	11,400.0	11,400.0	11,400.0	1.0E-99	1.0E99	Syst
1963	1,660.0	1,660.0	1,660.0	1.0E-99	1.0E99	Syst
1964	11,400.0	11,400.0	11,400.0	1.0E-99	1.0E99	Syst
1965	15,500.0	15,500.0	15,500.0	1.0E-99	1.0E99	Syst
1966	6,580.0	6,580.0	6,580.0	1.0E-99	1.0E99	Syst
1967	13,400.0	13,400.0	13,400.0	1.0E-99	1.0E99	Syst
1968	1,380.0	1,380.0	1,380.0	1.0E-99	1.0E99	Syst
1969	3,500.0	3,500.0	3,500.0	1.0E-99	1.0E99	Syst
1970	2,960.0	2,960.0	2,960.0	1.0E-99	1.0E99	Syst
1971	3,430.0	3,430.0	3,430.0	1.0E-99	1.0E99	Syst
1972	16,400.0	16,400.0	16,400.0	1.0E-99	1.0E99	Syst
1973	12,500.0	12,500.0	12,500.0	1.0E-99	1.0E99	Syst
1974	4,660.0	4,660.0	4,660.0	1.0E-99	1.0E99	Syst
1975	7,230.0	7,230.0	7,230.0	1.0E-99	1.0E99	Syst
1976	2,720.0	2,720.0	2,720.0	1.0E-99	1.0E99	Syst
1977	22,400.0	22,400.0	22,400.0	1.0E-99	1.0E99	Syst
1978	14,500.0	14,500.0	14,500.0	1.0E-99	1.0E99	Syst
1979	21,300.0	21,300.0	21,300.0	1.0E-99	1.0E99	Syst
1980	16,900.0	16,900.0	16,900.0	1.0E-99	1.0E99	Syst
1981	2,560.0	2,560.0	2,560.0	1.0E-99	1.0E99	Syst
1982	4,660.0	4,660.0	4,660.0	1.0E-99	1.0E99	Syst
1983	19,800.0	19,800.0	19,800.0	1.0E-99	1.0E99	Syst
1984	4,210.0	4,210.0	4,210.0	1.0E-99	1.0E99	Syst
1985	4,880.0	4,880.0	4,880.0	1.0E-99	1.0E99	Syst
1986	9,080.0	9,080.0	9,080.0	1.0E-99	1.0E99	Syst
1987	7,320.0	7,320.0	7,320.0	1.0E-99	1.0E99	Syst
1988	11,200.0	11,200.0	11,200.0	1.0E-99	1.0E99	Syst
1989	6,590.0	6,590.0	6,590.0	1.0E-99	1.0E99	Syst
1990	18,400.0	18,400.0	18,400.0	1.0E-99	1.0E99	Syst
1991	6,390.0	6,390.0	6,390.0	1.0E-99	1.0E99	Syst
1992	16,800.0	16,800.0	16,800.0	1.0E-99	1.0E99	Syst
1993	13,600.0	13,600.0	13,600.0	1.0E-99	1.0E99	Syst

1994	12,700.0		12,700.0	12,700.0		1.0E-99	1.0E99		Syst	
1995	21,400.0		21,400.0	21,400.0		1.0E-99	1.0E99		Syst	
1996	9,520.0		9,520.0	9,520.0		1.0E-99	1.0E99		Syst	
1997	22,200.0		22,200.0	22,200.0		1.0E-99	1.0E99		Syst	
1998	8,260.0		8,260.0	8,260.0		1.0E-99	1.0E99		Syst	
1999	10,900.0		10,900.0	10,900.0		1.0E-99	1.0E99		Syst	
2000	1,850.0		1,850.0	1,850.0		1.0E-99	1.0E99		Syst	
2001	25,300.0		25,300.0	25,300.0		1.0E-99	1.0E99		Syst	
2002	13,300.0		13,300.0	13,300.0		1.0E-99	1.0E99		Syst	
2003	8,130.0		8,130.0	8,130.0		1.0E-99	1.0E99		Syst	
2004	14,500.0		14,500.0	14,500.0		1.0E-99	1.0E99		Syst	
2005	4,390.0		4,390.0	4,390.0		1.0E-99	1.0E99		Syst	
2006	1,720.0		1,720.0	1,720.0		1.0E-99	1.0E99		Syst	
2007	14,400.0		14,400.0	14,400.0		1.0E-99	1.0E99		Syst	
2008	19,300.0		19,300.0	19,300.0		1.0E-99	1.0E99		Syst	
2009	8,980.0		8,980.0	8,980.0		1.0E-99	1.0E99		Syst	
2010	3,660.0		3,660.0	3,660.0		1.0E-99	1.0E99		Syst	
2011	4,740.0		4,740.0	4,740.0		1.0E-99	1.0E99		Syst	
2012	5,230.0		5,230.0	5,230.0		1.0E-99	1.0E99		Syst	
2013	5,110.0		5,110.0	5,110.0		1.0E-99	1.0E99		Syst	
2014	7,760.0		7,760.0	7,760.0		1.0E-99	1.0E99		Syst	
2015	7,340.0		7,340.0	7,340.0		1.0E-99	1.0E99		Syst	
2016	78,000.0		78,000.0	78,000.0		1.0E-99	1.0E99		Syst	
2017	6,645.0		6,645.0	6,645.0		1.0E-99	1.0E99		Syst	
----- ----- ----- -----										

Fitted log10 Moments		Mean	Variance
Std Dev	Skew		

EMA at-site data w/o regional info		3.879208	
0.121133	0.348041 -0.099441		
EMA w/ regional info and B17b MSE(G)		3.879208	
0.121133	0.348041 -0.042145		
EMA w/ regional info and specified MSE(G)		3.879208	
0.121133	0.348041 -0.042145		

EMA Estimate of MSE[G at-site]	0.075513
MSE[G at-site systematic]	0.075513
Effective Record Length [G at-site]	75.000000
Grubbs-Beck Critical Value	0.000000

--- Final Results ---

<< Plotting Positions >>

AmDarling2019-Olive Branch, LA-FLOW-ANNUAL PEAK

	Events Analyzed		Ordered Events	
--	-----------------	--	----------------	--

Day	Mon	Year	FLOW CFS	Rank	Water Year	FLOW CFS	H-S Plot Pos
06	Feb	1943	12,400.0	1	2016	78,000.0	1.32
24	Apr	1944	3,110.0	2	2001	25,300.0	2.63
29	Apr	1945	3,460.0	3	1977	22,400.0	3.95
16	Mar	1946	2,870.0	4	1997	22,200.0	5.26
14	Mar	1947	5,240.0	5	1995	21,400.0	6.58
03	Mar	1948	9,900.0	6	1979	21,300.0	7.89
17	Dec	1948	11,300.0	7	1961	19,900.0	9.21
07	Jan	1950	11,300.0	8	1983	19,800.0	10.53
29	Mar	1951	9,900.0	9	2008	19,300.0	11.84
04	Apr	1952	1,530.0	10	1990	18,400.0	13.16
18	May	1953	13,300.0	11	1980	16,900.0	14.47
09	Dec	1953	1,780.0	12	1992	16,800.0	15.79
13	Apr	1955	14,400.0	13	1972	16,400.0	17.11
12	Mar	1956	8,140.0	14	1965	15,500.0	18.42
29	Jun	1957	4,270.0	15	2004	14,500.0	19.74
24	Sep	1958	3,510.0	16	1978	14,500.0	21.05
02	Feb	1959	3,100.0	17	2007	14,400.0	22.37
18	Dec	1959	4,450.0	18	1955	14,400.0	23.68
18	Mar	1961	19,900.0	19	1993	13,600.0	25.00
28	Apr	1962	11,400.0	20	1967	13,400.0	26.32
21	Jan	1963	1,660.0	21	2002	13,300.0	27.63
03	Mar	1964	11,400.0	22	1953	13,300.0	28.95
05	Oct	1964	15,500.0	23	1994	12,700.0	30.26
17	Feb	1966	6,580.0	24	1973	12,500.0	31.58
15	Apr	1967	13,400.0	25	1943	12,400.0	32.89
15	Apr	1968	1,380.0	26	1964	11,400.0	34.21
13	Apr	1969	3,500.0	27	1962	11,400.0	35.53
07	Oct	1969	2,960.0	28	1950	11,300.0	36.84
18	Sep	1971	3,430.0	29	1949	11,300.0	38.16
07	Dec	1971	16,400.0	30	1988	11,200.0	39.47
25	Mar	1973	12,500.0	31	1999	10,900.0	40.79
06	Nov	1973	4,660.0	32	1951	9,900.0	42.11
09	Jun	1975	7,230.0	33	1948	9,900.0	43.42
25	Mar	1976	2,720.0	34	1996	9,520.0	44.74
22	Apr	1977	22,400.0	35	1986	9,080.0	46.05
30	Nov	1977	14,500.0	36	2009	8,980.0	47.37
22	Apr	1979	21,300.0	37	1998	8,260.0	48.68
28	Mar	1980	16,900.0	38	1956	8,140.0	50.00
11	Dec	1980	2,560.0	39	2003	8,130.0	51.32
17	Feb	1982	4,660.0	40	2014	7,760.0	52.63
06	Apr	1983	19,800.0	41	2015	7,340.0	53.95
13	Feb	1984	4,210.0	42	1987	7,320.0	55.26
23	Oct	1984	4,880.0	43	1975	7,230.0	56.58
30	Oct	1985	9,080.0	44	2017	6,645.0	57.89
19	Jan	1987	7,320.0	45	1989	6,590.0	59.21
03	Apr	1988	11,200.0	46	1966	6,580.0	60.53
01	Jan	1989	6,590.0	47	1991	6,390.0	61.84
25	Jan	1990	18,400.0	48	1947	5,240.0	63.16
20	Feb	1991	6,390.0	49	2012	5,230.0	64.47

	06 Mar 1992	16,800.0		50	2013	5,110.0	65.79	
	21 Jan 1993	13,600.0		51	1985	4,880.0	67.11	
	28 Jan 1994	12,700.0		52	2011	4,740.0	68.42	
	12 Apr 1995	21,400.0		53	1982	4,660.0	69.74	
	18 Dec 1995	9,520.0		54	1974	4,660.0	71.05	
	28 Apr 1997	22,200.0		55	1960	4,450.0	72.37	
	07 Jan 1998	8,260.0		56	2005	4,390.0	73.68	
	14 Mar 1999	10,900.0		57	1957	4,270.0	75.00	
	09 Oct 1999	1,850.0		58	1984	4,210.0	76.32	
	08 Jun 2001	25,300.0		59	2010	3,660.0	77.63	
	07 Aug 2002	13,300.0		60	1958	3,510.0	78.95	
	22 Feb 2003	8,130.0		61	1969	3,500.0	80.26	
	15 May 2004	14,500.0		62	1945	3,460.0	81.58	
	01 Feb 2005	4,390.0		63	1971	3,430.0	82.89	
	10 Jul 2006	1,720.0		64	1944	3,110.0	84.21	
	28 Oct 2006	14,400.0		65	1959	3,100.0	85.53	
	03 Sep 2008	19,300.0		66	1970	2,960.0	86.84	
	28 Mar 2009	8,980.0		67	1946	2,870.0	88.16	
	17 Oct 2009	3,660.0		68	1976	2,720.0	89.47	
	08 Mar 2011	4,740.0		69	1981	2,560.0	90.79	
	18 Feb 2012	5,230.0		70	2000	1,850.0	92.11	
	11 Jan 2013	5,110.0		71	1954	1,780.0	93.42	
	21 Feb 2014	7,760.0		72	2006	1,720.0	94.74	
	02 Mar 2015	7,340.0		73	1963	1,660.0	96.05	
	12 Aug 2016	78,000.0		74	1952	1,530.0	97.37	
	03 Jan 2017	6,645.0		75	1968	1,380.0	98.68	

* Low outlier plotting positions are computed using Median parameters.

<< Frequency Curve >>

AmDarling2019-Olive Branch, LA-FLOW-ANNUAL PEAK

Computed	Variance	Percent	Confidence Limits
Curve	Log (EMA)	Chance	0.10 0.90
FLOW, CFS		Exceedance	FLOW, CFS
72,968.8	0.01987	0.200	118,589.2 52,542.6
57,799.4	0.01401	0.500	86,679.2 43,771.8
47,651.0	0.01039	1.000	67,375.0 37,412.3
38,557.3	0.00746	2.000	51,520.2 31,301.5
30,439.8	0.00519	4.000	38,572.0 25,454.1
21,068.8	0.00315	10.000	25,134.0 18,169.8
14,887.3	0.00227	20.000	17,199.7 13,036.9
7,614.7	0.00181	50.000	8,642.9 6,706.8
3,863.9	0.00212	80.000	4,423.1 3,330.3
2,701.7	0.00283	90.000	3,147.3 2,247.6
2,007.2	0.00403	95.000	2,396.2 1,591.2
1,144.9	0.00894	99.000	1,473.6 791.7

<< Systematic Statistics >>

AmDarling2019-Olive Branch, LA-FLOW-ANNUAL PEAK

Log Transform:		Number of Events	
FLOW, CFS			
Mean	3.879	Historic Events	0
Standard Dev	0.348	High Outliers	0
Station Skew	-0.099	Low Outliers	0
Regional Skew	0.187	Zero Events	0
Weighted Skew	-0.042	Missing Events	0
Adopted Skew	-0.042	Systematic Events	75

--- End of Analytical Frequency Curve ---

USGS 07378000 Comite River near Comite, LA

Regional Skew: 0.02

Regional Skew MSE: 0.302

Plotting Position Type: Hirsch-Stedinger

Upper Confidence Level: 0.1

Lower Confidence Level: 0.9

Use non-standard frequencies

Frequency: 0.2

Frequency: 0.5

Frequency: 1.0

Frequency: 2.0

Frequency: 4.0

Frequency: 10.0

Frequency: 20.0

Frequency: 50.0

Frequency: 80.0

Frequency: 90.0

Frequency: 95.0

Frequency: 99.0

Display ordinate values using 1 digits in fraction part of value

--- End of Input Data ---

<< EMA Representation of Data >>

AmDarling2019-Comite, LA-FLOW-ANNUAL PEAK

Year	Peak	Value		Threshold		Type
		Low	High	Low	High	

1944	3,440.0	3,440.0	3,440.0	3,440.0	1.0E99	Syst	
1945	4,820.0	4,820.0	4,820.0	3,440.0	1.0E99	Syst	
1946	6,010.0	6,010.0	6,010.0	3,440.0	1.0E99	Syst	
1947	10,600.0	10,600.0	10,600.0	3,440.0	1.0E99	Syst	
1948	10,000.0	10,000.0	10,000.0	3,440.0	1.0E99	Syst	
1949	10,300.0	10,300.0	10,300.0	3,440.0	1.0E99	Syst	
1950	10,100.0	10,100.0	10,100.0	3,440.0	1.0E99	Syst	
1951	11,500.0	11,500.0	11,500.0	3,440.0	1.0E99	Syst	
1952	3,630.0	3,630.0	3,630.0	3,440.0	1.0E99	Syst	
1953	20,500.0	20,500.0	20,500.0	3,440.0	1.0E99	Syst	
1954	7,150.0	7,150.0	7,150.0	3,440.0	1.0E99	Syst	
1955	10,900.0	10,900.0	10,900.0	3,440.0	1.0E99	Syst	
1956	9,450.0	9,450.0	9,450.0	3,440.0	1.0E99	Syst	
1957	4,320.0	4,320.0	4,320.0	3,440.0	1.0E99	Syst	
1958	5,000.0	5,000.0	5,000.0	3,440.0	1.0E99	Syst	
1959	6,360.0	6,360.0	6,360.0	3,440.0	1.0E99	Syst	
1960	6,950.0	6,950.0	6,950.0	3,440.0	1.0E99	Syst	
1961	15,200.0	15,200.0	15,200.0	3,440.0	1.0E99	Syst	
1962	20,900.0	20,900.0	20,900.0	3,440.0	1.0E99	Syst	
1963	2,420.0	1.0E-6	3,440.0	3,440.0	1.0E99	Syst	
1964	15,400.0	15,400.0	15,400.0	3,440.0	1.0E99	Syst	
1965	20,100.0	20,100.0	20,100.0	3,440.0	1.0E99	Syst	
1966	13,200.0	13,200.0	13,200.0	3,440.0	1.0E99	Syst	
1967	17,600.0	17,600.0	17,600.0	3,440.0	1.0E99	Syst	
1968	2,360.0	1.0E-6	3,440.0	3,440.0	1.0E99	Syst	
1969	12,700.0	12,700.0	12,700.0	3,440.0	1.0E99	Syst	
1970	13,800.0	13,800.0	13,800.0	3,440.0	1.0E99	Syst	
1971	7,310.0	7,310.0	7,310.0	3,440.0	1.0E99	Syst	
1972	16,500.0	16,500.0	16,500.0	3,440.0	1.0E99	Syst	
1973	14,500.0	14,500.0	14,500.0	3,440.0	1.0E99	Syst	
1974	9,210.0	9,210.0	9,210.0	3,440.0	1.0E99	Syst	
1975	10,800.0	10,800.0	10,800.0	3,440.0	1.0E99	Syst	
1976	9,660.0	9,660.0	9,660.0	3,440.0	1.0E99	Syst	
1977	24,100.0	24,100.0	24,100.0	3,440.0	1.0E99	Syst	
1978	16,400.0	16,400.0	16,400.0	3,440.0	1.0E99	Syst	
1979	23,900.0	23,900.0	23,900.0	3,440.0	1.0E99	Syst	
1980	20,700.0	20,700.0	20,700.0	3,440.0	1.0E99	Syst	
1981	7,250.0	7,250.0	7,250.0	3,440.0	1.0E99	Syst	
1982	8,530.0	8,530.0	8,530.0	3,440.0	1.0E99	Syst	
1983	37,000.0	37,000.0	37,000.0	3,440.0	1.0E99	Syst	
1984	10,300.0	10,300.0	10,300.0	3,440.0	1.0E99	Syst	
1985	17,000.0	17,000.0	17,000.0	3,440.0	1.0E99	Syst	
1986	11,600.0	11,600.0	11,600.0	3,440.0	1.0E99	Syst	
1987	11,900.0	11,900.0	11,900.0	3,440.0	1.0E99	Syst	
1988	18,800.0	18,800.0	18,800.0	3,440.0	1.0E99	Syst	
1989	15,600.0	15,600.0	15,600.0	3,440.0	1.0E99	Syst	
1990	23,400.0	23,400.0	23,400.0	3,440.0	1.0E99	Syst	
1991	13,600.0	13,600.0	13,600.0	3,440.0	1.0E99	Syst	
1992	23,100.0	23,100.0	23,100.0	3,440.0	1.0E99	Syst	
1993	30,400.0	30,400.0	30,400.0	3,440.0	1.0E99	Syst	
1994	14,600.0	14,600.0	14,600.0	3,440.0	1.0E99	Syst	
1995	21,500.0	21,500.0	21,500.0	3,440.0	1.0E99	Syst	
1996	19,600.0	19,600.0	19,600.0	3,440.0	1.0E99	Syst	
1997	20,500.0	20,500.0	20,500.0	3,440.0	1.0E99	Syst	
1998	17,300.0	17,300.0	17,300.0	3,440.0	1.0E99	Syst	
1999	12,600.0	12,600.0	12,600.0	3,440.0	1.0E99	Syst	
2000	5,110.0	5,110.0	5,110.0	3,440.0	1.0E99	Syst	
2001	23,200.0	23,200.0	23,200.0	3,440.0	1.0E99	Syst	
2002	7,900.0	7,900.0	7,900.0	3,440.0	1.0E99	Syst	
2003	19,100.0	19,100.0	19,100.0	3,440.0	1.0E99	Syst	
2004	20,000.0	20,000.0	20,000.0	3,440.0	1.0E99	Syst	
2005	13,300.0	13,300.0	13,300.0	3,440.0	1.0E99	Syst	

2006	2,440.0		1.0E-6	3,440.0		3,440.0	1.0E99		Syst	
2007	21,300.0		21,300.0	21,300.0		3,440.0	1.0E99		Syst	
2008	23,800.0		23,800.0	23,800.0		3,440.0	1.0E99		Syst	
2009	13,700.0		13,700.0	13,700.0		3,440.0	1.0E99		Syst	
2010	9,560.0		9,560.0	9,560.0		3,440.0	1.0E99		Syst	
2011	9,570.0		9,570.0	9,570.0		3,440.0	1.0E99		Syst	
2012	10,000.0		10,000.0	10,000.0		3,440.0	1.0E99		Syst	
2013	11,300.0		11,300.0	11,300.0		3,440.0	1.0E99		Syst	
2014	9,100.0		9,100.0	9,100.0		3,440.0	1.0E99		Syst	
2015	9,420.0		9,420.0	9,420.0		3,440.0	1.0E99		Syst	
2016	71,000.0		71,000.0	71,000.0		3,440.0	1.0E99		Syst	
----- ----- ----- ----- -----										

Fitted log10 Moments				Mean	Variance
Std Dev	Skew				

EMA at-site data w/o regional info				4.074185	
0.076078	0.275823	-0.492743			
EMA w/ regional info and B17b MSE(G)				4.074864	
0.074975	0.273815	-0.325940			
EMA w/ regional info and specified MSE(G)				4.074864	
0.074975	0.273815	-0.325940			

EMA Estimate of MSE[G at-site]	0.101976
MSE[G at-site systematic]	0.101976
Effective Record Length [G at-site]	73.000000
Grubbs-Beck Critical Value	3,440.000000

--- Final Results ---

<< Plotting Positions >>

AmDarling2019-Comite, LA-FLOW-ANNUAL PEAK

Events Analyzed				Ordered Events					
FLOW				Water		FLOW		H-S	
Day	Mon	Year	CFS	Rank	Year	CFS	Plot	Pos	
25	Apr	1944	3,440.0	1	2016	71,000.0		1.35	
01	May	1945	4,820.0	2	1983	37,000.0		2.70	
16	May	1946	6,010.0	3	1993	30,400.0		4.05	
14	Mar	1947	10,600.0	4	1977	24,100.0		5.40	
04	Mar	1948	10,000.0	5	1979	23,900.0		6.75	
24	Mar	1949	10,300.0	6	2008	23,800.0		8.10	
08	Jan	1950	10,100.0	7	1990	23,400.0		9.45	
30	Mar	1951	11,500.0	8	2001	23,200.0		10.80	

05 Apr 1952	3,630.0	9	1992	23,100.0	12.16	
19 May 1953	20,500.0	10	1995	21,500.0	13.51	
10 Dec 1953	7,150.0	11	2007	21,300.0	14.86	
15 Apr 1955	10,900.0	12	1962	20,900.0	16.21	
13 Mar 1956	9,450.0	13	1980	20,700.0	17.56	
05 Apr 1957	4,320.0	14	1997	20,500.0	18.91	
24 Mar 1958	5,000.0	15	1953	20,500.0	20.26	
03 Feb 1959	6,360.0	16	1965	20,100.0	21.61	
18 Dec 1959	6,950.0	17	2004	20,000.0	22.96	
19 Mar 1961	15,200.0	18	1996	19,600.0	24.31	
29 Apr 1962	20,900.0	19	2003	19,100.0	25.66	
21 Jan 1963	2,420.0	20	1988	18,800.0	27.01	
04 Mar 1964	15,400.0	21	1967	17,600.0	28.36	
06 Oct 1964	20,100.0	22	1998	17,300.0	29.71	
12 Feb 1966	13,200.0	23	1985	17,000.0	31.06	
14 Apr 1967	17,600.0	24	1972	16,500.0	32.41	
23 Mar 1968	2,360.0	25	1978	16,400.0	33.76	
13 Apr 1969	12,700.0	26	1989	15,600.0	35.11	
07 Oct 1969	13,800.0	27	1964	15,400.0	36.47	
17 Sep 1971	7,310.0	28	1961	15,200.0	37.82	
08 Dec 1971	16,500.0	29	1994	14,600.0	39.17	
26 Mar 1973	14,500.0	30	1973	14,500.0	40.52	
20 Jan 1974	9,210.0	31	1970	13,800.0	41.87	
08 Jan 1975	10,800.0	32	2009	13,700.0	43.22	
26 Mar 1976	9,660.0	33	1991	13,600.0	44.57	
23 Apr 1977	24,100.0	34	2005	13,300.0	45.92	
01 Dec 1977	16,400.0	35	1966	13,200.0	47.27	
23 Apr 1979	23,900.0	36	1969	12,700.0	48.62	
29 Mar 1980	20,700.0	37	1999	12,600.0	49.97	
05 May 1981	7,250.0	38	1987	11,900.0	51.32	
16 Feb 1982	8,530.0	39	1986	11,600.0	52.67	
07 Apr 1983	37,000.0	40	1951	11,500.0	54.02	
11 Dec 1983	10,300.0	41	2013	11,300.0	55.37	
23 Oct 1984	17,000.0	42	1955	10,900.0	56.72	
31 Oct 1985	11,600.0	43	1975	10,800.0	58.07	
12 Aug 1987	11,900.0	44	1947	10,600.0	59.43	
03 Apr 1988	18,800.0	45	1984	10,300.0	60.78	
28 Jun 1989	15,600.0	46	1949	10,300.0	62.13	
26 Jan 1990	23,400.0	47	1950	10,100.0	63.48	
20 Feb 1991	13,600.0	48	2012	10,000.0	64.83	
07 Mar 1992	23,100.0	49	1948	10,000.0	66.18	
21 Jan 1993	30,400.0	50	1976	9,660.0	67.53	
29 Jan 1994	14,600.0	51	2011	9,570.0	68.88	
12 Apr 1995	21,500.0	52	2010	9,560.0	70.23	
19 Dec 1995	19,600.0	53	1956	9,450.0	71.58	
28 Apr 1997	20,500.0	54	2015	9,420.0	72.93	
08 Jan 1998	17,300.0	55	1974	9,210.0	74.28	
15 Mar 1999	12,600.0	56	2014	9,100.0	75.63	
06 May 2000	5,110.0	57	1982	8,530.0	76.98	
09 Jun 2001	23,200.0	58	2002	7,900.0	78.33	
10 Apr 2002	7,900.0	59	1971	7,310.0	79.68	
22 Feb 2003	19,100.0	60	1981	7,250.0	81.03	

	16 May 2004	20,000.0		61	1954	7,150.0	82.38	
	01 Feb 2005	13,300.0		62	1960	6,950.0	83.74	
	30 Apr 2006	2,440.0		63	1959	6,360.0	85.09	
	28 Oct 2006	21,300.0		64	1946	6,010.0	86.44	
	04 Sep 2008	23,800.0		65	2000	5,110.0	87.79	
	29 Mar 2009	13,700.0		66	1958	5,000.0	89.14	
	05 Feb 2010	9,560.0		67	1945	4,820.0	90.49	
	09 Mar 2011	9,570.0		68	1957	4,320.0	91.84	
	19 Feb 2012	10,000.0		69	1952	3,630.0	93.19	
	09 Jan 2013	11,300.0		70	1944	3,440.0	94.54	
	22 Feb 2014	9,100.0		71	2006	2,440.0*	96.32	
	03 Mar 2015	9,420.0		72	1963	2,420.0*	97.68	
	14 Aug 2016	71,000.0		73	1968	2,360.0*	99.05	

* Outlier

* Low outlier plotting positions are computed using Median parameters.

<< Frequency Curve >>

AmDarling2019-Comite, LA-FLOW-ANNUAL PEAK

	Computed	Variance		Percent		Confidence Limits	
	Curve	Log (EMA)		Chance		0.10 0.90	
	FLOW, CFS			Exceedance		FLOW, CFS	

	56,983.6	0.00823		0.200		78,785.7 45,254.0	
	49,707.3	0.00577		0.500		65,066.4 40,921.6	
	44,224.1	0.00426		1.000		55,645.6 37,357.7	
	38,752.6	0.00306		2.000		46,971.7 33,513.4	
	33,279.5	0.00217		4.000		38,977.6 29,357.3	
	25,991.8	0.00143		10.000		29,339.0 23,350.9	
	20,350.1	0.00117		20.000		22,591.8 18,409.4	
	12,294.6	0.00115		50.000		13,591.4 11,098.3	
	7,076.4	0.00171		80.000		7,935.6 6,177.5	
	5,197.5	0.00268		90.000		5,949.1 4,318.5	
	3,986.3	0.00425		95.000		4,687.9 3,112.8	
	2,361.3	0.01046		99.000		3,005.4 1,564.6	

<< Systematic Statistics >>

AmDarling2019-Comite, LA-FLOW-ANNUAL PEAK

	Log Transform:			
	FLOW, CFS		Number of Events	

	Mean	4.075	Historic Events	0
	Standard Dev	0.274	High Outliers	0
	Station Skew	-0.493	Low Outliers	3
	Regional Skew	0.020	Zero Events	0
	Weighted Skew	-0.326	Missing Events	0

Adopted Skew	-0.326	Systematic Events	73
--------------	--------	-------------------	----

--- End of Analytical Frequency Curve ---

USGS 07376000 Tickfaw River at Holden, LA

Regional Skew: 0.061

Regional Skew MSE: 0.302

Plotting Position Type: Hirsch-Stedinger

Upper Confidence Level: 0.1

Lower Confidence Level: 0.9

Use non-standard frequencies

Frequency: 0.2

Frequency: 0.5

Frequency: 1.0

Frequency: 2.0

Frequency: 4.0

Frequency: 10.0

Frequency: 20.0

Frequency: 50.0

Frequency: 80.0

Frequency: 90.0

Frequency: 95.0

Frequency: 99.0

Display ordinate values using 1 digits in fraction part of value

--- End of Input Data ---

<< EMA Representation of Data >>

AmDarling2019-Holden, LA-FLOW-ANNUAL PEAK

Year	Peak	Value		Threshold		Type
		Low	High	Low	High	
1941	5,740.0	5,740.0	5,740.0	1,260.0	1.0E99	Syst
1942	3,380.0	3,380.0	3,380.0	1,260.0	1.0E99	Syst
1943	9,680.0	9,680.0	9,680.0	1,260.0	1.0E99	Syst
1944	2,340.0	2,340.0	2,340.0	1,260.0	1.0E99	Syst
1945	2,230.0	2,230.0	2,230.0	1,260.0	1.0E99	Syst
1946	3,650.0	3,650.0	3,650.0	1,260.0	1.0E99	Syst
1947	6,640.0	6,640.0	6,640.0	1,260.0	1.0E99	Syst
1948	6,640.0	6,640.0	6,640.0	1,260.0	1.0E99	Syst
1949	6,640.0	6,640.0	6,640.0	1,260.0	1.0E99	Syst
1950	5,740.0	5,740.0	5,740.0	1,260.0	1.0E99	Syst
1951	4,770.0	4,770.0	4,770.0	1,260.0	1.0E99	Syst
1952	1,450.0	1,450.0	1,450.0	1,260.0	1.0E99	Syst
1953	8,400.0	8,400.0	8,400.0	1,260.0	1.0E99	Syst

1954	3,200.0		3,200.0	3,200.0		1,260.0	1.0E99	Syst	
1955	5,180.0		5,180.0	5,180.0		1,260.0	1.0E99	Syst	
1956	4,610.0		4,610.0	4,610.0		1,260.0	1.0E99	Syst	
1957	2,520.0		2,520.0	2,520.0		1,260.0	1.0E99	Syst	
1958	4,170.0		4,170.0	4,170.0		1,260.0	1.0E99	Syst	
1959	4,750.0		4,750.0	4,750.0		1,260.0	1.0E99	Syst	
1960	2,200.0		2,200.0	2,200.0		1,260.0	1.0E99	Syst	
1961	7,820.0		7,820.0	7,820.0		1,260.0	1.0E99	Syst	
1962	14,500.0		14,500.0	14,500.0		1,260.0	1.0E99	Syst	
1963	800.0		1.0E-6	1,260.0		1,260.0	1.0E99	Syst	
1964	6,200.0		6,200.0	6,200.0		1,260.0	1.0E99	Syst	
1965	6,160.0		6,160.0	6,160.0		1,260.0	1.0E99	Syst	
1966	12,900.0		12,900.0	12,900.0		1,260.0	1.0E99	Syst	
1967	12,000.0		12,000.0	12,000.0		1,260.0	1.0E99	Syst	
1968	4,430.0		4,430.0	4,430.0		1,260.0	1.0E99	Syst	
1969	6,170.0		6,170.0	6,170.0		1,260.0	1.0E99	Syst	
1970	1,340.0		1,340.0	1,340.0		1,260.0	1.0E99	Syst	
1971	2,780.0		2,780.0	2,780.0		1,260.0	1.0E99	Syst	
1972	6,570.0		6,570.0	6,570.0		1,260.0	1.0E99	Syst	
1973	11,200.0		11,200.0	11,200.0		1,260.0	1.0E99	Syst	
1974	19,000.0		19,000.0	19,000.0		1,260.0	1.0E99	Syst	
1975	6,020.0		6,020.0	6,020.0		1,260.0	1.0E99	Syst	
1976	1,470.0		1,470.0	1,470.0		1,260.0	1.0E99	Syst	
1977	18,100.0		18,100.0	18,100.0		1,260.0	1.0E99	Syst	
1978	9,100.0		9,100.0	9,100.0		1,260.0	1.0E99	Syst	
1979	17,600.0		17,600.0	17,600.0		1,260.0	1.0E99	Syst	
1980	13,100.0		13,100.0	13,100.0		1,260.0	1.0E99	Syst	
1981	1,710.0		1,710.0	1,710.0		1,260.0	1.0E99	Syst	
1982	2,960.0		2,960.0	2,960.0		1,260.0	1.0E99	Syst	
1983	22,500.0		22,500.0	22,500.0		1,260.0	1.0E99	Syst	
1984	2,500.0		2,500.0	2,500.0		1,260.0	1.0E99	Syst	
1985	3,910.0		3,910.0	3,910.0		1,260.0	1.0E99	Syst	
1986	7,120.0		7,120.0	7,120.0		1,260.0	1.0E99	Syst	
1987	5,870.0		5,870.0	5,870.0		1,260.0	1.0E99	Syst	
1988	6,030.0		6,030.0	6,030.0		1,260.0	1.0E99	Syst	
1989	4,330.0		4,330.0	4,330.0		1,260.0	1.0E99	Syst	
1990	13,500.0		13,500.0	13,500.0		1,260.0	1.0E99	Syst	
1991	7,250.0		7,250.0	7,250.0		1,260.0	1.0E99	Syst	
1992	7,830.0		7,830.0	7,830.0		1,260.0	1.0E99	Syst	
1993	18,300.0		18,300.0	18,300.0		1,260.0	1.0E99	Syst	
1994	12,800.0		12,800.0	12,800.0		1,260.0	1.0E99	Syst	
1995	11,700.0		11,700.0	11,700.0		1,260.0	1.0E99	Syst	
1996	7,950.0		7,950.0	7,950.0		1,260.0	1.0E99	Syst	
1997	6,550.0		6,550.0	6,550.0		1,260.0	1.0E99	Syst	
1998	8,220.0		8,220.0	8,220.0		1,260.0	1.0E99	Syst	
1999	6,680.0		6,680.0	6,680.0		1,260.0	1.0E99	Syst	
2000	435.0		1.0E-6	1,260.0		1,260.0	1.0E99	Syst	
2001	7,640.0		7,640.0	7,640.0		1,260.0	1.0E99	Syst	
2002	4,910.0		4,910.0	4,910.0		1,260.0	1.0E99	Syst	
2003	5,300.0		5,300.0	5,300.0		1,260.0	1.0E99	Syst	
2004	8,680.0		8,680.0	8,680.0		1,260.0	1.0E99	Syst	
2005	4,250.0		4,250.0	4,250.0		1,260.0	1.0E99	Syst	
2006	1,260.0		1,260.0	1,260.0		1,260.0	1.0E99	Syst	
2007	5,340.0		5,340.0	5,340.0		1,260.0	1.0E99	Syst	
2008	5,140.0		5,140.0	5,140.0		1,260.0	1.0E99	Syst	
2009	9,790.0		9,790.0	9,790.0		1,260.0	1.0E99	Syst	
2010	5,880.0		5,880.0	5,880.0		1,260.0	1.0E99	Syst	
2011	10,700.0		10,700.0	10,700.0		1,260.0	1.0E99	Syst	
2012	4,380.0		4,380.0	4,380.0		1,260.0	1.0E99	Syst	
2013	9,660.0		9,660.0	9,660.0		1,260.0	1.0E99	Syst	
2014	3,940.0		3,940.0	3,940.0		1,260.0	1.0E99	Syst	
2015	3,100.0		3,100.0	3,100.0		1,260.0	1.0E99	Syst	
2016	35,800.0		35,800.0	35,800.0		1,260.0	1.0E99	Syst	

2017	5,242.0	5,242.0	5,242.0	1,260.0	1.0E99	Syst
------	---------	---------	---------	---------	--------	------

Fitted log10 Moments			Mean	Variance
Std Dev	Skew			
EMA at-site data w/o regional info			3.751940	
0.104299	0.322953	-0.353858		
EMA w/ regional info and B17b MSE (G)			3.752269	
0.103677	0.321989	-0.243561		
EMA w/ regional info and specified MSE (G)			3.752269	
0.103677	0.321989	-0.243561		

EMA Estimate of MSE[G at-site]	0.088423
MSE[G at-site systematic]	0.088423
Effective Record Length [G at-site]	77.000000
Grubbs-Beck Critical Value	1,260.000000

--- Final Results ---

<< Plotting Positions >>

AmDarling2019-Holden, LA-FLOW-ANNUAL PEAK

Events Analyzed				Ordered Events			
Day	Mon	Year	FLOW CFS	Rank	Water Year	FLOW CFS	H-S Plot Pos
17	Dec	1940	5,740.0	1	2016	35,800.0	1.28
19	Sep	1942	3,380.0	2	1983	22,500.0	2.56
22	Mar	1943	9,680.0	3	1974	19,000.0	3.84
01	Apr	1944	2,340.0	4	1993	18,300.0	5.13
02	May	1945	2,230.0	5	1977	18,100.0	6.41
18	Mar	1946	3,650.0	6	1979	17,600.0	7.69
03	Apr	1947	6,640.0	7	1962	14,500.0	8.97
05	Mar	1948	6,640.0	8	1990	13,500.0	10.25
24	Mar	1949	6,640.0	9	1980	13,100.0	11.53
09	Jun	1950	5,740.0	10	1966	12,900.0	12.82
31	Mar	1951	4,770.0	11	1994	12,800.0	14.10
07	Apr	1952	1,450.0	12	1967	12,000.0	15.38
20	May	1953	8,400.0	13	1995	11,700.0	16.66
06	Dec	1953	3,200.0	14	1973	11,200.0	17.94
04	Aug	1955	5,180.0	15	2011	10,700.0	19.22
14	Mar	1956	4,610.0	16	2009	9,790.0	20.51

21 Sep 1957	2,520.0	17	1943	9,680.0	21.79	
16 Nov 1957	4,170.0	18	2013	9,660.0	23.07	
04 Jun 1959	4,750.0	19	1978	9,100.0	24.35	
07 Feb 1960	2,200.0	20	2004	8,680.0	25.63	
23 Feb 1961	7,820.0	21	1953	8,400.0	26.91	
29 Apr 1962	14,500.0	22	1998	8,220.0	28.20	
26 Feb 1963	800.0	23	1996	7,950.0	29.48	
05 Mar 1964	6,200.0	24	1992	7,830.0	30.76	
07 Oct 1964	6,160.0	25	1961	7,820.0	32.04	
14 Feb 1966	12,900.0	26	2001	7,640.0	33.32	
15 Apr 1967	12,000.0	27	1991	7,250.0	34.60	
12 Apr 1968	4,430.0	28	1986	7,120.0	35.89	
15 Apr 1969	6,170.0	29	1999	6,680.0	37.17	
05 Mar 1970	1,340.0	30	1949	6,640.0	38.45	
20 Sep 1971	2,780.0	31	1948	6,640.0	39.73	
09 Dec 1971	6,570.0	32	1947	6,640.0	41.01	
26 Mar 1973	11,200.0	33	1972	6,570.0	42.29	
23 May 1974	19,000.0	34	1997	6,550.0	43.57	
10 Jan 1975	6,020.0	35	1964	6,200.0	44.86	
27 Mar 1976	1,470.0	36	1969	6,170.0	46.14	
22 Apr 1977	18,100.0	37	1965	6,160.0	47.42	
01 Dec 1977	9,100.0	38	1988	6,030.0	48.70	
23 Apr 1979	17,600.0	39	1975	6,020.0	49.98	
31 Mar 1980	13,100.0	40	2010	5,880.0	51.26	
12 Feb 1981	1,710.0	41	1987	5,870.0	52.55	
20 Feb 1982	2,960.0	42	1950	5,740.0	53.83	
07 Apr 1983	22,500.0	43	1941	5,740.0	55.11	
30 Dec 1983	2,500.0	44	2007	5,340.0	56.39	
28 Feb 1985	3,910.0	45	2003	5,300.0	57.67	
31 Oct 1985	7,120.0	46	2017	5,242.0	58.95	
02 Mar 1987	5,870.0	47	1955	5,180.0	60.24	
04 Apr 1988	6,030.0	48	2008	5,140.0	61.52	
04 Jan 1989	4,330.0	49	2002	4,910.0	62.80	
27 Jan 1990	13,500.0	50	1951	4,770.0	64.08	
12 May 1991	7,250.0	51	1959	4,750.0	65.36	
07 Mar 1992	7,830.0	52	1956	4,610.0	66.64	
22 Jan 1993	18,300.0	53	1968	4,430.0	67.93	
30 Jan 1994	12,800.0	54	2012	4,380.0	69.21	
13 Apr 1995	11,700.0	55	1989	4,330.0	70.49	
21 Dec 1995	7,950.0	56	2005	4,250.0	71.77	
27 Feb 1997	6,550.0	57	1958	4,170.0	73.05	
08 Jan 1998	8,220.0	58	2014	3,940.0	74.33	
15 Mar 1999	6,680.0	59	1985	3,910.0	75.62	
14 Sep 2000	435.0	60	1946	3,650.0	76.90	
08 Jun 2001	7,640.0	61	1942	3,380.0	78.18	
29 Sep 2002	4,910.0	62	1954	3,200.0	79.46	
10 Apr 2003	5,300.0	63	2015	3,100.0	80.74	
17 May 2004	8,680.0	64	1982	2,960.0	82.02	
03 Feb 2005	4,250.0	65	1971	2,780.0	83.30	
28 Feb 2006	1,260.0	66	1957	2,520.0	84.59	
02 Jan 2007	5,340.0	67	1984	2,500.0	85.87	
04 Sep 2008	5,140.0	68	1944	2,340.0	87.15	

30 Mar 2009	9,790.0	69	1945	2,230.0	88.43	
20 Dec 2009	5,880.0	70	1960	2,200.0	89.71	
11 Mar 2011	10,700.0	71	1981	1,710.0	90.99	
01 Sep 2012	4,380.0	72	1976	1,470.0	92.28	
11 Jan 2013	9,660.0	73	1952	1,450.0	93.56	
24 Feb 2014	3,940.0	74	1970	1,340.0	94.84	
07 Jan 2015	3,100.0	75	2006	1,260.0	96.12	
13 Aug 2016	35,800.0	76	1963	800.0*	97.80	
23 Jan 2017	5,242.0	77	2000	435.0*	99.10	
----- -----						

* Outlier

* Low outlier plotting positions are computed using Median parameters.

<< Frequency Curve >>

AmDarling2019-Holden, LA-FLOW-ANNUAL PEAK

Computed	Variance	Percent	Confidence Limits	
Curve	Log (EMA)	Chance	0.10	0.90
FLOW, CFS		Exceedance	FLOW, CFS	
-----		-----	-----	
38,413.3	0.01190	0.200	56,915.7	29,208.1
32,211.1	0.00833	0.500	44,674.5	25,574.4
27,749.5	0.00615	1.000	36,685.6	22,721.2
23,484.8	0.00441	2.000	29,664.8	19,776.4
19,413.0	0.00311	4.000	23,510.6	16,742.5
14,309.0	0.00202	10.000	16,548.8	12,621.4
10,625.9	0.00161	20.000	12,022.4	9,458.3
5,825.4	0.00152	50.000	6,537.0	5,182.9
3,060.4	0.00213	80.000	3,480.5	2,633.7
2,148.5	0.00326	90.000	2,495.3	1,756.2
1,589.7	0.00510	95.000	1,899.9	1,216.9
883.3	0.01241	99.000	1,150.2	567.7
-----		-----	-----	

<< Systematic Statistics >>

AmDarling2019-Holden, LA-FLOW-ANNUAL PEAK

Log Transform:		Number of Events	
FLOW, CFS			
Mean	3.752	Historic Events	0
Standard Dev	0.322	High Outliers	0
Station Skew	-0.354	Low Outliers	2
Regional Skew	0.061	Zero Events	0
Weighted Skew	-0.244	Missing Events	0
Adopted Skew	-0.244	Systematic Events	77

--- End of Analytical Frequency Curve ---

USGS 07373550 MOORES BRANCH NR WOODVILLE, MS

Regional Skew: -0.025

Regional Skew MSE: 0.3025

Plotting Position Type: Hirsch-Stedinger

Upper Confidence Level: 0.1

Lower Confidence Level: 0.9

Use non-standard frequencies

Frequency: 0.2

Frequency: 0.5

Frequency: 1.0

Frequency: 2.0

Frequency: 4.0

Frequency: 10.0

Frequency: 20.0

Frequency: 50.0

Frequency: 80.0

Frequency: 90.0

Frequency: 95.0

Frequency: 99.0

Display ordinate values using 1 digits in fraction part of value

--- End of Input Data ---

<< EMA Representation of Data >>

MOORES BRANCH-WOODVILLE, MS-FLOW-ANNUAL PEAK

		Value		Threshold		Type
Year	Peak	Low	High	Low	High	
1955	416.0	416.0	416.0	1.0E-99	1.0E99	Hist
1956	---	1.0E-99	416.0	416.0	1.0E99	Cens
1957	100.0	100.0	100.0	1.0E-99	1.0E99	Syst
1958	200.0	200.0	200.0	1.0E-99	1.0E99	Syst
1959	138.0	138.0	138.0	1.0E-99	1.0E99	Syst
1960	178.0	178.0	178.0	1.0E-99	1.0E99	Syst
1961	206.0	206.0	206.0	1.0E-99	1.0E99	Syst
1962	353.0	353.0	353.0	1.0E-99	1.0E99	Syst
1963	260.0	260.0	260.0	1.0E-99	1.0E99	Syst
1964	202.0	202.0	202.0	1.0E-99	1.0E99	Syst
1965	193.0	193.0	193.0	1.0E-99	1.0E99	Syst
1966	182.0	182.0	182.0	1.0E-99	1.0E99	Syst
1967	241.0	241.0	241.0	1.0E-99	1.0E99	Syst
1968	246.0	246.0	246.0	1.0E-99	1.0E99	Syst
1969	66.0	66.0	66.0	1.0E-99	1.0E99	Syst
1970	120.0	120.0	120.0	1.0E-99	1.0E99	Syst
1971	110.0	110.0	110.0	1.0E-99	1.0E99	Syst
1972	346.0	346.0	346.0	1.0E-99	1.0E99	Syst

1973	455.0		455.0	455.0		1.0E-99	1.0E99	Syst	
1974	225.0		225.0	225.0		1.0E-99	1.0E99	Syst	
1975	354.0		354.0	354.0		1.0E-99	1.0E99	Syst	
1976	180.0		180.0	180.0		1.0E-99	1.0E99	Syst	
1977	224.0		224.0	224.0		1.0E-99	1.0E99	Syst	
1978	330.0		330.0	330.0		1.0E-99	1.0E99	Syst	
1979	148.0		148.0	148.0		1.0E-99	1.0E99	Syst	
1980	255.0		255.0	255.0		1.0E-99	1.0E99	Syst	
1981	264.0		264.0	264.0		1.0E-99	1.0E99	Syst	
1982	215.0		215.0	215.0		1.0E-99	1.0E99	Syst	
1983	423.0		423.0	423.0		1.0E-99	1.0E99	Syst	
1984	198.0		198.0	198.0		1.0E-99	1.0E99	Syst	
1985	360.0		360.0	360.0		1.0E-99	1.0E99	Syst	
1986	167.0		167.0	167.0		1.0E-99	1.0E99	Syst	
1987	218.0		218.0	218.0		1.0E-99	1.0E99	Syst	
1988	126.0		126.0	126.0		1.0E-99	1.0E99	Syst	
1989	257.0		257.0	257.0		1.0E-99	1.0E99	Syst	
1990	235.0		235.0	235.0		1.0E-99	1.0E99	Syst	
1991	138.0		138.0	138.0		1.0E-99	1.0E99	Syst	
1992	224.0		224.0	224.0		1.0E-99	1.0E99	Syst	
1993	345.0		345.0	345.0		1.0E-99	1.0E99	Syst	
1994	360.0		360.0	360.0		1.0E-99	1.0E99	Syst	
1995	223.0		223.0	223.0		1.0E-99	1.0E99	Syst	
1996	248.0		248.0	248.0		1.0E-99	1.0E99	Syst	
1997	138.0		138.0	138.0		1.0E-99	1.0E99	Syst	
1998	130.0		130.0	130.0		1.0E-99	1.0E99	Syst	
1999	254.0		254.0	254.0		1.0E-99	1.0E99	Syst	
2000	114.0		114.0	114.0		1.0E-99	1.0E99	Syst	
2001	121.0		121.0	121.0		1.0E-99	1.0E99	Syst	
2002	370.0		370.0	370.0		1.0E-99	1.0E99	Syst	
2003	131.0		131.0	131.0		1.0E-99	1.0E99	Syst	
2004	218.0		218.0	218.0		1.0E-99	1.0E99	Syst	
2005	220.0		220.0	220.0		1.0E-99	1.0E99	Syst	
2006	131.0		131.0	131.0		1.0E-99	1.0E99	Syst	
2007	178.0		178.0	178.0		1.0E-99	1.0E99	Syst	
2008	130.0		130.0	130.0		1.0E-99	1.0E99	Syst	
2009	283.0		283.0	283.0		1.0E-99	1.0E99	Syst	
2010	137.0		137.0	137.0		1.0E-99	1.0E99	Syst	
2011	132.0		132.0	132.0		1.0E-99	1.0E99	Syst	
2012	148.0		148.0	148.0		1.0E-99	1.0E99	Syst	
2013	177.0		177.0	177.0		1.0E-99	1.0E99	Syst	
2014	191.0		191.0	191.0		1.0E-99	1.0E99	Syst	
2015	158.0		158.0	158.0		1.0E-99	1.0E99	Syst	
2016	272.0		272.0	272.0		1.0E-99	1.0E99	Syst	
2017	310.0		310.0	310.0		1.0E-99	1.0E99	Syst	

Fitted log10 Moments			Mean	Variance
Std Dev	Skew			
EMA at-site data w/o regional info			2.308364	
0.031434	0.177295	-0.137544		
EMA w/ regional info and B17b MSE (G)			2.308358	
0.031431	0.177288	-0.111338		
EMA w/ regional info and specified MSE (G)			2.308358	
0.031431	0.177288	-0.111164		

```

-----
EMA Estimate of MSE[G at-site]          0.091613
MSE[G at-site systematic]              0.093514
Effective Record Length [G at-site]    62.266299
Grubbs-Beck Critical Value             0.000000

```

--- Final Results ---

<< Plotting Positions >>

MOORES BRANCH-WOODVILLE, MS-FLOW-ANNUAL PEAK

Events Analyzed				Ordered Events			
				Water	FLOW	H-S	
Day	Mon	Year	CFS	Year	CFS	Plot	Pos
12	Apr	1955	416.0	1973	455.0	1.19	
01	Jan	1956	---	1983	423.0	2.38	
22	Dec	1956	100.0	1955	416.0	3.57	
13	Nov	1957	200.0	2002	370.0	6.35	
24	Jul	1959	138.0	1994	360.0	7.94	
17	Dec	1959	178.0	1985	360.0	9.52	
17	Mar	1961	206.0	1975	354.0	11.11	
13	Nov	1961	353.0	1962	353.0	12.70	
20	Jan	1963	260.0	1972	346.0	14.29	
02	Mar	1964	202.0	1993	345.0	15.87	
01	Mar	1965	193.0	1978	330.0	17.46	
18	Sep	1966	182.0	2017	310.0	19.05	
14	Apr	1967	241.0	2009	283.0	20.63	
07	Jun	1968	246.0	2016	272.0	22.22	
01	Dec	1968	66.0	1981	264.0	23.81	
02	Jun	1970	120.0	1963	260.0	25.40	
16	Sep	1971	110.0	1989	257.0	26.98	
02	Mar	1972	346.0	1980	255.0	28.57	
24	Mar	1973	455.0	1999	254.0	30.16	
13	Apr	1974	225.0	1996	248.0	31.75	
06	May	1975	354.0	1968	246.0	33.33	
30	Jun	1976	180.0	1967	241.0	34.92	
03	Mar	1977	224.0	1990	235.0	36.51	
30	Nov	1977	330.0	1974	225.0	38.10	
20	Jan	1979	148.0	1992	224.0	39.68	
11	Jan	1980	255.0	1977	224.0	41.27	
04	Mar	1981	264.0	1995	223.0	42.86	
16	Feb	1982	215.0	2005	220.0	44.44	
01	Feb	1983	423.0	2004	218.0	46.03	
23	Nov	1983	198.0	1987	218.0	47.62	
22	Oct	1984	360.0	1982	215.0	49.21	
30	Oct	1985	167.0	1961	206.0	50.79	

18 Mar 1987	218.0	33	1964	202.0	52.38	
25 Mar 1988	126.0	34	1958	200.0	53.97	
27 Jun 1989	257.0	35	1984	198.0	55.56	
15 Feb 1990	235.0	36	1965	193.0	57.14	
11 Aug 1991	138.0	37	2014	191.0	58.73	
05 Mar 1992	224.0	38	1966	182.0	60.32	
20 Jan 1993	345.0	39	1976	180.0	61.90	
27 Jan 1994	360.0	40	2007	178.0	63.49	
23 Apr 1995	223.0	41	1960	178.0	65.08	
18 Dec 1995	248.0	42	2013	177.0	66.67	
27 Apr 1997	138.0	43	1986	167.0	68.25	
22 Jan 1998	130.0	44	2015	158.0	69.84	
30 Jan 1999	254.0	45	2012	148.0	71.43	
03 Apr 2000	114.0	46	1979	148.0	73.02	
19 Jan 2001	121.0	47	1997	138.0	74.60	
26 Mar 2002	370.0	48	1991	138.0	76.19	
22 Feb 2003	131.0	49	1959	138.0	77.78	
14 May 2004	218.0	50	2010	137.0	79.37	
09 Dec 2004	220.0	51	2011	132.0	80.95	
15 Dec 2005	131.0	52	2006	131.0	82.54	
05 Jan 2007	178.0	53	2003	131.0	84.13	
11 Mar 2008	130.0	54	2008	130.0	85.71	
27 Mar 2009	283.0	55	1998	130.0	87.30	
16 Oct 2009	137.0	56	1988	126.0	88.89	
09 Mar 2011	132.0	57	2001	121.0	90.48	
04 Apr 2012	148.0	58	1970	120.0	92.06	
11 Feb 2013	177.0	59	2000	114.0	93.65	
28 Mar 2014	191.0	60	1971	110.0	95.24	
05 Apr 2015	158.0	61	1957	100.0	96.83	
03 Feb 2016	272.0	62	1969	66.0	98.41	
03 Apr 2017	310.0	63	1956	---	---	

* Low outlier plotting positions are computed using Median parameters.

<< Frequency Curve >>

MOORES BRANCH-WOODVILLE, MS-FLOW-ANNUAL PEAK

Computed	Variance	Percent	Confidence Limits
Curve	Log (EMA)	Chance	0.10 0.90
FLOW, CFS		Exceedance	FLOW, CFS
623.4	0.00486	0.200	805.0 524.3
557.8	0.00344	0.500	691.1 481.7
508.4	0.00257	1.000	611.0 447.5
459.0	0.00186	2.000	535.7 411.0
409.1	0.00132	4.000	464.6 371.9
341.5	0.00084	10.000	375.7 315.2
287.4	0.00064	20.000	311.0 267.2
204.9	0.00057	50.000	220.0 190.9
144.6	0.00073	80.000	156.1 132.7

	120.0	0.00102		90.000		130.9	107.7	
	102.6	0.00150		95.000		113.5	89.5	
	76.1	0.00336		99.000		87.8	61.2	
	-----			-----			-----	

<< Systematic Statistics >>

MOORES BRANCH-WOODVILLE, MS-FLOW-ANNUAL PEAK

	Log Transform:			Number of Events		
	FLOW, CFS					
	-----			-----		
	Mean	2.308		Historic Events	1	
	Standard Dev	0.177		High Outliers	0	
	Station Skew	-0.138		Low Outliers	0	
	Regional Skew	-0.025		Zero Events	0	
	Weighted Skew	-0.111		Missing Events	1	
	Adopted Skew	-0.111		Systematic Events	61	
				Historic Period	63	
	-----			-----		

--- End of Analytical Frequency Curve ---

USGS 07375500 Tangipahoa River at Robert, LA

Regional Skew: 0.091

Regional Skew MSE: 0.302

Plotting Position Type: Hirsch-Stedinger

Upper Confidence Level: 0.1

Lower Confidence Level: 0.9

Use non-standard frequencies

Frequency: 0.2

Frequency: 0.5

Frequency: 1.0

Frequency: 2.0

Frequency: 4.0

Frequency: 10.0

Frequency: 20.0

Frequency: 50.0

Frequency: 80.0

Frequency: 90.0

Frequency: 95.0

Frequency: 99.0

Display ordinate values using 1 digits in fraction part of value

--- End of Input Data ---

<< EMA Representation of Data >>

AmDarling2019-Robert, LA-FLOW-ANNUAL PEAK

Year	Peak	Value		Threshold		Type
		Low	High	Low	High	
1939	6,000.0	6,000.0	6,000.0	1.0E-99	1.0E99	Syst
1940	7,690.0	7,690.0	7,690.0	1.0E-99	1.0E99	Syst
1941	11,200.0	11,200.0	11,200.0	1.0E-99	1.0E99	Syst
1942	6,250.0	6,250.0	6,250.0	1.0E-99	1.0E99	Syst
1943	35,500.0	35,500.0	35,500.0	1.0E-99	1.0E99	Syst
1944	8,860.0	8,860.0	8,860.0	1.0E-99	1.0E99	Syst
1945	5,920.0	5,920.0	5,920.0	1.0E-99	1.0E99	Syst
1946	9,410.0	9,410.0	9,410.0	1.0E-99	1.0E99	Syst
1947	18,200.0	18,200.0	18,200.0	1.0E-99	1.0E99	Syst
1948	24,000.0	24,000.0	24,000.0	1.0E-99	1.0E99	Syst
1949	27,700.0	27,700.0	27,700.0	1.0E-99	1.0E99	Syst
1950	14,300.0	14,300.0	14,300.0	1.0E-99	1.0E99	Syst
1951	11,500.0	11,500.0	11,500.0	1.0E-99	1.0E99	Syst
1952	2,800.0	2,800.0	2,800.0	1.0E-99	1.0E99	Syst
1953	50,500.0	50,500.0	50,500.0	1.0E-99	1.0E99	Syst
1954	12,400.0	12,400.0	12,400.0	1.0E-99	1.0E99	Syst
1955	13,200.0	13,200.0	13,200.0	1.0E-99	1.0E99	Syst
1956	11,900.0	11,900.0	11,900.0	1.0E-99	1.0E99	Syst
1957	7,690.0	7,690.0	7,690.0	1.0E-99	1.0E99	Syst
1958	9,540.0	9,540.0	9,540.0	1.0E-99	1.0E99	Syst
1959	11,500.0	11,500.0	11,500.0	1.0E-99	1.0E99	Syst
1960	5,770.0	5,770.0	5,770.0	1.0E-99	1.0E99	Syst
1961	38,200.0	38,200.0	38,200.0	1.0E-99	1.0E99	Syst
1962	30,100.0	30,100.0	30,100.0	1.0E-99	1.0E99	Syst
1963	2,040.0	2,040.0	2,040.0	1.0E-99	1.0E99	Syst
1964	15,400.0	15,400.0	15,400.0	1.0E-99	1.0E99	Syst
1965	14,800.0	14,800.0	14,800.0	1.0E-99	1.0E99	Syst
1966	30,800.0	30,800.0	30,800.0	1.0E-99	1.0E99	Syst
1967	28,100.0	28,100.0	28,100.0	1.0E-99	1.0E99	Syst
1968	4,730.0	4,730.0	4,730.0	1.0E-99	1.0E99	Syst
1969	18,200.0	18,200.0	18,200.0	1.0E-99	1.0E99	Syst
1970	3,680.0	3,680.0	3,680.0	1.0E-99	1.0E99	Syst
1971	18,500.0	18,500.0	18,500.0	1.0E-99	1.0E99	Syst
1972	18,400.0	18,400.0	18,400.0	1.0E-99	1.0E99	Syst
1973	37,900.0	37,900.0	37,900.0	1.0E-99	1.0E99	Syst
1974	39,500.0	39,500.0	39,500.0	1.0E-99	1.0E99	Syst
1975	15,700.0	15,700.0	15,700.0	1.0E-99	1.0E99	Syst
1976	4,010.0	4,010.0	4,010.0	1.0E-99	1.0E99	Syst
1977	33,600.0	33,600.0	33,600.0	1.0E-99	1.0E99	Syst
1978	13,800.0	13,800.0	13,800.0	1.0E-99	1.0E99	Syst
1979	26,300.0	26,300.0	26,300.0	1.0E-99	1.0E99	Syst
1980	35,300.0	35,300.0	35,300.0	1.0E-99	1.0E99	Syst
1981	10,800.0	10,800.0	10,800.0	1.0E-99	1.0E99	Syst
1982	7,190.0	7,190.0	7,190.0	1.0E-99	1.0E99	Syst
1983	85,000.0	85,000.0	85,000.0	1.0E-99	1.0E99	Syst
1984	11,800.0	11,800.0	11,800.0	1.0E-99	1.0E99	Syst
1985	11,800.0	11,800.0	11,800.0	1.0E-99	1.0E99	Syst
1986	9,570.0	9,570.0	9,570.0	1.0E-99	1.0E99	Syst
1987	20,800.0	20,800.0	20,800.0	1.0E-99	1.0E99	Syst
1988	21,400.0	21,400.0	21,400.0	1.0E-99	1.0E99	Syst
1989	14,800.0	14,800.0	14,800.0	1.0E-99	1.0E99	Syst
1990	36,200.0	36,200.0	36,200.0	1.0E-99	1.0E99	Syst
1991	14,700.0	14,700.0	14,700.0	1.0E-99	1.0E99	Syst

1992	17,700.0		17,700.0	17,700.0		1.0E-99	1.0E99		Syst	
1993	37,800.0		37,800.0	37,800.0		1.0E-99	1.0E99		Syst	
1994	22,900.0		22,900.0	22,900.0		1.0E-99	1.0E99		Syst	
1995	20,800.0		20,800.0	20,800.0		1.0E-99	1.0E99		Syst	
1996	12,700.0		12,700.0	12,700.0		1.0E-99	1.0E99		Syst	
1997	13,700.0		13,700.0	13,700.0		1.0E-99	1.0E99		Syst	
1998	16,200.0		16,200.0	16,200.0		1.0E-99	1.0E99		Syst	
1999	13,500.0		13,500.0	13,500.0		1.0E-99	1.0E99		Syst	
2000	1,480.0		1,480.0	1,480.0		1.0E-99	1.0E99		Syst	
2001	13,700.0		13,700.0	13,700.0		1.0E-99	1.0E99		Syst	
2002	18,600.0		18,600.0	18,600.0		1.0E-99	1.0E99		Syst	
2003	23,500.0		23,500.0	23,500.0		1.0E-99	1.0E99		Syst	
2004	14,600.0		14,600.0	14,600.0		1.0E-99	1.0E99		Syst	
2005	8,140.0		8,140.0	8,140.0		1.0E-99	1.0E99		Syst	
2006	3,190.0		3,190.0	3,190.0		1.0E-99	1.0E99		Syst	
2007	11,700.0		11,700.0	11,700.0		1.0E-99	1.0E99		Syst	
2008	8,800.0		8,800.0	8,800.0		1.0E-99	1.0E99		Syst	
2009	22,400.0		22,400.0	22,400.0		1.0E-99	1.0E99		Syst	
2010	12,700.0		12,700.0	12,700.0		1.0E-99	1.0E99		Syst	
2011	13,400.0		13,400.0	13,400.0		1.0E-99	1.0E99		Syst	
2012	32,500.0		32,500.0	32,500.0		1.0E-99	1.0E99		Syst	
2013	22,800.0		22,800.0	22,800.0		1.0E-99	1.0E99		Syst	
2014	9,830.0		9,830.0	9,830.0		1.0E-99	1.0E99		Syst	
2015	6,120.0		6,120.0	6,120.0		1.0E-99	1.0E99		Syst	
2016	120,000.0		120,000.0	120,000.0		1.0E-99	1.0E99		Syst	
2017	9,875.0		9,875.0	9,875.0		1.0E-99	1.0E99		Syst	
----- ----- ----- -----										

```
-----
-----
Fitted log10 Moments                                Mean      Variance
Std Dev      Skew
-----
```

```
-----
EMA at-site data w/o regional info                4.150645
0.113722      0.337227      -0.250359
EMA w/ regional info and B17b MSE(G)              4.150645
0.113722      0.337227      -0.178662
EMA w/ regional info and specified MSE(G)         4.150645
0.113722      0.337227      -0.178662
-----
```

```
EMA Estimate of MSE[G at-site]                    0.080295
MSE[G at-site systematic]                          0.080295
Effective Record Length [G at-site]               79.000000
Grubbs-Beck Critical Value                        0.000000
```

--- Final Results ---

<< Plotting Positions >>
AmDarling2019-Robert, LA-FLOW-ANNUAL PEAK

Events Analyzed				Ordered Events			
			FLOW			FLOW	H-S
Day	Mon	Year	CFS	Rank	Water Year	CFS	Plot Pos
06	Jun	1939	6,000.0	1	2016	120,000.0	1.25
02	May	1940	7,690.0	2	1983	85,000.0	2.50
18	Dec	1940	11,200.0	3	1953	50,500.0	3.75
19	Sep	1942	6,250.0	4	1974	39,500.0	5.00
22	Mar	1943	35,500.0	5	1961	38,200.0	6.25
31	Mar	1944	8,860.0	6	1973	37,900.0	7.50
01	May	1945	5,920.0	7	1993	37,800.0	8.75
26	Sep	1946	9,410.0	8	1990	36,200.0	10.00
03	Apr	1947	18,200.0	9	1943	35,500.0	11.25
06	Mar	1948	24,000.0	10	1980	35,300.0	12.50
04	May	1949	27,700.0	11	1977	33,600.0	13.75
14	Feb	1950	14,300.0	12	2012	32,500.0	15.00
31	Mar	1951	11,500.0	13	1966	30,800.0	16.25
05	Apr	1952	2,800.0	14	1962	30,100.0	17.50
03	May	1953	50,500.0	15	1967	28,100.0	18.75
04	Dec	1953	12,400.0	16	1949	27,700.0	20.00
16	Apr	1955	13,200.0	17	1979	26,300.0	21.25
05	Feb	1956	11,900.0	18	1948	24,000.0	22.50
19	Sep	1957	7,690.0	19	2003	23,500.0	23.75
16	Nov	1957	9,540.0	20	1994	22,900.0	25.00
02	Jun	1959	11,500.0	21	2013	22,800.0	26.25
04	Apr	1960	5,770.0	22	2009	22,400.0	27.50
22	Feb	1961	38,200.0	23	1988	21,400.0	28.75
14	Nov	1961	30,100.0	24	1995	20,800.0	30.00
25	Feb	1963	2,040.0	25	1987	20,800.0	31.25
03	Mar	1964	15,400.0	26	2002	18,600.0	32.50
07	Oct	1964	14,800.0	27	1971	18,500.0	33.75
14	Feb	1966	30,800.0	28	1972	18,400.0	35.00
15	Apr	1967	28,100.0	29	1969	18,200.0	36.25
13	May	1968	4,730.0	30	1947	18,200.0	37.50
14	Apr	1969	18,200.0	31	1992	17,700.0	38.75
05	Mar	1970	3,680.0	32	1998	16,200.0	40.00
17	Sep	1971	18,500.0	33	1975	15,700.0	41.25
07	Dec	1971	18,400.0	34	1964	15,400.0	42.50
19	Apr	1973	37,900.0	35	1989	14,800.0	43.75
23	May	1974	39,500.0	36	1965	14,800.0	45.00
15	Apr	1975	15,700.0	37	1991	14,700.0	46.25
26	Mar	1976	4,010.0	38	2004	14,600.0	47.50
22	Apr	1977	33,600.0	39	1950	14,300.0	48.75
01	Dec	1977	13,800.0	40	1978	13,800.0	50.00
23	Apr	1979	26,300.0	41	2001	13,700.0	51.25
31	Mar	1980	35,300.0	42	1997	13,700.0	52.50
11	Feb	1981	10,800.0	43	1999	13,500.0	53.75
18	Feb	1982	7,190.0	44	2011	13,400.0	55.00
07	Apr	1983	85,000.0	45	1955	13,200.0	56.25
29	Dec	1983	11,800.0	46	2010	12,700.0	57.50
27	Feb	1985	11,800.0	47	1996	12,700.0	58.75

	31 Oct 1985	9,570.0		48	1954	12,400.0	60.00	
	28 Feb 1987	20,800.0		49	1956	11,900.0	61.25	
	02 Feb 1988	21,400.0		50	1985	11,800.0	62.50	
	31 Mar 1989	14,800.0		51	1984	11,800.0	63.75	
	27 Jan 1990	36,200.0		52	2007	11,700.0	65.00	
	11 May 1991	14,700.0		53	1959	11,500.0	66.25	
	27 Aug 1992	17,700.0		54	1951	11,500.0	67.50	
	22 Jan 1993	37,800.0		55	1941	11,200.0	68.75	
	30 Jan 1994	22,900.0		56	1981	10,800.0	70.00	
	12 Apr 1995	20,800.0		57	2017	9,875.0	71.25	
	20 Dec 1995	12,700.0		58	2014	9,830.0	72.50	
	26 Feb 1997	13,700.0		59	1986	9,570.0	73.75	
	08 Jan 1998	16,200.0		60	1958	9,540.0	75.00	
	15 Mar 1999	13,500.0		61	1946	9,410.0	76.25	
	21 Dec 1999	1,480.0		62	1944	8,860.0	77.50	
	05 Mar 2001	13,700.0		63	2008	8,800.0	78.75	
	29 Sep 2002	18,600.0		64	2005	8,140.0	80.00	
	01 Jul 2003	23,500.0		65	1957	7,690.0	81.25	
	17 May 2004	14,600.0		66	1940	7,690.0	82.50	
	03 Feb 2005	8,140.0		67	1982	7,190.0	83.75	
	27 Feb 2006	3,190.0		68	1942	6,250.0	85.00	
	01 Jan 2007	11,700.0		69	2015	6,120.0	86.25	
	16 May 2008	8,800.0		70	1939	6,000.0	87.50	
	30 Mar 2009	22,400.0		71	1945	5,920.0	88.75	
	19 Dec 2009	12,700.0		72	1960	5,770.0	90.00	
	11 Mar 2011	13,400.0		73	1968	4,730.0	91.25	
	01 Sep 2012	32,500.0		74	1976	4,010.0	92.50	
	11 Jan 2013	22,800.0		75	1970	3,680.0	93.75	
	24 Feb 2014	9,830.0		76	2006	3,190.0	95.00	
	04 Mar 2015	6,120.0		77	1952	2,800.0	96.25	
	13 Aug 2016	120,000.0		78	1963	2,040.0	97.50	
	23 Jan 2017	9,875.0		79	2000	1,480.0	98.75	

* Low outlier plotting positions are computed using Median parameters.

<< Frequency Curve >>

AmDarling2019-Robert, LA-FLOW-ANNUAL PEAK

Computed	Variance	Percent	Confidence Limits
Curve	Log (EMA)	Chance	0.10 0.90
FLOW, CFS		Exceedance	FLOW, CFS
111,802.5	0.01357	0.200	169,959.0 83,409.4
91,765.9	0.00955	0.500	130,362.4 71,721.3
77,733.5	0.00708	1.000	105,076.8 62,800.2
64,640.7	0.00509	2.000	83,293.2 53,826.1
52,454.7	0.00358	4.000	64,601.3 44,825.9
37,657.9	0.00228	10.000	44,039.0 32,993.0
27,352.2	0.00177	20.000	31,153.9 24,222.8
14,477.1	0.00162	50.000	16,312.2 12,834.0

	7,415.6	0.00215		80.000		8,458.9	6,406.5	
	5,158.6	0.00309		90.000		6,005.0	4,288.3	
	3,796.3	0.00462		95.000		4,540.4	2,996.0	
	2,099.6	0.01073		99.000		2,717.7	1,428.2	
	-----	-----		-----		-----	-----	

<< Systematic Statistics >>

AmDarling2019-Robert, LA-FLOW-ANNUAL PEAK

Log Transform:		Number of Events	
FLOW, CFS			
Mean	4.151	Historic Events	0
Standard Dev	0.337	High Outliers	0
Station Skew	-0.250	Low Outliers	0
Regional Skew	0.091	Zero Events	0
Weighted Skew	-0.179	Missing Events	0
Adopted Skew	-0.179	Systematic Events	79

--- End of Analytical Frequency Curve ---

APPENDIX 4: BOUNDARY CONDITIONS SUPPORTING RESEARCH

Boundary Conditions Supporting Research

Amite River Basin Hydraulic Model Boundary Conditions

JULY 30, 2018

AMITE RIVER BASIN HYDRAULIC MODEL
BOUNDARY CONDITIONS

Prepared for

Dewberry Consultants, LLC.
2835 Brandywine Road, Suite 100
Atlanta, GA 30341-4015

Prepared by

FTN Associates, Ltd.
124 West Sunbridge, Suite 3
Fayetteville, AR 72703

FTN Project No. 10568-1488-001

July 30, 2018



TABLE OF CONTENTS

1.0	INTRODUCTION	A4-6
2.0	DATA SOURCES	A4-8
3.0	TYPICAL LAKE ELEVATION	A4-11
4.0	ELEVATION OF RECORD.....	A4-155
5.0	FLOODING LAKE ELEVATIONS.....	A4-188
6.0	WIND INDUCED LAKE ELEVATIONS	A4-20
7.0	REFERENCES	A4-21

LIST OF TABLES

Table 1	Station Location Information.....	A4-9
Table 2	Amite River Peak Discharges vs. Measured Lake Maurepas WSEL	A4-19
Table 3	Average Daily Wind Speed vs. Measured Lake Maurepas WSEL	A4-20

LIST OF FIGURES

Figure 1	Project Location Map.....	A4-7
Figure 2	Streamflow, WSEL, and wind gage station locations in the study area.	A4-8
Figure 3	Pass Manchac Stage Data	A4-11
Figure 4	Pass Manchac Stage Duration Curve.....	A4-12
Figure 5	Water Surface Elevations at Pass Manchac (May 14-24, 2018).....	A4-14
Figure 6	Rainfall Totals from Hurricane Isaac. Adapted from Berg (2013).....	A4-15
Figure 7	Amite River Discharge vs. Pass Manchac WSEL during Hurricane Isaac.....	A4-21

1.0 INTRODUCTION

This report describes work done by FTN Associates, Ltd. (FTN) under subcontract to Dewberry Consultants LLC (Dewberry) who is under contract with the Louisiana Department of Transportation and Development (DOTD) as their consultant for the Federal Emergency Management Agency (FEMA) Cooperating Technical Partner program. This work fulfills the requirements for the “Hydrologic and Hydraulic Numerical Modeling of the Amite River Basin” Task Order Task 7.3 “Develop Boundary Options.”

FTN was tasked with developing a set of downstream boundary conditions for the Amite River Basin Hydraulic Model (model). The downstream end of the model terminates where the Amite River meets Lake Maurepas. A stage hydrograph boundary condition is appropriate for this location due to the backwater effects caused by the lake. The lake is also influenced by diurnal tidal fluctuations and experiences periodic water surface elevation (WSEL) changes due to its connection with the Gulf of Mexico, through the Lake Pontchartrain basin estuary. In developing the boundary condition at this location, the following four conditions were considered at Lake Maurepas:

1. Average or “typical” WSEL and tidal fluctuation.
2. WSEL of record.
3. WSEL during the largest measured flooding events on the Amite River.
4. Wind and storm surge influenced WSEL.

Lake Maurepas receives flow from four principal river systems: Amite River, Tickfaw River, Blind River, and Dutch Bayou, along with several minor channels that discharge from the surrounding swamp (see Figure 1). However, direct exchange of flow from the swamp surrounding the lake is limited to the main channels over the normal range of lake elevations by a natural berm along the lake shoreline (URS, 2006). Lake Maurepas normally discharges into Lake Pontchartrain to the northeast through Pass Manchac.



Figure 1: Project Location Map.

2.0 DATA SOURCES

Streamflow, WSEL, and wind speed data were collected from the U.S. Army Corps of Engineers (USACE), U.S. Geological Survey (USGS), and National Oceanic and Atmospheric Administration (NOAA), respectively, for the project area. The location of the stations used in this analysis are shown in Figure 2. Location information is also provided in Table 1.



Figure 2: Streamflow, WSEL, and wind gage station locations in the study area.

Table 1. Station Location Information.

AGENCY	STATION	NAME	NAD83	
			LATITUDE	LONGITUDE
USGS	07380120	Amite River at Port Vincent, LA	30.332694	-90.852042
USGS	07380200	Amite River near French Settlement, LA	30.275473	-90.779262
USGS	07380215	Amite River at Hwy 22 near Maurepas, LA	30.309362	-90.610368
USACE	85420	Pass Manchac near Pontchatoula	30.281389	-90.400278
NOAA	USW00012916	New Orleans Airport, LA	29.996910	-90.277510
NOAA	8761927	New Canal Station, LA	30.026666	-90.113333

The USACE operates the Pass Manchac near Pontchatoula gage (USACE gage no. 85420), which is located on the Louisiana State Highway 51 bridge on the south side of Pass Manchac. Daily stage data for this gage were obtained, from the USACE New Orleans District. Stage values at this location have been recorded since July 1955 but there is a considerable gap in the data that starts in September 2005 and extends through April 2009. Furthermore, a consistent vertical datum was not used throughout the period of record, and before March 1983 a vertical datum was not established, so that data cannot be used for this analysis.

The USACE originally established the Pass Manchac gage to a vertical datum of 0 feet, NGVD29 in March 1983. Adjustments factors were then used to calibrate the gage back to the zero datum in May 1987 and March 1988 using new target epochs. One final calibration was completed in April 2009, and at this time, the gage adjustment factor was used to shift the gage datum to a 0 feet, NAVD88 datum. Using gage calibration notes from the USACE, all available stage data was first converted to a NAVD88 datum for use in the project.

Streamflow and stage data were downloaded from the USGS's National Water Information System (NWIS) website (<https://waterdata.usgs.gov/nwis>). The USGS operates three gages on the Amite River in close proximity to Lake Maurepas. However, only the Amite River at Port Vincent, LA (07380120) site records both streamflow and stage. Streamflow data from the USGS's Port Vincent site were used to examine the likelihood of extreme flooding events occurring when lake levels were high in Lake Maurepas. Peak streamflow values have been recorded at the Port Vincent site since 1985. This record coincides with most of the stage data recorded at Pass Manchac. Stage data at the Amite River at Louisiana State Highway 22

near Maurepas, LA (USGS gage no. 07380215) station were also used to examine the water surface slope in Lake Maurepas.

Wind speed data for this project was obtained from NOAA's Climate Data Online website (<https://www.ncdc.noaa.gov/cdo-web/>). The New Orleans Airport, LA (NOAA station USW00012916) site has recorded daily average wind speed from January 1984. This data was used to examine the effect that high wind speed has on lake levels and the likelihood of an extreme flooding event coinciding with high lake levels that were developed during high wind speed events.

3.0 TYPICAL LAKE ELEVATION

Daily and hourly stage¹ data from the USACE's Pass Manchac near Pontchatoula station were used to develop the "typical" or average downstream boundary condition for the Amite River Basin hydraulic model. Daily values were used to determine the long-term average WSEL and hourly data were used to develop the average diurnal tidal pattern in Lake Maurepas. Figure 3 presents the daily stage data that has been recorded at the Pass Manchac site since March 1983 (i.e., when measurements were referenced to an elevation datum). A stage duration curve was also developed using these data and is presented in Figure 4. The average or "typical" WSEL in Lake Maurepas during this time period is 0.73 feet, NAVD88. The median WSEL during this period is 0.71 feet, NAVD88, and over 98% of the values recorded are between -0.7 and 2.5 feet, NAVD88.

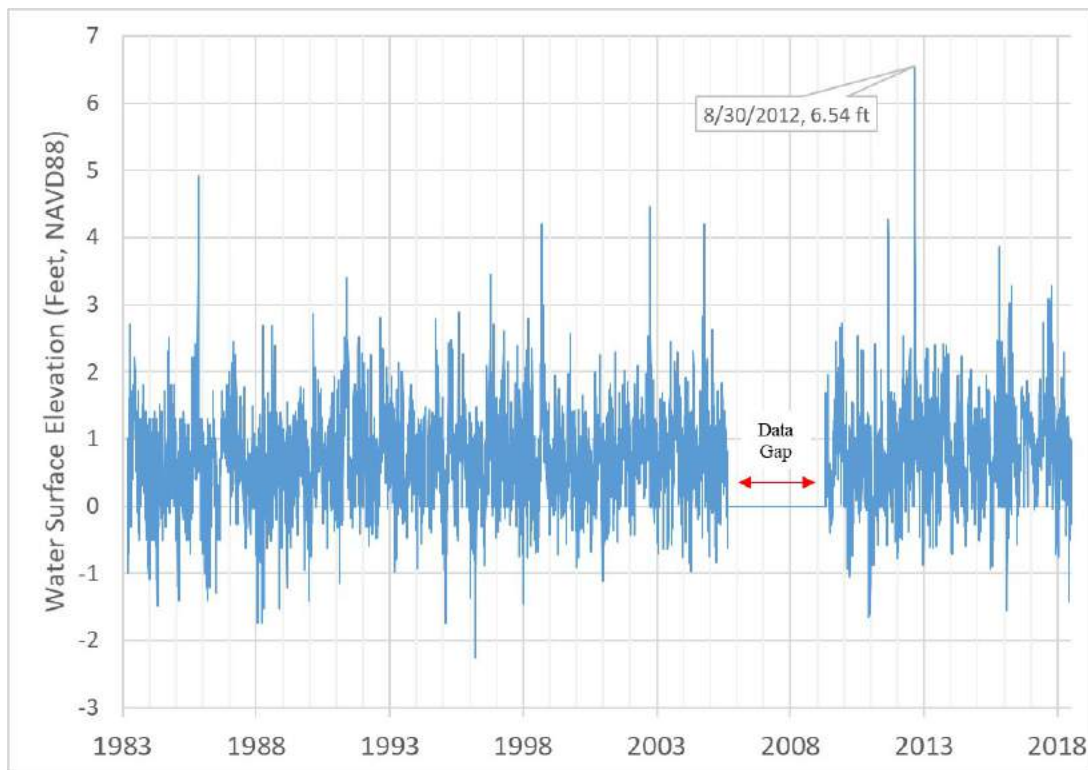


Figure 3: Pass Manchac Stage Data.

¹ Datum of gage is 0.0 ft NAVD88, so stage and WSEL values are the same.

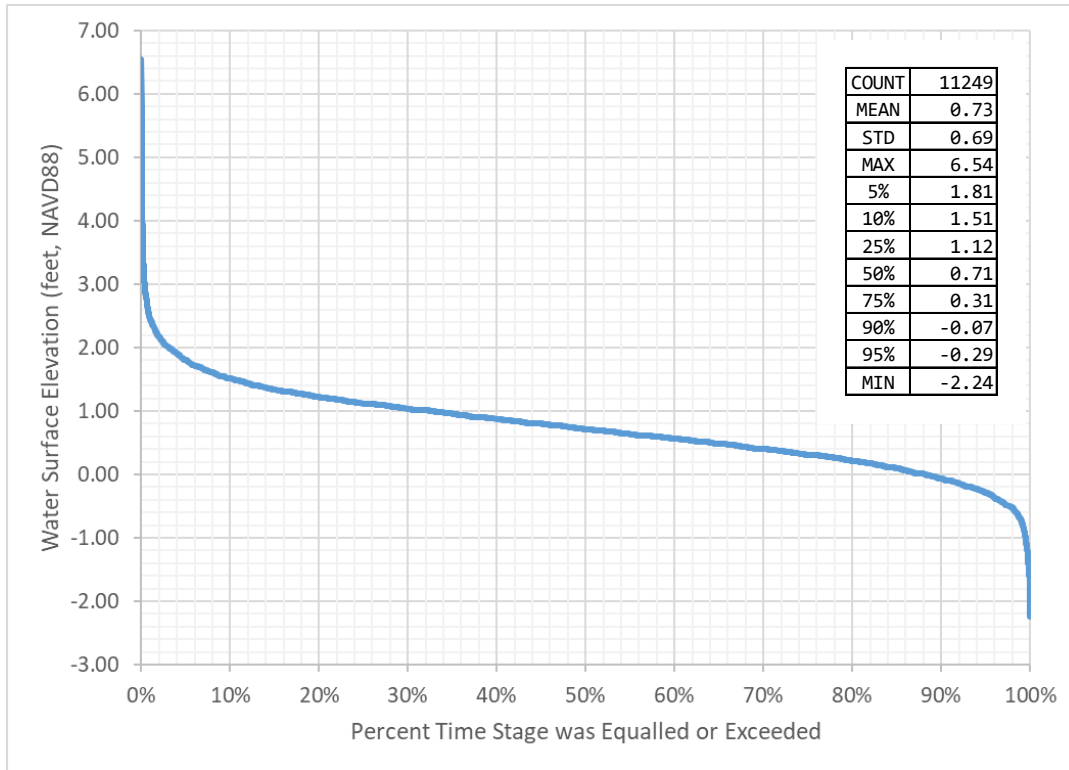


Figure 4. Pass Manchac Stage Duration Curve.

Lake Maurepas is influenced by diurnal tidal fluctuations and experiences periodic WSEL changes due to its connection with the Gulf of Mexico through the Lake Pontchartrain. NOAA operates the New Canal Station, LA (NOAA station no. 8761927) monitoring station in Lake Pontchartrain (NOAA, 2018). This station has been in operation since November 1982 and according to NOAA’s website, the normal diurnal range at this station is 0.54 feet. According to hourly data collected from January-June 2018 at Pass Manchac, the average diurnal range in Lake Maurepas is 0.24 feet. The diurnal range in Lake Maurepas is likely less than that of Lake Pontchartrain due to the damping effect caused by the reduced conveyance capacity in Pass Manchac, and resistance factors such as shear stress, drag, and the width of the pass.

For the “typical” boundary condition, a WSEL time-series for Lake Maurepas can be generated using the average lake level and diurnal tidal range. The diurnal tidal pattern in Lake Maurepas can easily be modeled as a periodic sine function according to Equation 1.

Equation 1

$$f(x) = A * \sin(Bx + C) + D$$

Where:

A = Amplitude

B = $2\pi \div \text{Period}$

C = -Phase Shift * B

D = Vertical Shift

For the “typical” condition, the amplitude is equal to one half the average diurnal range (A=0.12), the period is equal to one lunar day (~24 hrs and 50 minutes [B=0.253]), the vertical shift is equal to the average lake elevation (D=0.73), and the phase shift is dependent on position of the moon, sun and other minor variables (“C” can be set to any real value, however the timing of the High and Low Tides will be set by this value). This simplified procedure doesn’t account for more complex factors that effect tidal fluctuations, but it does produce sub-daily variations that are similar to “typical” conditions in Lake Maurepas. Measured hourly WSEL values at Pass Manchac from May 14th-24th, 2018 are shown in Figure 5, along with modeled output using Equation 1. During this period, lake levels were relatively constant, and the sinusoidal pattern generated from tidal fluctuations is especially evident.

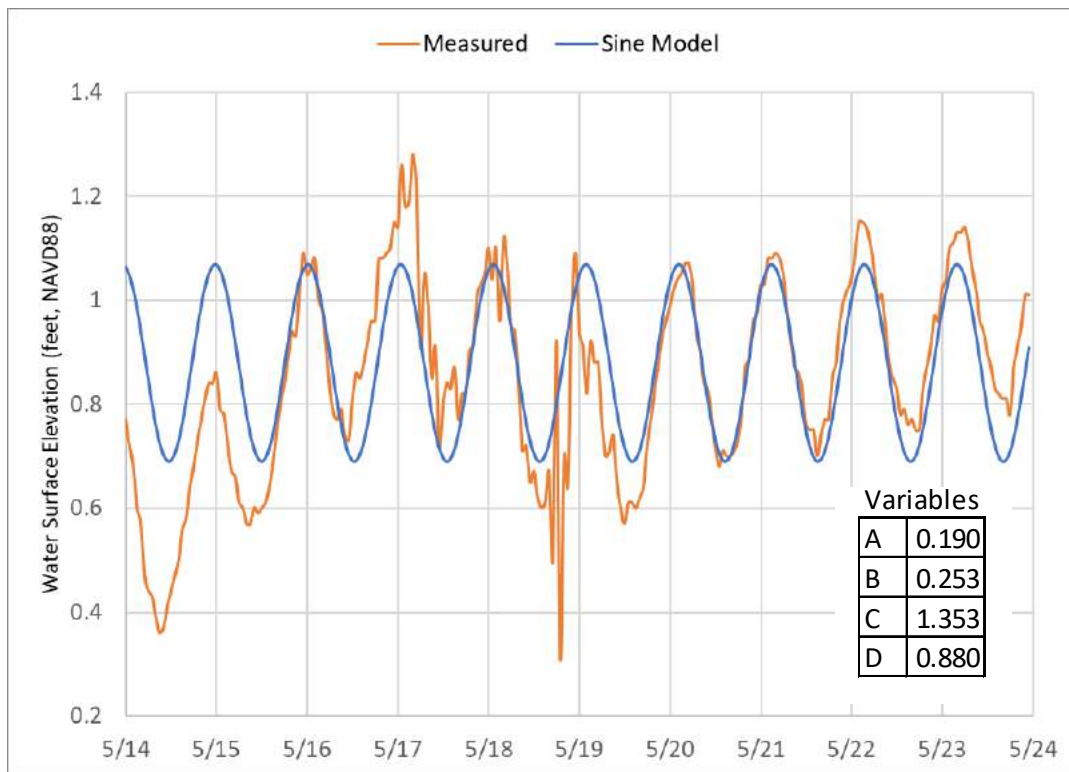


Figure 5. Water Surface Elevations at Pass Manchac (May 14-24, 2018).

4.0 ELEVATION OF RECORD

The water surface elevation (WSEL) of record in Lake Maurepas, as measured at the Pass Manchac station, occurred on August 30, 2012. On this date the WSEL at Pass Manchac reached 6.54 feet, NAVD88, at the same time that Hurricane Isaac made landfall along the Louisiana-Mississippi coast southeast of Lake Maurepas. Isaac's strong winds produced a large storm surge in southeastern Louisiana and Mississippi. Isaac was also responsible for producing over 23 inches of rain in Hammond, LA from August 25th – September 3rd, 2012 (Figure 6), produced maximum wind gusts of over 70 mph at the New Orleans Airport, and the USGS reported that the storm surge was so strong that the Mississippi River flowed backwards for almost 24 hours (Berg, 2013).

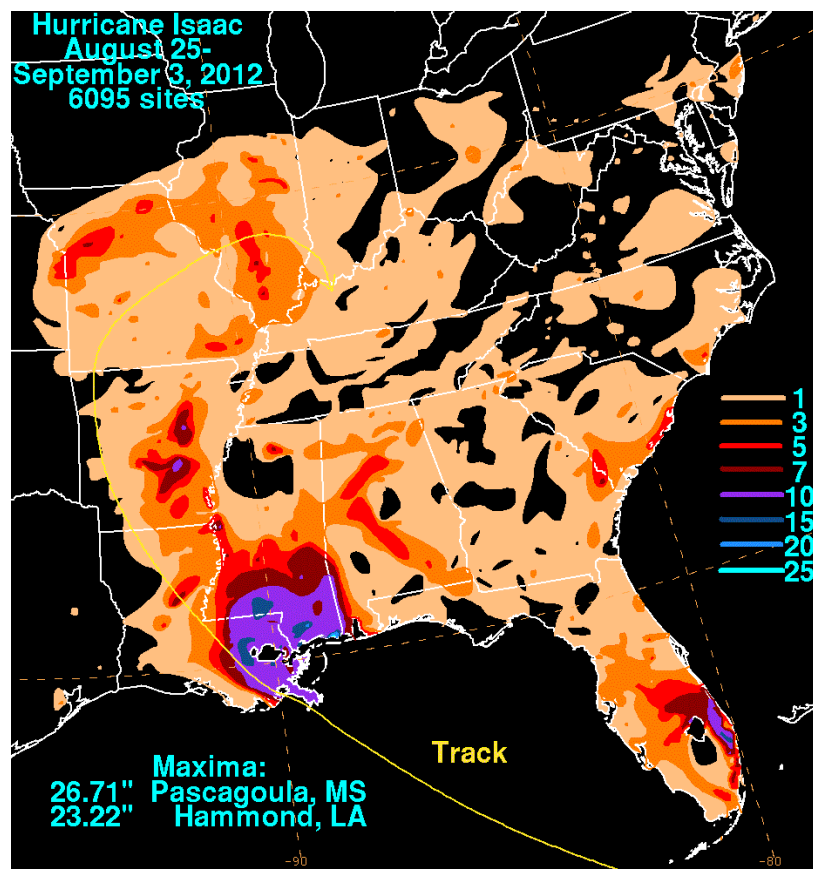


Figure 6. Rainfall Totals from Hurricane Isaac. Adapted from Berg (2013).

During Hurricane Isaac, measured streamflow at the USGS's Amite River at Port Vincent (07380120) gaging station peaked at 21,300 cfs. Also, as evident by the negative discharges measured during August 29th, 2012, the Amite River actually flowed backwards as the WSEL in Lake Maurepas rose rapidly due to the strong storm surge (Figure 7).

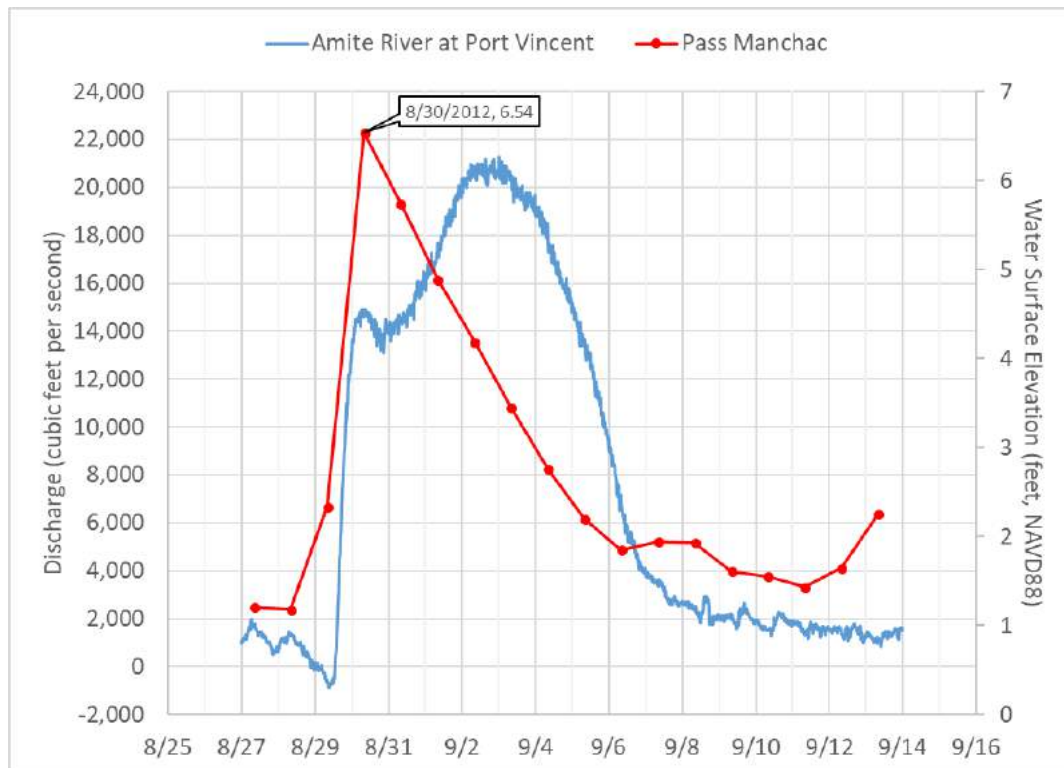


Figure 7. Amite River Discharge vs. Pass Manchac WSEL during Hurricane Isaac.

Using the WSEL of record as a constant stage boundary condition in the Amite River Hydraulic model is an option, however the probability of the peak streamflow and peak WSEL occurring at the same time appears to be unlikely. The highest measured WSELs in Lake Maurepas were caused by storm surges due to tropical systems, and high storm surges produced by tropical systems preceded flooding events due to strong winds at the edge of the system that create the surge; then flooding occurs later as the system produces rainfall on land. One alternative to creating the elevation of record boundary condition would be to use the WSEL values recorded during Hurricane Isaac (August 27th through September 6th, 2012), but shift the

peak stage time to occur approximately three days prior to the peak discharge in the hydraulic model.

5.0 FLOODING LAKE ELEVATIONS

The 15 largest discharge measurements from 1985-2018 at the USGS Amite River at Port Vincent (07380120) gage are listed in Table 2. Lake Maurepas WSEL values measured at the USACE's Pass Manchac station are also reported for the same day as the measured peak flow along with the maximum stage recorded during the 5-day window around the peak flow date. Thirteen of the fifteen largest discharges, occurred during winter or spring months and only two of the events occurred during the northern Atlantic hurricane season (June 1st – November 30th) when storm surges produced by tropical storms are typically the largest. The flood of record on the Amite River occurred on August 15th, 2016 during the hurricane season but was not the result of a named tropical system and was instead caused by a slow-moving tropical low-pressure system interacting with an eastward traveling baroclinic trough to the north (Wang, Zhao, and Gillies, 2016). Luckily, this system was not accompanied with large storm surges or flooding in region would have been further exacerbated. The only peak discharge event in Table 2 that was the result of a named tropical storm (Hurricane Juan), occurred on November 1st, 1985. This event also produced the largest peak and 5-day max WSEL values that were recorded, coinciding with one of the 15 largest discharges in the Amite River.

FTN was not tasked with developing joint probability statistics describing the likelihood of extreme flooding events coinciding with high WSELs in Lake Maurepas. The data in Table 2, however, show that, in general, peak flooding events occur much more frequently during the winter and spring months and are less likely to occur as a result of a major tropical storm. This means that the likelihood of extreme flooding occurring at the same time as a high WSEL event in Lake Maurepas is minimal. One possible alternative for developing a boundary condition from these data is to use the statistics from the 5-day maximum WSEL values to generate an average and worst-case scenario. With the exception of the Hurricane Juan peak (11/1/1985), the remaining 5-day peak values are between 0.83 and 3.03 feet, NAVD88, and the mean of all the 5-day peak values is 2.15 feet, NAVD88. This value could be used to represent the average flooding scenario stage boundary condition. The worst-case scenario flooding scenario could

also be modeled using the 5-day peak value measured during Hurricane Juan (4.91 feet, NAVD88).

Table 2. Amite River Peak Discharges vs. Measured Lake Maurepas WSEL.

DATE	USGS 07380120 Discharge (cfs)	Value Code ¹	Pass Manchac (85420)	
			Peak Discharge WSEL ² (feet, NAVD88)	5-day Max WSEL (feet, NAVD88)
8/15/2016	199,000	P	1.30	1.72
1/28/1990	69,500	P	0.73	1.02
1/23/1993	48,400	P	1.79	1.93
4/30/1997	45,300	P	1.08	2.02
4/13/1995	44,700	P	1.92	2.48
3/8/1992	43,100	P	1.05	2.03
11/1/1985	42,200	P	3.62	4.91
2/24/2003	42,100	P	0.95	1.59
1/9/1998	41,000	P	NA	1.84
3/14/2016	41,700	A	2.59	3.03
4/4/1988	38,300	P	2.29	2.69
1/13/2013	35,200	P	2.05	2.18
3/17/1999	33,900	P	0.72	0.83
2/28/1997	31,800	A	1.33	1.88
5/18/2004	31,400	P	2.09	2.09

1. P=Peak Value / A=Average Daily Value.

2. NA = Not Available.

6.0 WIND INDUCED LAKE ELEVATIONS

The 10 largest daily average wind speeds recorded at the New Orleans Airport (USW00012916) from January 1984 through June 2018 are presented in Table 3. The top nine recorded values occurred during tropical storms that developed in August through October during the peak of the northern Atlantic Hurricane season. The tenth highest wind speed, however, was recorded during the spring, was one of the most intense extratropical cyclones ever observed and was dubbed the “1993 Storm of the Century” (Kocin, Schumacher, Morales, & Uccellini, 1994). The average wind speed during Hurricane Isaac is the largest on record and resulted in a powerful storm surge that resulted in the water surface elevation of record in Lake Maurepas. However, wind speed alone is not the only factor contributing to high WSELs in Lake Maurepas. Other factors such as storm intensity, forward speed, size, and angle of approach to the coast can affect storm surge intensity and drive the WSEL. This is evident by the low 10-day maximum WSEL associated with the 1993 Storm of the Century and the fact that similar wind speeds resulted in substantially different WSELs in Lake Maurepas during other events.

Table 3. Average Daily Wind Speed vs. Measured Lake Maurepas WSEL.

Date	Storm Name	USW00012916 Average Daily Wind Speed (mph)	Pass Manchac 10-day Max WSEL (feet, NAVD88)
8/29/2012	Hurricane Isaac	35.34	6.54
9/1/2008	Hurricane Gustav	29.53	NR
9/27/1998	Hurricane Georges	26.40	2.86
8/26/1992	Hurricane Andrew	25.50	2.81
9/24/2005	Hurricane Katrina	24.38	NA
9/12/2008	Hurricane Ike	24.38	NA
10/27/1985	Hurricane Juan	24.16	4.91
9/25/2002	Hurricane Isidore	22.82	4.45
9/15/2004	Hurricane Ivan	22.59	2.82
3/13/1993	1993 Storm of Century	22.15	1.22

One possible alternative for developing a boundary condition from these data is to use the statistics from the 10-day maximum WSEL values to generate an average scenario. Using this approach, the wind induced stage boundary condition would be equal to 3.66 feet, NAVD88, which is in-between the two scenarios that were suggested in Section 5.0.

7.0 REFERENCES

- Berg, R. (2013). Tropical Cyclone Report – Hurricane Isaac (AL092012). National Hurricane Center. January 28, 2013.
- Kocin, P., Schumacher, P., Morales, R., and Uccellini, L. (1994). Overview of the 12-14 March 1993 Superstorm. National Weather Service.
- NOAA. (2018). National Oceanic and Atmospheric Administration Tides and Currents - Station 8761927. Retrieved from: <https://tidesandcurrents.noaa.gov/stationhome.html?id=8761927> [Accessed July 2018].
- URS. (2006). Mississippi River Reintroduction into Maurepas Swamp Project (PO-29). Volume IV of VII – Hydrologic Data. June 29, 2006.
- Wang, S. Y. S., Zhao, L., & Gillies, R. R. (2016). Synoptic and quantitative attributions of the extreme precipitation leading to the August 2016 Louisiana flood. *Geophysical Research Letters*, 43(22).

APPENDIX 5: HYDROLOGIC AND HYDROMETEOROLOGIC STATIONARITY ASSESSMENT

Supporting Research

Background

In 2016, the United States Army Corps of Engineers (USACE) issued Engineering and Construction Bulletin No. 2016-25 (hereafter, ECB 2016-25) [8], which stipulated that climate change should be considered for all Federally funded projects in planning stages. A qualitative analysis of historical climate trends as well as an assessment of future projections was provisioned by ECB 2016-25. Even if climate change does not appear to be an impact for a particular region of interest, the formal analysis outlined in ECB 2016-25 results in better informed planning and engineering decisions. For example, an increase in impervious area can often result in higher streamflow, even with no trend in heavy rainfall. Stationarity tests were performed on long-record precipitation and streamflow gages to assess whether non-stationarity needs to be factored in for future planning projects.

Precipitation

A stationarity analysis was performed on long-term precipitation gages belonging to the Global Historical Climatology Network. Only gages with 60 qualifying years were used, with a qualifying year being defined as one with less than 10 missing days of observations. In addition, given that climate change is expected to have an impact in the relatively recent period, only gages with one qualifying year later than 2007 were used. In all, 35 gages within and in the vicinity of the study region qualified for the analysis.

Three stationarity tests were performed:

- Trends in annual maximum series through 2015 and 2016.
- Trends in peaks over threshold (threshold: 2.5 in. per day).
- Percent change in the 99th percentile of rainy day rainfall intensity.

Results for the tests are shown in **Figure A5-1a** through **Figure A5-1d**. All trend estimates were determined using both Pearson and Spearman correlation coefficients (i.e. correlating the year with the magnitude). A null hypothesis of stationarity was assumed, and trends, if found, were only classified as significant if the confidence level exceeded 90%.

Figure A5-1b shows trend test results for Annual Maximum Series (AMS) using data through 2016. Of 35 gages, 7 were identified as having significant positive trends with none having significant negative trends. Assuming independence between gages, only about 4 gages are expected to show a trend by chance. Thus, the results suggest there is regional-scale non-stationarity towards higher AMS daily rainfall in the area. A similar test, but limiting data through 2015, showed a similar result with 6 of 35 gages showing significant upward trends. Thus, the 2016 heavy rainfall event does not appear to have an outsized influence on the AMS trend analysis.

Because AMS events measure only one daily rainfall per year, it could be prone to being affected by rare, very extreme events. To investigate trends in a larger number of rainfall events, a Peaks-Over-Threshold (POT) approach was also used. A threshold of 2.5 in. per day was used, which results in roughly two to five POT days identified depending on the exact location. For example, the POT time series from the Baton Rouge Ryan Airport gage is shown in **Figure A5-2**. Note the clear upward trend in the number of such events, with a maximum of eight events being recorded during exceptionally wet 2016. **Figure A4-1c** shows that 8 of 35 gages have significant upward trends in POT, with zero trends having downward trends. This corroborates the AMS trend results in **Figure A5-1a** and **Figure A5-1b**.

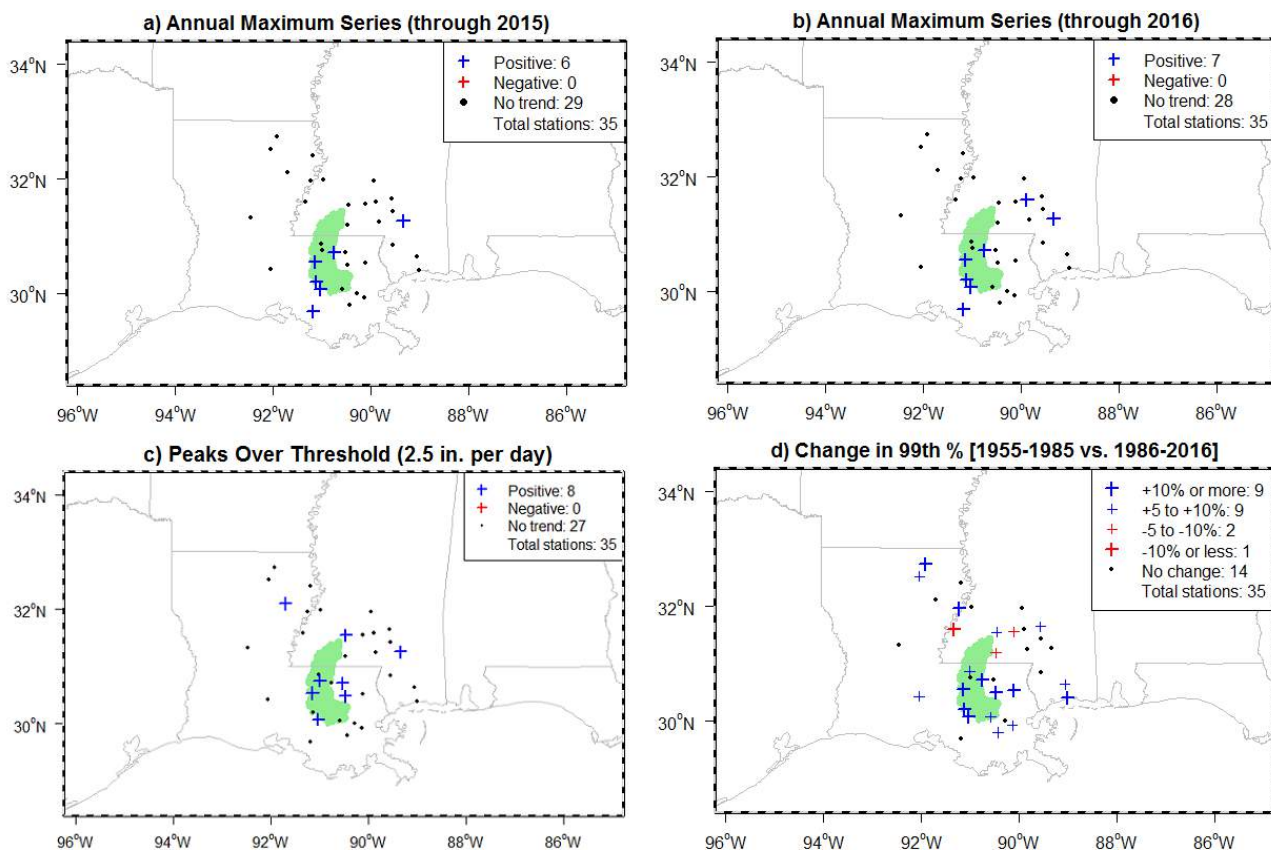


Figure A5-1a through Figure A5-1c: Stationarity Test Results Of Qualifying Long-Term Rain Gages: (a and b) Trends in Annual Maximum Series through (a) 2015 and (b) 2016, (c) Trends in Peaks Over Threshold (threshold: 2.5 in. per day), and (d) percent change in the 99th percentile of rainy day rainfall intensity.

Figure A5-1d shows the percent change in the 99th percentile of rainy day rainfall across the qualifying gages, from the 1955-1985 period to the 1986-2016 period. For example, at the Baton Rouge Ryan Airport gage, the magnitude of the 99th percentile over the earlier period was 3.53 in., while during the latter period it is 3.98 in. (an increase of 13%). Of the 35 gages, 18 showed increases of at least 5%, while only three showed decreases of that magnitude. Collectively, these tests suggest that there is clear non-stationarity towards an increase in the magnitude and occurrence of heavy rainfall in the area.

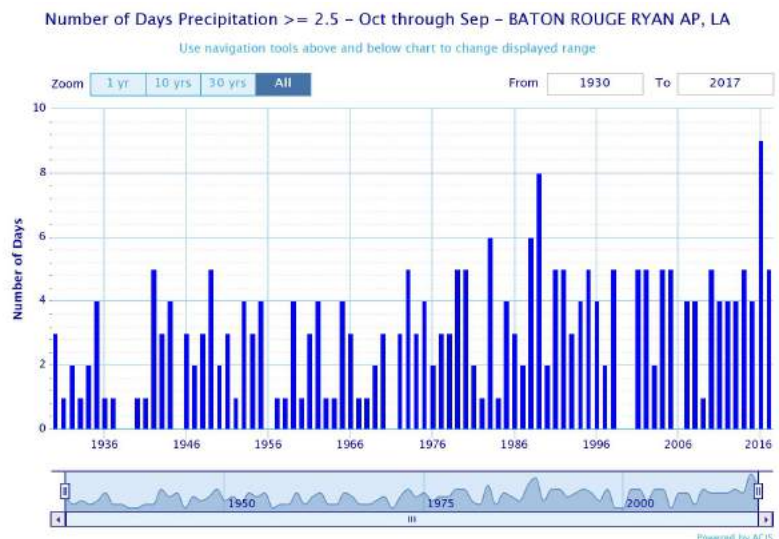


Figure A5-2: Days with three or more inches of rainfall at Baton Rouge Ryan Airport, LA.

Streamflow

In accordance with ECB 2016-25, a stationarity analysis was performed to determine if there are long-term changes in streamflow statistics within the ARB, and its vicinity. Non-stationarity in stream flow can be a result of many processes, most notably changes in land cover, addition/removal/modification of water control structures, and changes in regional rainfall characteristics. To test for stationarity, the guidance provided by the USACE Non-Stationarity Detection Tool was used. This is a compilation of 16 tests measuring changes in the distribution, mean, variance, and trend of long-term time series. The tests can be broadly grouped into two categories: change point and trend. The former measures relatively abrupt “step-like” changes in the time series, while the latter measure longer term, steadier changes. Note that a time series with a trend can often also have an identified change point. Water Year Annual Maximum Series of streamflow (data through 2016) at the following six gages were used in the analysis and the data from these gages can be seen in **Table A5-1**.

Table A5-2 outlines the tests that were performed. The null hypothesis for all tests was stationarity; the alternative hypothesis of non-stationarity was accepted if confidence exceeded the 90% level of statistical significance. In addition to conducting the tests, each time series was manually inspected.

Results of the stationarity tests are shown in **Table A5-3**. For change point tests 1-12, the table shows the year(s) identified as a change point. For trend tests 13-16, tests 13 and 14 show whether a trend is detected, while tests 15 and 16 also provide information about the direction of the trend. Blanks indicate the null hypothesis (i.e. stationarity) was not rejected. Positive trends in streamflow were noted at three of the six gages: the Comite River near Olive Branch, Comite River near Comite and Amite River near Denham Springs. However, for the Olive Branch site, only two of the four trend tests found significant results, making it difficult to definitively confirm that non-stationarity was present. The two other sites had more convincing evidence to support an increase in streamflow over time. However, a significant complication was that numerous change point tests for these two gages revealed the 1970s as a period when there was a stepwise increase in flow. This appears to coincide favorably with data showing that the number of residential structures increased markedly during this time as shown in **Figure A5-3** (Source: InfoGroup®). Thus, based on our experience, the increase in buildings and associated impervious area, appears to be the more plausible explanation for recent higher streamflow at this time. However, it is important to note that the 2016 flooding event was unprecedented within the context of the historical (gaged) streamflow records. Thus, it will be important to monitor trend tests over the coming years to check for any newly detected trends.

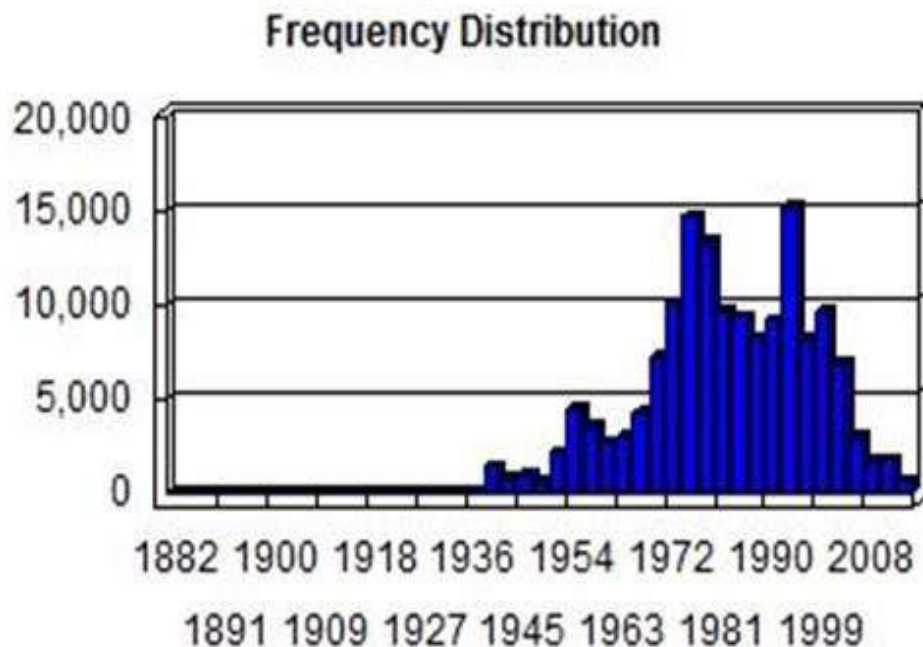


Figure A5-3: Residential Structures Built, By Date

Table A5-1: Streamgages Used in the Stationarity Analysis.

Gage	Location	Years of record
07377500	Comite R nr Olive Br, LA	74
07378000	Comite R nr Comite, LA	72
07378500	Amite R nr Denham Springs, LA	79
07377000	Amite R nr Darlington, LA	67
07376000	Tickfaw R at Holden, LA	76
07375500	Tangipahoa R at Roberts	78

Table A5-2: Stationarity Tests Performed

Test	Type
Cramer-von-Mises distribution	Change point
Kolmogorov-Smirnov distribution	Change point
LePage distribution	Change point
Energy Divisive distribution	Change point
Lombard (Wilcoxon) abrupt mean	Change point
Pettitt mean	Change point
Mann-Whitney mean	Change point
Bayesian mean	Change point
Lombard (Mood) abrupt variance	Change point
Mood variance	Change point
Lombard (Wilcoxon) smooth mean	Change point
Lombard (Mood) smooth variance	Change point
Mann-Kendall trend	Trend
Spearman correlation trend	Trend
Parametric trend	Trend
Parametric trend with Sens slope	Trend
Test	Type
Cramer-von-Mises distribution	Change point
Kolmogorov-Smirnov distribution	Change point
LePage distribution	Change point
Energy Divisive distribution	Change point
Lombard (Wilcoxon) abrupt mean	Change point

Table A5-3a: Stationarity Test Results Using Annual Peak Streamflow.

Location	Test1	Test2	Test3	Test4	Test5	Test6	Test7	Test8
Comite R nr Olive Br, LA			1976	1977	1975			
Comite R nr Comite, LA	1960	1960	1976	1977	1959	1976	1960	
Amite R nr Denham Springs, LA		1991		1972	1970	1971	1976	
Amite R nr Darlington, LA				1984	2014			
Tickfaw R at Holden, LA				1972	1959			
Tangipahoa R at Roberts				1971	1941			

Table A5-3b: Stationarity Test Results Using Annual Peak Streamflow.

Location	Test9	Test10	Test11	Test12	Test13	Test14	Test15	Test16
Comite R nr Olive Br, LA	2014						positive	positive
Comite R nr Comite, LA	1944			1944/1946	trend	trend	positive	positive
Amite R nr Denham Springs, LA	1921				trend	trend	positive	positive
Amite R nr Darlington, LA	2014							
Tickfaw R at Holden, LA	2014							
Tangipahoa R at Roberts	1982							

*Note that Blanks indicate stationarity was not rejected.

Conclusion for Stationarity Assessment

The Flood of August 2016 significantly increased the estimated 1% Annual Exceedance Probability flows for the lower reaches of Amite and Comite Rivers. The 1% AEP is still considerably lower than the flows recorded during that event.

The stationarity tests show positive trends in both precipitation and streamflow. For precipitation gages, regional-scale changes in Annual Maximum Series, Peaks-Over-Threshold and the 99th percentile of daily rainfall all suggest an upward increase in heavy rainfall magnitude and intensity. For streamflow, increases were found at 3 of the 6 tested gages (with no significant changes at the other sites): the Comite River near Olive Branch, Comite River near Comite and Amite River near Denham Springs. For the Olive Branch site, only two of the four trend tests found significant results, making it difficult to definitively confirm that non-stationarity was present. The two other sites had more convincing evidence of increased streamflow over time, though it is difficult to determine if this is due to changes in precipitation or impervious cover owing to a marked increase in the number of residential structures being built around the time of the changes in streamflow.